SAPIENZA
UNIVERSITÀ DI ROMA

Facoltà di Ingegneria

DOTTORATO DI RICERCA IN MECCANICA TEORICA E APPLICATA
XXV Ciclo

MODELLING OF MEMS/NEMS RESONATORS AND FUNCTIONAL DESIGN OF A MECHANICAL TRANSISTOR

Candidato
ALESSANDRO SCORRANO

Docente Guida
Prof. ANTONIO CARCATERRA

Tutor
Prof. ALDO SESTIERI

all'Uomo,

alla Scienza,

al Mondo.

"I do not know what I may appear to the world,
but to myself I seem to have been only like a boy
playing on the sea-shore and diverting myself in now and then
finding a smoother pebble or a prettier shell than ordinary,
whilst the great ocean of truth lay all undiscovered before me."
Isaac Newton

"What is an ocean but a multitude of drops?"
Adam Ewing (Cloud Atlas)

Acknowledgements

First of all, thanks to the *Italy* and to the late *Twentieth Century*: nothing of what I know, I like to do, I love, and I am, would have been the same, without such a fortunate anagraphics. Secondly, I am grateful to my *Family*: my parents gave me the chance to grow in a timeless, inspiring, emancipated, and unrestricted environment that continuously stimulated my curiosity. From the point of view of my formation, I owe so much to *Maestra Agnese*, *Nonno Italo*, and *Mike Bongiorno*: three muses for my culture, three molds for the shape of my brain.

Jumping to (very) more recent times, *Prof. Augusto Di Benedetto*, *Prof. Nicola Pio Belfiore*, and *Prof. Antonio Carcaterra*, respectively embodied the light, the hearth, and the brain of my academic studies. Among them, I particularly thank *Antonio*: a precious and irreplaceable guide along the route towards the Doctorate. Without him, my PhD simply couldn't have been reality. Many others companions shared with me emotions, intelligence, and good debates around Engineering and Science, contributing to make these 3-years-long experience unforgettable. I am mainly thinking to my "teammate" *Gianluca Pepe*, and my "exemplar" *Nicola Roveri*.

Very special thanks are for *Prof. Leonid Y. Gorelik* and *Milton Eduardo Peña-Aza*, due to the limitless hospitality and availability they both showed during my period of stay in Goteborg. Their genuine Russian and Colombian tempers produced a miracle: I don't missed the Mediterranean way of life a single day, even being in the cold Scandinavia!
A goodbye to the whole staff of the Department of Applied Physics at CHALMERS University of Technology. Really, that was a brief but intense period of professional growth for myself.

Last (and most importantly?) I express gratitude to the two halves of my heart: *Valentina*, my Twin Brain, and *Roberta*, my Twin Behavior, who supported a difficult-to-deal-with habit person like me (respectively during the first and second part of the Doctorate – I swear – with no superpositions!), in complementary ways.

Thanks to the *SEALAB Project*, for the chance to periodically detach my brain from my main research topic, every time re-focusing on it with different point of views and a more clear mind.

Last, thanks to the *Inspiration* who seized me to write this Thesis, which I consider my best creation so far…

Contents

Preface

The most basic example of charge transport is represented by the collective motion of charge carriers in a conductive medium – valence electrons in a metal, ions and free electrons in a plasma – under the effect of an external electromagnetic field.
However, more complex conductive working principles exist. For example, in the context of electromechanical devices, peculiar forms of charge transport labeled with the umbrella term *electron shuttle* are experienced by a relatively small group of specifically designed systems.
The simplest configuration capable to realize such "shuttle mechanism" comprises a set of three conductors: two fixed electrodes and an oscillator element between them, separated by a dielectric fluid. Under certain boundary conditions, such system exhibits a symmetry breaking: the oscillator starts vibrating and a limit-cycle can be established, in which a finite amount of electrons per cycle is alternatively collected and released – *shuttled* – when approaching either the fixed electrodes. Consequently, a net current, whose absolute value is strictly related to the frequency of the mechanical oscillations, is produced. Notice that, since the existence of this form of charge transport does not depend on the mobility of unbound electrons, but relies on the motion of a vibrating element; this latter constitutes, in the context of the shuttle mechanism, the archetype of a proper "mechanical charge carrier".

Although the first realization of an electron shuttle device dates at least two centuries ago – the so-called "Franklin bells" represent a first example – only in recent times [Gorelik and Isacsson, 1998] it found reinvigorated interest in the field of nanotechnology, producing a whole novel branch of both theoretical and experimental research. In fact, the presence of quantum effects – in particular *Coulomb blockade* and *quantum tunneling* – opens the way to more interesting – in some cases chaotic – dynamics for the vibrating element of such devices: motion regimes which are peculiar of the nanoscale and not accessible by macro systems.
Collectively refer to these systems as *Quantum Shuttle Modules* (QSMs).

Many original architectures comprising one or more QSMs have been conceptualized and realized in the last decade. From this point of view, one of the most prolific research teams is the Blick's group. An especially promising application is contained in a patent [Blick and Marsland, 2008], in which the idea to realize logic circuits whose switching elements make use of the shuttle mechanism is proposed for the first time. In the inventor's claims, an information technology in which the flux of data relies on vibrating mechanical elements instead of solid state electronic components would have the advantages of low power consumptions, robustness to radiation and wider range of operating temperatures.
In the depicted embodiment of the invention, a switching element is obtained by mechanically couple a set of QSM subsystems, whose vibrating elements are realized with a nanocantilevers geometry. Since each switching element is capable to reproduce the main functionalities of a conventional transistor – namely voltage-driven switching and current amplification – refer to one of them as a *NanoMechanical Transistor* (NMT).

At the present day, the NMT is a mainly unexplored device: no experimental setup has been realized nor predictive theoretical models have been proposed yet. The situation is diametrically opposite in the field of QSMs, whose literature is rather wide, although recent, and a number of QSM devices have been realized at different scales, architectures and materials, exhibiting in most cases a behavior in agreement with the theoretical models. The work presented in this thesis is aimed to fill this gap, providing a first theoretical description of the NMT depicted in the cited patent, finalized to develop an early design stage.

The individuation of such a research topic derived from the opinion the NMT is a good example of concept design introducing original ingredients from the dual point of view of the core working principle – the electron shuttle – and the functional interaction between its constitutive elements – the QSMs. In the Author's belief, these characteristics make the NMT worthy of theoretical investigations, independently from the factual chance to represent a step innovation for both the electronic and information industry – as advocated in the patent claims – and from the technological issues in definitely producing a working prototype.

Notice that, since the NMT is composed by a set of QSMs, its study requires a preliminary comprehension of the dynamical regimes and electrical characterization of these systems. In turn, this will allow to: i) choose the most appropriate typology of QSM to obtain the desired transistor functionalities; ii) determine the characteristic scales of the device; iii) select the correct analytical approach, form of equations and suitable approximations to simulate the dynamics of the whole NMT system with a series of numerical experiments.

This thesis is consequently divided into two Parts: the first one focusing on a theoretical study of QSMs; the second one intended to assess the feasibility of a real application, the NMT.

A brief description of the contents of this work is presented ahead.

In the introduction, a general, conceptual picture of the shuttle mechanism is given, with emphasis on its historical origins. Then, the influence of nanoscale-related phenomena on shuttle devices is discussed: follows a detailed analysis of recent landmarks in QSM literature and a preliminary overview of the NMT patent.

Part One begins with the description of some nanoscale devices exhibiting different forms of charge transport. Then, attention focuses on the shuttle mechanism, whose fundamental concepts and classifications are presented, such as: shuttle and tunnel current contributions, electromechanical coupling, soft/hard nature of oscillations, tunneling region, transport factor.

A prototypal architecture for a QSM, representing the most simple system capable to exhibit the shuttle mechanism at nanoscale, is introduced. As usual in literature, a concentrated parameters model is used, the state of the system reduced to a couple of lagrangian descriptors, namely the oscillator position and charge. Ordinary differential equations describe the evolution of the electromechanical system: both numerical and analytical approaches are used to investigate the dynamics of a QSM under the effect of different boundary conditions. In particular, it is possible to discern two distinct kinds of shuttle mechanism, called *direct* and *inverse* shuttle.

In direct shuttle, a potential difference between two electrodes produces a self-excitation which sustains the motion of the vibrating element and results in a shuttle current between them.

In inverse shuttle, the motion of the vibrating element is triggered by the parametric resonance, and a shuttle current is established between two electrodes maintained at the same voltage.

The two described phenomenologies are somehow complementary and, since the more or less propensity of a system to the first or the second shuttle mechanism only depends on the boundary conditions, it means every QSM referring to the prototypal system presents a superimposition of these two basic forms of shuttle. Consequently, the possibility of *hybrid* shuttle is conceived. In these systems, the overall current can be obtained as a linear combination of and direct and inverse shuttle currents, weighted on the basis of the boundary conditions used.

Part Two opens with a brief historical account of conventional – electronic – transistors. Follows a more detailed analysis of the NMT patent, aimed to critically discuss and delineate the best strategies to reproduce the main functionalities of a transistor. Consequently, the choice of the typology of QSM to be the best candidate as a subsystem of the NMT – direct shuttle with hard nature of oscillations and strong electromechanical coupling – is carried out. In turn, these preliminary design choices individuate the most appropriate form of equations – a semi-classical continuous-charge model – to be used to describe the system dynamics. In particular, closed-form relations for capacitances, equivalent quantum tunneling conductances and force on the oscillator are produced. The attention paid to qualitatively include all the relevant physical effects and quantitatively relate them to the choice of the system parameters, leads to an high flexible set of equations which allowed to develop an interpretative analysis of the results coming from a large number of numerical experiments.

As a first step, a single QSM subsystem is analyzed. A distinction between internal, external and control parameters is suggested. A predictive model is proposed in which a QSM can be put into relation to a Turing machine whose present state is represented by the permanent motion regime established and the value on the input tape corresponds to the applied bias voltage: the control parameter. Transitions between different states occur in correspondence of some threshold values for the external parameter, whose values depend on the set of internal parameters. Also, an interpretative model for the activation/deactivation processes is presented, together with a physical explanation of the current-voltage hysteresis peculiar of hard shuttle regimes. Last, a general characterization of QSM systems is given, and a set of qualitative features of a QSM is defined and quantitatively related to its internal parameters.

As a second and last step, $N+1$ QSM subsystems are arranged to realize the multiple-module NMT, so that the whole system is described by $2(N+1)$ equations. Each QSM is considered electrostatically decoupled from the others, but mechanically coupled with its nearest neighbors. Once the distinction between the only drive module and the remaining N slave modules is introduced, a functional analysis of the NMT in reproducing both the current interruption and amplification features is presented. First, a rigorous definition of ON and OFF states is proposed, then, peculiar motion regimes and failure conditions are individuated and investigated. This Part leads to synthetize a set of "thumb rules": a basic control strategy aimed to obtain a system which correctly mimics the functionalities of an electrical switch and/or amplifier. Last, a black-box characterization of the NMT is outlined, its electric performances compared with conventional devices, and an heuristic procedure to estimate the current gain is suggested.

This completes the description of the thesis contents.

Two main original contributions can be individuated in this work, as it is summarized ahead.

i) The theoretical study of an innovative device, the Blick's NMT, developed through the consecutive steps of: equation modeling, numerical simulations, functional analysis and characterization of its black-box conductive properties. The whole process is synthetized by the proposal of a set of design requirements and control strategies.
ii) The conceptualization and the quali-quantitative analysis of a form of shuttle mechanism triggered by parametric resonance (here termed "inverse shuttle"), able to realize a current flow between two electrodes at the same voltage. This represents, differently from self-excited QSMs introduced by Gorelik ("direct shuttle"), a new archetype of shuttle.

The study presented here constitutes the outcome of a period of fructuous collaboration of the Author with Gorelik himself at the CHALMERS University of Technology.

Alessandro Scorrano *Göteborg, August 24th, 2012*

Nomenclature

MEMS/NEMS	*Micro/Nano ElectroMechanical System*
CS	*Conductive Solid*
SM	*Shuttle Module*
QSM	*Quantum Shuttle Module*
NMT	*NanoMechanical Transistor*
TJ	*Tunnel Junction*
DTJ	*Double (Tunnel) Junction*
SET	*Single-Electron Transistor*
Q-dot	*Quantum Dot*
QT	*Quantum Tunneling*
CB	*Coulomb Blockade*
DC/AC	*Direct/Alternate Current*
RCF	*Resonant Coulomb Force*
STM	*Scanning Tunneling Microscope*
IC	*Integrated Circuit*
CNT	*Carbon NanoTube*
BJT	*Bipolar Junction Transistor*
FET	*Field-Effect Transistor*

List of Symbols

e	elementary charge	$1.602 \times 10^{-19}\ C$
h	Planck constant	$6.626 \times 10^{-34}\ J \cdot s$
c	speed of light	$2.998 \times 10^{8}\ m/s$
k_B	Boltzmann constant	$1.381 \times 10^{-23}\ J/K$
ε_0	vacuum permittivity	$8.854 \times 10^{-23}\ F/m$

$x(t)$	shuttling element position
$Q_S(t)$	total electric charge on the shuttling element
$N_S(t)$	(positive) charge carriers on the shuttling element

$I(t)$ or $\bar{I}_{\Delta t}$	instant or average current
dQ or ΔQ	electric charge passed though the charge detector in a time $\mathrm{d}t$ or Δt
dN or ΔN	(positive) charge carriers passed though the charge detector in a time $\mathrm{d}t$ or Δt
n	charge carriers density for the whole oscillation volume
n^*	charge carriers density within the shuttling element
N^*	maximum (positive) charge carriers the shuttling element can contain
N_s	(positive) charge carriers (actually) shuttled per oscillation
T_s	(actual) shuttle period of oscillation
f_s	(actual) shuttle frequency
A	amplitude of oscillation
χ	phase shift between $x(t)$ and $V_G(t)$
v	drift velocity

d	half-distance between fixed electrodes
g	distance between the gate and the shuttling element
r	shuttling element radius
R	fixed electrodes radius
S	(average) area of the tunneling surfaces
m	shuttling element mass
k	shuttling element stiffness
γ	damping for the shuttling element
ζ	damping ratio for the shuttling element
f or ω	natural or radian frequency for the shuttling element

F	electrostatic force
V or ΔV	voltage or voltage difference
E	electric field
G	conductance
R	resistance
C	capacitance
P	elastance

ρ	density
ϱ	resistivity
λ	tunneling length
ϕ	work function
ε	permittivity
$\mathcal{A}$	area enclosed within the shuttle phase curve
$\mathcal{T}$	tunneling region
$\mathcal{O}$	oscillating region
$\mathcal{G}$	system geometry
$\mathcal{B}$	boundary conditions
$\mathcal{X}$	vibrational state
$\mathcal{Q}$	electrodynamics
$\mathcal{J}$	conductive behavior
Ψ	characteristic ratio
Φ	characteristic phase
K	electromechanical coupling
H	mechanical advantage
η	transport factor
A	activation index
M	modulation index
R	robustness index
$P_1(t)$	occupation probability of a single-electron Q-dot
f	Fermi-Dirac distribution
Γ	tunneling rates
μ	chemical potential
Θ	temperature
σ_x	expected value of thermal vibrations
ω_{LR}	bias voltage radian frequency
ω_G	gate voltage radian frequency
ω_I	shuttle current radian frequency
$\xi(t)$	flexural deflection of the pillar
$\vartheta(t)$	torsional angle of the web
κ	torsional coupling
J	local moment of inertia of the web
L	pillar length
$2b$	pillar thickness
N	number of slave modules
α	current gain
$\mathcal{E}$	total energy
$\mathcal{U}$	potential energy
$\mathcal{K}$	kinetic energy
$\Delta\mathcal{E}_{es}$	electrostatically injected energy per oscillation
$\Delta\mathcal{E}_d$	mechanically dissipated energy per oscillation
$\Delta\mathcal{E}_{i\to j}$	energy transfer from i to j per oscillation

$(\circ)_f$	free-charge (…)
$(\circ)_p$	polarization (…)
$(\circ)_m$	magnetization (…)
$(\circ)_s$	shuttle (…)
$(\circ)_t$	tunneling (…)
$(\circ)_L$	left electrode's (…)
$(\circ)_R$	right electrode's (…)
$(\circ)_G$	gate electrode's (…)
$(\circ)_I$	island's (…)
$(\circ)_S$	shuttling element's (…)
$(\circ)_D$ or $(\circ)_P$	Q-dot or pillar realization of a shuttling element's (…)
$(\circ)_D$	drain terminal's (…)
$(\circ)_S$	source terminal's (…)
$(\circ)_{dr}$	drive module's (…)
$(\circ)_{sl}$	slave module's (…)
$(\circ)_i$	*i*-th pillar's (…)

INTRODUCTION

Mass and electric charge

Mass and electric charge are fundamental properties of matter, whose presence manifests in a multitude of natural phenomena. In a classical frame, massive objects are subjected to the laws of Classical Mechanics, while electrically charged substances are governed by the Classical ElectroDynamics.

However, roles of mass and electric charge are not analogue: an important difference arises from the inertial/gravitational mass dichotomy. Actually, mass is *not only* the property of matter responsible for the gravitational interaction (gravitational mass), but it is *also* a quantitative measure of an object resistance to acceleration (inertial mass). These are two conceptually distinct physical effects, however, the universality of free fall (*Galileian equivalence principle*) guarantees their identity. In modern physics, this scenario is – if possible – more complex [1] and at least four distinct phenomena are related with such many attributes of mass: inertia, space-time curvature †, Compton wavelength ‡, energy (*Einstein's equivalence principle*) ‡†; and only their proportionality individuates the abstract concept of (rest) mass ‡‡.

On the other hand, the concept of electric charge still maintains an univocal interpretation because, even after the advent of Quantum ElectroDynamics ‡‡†, it is still related to only one physical phenomenology (the electromagnetic interaction), thus preserving its intuitiveness also in a contemporary frame.

In this context, it is not surprising that some formal classical definitions on electrodynamics are still valid today with minimal revisions. For example, introducing electric current as "flow of electric charge through a surface" provides the rather polite concept reassumed by formula $I(t) \triangleq dQ/dt$. However, electric charge, like mass, has a discrete space distribution localized in particles – *charge carriers*. Also, unlike mass, electric charge always appears quantized – in units of e. The last feature is important, since means that, in principle, one can simply count the net number of charge carriers $\Delta N = N_+ - N_-$ which cross through a surface in a given time, and then use the formula $\bar{I}_{\Delta t} \triangleq \Delta Q/\Delta t = e\Delta N/\Delta t$. This is an alternative, *operative*, definition of current, which can be helpful in certain situations.

Notice that both formulae can be interpreted from the given formal definition, the first one referring to an *instant* current, the second being the *average* one. Trivially, these two quantities match in the stationary case, the original definition regaining its original univocality.

† In General Relativity, gravitation is not a force, and massive body interactions are actually an effect of the space-time curvature caused by their space distribution. Thus, mass *is no more* a property of matter on which a fundamental interaction relies. This produces two consequences: i) the inertial/gravitational mass dichotomy is apparently solved, since mass is a general feature of matter which – shaping of geodesics of minimal action – reassumes both the effects of resistance to acceleration and space-time curvature; ii) since gravitation is not a force, this can be the core reason for which all attempts to unify it with the other three fundamental interactions of the Standard Model within the frame of a unified theory has failed to the present day; also, it could explain why the existence of graviton, the hypothetical mediator for gravitation force, has not been proved yet.

‡ Since $m = h/\lambda c$, being λ the Compton wavelength, c the speed of light and m the quantum mass.

‡† Conversely to the erroneous common belief, mass cannot be transformed in energy, nor vice versa. The equivalence principle $E = mc^2$ simply states mass *is* a form of energy – or energy is a form of mass. In special relativity rest mass can be transformed in more mobile forms of mass, but remains mass, similarly for different forms of energy. An isolated system does not conserve the sum of mass and energy: instead, it conserves, independently *both*. If a not isolated system undergoes a variation of energy dE, the same is for an amount of mass dE/c^2. Matter, if considered as some types of particles, can be created or annihilated, but the whole obtained system retains both the original mass and energy [2].

‡‡ In recent years, the pedagogic importance of relativistic mass when dealing with Special Relativity is debated. Since, the "real" mass is referred to the invariant one, also called *rest mass*.

‡‡† The Quantum ElectroDynamics is accredited as "the jewel of physics", by Richard Feynman, due to the fact it was the first theory where full agreement between Quantum Mechanics and Special Relativity has been achieved. It describes phenomena involving electrically charged particles interacting by exchange of photons, elegantly generalizing Classical ElectroDynamics.

Different forms of charge transport: conceiving the shuttle mechanism

Suppose we are interested to identify any conceptually distinct phenomenon able to produce a form of charge transport, thus – potentially – a current. We propose a thought experiment in which a flat surface of given area S and normal versor $\hat{n}$ – representing an ideal "charge detector" – is used to measure current in situations of increasing complexity.

Start by considering an ideal case in which a certain volume is filled with a charge carriers density n, each charge carrier moving with a velocity $\vec{v} \parallel \hat{n}$. The current I_{id} is given by:

$$I_{id} = \bar{I}_{\Delta t} = e\frac{\Delta N}{\Delta t} = enSv \equiv I(t) \tag{I}$$

Since the velocity field is uniform, the average and instant currents match, and a simple formula $\Delta N = nSv\Delta t$ relates the number of counted charge carriers ΔN to their common velocity v .

Now consider a volume of real matter. Here, the charge carriers velocity field is all but uniform – though we can still assume for them a uniform density n. We can calculate current by the means of the current density $\mathbf{J}$, in general arising from three contributions $\mathbf{J} = \mathbf{J_f} + \mathbf{J_p} + \mathbf{J_m}$. The term J_f represents the *free-charge current density*, and depends on the collective motion of charge carriers in the conductor: valence electrons, (if a metal) or ions and free electrons (if a plasma). Then, $\mathbf{J_p}$ represents the *polarization current density* (produced by the rate of polarization in dielectric materials), and $\mathbf{J_m}$ the *magnetization current density* (related to circulations of magnetic dipole moments). Limit our analysis to a conductive material, so that the *bound-current density* $\mathbf{J_b} = \mathbf{J_p} + \mathbf{J_m}$ is not present. In this case, our current detector measures a current I_f depending only on the mobility of free charge carriers. One obtains:

$$I_f = I(t) = \int_S \mathbf{J_f}(t) \cdot \hat{n}\, dS = enSv_f(t) \tag{II}$$

Since, in general, the velocity field is chaotic and time-variable, this relation gives an instant current which does not match its average value. However, it is possible to relate it to a single velocity $v_f(t)$, the *drift velocity*, defined as the average velocity of charge carriers in the direction normal to S †. Trivially, (I) represents the special case of (II) in which the drift velocity v_f is constant and corresponds to the actual, uniform velocity v of individual charge carriers.

So far, our analysis has been limited to continuum media. Now, extend our thought experiment to a system composed by more elements.

Consider a simple system composed by only two elements: a dielectric fluid and a solid conductor within it. Let the conductor a cylinder moving through the dielectric with a velocity v parallel to its height $2r$ and normal to its surface S (Fig.Ia). Within the conductor, a uniform charge carrier density $n^* = N^*/2Sr$ exists, being N^* the defect of electrons (or excess of positive charge carriers). Electrons can't move towards the dielectric, thus n^* (or N^*) is a constant. Place our charge detector normal to the velocity v and perfectly overlapping the body trajectory.

First, assume the velocity v is constant. To measure the current, let $\Delta t = 2r/v$, so that the whole body has passed through the surface and $\Delta N = N^*$. Therefore the current is:

$$\bar{I}_{\Delta t} = e\frac{\Delta N}{\Delta t} = e\frac{N^*}{2r}v = en^*Sv \equiv I(t) \tag{III}$$

† The drift velocity is typically very slow, compared to the propagation of electromagnetic field. A current of some *amperes* in a copper wire corresponds to a drift velocity of the order of mm/s .

Notice that relation (III) is analogous to (I), except now the uniform velocity field v is not consequent to the mobility of free electrons, but relies on the movement of a rigid body, which can be in this sense considered a "mechanical charge carrier" *shuttling* electrons with its motion. In this thesis we'll refer to this archetypal form of charge transport as *electron shuttle*.

Now consider the case in which the shuttling element undergoes oscillations of period T_s, its center moving back and forth describing positions $x \in [x_0 - (d-r), x_0 + (d-r)]$, with $d > r$ and x_0 the fixed position of the charge detector. Similarly to (III), one can calculate:

$$\bar{I}_{\Delta t} = e\frac{\Delta N}{\Delta t} = \begin{cases} 0 & if\ \Delta t = hT_s \\ I_h & if\ \Delta t \neq hT_s \end{cases} \quad , \quad h \in \mathbb{N}$$

In this case, the time profile of instant current is trivially intermittent and with null mean value: if the observation lasts an integer number of oscillations, no average current is obtained, otherwise, a residual value I_h exists, with $I_h \to 0$ for $h \to \infty$ (Fig.Ib).

Generalize the latter case by considering a body with the same kinematics, but shuttling either N_l or N_r charge carriers depending on its motion direction (Fig.Ic). For simplicity's sake, let $N_r = -N_l \equiv N^*$. If the current detection lasts an integer number of oscillations, so that $\Delta t = hT_s$, the current I_s can be calculated as:

$$I_s = \bar{I}_{T_s} = e\frac{\Delta N}{\Delta t} = e\frac{h(N_r - N_l)}{hT_s} = e\frac{2N^*}{T_s} = eN_s f_s \qquad \text{(IV)}$$

The latter term in (IV) is an expression to calculate the *shuttle current* I_s – namely its average value † in a cycle of oscillation – by knowing the *shuttled charges* per cycle $N_s = 2N^*$ and the *shuttling frequency* $f_s = 1/T_s$. The possibility of obtain a net shuttle current relies on having $N_s \neq 0$: we'll discuss later about this possibility, in the meantime simply assume it as true.

Last, the concept of *shuttle drift velocity* v_s can be related to two alternative definitions. The first is similar to relation (III) for the drift velocity v_f , and depends on the actual charge carrier density $n^* = N^*/2Sr$; the second is analogous to (II) and comes by considering charge carriers distributed on the *whole* oscillation volume, so that $n = N^*/2Sd$. The two definitions are:

$$v_s{}^I \triangleq \frac{I_s}{en^*S} = \frac{r}{d}\bar{v} \quad , \qquad v_s{}^{II} \triangleq \frac{I_s}{enS} = \bar{v} \qquad \text{(V)}$$

The second definition is more convenient since the shuttle velocity matches the half-period average speed $\bar{v} = 4d/T_s$, this formula invariant with the geometry and depending only on the oscillation frequency. Other advantages of such formulation will be clear in following Sections. This completes, for now, our thought experiment about possibilities of charge transport.

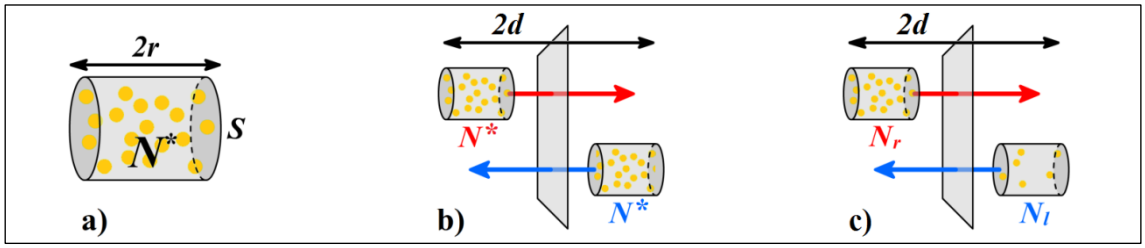

Figure I – *A conductor with geometry (a) oscillates back and forth. If the number of shuttled electrons is constant, the charge detector measures a null current (b). Otherwise, a non-zero current is produced (c).*

† An important point about shuttle current is that only its average value can be calculated, while its instant value is undefined.

In conclusion, the conceptualization of a form of charge transport relying on mechanical oscillations has been presented, calling it *electron shuttle*. Since it can be exhibited only in specifically designed systems comprising at least one vibrating conductor element, this mechanism is alternative to conventional conduction phenomena which occur in natural media.

Symmetry breaking and continuative oscillations: feasibility of a shuttle device

The occurrence of a form of charge transport within a system is a necessary but not sufficient condition for such a system to produce a *macroscopic* current. This consideration is valid also in the case of electron shuttle: a shuttle device *works* when it is able to produce a current: i) not null, ii) in a continuative way. Distinctly analyze these two goals.

Consider the first one. Trivially, if electrons are shuttled back and forth by the moving conductor body, the average current in a cycle is zero (Fig.Ib). To produce a net shuttle current $I_s \neq 0$, one needs $N_s \neq 0$: this condition was simply assumed *possible* when relation (III) has been presented. Here we discuss *how* to produce this fact: since N_s are the shuttled charges per cycle, we want a device in which *some electrons* are actually taken from one side and released to the other one (Fig.Ic). The system introduced in the previous Section, formed by a conductor oscillating within a dielectric, is obdurately symmetric: how to choose from *which* side electrons move to the other one? We are in the standard situation in which a symmetric system whose desired functionality requires *directionality* (current direction) demands for a *symmetry breaking* effect to univocally determine such a direction – and successfully achieve its goal.

From an engineering point of view, individuating the most effective symmetry breaking effect to make a device work, is a challenging clue. Many fascinating and instructive examples can be found in various disciplines of science, one of the most recent, for example, an intriguing way to obtain work from swimming bacteria by using asymmetrical gears [3].
Depending on the case, the invasive introduction of a rectifying mechanism (a ratchet or one-way clutch in a mechanical system, a non-return valve in a hydraulic circuit, a half-wave rectifier in an electrical one) could be needed to break the symmetry; otherwise, the application of a certain field could be sufficient. A shuttle device belongs to the second case: we expect the presence of a certain electric field E in the direction parallel to the body velocity v is effective to provide the required symmetry breaking effect. To produce such an electric field, one needs to introduce two new conductors in the system to which a voltage $V = 2Ed$ is applied.

Referring to Fig.II, consider two electrodes, labeled with L and R, fixed and placed to the leads of the trajectory of the shuttling element, marked with S. The three bodies are separated by the dielectric, except when S is in its reverse points: this means S alternatively touches L and R during its oscillation. The depicted L-S-R three-conductors system represents the most simple case producing not only the shuttle charge transfer, but also a net average current per cycle.
The exact description of the phenomenology responsible for this current will be detailed in Part One. Here, it is sufficient to know that, if, for example, L is the positive biased electrode, S takes (*loads*) an amount N_s of electrons from R , shuttles them to L , and releases (*unload*s) the (in average) same amount N_s in L , and last shuttles them to R . This mechanism produces an R to L electron transport corresponding to an L to R shuttle current (Fig.III) given by formula (IV). Vice versa, the same current flows from R to L when R is the positive biased electrode.

However, the application of a DC voltage between the leads of oscillation is only one of the possible symmetry breaking effects capable of shuttle charge transfer to produce a net current †.

† Notice that not every attempt to de-symmetrize a shuttle system leads an effective symmetry breaking effect: for example, not symmetrical oscillations of the shuttling body do not produce any current if the applied voltage is not present.

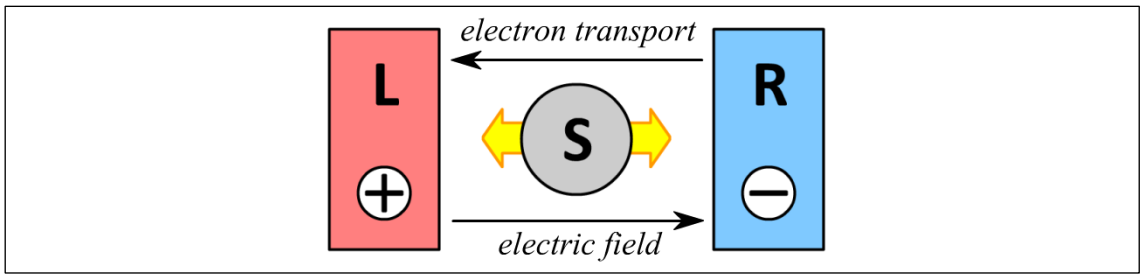

Figure II – *Schematic representation of the most basic shuttle device.*

Once a shuttle device is able to produce a net current, such a current has to be produced in a continuative way. Since it relies on the motion of the shuttling element, the second goal to build an actual shuttle device consists in specify *how* its continuative oscillations are guaranteed.
In presence of a dissipative effect (always present in real systems), one needs to provide it a certain amount of energy per cycle, to maintain constant the amplitude of the shuttling element oscillations. Depending on the process occurring, one can discern two situations:

- *Induced shuttle*. A power source external to the core shuttle mechanism directly controls frequency and amplitude of the shuttling element.
- *Autonomous shuttle*. Once the shuttle mechanism is triggered for the first time, the symmetry breaking effect itself provides the required energy to maintain the oscillating regime of the shuttling element. (Notice that, in this case, there is no way to directly control of the oscillations frequency and amplitude.)

In this thesis we are mainly interested in investigating devices capable of *autonomous shuttle*, since they represent an interesting case of study from an exquisite mechanical point of view.
Also, without further clarifications (which will be again detailed in Part One), here we only anticipate that, referring to the L-S-R three-conductors system, the applied voltage itself – if some conditions hold – is sufficient to provide for the continuity of oscillations.

Therefore, the system depicted in Fig.II is a good candidate to be the scheme for an actual, autonomous, shuttle device whose dynamics has been reassumed in Fig.III.

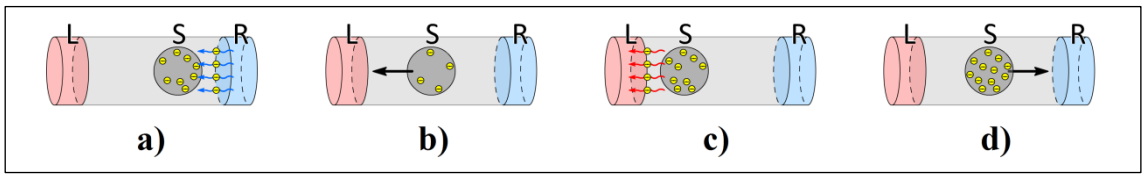

Figure III: *Schematic representation of the shuttle mechanism as divided in four steps (a-d).*

Refer as a *Shuttle Module* (SM) to any device capable of the shuttle mechanism in which have been provided: i) a symmetry breaking effect; ii) a way to maintain continuative oscillations.
Notice how the shuttle mechanism is a form of charge transport completely different from the traditional ones occurring in a continuous medium.
This gives the opportunity to propose a new thought experiment.

Consider a black-box cylinder with length $2d$ and base area S. We want to characterize its electrical behavior. If no information is available on the charge transport mechanism occurring inside, one can only apply a certain voltage V^* at its terminals and measure the consequent I^* current. Then, one can estimate a value for n and conclude the charge carriers inside the cylinder have an average velocity I^*/enS . After a series of measurements, the *external characteristic* of the cylinder $I = I(V)$ is obtained, its local derivative dI/dV giving the device conductance $G(V)$ for any value of V. This example represents the most general case.
Now, imagine we have the information about the nature of system inside the black-box.

First consider the case in which the cylinder is a Conductive Solid (CS) (Fig.IVa). We know the only allowed charge transport mechanism is the movement of free electrons under the effect of an electric field. So, it is possible to use both relation (II) and Ohm's law and obtain:

$$I_f = enSv_f \equiv G_f V \tag{VI}$$

where G_f is the free-charge conductance, which, from Pouillet law, is $G_f = S/2\varrho d$. As it is well-known, in a CS the resistivity ϱ is constant for a wide range of voltage values, so that the current-voltage dependence $I_f = I_f(V)$ is linear. Also, relation (VI) highlights the intuitive fact that the drift velocity v_f and the applied voltage V are proportional. Last, the application of an AC signal $V(t) = V_0 \cos(\omega_V t)$ at the cylinder terminals produces periodic fluctuations in $v_f(t)$ and $I_f(t)$ but no time averaged charge carrier movement since $\overline{v_f} = 0$, nor average current $\overline{I_f}$ †.

Now consider the case in which the cylinder is a complex system exhibiting shuttle: thus, a Shuttle Module (SM) (Fig.IVb). Conceptually, one can again apply – with a certain abuse of notation – the Ohm's law. Notice that, being the device a black-box, an external observer doesn't know the internal geometry of the system (the ratio r/d): he can only assume a certain charge carrier density n is distributed all over cylinder volume , and relate the measured current I_s to the *second* definition proposed for the shuttle drift velocity, ${v_s}^{II} \triangleq I_s/enS$. Summarizing:

$$I_s = enS{v_s}^{II} \equiv G_s V \tag{VII}$$

We refer to G_s as the *shuttle conductance* . To conclude, some considerations on (VI) and (VII).
First, differently from G_f in (VI), here G_s is not, in general, constant: thus the external characteristic of a SM is not linear.
Second, since $I_s = eN_s f_s$, the shuttle current physically arises from the number of shuttled charge carriers N_s, which is different from zero only in presence of a symmetry breaking effect. In the case presented in Fig.II and Fig.III, this role is provided by the voltage V itself, so that $N_s = N_s(V)$. However, in Part One, a different kinds of SMs will be presented, in which the symmetry breaking effect *does not require* the application of a DC voltage V. This means such exotic systems experience $N_s \neq 0$ and $I_s \neq 0$ also when $V = 0$, thus, using the definition (VII), they are characterized by a conductance $G_s \to \infty$. This possibility is *unique* of complex systems like SMs, and *excludes* natural materials.
Third, formulae (VI)-(VII) require different approaches. In a CS, by knowing the visible geometry of the cylinder S and $2d$, and *one* internal parameter (i.e. ϱ) one can anticipate G_f and calculate the value of I_f by using (VI), and only *later* inference from it the drift velocity v_f . Instead, in the case of a SM, in addition to the visible geometry, S and $2d$, one needs *two* internal parameters to anticipate the value of I_s (i.e. f_s , and r), so that $n = n^* r/Sd$ and ${v_s}^{II} = \bar{v} = 4df_s$: once the current has been calculated, one can finally compute G_s by using the Ohm's law.

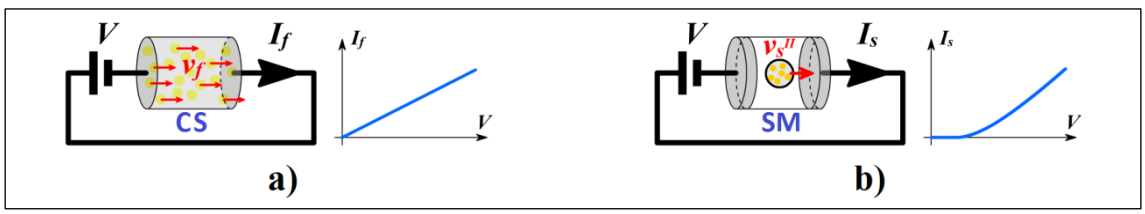

Figure IV – *Black-box testing of a (a) Conductive Solid (CS) and a (b) Shuttle Module (SM).*

† This situation inhibits the system to produce a net current in a manner analogous to a SM without a symmetry breaking effect.

Historical overview of shuttle devices at macroscale

The first historical account of a shuttle device originates from the roots of electrostatics. The so-called *Franklyn bells* (or *lightning bells*) were actually invented in 1742 by Andrew Gordon in Germany, although they are often referred to Benjamin Franklyn due to one of its famous attempts to understand nature of static electricity related to atmospheric phenomena.
A proposed reconstruction of their realization is in the photo in Fig.Va; however, no clear figurative documentation of the original installment is available.
Franklyn mounted such device in his house to warn him of approaching thunderstorms, connecting a first bell to a pointed rod on his chimney and a second one to the ground; then, a brass sphere was appended between the bells (Fig.Vb). Here a famous portrait of its experiment:

> *"In September 1752, I erected an Iron Rod to draw the Lightning down into my House, in order to make some Experiments on it, with two Bells to give Notice when the Rod should be electrified. A contrivance obvious to every Electrician. I found the Bells rang sometimes when there was no Lightning or Thunder, but only a dark Cloud over the Rod; that sometimes after a Flash of Lightning they would suddenly stop; and at other times, when they had not rang before, they would, after a Flash, suddenly begin to ring; that the Electricity was sometimes very faint, so that when a small Spark was obtained, another could not be got for sometime after; at other times the Sparks would follow extremely quick, and once I had a continual Stream from Bell to Bell, the size of a Crow-Quill. Even during the same Gust there were considerable variations."*
>
> *letter from Benjamin Franklin to Peter Collinson, 1753*

The explanation of these phenomenology is rather clear: the approaching clouds accumulated a potential difference between the two bells, which, when reached a threshold value, started to attract the brass sphere by electrostatic induction, triggering a first oscillation and then continuatively convert electrical energy into mechanical energy with a self-sustained shuttle mechanism.
Franklyn bells represent the first historical – though rude –realization of an actual SM, working in a manner completely similar to the L-S-R three-conductors system depicted in Fig.II and Fig.III. In fact, the two bells represent the fixed electrodes L and R , and the brass sphere is the shuttling element S: last the DC voltage which breaks the system symmetry is provided by the atmospheric electrostatic energy in bad weather conditions.

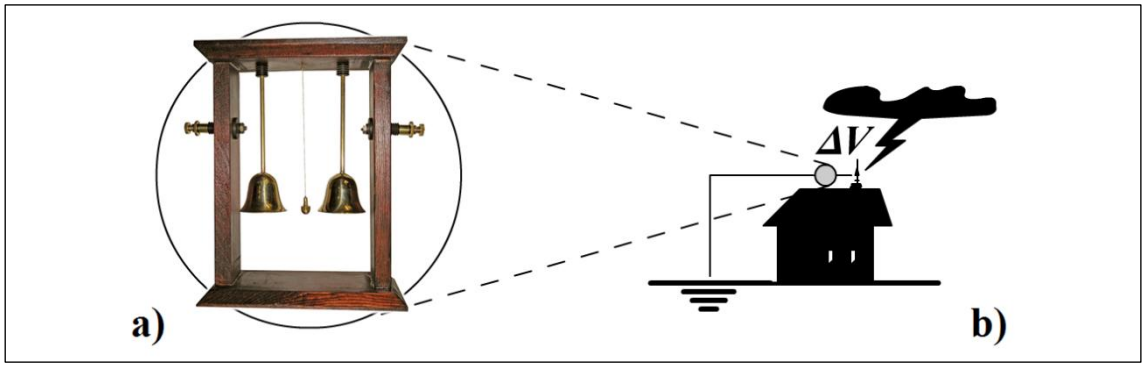

Figure V – *a) model of Franklyn bells; b) schematic reconstruction of the Franklyn experiment.*

Centuries later, when electricity was understood and interpreted at a much deeper level, similar concepts were used in some electromechanical devices feasible of commercial applications like doorbells, school bells or security alarms, in some cases still used nowadays.

Some embodiments are similar to the device depicted in Fig.VIa. A restoring spring maintains the clapper element in contact with one of the electrodes. Then, a DC voltage is applied, and current start flow within the clapper. When the electric charge reaches a threshold value, the electrostatic repulsion surpasses the spring stiffness and suddenly the clapper is accelerated, knocking the opposite (grounded) electrode, and releasing to it the excess charges. Later, it returns in the initial position due to the restoring mechanical force. (Fig.VIb).
Differently from the Franklyn bells, here oscillations are not continuous, but exhibit alternate periods of *dwell* (so that its motion law is much more similar to a *shishi odoshi*, see Fig.VIc), also, the triggering mechanism is completely different.

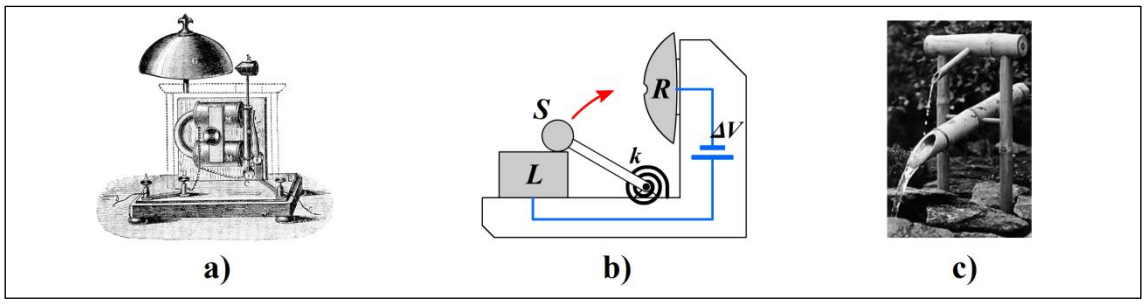

Figure VI – *(a) Old-fashioned doorbell; (b) schematics showing the three conductors and the torsional spring, labeled similarly to the SM in Fig.II; (c) a shishi odoshi (from the Japanese, "scare the deer") works in manner somehow similar to the shuttle mechanism: gravity plays the role of the restoring force and the movement of electrons is substituted by the flow of water.*

However, similarities between an electromechanical doorbell and Franklyn bells are not over. Both systems are composed by two fixed conductors and a moving one which represents the shuttling element, its motion being periodic and *autonomous* (since the required energy comes from the symmetry breaking effect itself), the symmetry breaking effect provided, in both cases, by a DC voltage. Differences in motion law only depend on the presence of a spring with different rest position: in the center in the case of Franklyn bells, at one of the leads for the doorbell †.

Although the presence of a current is the very origin of the self-excitation mechanism which maintains oscillations, the presence of the current itself produces the drawback of discharging the two fixed electrodes. Therefore, if no external power supply is provided among the leads, oscillations stop after a brief transient, since the electrostatic-kinetic energy conversion cannot occur anymore (as in the case of Franklyn). This means that, ironically, in the two presented examples, the shuttle current is only a *collateral effect* of devices whose function *is not* charge transport, but respectively "advice of cloud approaching" and "emit sound", and for which the presence of this current is a disturbance element. Considerably, this is a common feature of macroscopic shuttle devices: no convenient application for the conduction shuttle mechanism *in se* have been glimpsed to the present day. This fact, together with the connate simplicity of the working principle of these devices, has contributed to produce a desolate scenario in which the shuttle mechanism at macroscale has been relegated to a didactic trick in some school laboratories, a mere gadget not worthy of further theoretical investigations.
As we will see, this situation is going to change when electron shuttle is performed in a nanoscale environment.

† Actually, the presence of a spring or a sort of centering mechanism is not needed at all to produce electron shuttle. In fact the shuttling element could be free and simply alternating moving back and forth due to the self-excited mechanism, with sawtooth-profile oscillations.

Shuttle at nanoscale. Introduction to Quantum Tunneling and Coulomb Blockade

Imagine to progressively reduce the scale of a shuttle device.
When nanoscale is reached, two additional physical phenomena have to be considered:

- a non-classical form of charge transfer, the *Quantum Tunneling* (QT);
- charge quantization becomes considerable and can produce *Coulomb Blockade* (CB) effects.

Both QT and CB imply huge consequences to the shuttle mechanism, which influence in a conceptually substantial way both the dynamical regimes and conduction properties of a shuttle device. Introduce these two concepts one by one.

QUANTUM TUNNELING. The minimum energy required to remove an electron from a solid is the work function ϕ . These effects are well described by Classical ElectroDynamics †.
At nanoscale, however, an additional phenomenon, the *Quantum Tunneling* (QT), is present, which allows an electron to escape a material also when a classical model would not allow so. QT is generally exhibited between two faced electrodes separated by a layer of dielectric. If a potential difference is applied, some electrons can move – *tunnel* – from one surface to the other one. This is even possible with amounts of energy below the work function ϕ, provided a very thin distance – of the order of a few nanometers – between the electrodes yields. If this is the case, the two electrodes constitute a *Tunnel Junction* (TJ). A more detailed explanation of the physics of QT will be presented in Chapter 1. In this Introduction, it is sufficient to deal with QT by considering the measurable, macroscopic effect it produces, which is *equivalent to* (but not strictly *the same of*, given the "complicate intercourse" between quantum mechanics and the concept of "motion") admit the presence of an additional form of charge transport.

When does the phenomenon of QT occurs in a shuttle device? Consider the archetypal L-S-R three-conductors shuttle system depicted in Fig.VIIa. If the characteristic dimension of the device, $2d$, is of the order of nanometers, the distance between the conductors is compatible with QT. If this occurs, when a voltage V is applied, a *tunnel current* I_t is established. This current does not affect the possibility to exhibit the shuttle mechanism, and can therefore *coexist* with the shuttle current I_s , so that an overall current $I_{s,t} \triangleq I_s + I_t$ flows through the system.
In a shuttle device, the tunnel current I_t is operatively defined as "the current which passes through L and R electrodes when the shuttling element is at rest". It has to be remarked that this definition is not trivial as it appears and requires a couple of considerations.

First, since a shuttle device is formed by three conductors, the tunnel current I_t is the combination of two distinct phenomenologies: two partial "jumps", among L and S, and then S and R (*short* tunnel, Fig.VIIb); or a direct, single "jump" from L and R (*long* tunnel, Fig.VIIc).
However, in an experimental setup, not only we cannot separate these two efforts to QT: there is even a practical difficulty in discerning the value of the whole tunnel current I_t with respect to the shuttle current I_s. In fact, by strictly applying the proposed definition, a direct measure of I_t requires a shuttling element at rest: this is largely unfeasible since its oscillations depend by the same voltage V needed to detect I_t ; but, because of the nanoscale, we cannot simply "stop by hand" the oscillations. In this scenario the only way to *experimentally* measure the two contributions to current could be realize two *twin* embodiments, as detailed in Section 2.1.1.

† Phenomena related to the surpass of such energy threshold are labeled with the umbrella term *emission.* Two main kinds of emission exist: *thermionic (hot) emission* and *field (cold) emission*; in the first case the required energy is supplied by high temperatures, in the second one by a strong (quasi)static electric field. Emission usually occurs in a myriad of natural or artificially induced phenomena and produces well-known manifestations in dielectric breakdowns like electric arcs or sparks. Actually, field emission was explained in a non-classical way by introducing quantum tunneling in the late 1920s.

‡ As it will be clear in Chapter 1, long tunnel phenomenology is always negligible with respect to short tunnel.

Actually, the tunnel current can be more profitably estimated in a *theoretical* model, by calculating the overall current from L to R , and subtracting the shuttle contribution using formula (IV):

$$I_t = \bar{I}_{T_s} \triangleq I_{s,t} - I_s = I_{s,t} - eN_s f_s \qquad \text{(VIII)}$$

Once we calculated the value of I_t, we can introduce the concept of *tunnel drift velocity* v_t in a way similar to (V), assuming – compatibly with the definition of v_s^{II} – a charge carriers density n distributed on the *whole* oscillation volume:

$$I_t \triangleq enSv_t \qquad \text{(IX)}$$

As a second point, the presence of QT in shuttle devices has a strong influence *also* when $I_t = 0$. In fact, even in the case d is too large to allow both *short* and *long* tunnel, during its oscillations, the shuttling element S alternatively approaches to L and R at distances $\lambda \ll d$ compatible with QT. This fact has an enormous impact on the functionality of a shuttle device. It means that, in nanoscale, *the shuttling element does not require any contact with the fixed electrodes to make the device work* – differently from macroscale shuttle devices like the Franklyn bells – *but it is only required it approaches to distances* $\sim\lambda$, with λ representing the characteristic *tunnel length*. Both shuttle current and continuative oscillations (if it is an autonomous device) are guaranteed, but (refer now to Fig.III) *the load/unload transients consist in a transfer of electrons from R ro S or from S to L which relies on QT instead of contact*.
In turn, this implies two further consequences.
First, a nanoscale shuttle device has a more various dynamical behavior: oscillations of the shuttling element can, in principle, be modulated in amplitude in the range $A \gtrsim (d - r) - \lambda$ (this is not possible in absence of QT, when contact strictly requires $A \equiv d - r$); also, their shape can be more similar to a sinusoid since now collisions with electrodes are not required.
Second, the total current $I_{s,t}$ (needed to calculate the tunnel contribution I_t by using (VIII)) has to be calculated by using QT-related formulae. Thus, in a nanoscale shuttle device, both shuttle and tunnel currents, conceptually, rely on QT. This apparently paradoxical statement can be correctly understood if one carefully interprets the (in words) definition of tunnel current.

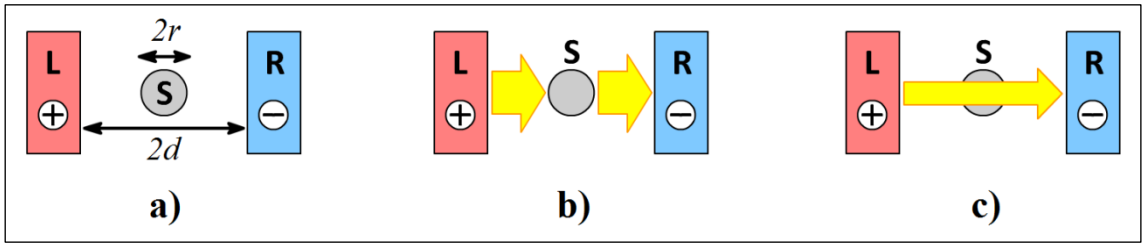

Figure VII – *Different kinds of QT in a shuttle device with geometry (a): short tunnel (b), long tunnel (c).*

The described considerations are outstanding. A neat distinction between shuttle at macroscale and the just described phenomenology, peculiar of nanoscale, is required at this point. Therefore, in the rest of this thesis, we'll refer to nanoscale shuttle devices characterized by the presence of QT as *Quantum Shuttle Modules* (QSM), to discern them from macroscale devices (like Franklyn Bells), for which we maintain the original *Shuttle Modules* (SMs) denomination.

To conclude this preliminary discussion about QT, we can extend our thought experiment dealing with the electrical characterization of a black-box cylinder, and obtain a complete overview of the charge transport mechanisms presented in this thesis.

Start by considering a cylinder filled with a dielectric and with length $d \sim \lambda$. In this case, an external observer could conclude he is in front of a TJ (Fig.VIIIa,b). Consequently, he expects a current coming from the only contribution of QT, so that, from (IX):

$$I_t = enSv_t \equiv G_t V \tag{X}$$

A number of models exist in literature to estimate the *tunnel conductance* G_t, usually dependent on both distance and voltage: $G_t = G_t(d,V)$. In Part One and Appendix A we'll discuss some.

Last, if the black-box internal structure is that of a shuttle device and $d \sim \lambda$, then the external observer recognizes in it a QSM (Fig.VIIIc,d) †. In this case, we expect two contributions to the total current. Thus, combining (VII) and (X) one obtains:

$$I_{s,t} = I_s + I_t = eN_s f_s + I_t = enS(v_s{}^{II} + v_t) = enSv_{s,t} \equiv (G_s + G_t)V \tag{XI}$$

Imagine the observer is interested in estimate the tunnel current I_t . We already know it is not possible experimentally: applying a voltage at the terminals of the cylinder, one would measure an overall current $I_{s,t}$ which cannot be decomposed. Its analytical calculation, also, is a complicated procedure, reassuming the whole discussion about QT: first $I_{s,t}$ is calculated as an average current per cycle by using formulae for QT; then I_s is defined as an average value from $eN_s f_s$; last, their difference gives the average value of I_t ‡. Notice how this scenario is completely different from the direct procedure to calculate of the tunnel current in a simple TJ (relation (X)), where the mere usage of a closed-form formula for the conductance $G_t = G_t(d,V)$ is effective to calculate I_t. Another important point is that, while in a TJ it is possible to calculate the instant tunnel current $I_t(t)$ by knowing G_t , this is not the case of a QSM. In fact, from formula (VIII), since the shuttle current is defined *only* as an *average quantity* referred to a period T_s, and the tunnel current has to be calculated indirectly from the shuttle contribution, then the tunnel current inherits the lacking of an instant value, which remains *undefined*. Methodologies to calculate current in a QSM are analyzed more closely in Chapter 2.

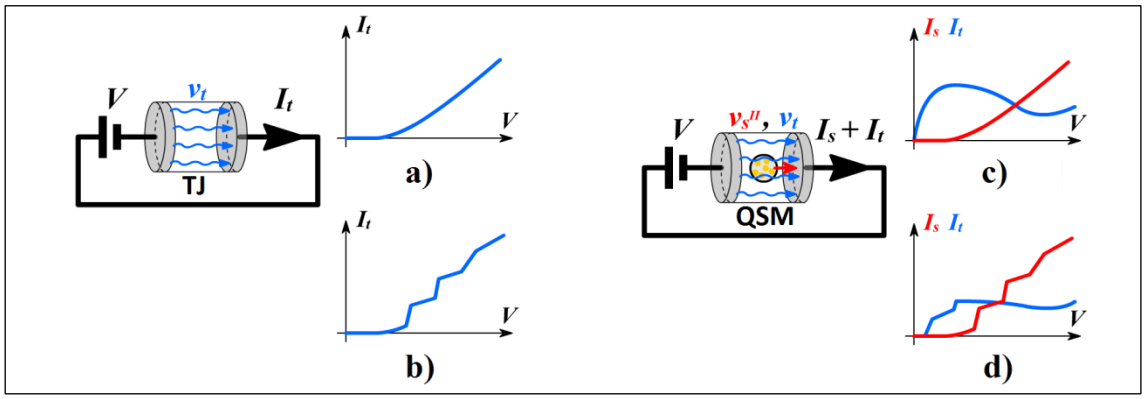

Figure VIII – *Black-box testing of a Tunnel Junction (TJ) and a Quantum Shuttle Module (QSM). Curves (a) and (c) refer to the absence of Coulomb blockade; in (b) and (d) Coulomb staircase is visible.*

Formulae (VI), (VII), (X), (XI) and Fig.IV and Fig.VIII complete the scenario on the conduction mechanisms of interest for this thesis: free conduction (in a CS), shuttle (in a SM), tunnel (in a TJ), and shuttle-tunnel combination (in a QSM).

† Notice that more instances of the same QSM, can, in principle, compose the periodic structure of a metamaterial.

‡ The tunnel current can be related to the tunnel drift velocity v_t; which, in turn, can be combined with $v_s{}^{II}$ – another reason for which $v_s{}^{II}$ is preferable to $v_s{}^{I}$ – to calculate the *shuttle-current drift velocity* $v_{s,t}$.

COULOMB BLOCKADE. Consider relations (I), (II) and (IV). They respectively refer to an ideal flux of charge carriers, to the free electrons mobility in a real medium, and to a macroscopic SM. Set a value for Δt multiple of T_s and compare the formulae. Notice that, while the current obtained in the ideal environment with (I) is *discrete*, the effect of charge carriers quantization is lost when integrating a chaotic velocity field in (II) so that, in a real medium, the current can assume continuous values. Notice how, in (III), such discreteness is regained: over a period of oscillation, a SM shuttles an integer number of electrons. However, at macroscale, the effect of charge quantization is negligible, and formulae (I), (II) and (IV) are rather accurate.
On the other hand, at nanoscale, we introduced another form of charge transport, the QT, and a SM becomes a QSM for which relations (X) and (XI) yield. In a QSM, the discrete nature of charge is not only detectable, but sometimes produces interesting effects. Such effects are not included in (X) and (XI), which rely on the continuous charge hypothesis. Specifically, the term *Coulomb Blockade* (CB) refers to charge quantization effects which occur in presence of QT.

Consider for example a TJ, the most simple device exhibiting QT. The effect of CB is that of increasing its resistance for very small values of the applied voltage, actually "blocking" the current. This means the external characteristic $I_t = I_t(V)$ has a null slope in $V = 0$.

However, our case of interest is the QSM: since it can be considered as a couple of TJ with time-dependent distances, we anticipate here that the effect of CB is more complex than a TJ and is, in some sense, a generalization. In fact, in a QSM, CB manifests by producing a peculiar step-like structure in the current $I_{s,t} = I_{s,t}(V)$, called *Coulomb staircase*.

We can conclude our thought experiment about the black-box cylinder, by considering a TJ and a QSM in presence of CB. Relations (X) and (XI) remain valid apart for the described minor effects related to charge quantization, and Fig.VIII sketches the differences in the external characteristics $I_t = I_t(V)$ and $I_{s,t} = I_{s,t}(V)$ with (Fig.VIIIa,c) and without (Fig.VIIIb,d) CB.

When does CB effects appear in a QSM? Since CB is related with charge discreteness, one could conclude a QSM shuttling $5 \div 10$ electrons per cycle surely exhibits the Coulomb staircase effect. However, this statement is not correct, since, actually, the possibility of observe CB depends (such as in a TJ) on a series of requirements, the hardest to accomplish being a relation between temperature and the shuttling element self-capacitance. (A complete overview of the requirements to observe CB will be given in in Section 1.2 for a TJ, and in 2.2.10 for a QSM).
Therefore, "shuttle a small number of charges" is not (the only) good indicator to observe effects of their discreteness: depending on the case, CB occurs when tens, a few, or even only one electron are shuttled. Last, since the chance to observe CB involves *temperature*, the same device can, in principle, exhibit or not it depending on the environment.
Also, differences introduced by CB are not preponderant as them produced by QT, which differentiate a QSM from a SM. Therefore, consider a further distinction between QSM devices characterized by CB and others which are not, is inopportune in the context of this thesis.

In conclusion, Tab.I gives a picture of some general features of shuttle devices.
Notice how CB can be exhibited by some QSMs, but never by SMs. Since we are interested to study nanoscale devices, from here now, the thesis is going to focus exclusively on QSM.

Tab.I – *Comparison between macroscale SM and nanoscale QSM.*

Kind of device	***Presence of***				***Load/unload transients occurring by***	***Contributions to the overall current***	***Oscillations amplitude***	***Shape of I-V curve***
	symmetry breaking	***continuative oscillations***	***QT***	***CB***				
SM	yes	yes	no	unable	contact	shuttle	$A = d$	smooth
QSM	yes	yes	yes	no	QT, contact	QT, shuttle	$A \gtrsim d - \lambda$	smooth
				yes	QT, contact	QT, shuttle	$A \gtrsim d - \lambda$	staircase

State of the art: recent NEMS literature on shuttle

We interrupted our historical overview on the shuttle mechanism by discussing the reasons beyond the limited scientific and industrial interest around shuttle devices at macroscale (SMs).

In the last Section, we highlighted the consequences of a relocation of such a working principle to nanoscale devices (QSMs), in particular considering the presence of a novel kind of charge transport, the QT, and effects related to the quantization of charge, the CB. It can be remarked the archetype of electron shuttle can benefit from the shift SM → QSM .
First, due to QT, dynamical regimes of a QSM are more rich of possibilities with respect to SM.
Second, due to CB, electrical characteristics of a QSM exhibit non-linearities absent in SM.
These two key-points together explain the renewed interest for the shuttle mechanism in the context of NEMS literature, demonstrated, in recent years, by a widespread of both theoretical and experimental papers. This research has already produced a number of original concepts and working prototypes, possibly bearer of technological innovation. In this Section, we resume our historical analysis on the shuttle mechanism by discussing the most important research landmarks around nanoscale shuttle devices (QSMs).

APPLICATIONS OF QT AND CB. To begin, a brief reference to some less or more recent milestones in electronics and nanotechnology involving QT and CB, to provide a general picture of the precursor scenario from which the NEMS literature around QSM will develop.

QT was predicted at the beginning of the XX century. In 1928, QT gave the first explanation for the alpha decay [4], although its complete acceptance arrived only after its first technological application: the *tunnel diode* [5,6], invented by Leo Esaki in 1957. Tunnel diode represents still today the most popular diode characterized by a negative resistance region, however, despite its working principle involves QT, it remains a conventional semiconductor electronic device. In 1973, Esaki, Josephson and Giaever were awarded with the Nobel prize in physics [7] for the discovery of the tunneling of superconducting Cooper pairs. The same prize was granted to Binnig and Rohrer in 1986 [8] for the invention of the *Scanning Tunneling Microscope* (STM). The STM represents the most sensible application of QT at present days, consenting to manipulate individual atoms to reach resolutions up to $0.1\ nm$.

In 1911, in his famous experiment with oil drops, Millikan was the first to observe single-electron effects [9]. Charge discreteness in QT was investigated in solids in 1968 by Giaever and Zeller [10], after being conjectured to interpret some data on the conductivity of granular thin films [11,12]. Later named with the umbrella term CB, a first comprehensive theory of these effects in a TJ was given by Klein [13] and Shekter [14]. In 1986 Averin and Likharev suggested the concept of the *Single Electron Transistor* (SET) by using a double-junction geometry [15].
Since its core working principle is based on charge quantization, the SET is not only the first technological application of CB, but also represents the first electronic device whose concept truly relies on nanoscale. It is formed by a low-capacitance conductor (the island) separated from the output terminals by two TJ. By applying an appropriate voltage to the gate, if CB requirements hold, a drain-to-source current in which electrons are transferred one-by-one is triggered. (A more detailed description of the SET is given in Section 1.3.)
First working SETs were realized in 1987 [16,17], operating only in cryogenic environments due to the strict requirements to observe CB. In recent times, however, room temperature SET have been successfully developed [18,19,20] and some predictive theoretical models have been already proposed [21,22]. Although the SET is one of the main successes of recent nanotechnology, it cannot be strictly considered a NEMS: it is a completely static device which doesn't involve any mechanical concept. Furthermore, up to the end of the 90s, the integration of mechanical elements and concepts in MENS/NEMS was typically limited to *static* devices, for example cantilever electrical switches actuated by Coulomb force or opto-mechanical applications [23,24].

GORELIK AND BLICK. This is the general scenario in which the idea of using a shuttle charge transfer mechanism was suggested for the first time in NEMS literature. Two authors, in particular, are worthy of the consequent success of this branch of research. In 1998, with a couple of most-cited articles, *L. Y. Gorelik* [25] and *R. H. Blick* [26] disclosed for the first time the enormous potential electron shuttle could have in the context of NEMS.

From the abstract of "Shuttle mechanism for charge transfer in Coulomb blockade nanostructures" [25]: *"Room-temperature Coulomb blockade of charge transport through composite nanostructures containing organic interlinks has recently been observed. […] For a simple model system […] we show that self-excitation of periodic cluster oscillations in conjunction with sequential processes of cluster charging and decharging appears for a sufficiently large bias voltage. This new 'electron shuttle' mechanism of discrete charge transfer gives rise to a current through the nanostructure, which is proportional to the cluster vibration frequency."*
The paper opens by suggesting an explanation for the CB effects recently observed in some experiments involving a metallic cluster in organic interlinks. The measured current could not merely due to a SET-like phenomenon, thus Gorelik proposes a *generalization* of it, in which the island can oscillate. With a series of qualitative arguments, the possibility for such oscillations to produce the mechanism shown in Fig.III is suggested, this archetypal motion regime named "electron shuttle" †. In particular, the possibility of self-excitation induced by a DC voltage is re-demonstrated at nanoscale, where QT is present and plays a central role. To support this qualitative arguments, the article elegantly closes with analytical and numerical results confirming: i) the achievement of stable limit-cycles; ii) the existence of a novel current contribution, the shuttle current, *in addition* to the tunnel one, already well-known in TJ devices. A central mark of the paper is the first proposition in literature of a formula like (IV), in which a current is proportional to a mechanical oscillation frequency. The work also analyzes how the presence of CB affects the conduction properties of the system. Summarizing, this article by Gorelik sets the theoretical starting point for the whole QSM literature.

On the other hand, Blick immediately recognized the applicative relevance this novel charge transport mechanism could have and, some months later, realized the first embodiment of a shuttle device. From the abstract of "A mechanically flexible tunneling contact operating at radio frequencies" [26]: *"Old fashioned doorbells apply simple electromechanical resonators to generate sound.[…] Naturally, many different realizations of bells exist, but basically we can notice that the combination of electrostatic and mechanical forces in such a bell lead to a resonant transport of electrons. Since the electron's charge is quantized a bell can in principle be used to count single electrons, much in the same way as in Millikan's famous experiment with oil drops or by using SETs. Here, we demonstrate a new technique for counting electrons with an electromechanical resonator, based on a mechanically flexible tunneling contact. In the case of macroscopic bells the granularity of the charge carriers is not observed, because of the large currents used. In our case the underlying idea is to scale down a classical bell - the resonator - in order to build a ''quantum bell'' with which single electrons can be transferred."*
Aware of the historical macroscale origins of the shuttle mechanism, Blick conceives a device which benefits from charge quantization to count single electrons. In his paper, the results of an experimental apparatus in which the shuttling element – with a cantilever geometry (*nanopillar*) – shuttles $N_s = 0 \sim 10$ electrons per cycle, are presented. This work represents the first realization of a shuttle device at nanoscale, but it doesn't exhibit self-excitation highlighted in [25]: the nanopillar oscillations are forced by an external AC voltage – by using the *Resonant Coulomb Force* (RCF) methodology – applied at half its height, while electrons are shuttled by its tip

† So that, actually, in this work, when we refer to macroscopic devices like the Franklyn Bells as "shuttle" we use a generalization from this nomenclature first proposed by Gorelik, in this 1998 paper for nanoscale devices.

among another pair of electrodes. Thus, this shuttle device is not *autonomous* at all (see definition in Section 2.2.3). Nonetheless, at the end of its article, Blick mentions Gorelik, envisaging a future setup in which electron shuttle will be self-excited as suggested by him in [25].

Both authors, nearly independently, recognized the importance of nanoscale in electron shuttle, the first one focusing more on the theoretical chances given by the presence of QT on the motion regimes; the second one on the applicative usages coming from CB effects due to the discrete nature of electric charge. Still, both authors will continue to focus on their respective – and in some sense complementary – approaches to develop this branch of research.

YEARS 1998-2004. In the following years, Gorelik et al. introduce the concept of *soft* or *hard* shuttle regime (Section 2.2.8) and, in the latter case, the existence of an *hysteretic effect* in the current-voltage curve (see Section 2.2.11 and 3.3) is investigated through analytical and numerical arguments [27,28]. Shortly after, they generalize the geometry used in [25] by investigating a three-terminals shuttle system – partly inspired to a SET – exhibiting a chaotic behavior [29].

In the same years, Blick sets up a research team, the BLICK group [30] which will constitute a firm reference point for every experimental progress for nanoscale shuttle literature. In particular, the two-terminals geometry with a nanopillar under RCF continues to be investigated.
At the beginning, the concept of "quantum bell" is further explored [31,32]. Notice it is not the first time a single-charge detector is proposed in NEMS literature [33,34]: SETs can conceptually operate as electron detectors, but the shuttle mechanism has better accuracy, working speed and resistance to electromagnetic shocks. Also, SET requires cryogenic temperatures and/or very small scale to work; while a quantum bell has to avoid collisions with the leads [32]. Then, the non-linear dynamic behavior of the shuttling element is investigated from a more exquisite mechanical point of view, comparing the experimental results with those of an hardening *Duffing oscillator* [35] and providing a first theoretical model for these phenomena [36].
In 2002, new architectures are investigated, the Q-factor is regulated by mixing capacitive and magnetomotive effects (Q-tuning), and self-excitation possibilities start to be discussed, by introducing the concept of *transport factor* (see Section 2.2.9) [37] in the shuttle theory.
In 2003, the possibility of coupling more double-clamped resonators is explored for the first time, both experimentally and numerically [38,39,40].
In 2004, two twin papers by BLICK group [41,42] set some experimental achievements: i) the use of a new fabrication technique able to produce smaller gold-capped silicon nanopillars with a simpler two-steps etching process; ii) the superimposition of the AC voltage for RCF with a DC signal, to produce a better tuning of charge transport through mechanical mixing. With i) and ii), the original goal of obtaining a more stable single-electron shuttle is finally achieved.
The same year, Blick's popularity grows, not only in the academic field – he writes the editorial "Focus on Nano-electromechanical Systems" for *New Journal of Physics* [43] – but also in popular press and media [44,45], where its latest setups are interpreted as "mechanical transistors" †.
A consideration is needed at this point. The BLICK group experimental setups still make use of an AC excitation because, as explicitly reported in [41], a shuttling element realized with a cantilever geometry is *too stiff* to exhibit the self-excitation mechanism proposed by Gorelik (who, in [25], refers to a lighter metallic grain solution). Nicely, years later the BLICK group will contradict itself by succeeding in the goal of nanopillar self-excitation.

In the meantime, others research groups begin to interest to the nanoscale shuttle, most from a theoretical point of view, by using different analytical approaches: Master equation/density matrices [46,47,48,49,50], quantum oscillator [51], semi-classical models [52,53], by exploring new geometries coupling a SET and a shuttling element [47], or rather exhaustive reviews [54].

† As it will be clear in the next Section, this term was, if not misleading, at least *premature*, in 2004. In fact, Blick proposes an "orthodox" mechanical transistor concept, working with a DC gate voltage, only in 2007-2008.

YEARS 2004-2011. On one hand, Gorelik et al. [55,56,57] continue their theoretical researches. On the other hand, BLICK group produces new experimental goals. Here, we focus on them.

First, the presence of a modified Fowler-Nordheim field-emission is observed and attributed to the AC-driven pillar oscillations [58] after it was only glimpsed in a previous work [59].

In 2007, Blick et al. set a milestone in recent shuttle literature with: "A Nano-Mechanical Computer: Exploring New Avenues of Computing" [60]. This is the first time the results of BLICK group on shuttle are explicitly related to the chance of a "new electronics" based on mechanical elements. From the abstract: *"We propose a fully mechanical computer based on nanoelectromechanical elements. Our aim is to combine this classical approach with modern nanotechnology to build a nanomechanical computer (NMC) based on nanomechanical transistors. The main motivation behind constructing such a computer is threefold: (i) mechanical elements are more robust to electromagnetic shocks than current dynamic random access memory (DRAM) based on metal oxide semiconductor (CMOS) technology, (ii) the power dissipated can be orders of magnitude below CMOS and (iii) the operating temperature of such an NMC can be an order of magnitude above that of conventional CMOS."*

Most importantly, the article refers for the first time to some recent experiments in which DC self-excitation has been successfully achieved: *"We estimate that operation with externally applied DC voltages is feasible. These voltages can be generated either by a battery or by a manually actuated battery charger. […] As we have found in recent measurements †, self-excitation can be exploited to generate mechanical oscillations without any AC excitation. Hence, DC voltages are sufficient to operate the NMC. Basically, a DC voltage creates an electric field to support mechanical oscillations of the nanopillars. […] It has to be noted that onset of the mechanical oscillations is induced by a thermal fluctuation, which is found to be enhanced, if the electrical field is inhomogeneous."*

The paper continues by explaining the core elements of such a "mechanical computer" could be similar to the shuttling resonators he investigated in much of previous BLICK group works, describing how they can be combined in logic gates. With this article, Blick starts to be accredited as the "father of the mechanical computer" [61,62].

After a few other papers, further investigating new geometries [63,64] and field-emission [65,66], in 2010 BLICK group finally presents its results on a self-excited electromechanical resonator in a most-cited article [67]. From the abstract: *"Self-excitation is a mechanism that is ubiquitous for electromechanical power devices such as electrical generators. This is conventionally achieved by making use of the magnetic field component in electrical generators, a good and widely visible example of which is the wind turbine farm. In other words, a static force, such as the wind acting on rotor blades, can generate a resonant excitation at a certain mechanical frequency. For nanomechanical systems, such a self-excitation mechanism is also highly desirable, because it can generate mechanical oscillations at radio frequencies by simply applying a DC bias voltage. This is of great importance for low-power signal communication devices and detectors, as well as for mechanical computing elements. For a particular system – the single electron shuttle – this effect was predicted some time ago by Gorelik et al"*.

In this experimental article, self-excitation of a nanopillar with a simple DC voltage is successfully achieved. It is not the first time a self-excited shuttle mechanism is produced since 1998 [68,69], but it was never obtained by using a mechanical element characterized by the most-versatile (and mechanically-representative) cantilever geometry. Another important clue of this paper is that both soft and hard self-excitation regimes are investigated, by using different pillar geometries, the latter case demonstrating the hysteretic effect on the current-voltage curve first theoretically anticipated by Isacsson, Gorelik et al. in 1998 [27].

†: Here the abstract cites a submitted work by Blick et al. However, the actual publication of such results is in 2010.

In recent years, Blick partly concentrated on collateral themes: thus, article [67] elegantly concludes, for now, this experimental race on electron shuttle produced by nanoscale resonators.

Other groups, in recent years, continued to explore the possibilities of QSMs, some proposing architectures more complex with respect to the conventional two-terminals (preferred by Blick) or three-terminals (preferred by Gorelik) geometries. A brief, not comprehensive, list includes: Pistolesi and Fazio [70,71], Wang [72,73], Koenig [74,75].

To conclude this general picture around the state of the art of nanoscale shuttle, a brief technological discussion on how the shuttling element can be realized seems opportune.

If the QSM is designed to shuttle a relatively large amount of electrons per cycle, it is sufficient a metallic grain or metallic cap on the tip of a nanopillar. However, in QSMs shuttling one only electron, such as in a SET, one needs to carefully conceive the shuttling element. A recurrent concept in nanotechnology satisfying exactly this need is that of *Quantum Dot* (Q-dot).

A Q-dot is a small portion of semiconductor in which electrons are three-dimensionally confined, and therefore exhibit a peculiar behavior, a sort of hybrid between a particle and a bulk material (in Section 1.4 a more detailed overview of Q-dots is given). Q-dots have been discovered by Alexei Ekimov at the beginning of the 1980s [76], the most interesting application happened in the last decade. In particular, Q-dots easily show CB effects and some Q-dot-based SETs have been achieved. Last years, molecular-size Q-dots have been realized and Q-bits application to "quantum computers" proposed (again, see Section 1.4 for references).

Blick's NanoMechanical Transistor consisting of a set of Quantum Shuttle Modules

In the 2007 article "A Nano-Mechanical Computer: Exploring New Avenues of Computing", Blick promotes an information industry in which the flux and stock of data relies on the vibration of mechanical elements – thus, on the shuttle mechanism. Notice how, since the fundamental brick of conventional computing is the *transistor* †, similarly, a "mechanical computer" would demand for a specifically conceived "mechanical transistor".

Let us consider the QSM depicted in Fig.II and exhibiting the shuttle mechanism in Fig.III. Such a device exhibits an electrical behavior analogous to that of a mere non-linear passive circuital component, its external characteristic quali-quantitatively described by Fig.VIIIb,d and formula (XI), respectively. This is because the input symmetry-breaking voltage is applied among the *same* pair of terminals between which the output shuttle current is established.

A transistor requires indeed *two* pairs of terminals: one for the input and one for the output. In order to answer this requirement, Blick, in the 2008 United States patent "Nanomechanical computer" [77] ‡, suggests the original concept for a transistor shuttle device whose internal architecture is necessarily more complex than the QSM described above.

The idea is to build a device assembled with a set QSMs similar to those in Fig.II. The first group of shuttling elements are called *drives*, and oscillate between a first pair of electrodes; the remaining resonators, being the *slaves*, oscillate between another pair of them.

Blick proposes to realize the shuttling elements with the peculiar cantilever (nanopillars) geometry he investigated in many of its works listed in the previous Section. This allows to mechanically couple all the cantilevers in a simple way, by the means of a common torsional element – called *web* – to which all of them are clamped.

Schematic drawings of this embodiment are reported in Fig.IX.

† In conventional electronics, both logic gates and memory elements are realized with different circuital topologies which often comprise at least a transistor.

‡ In this patent, Blick also proposes the circuital topology for logic gates and memory elements whose core working principle relies on electron shuttle.

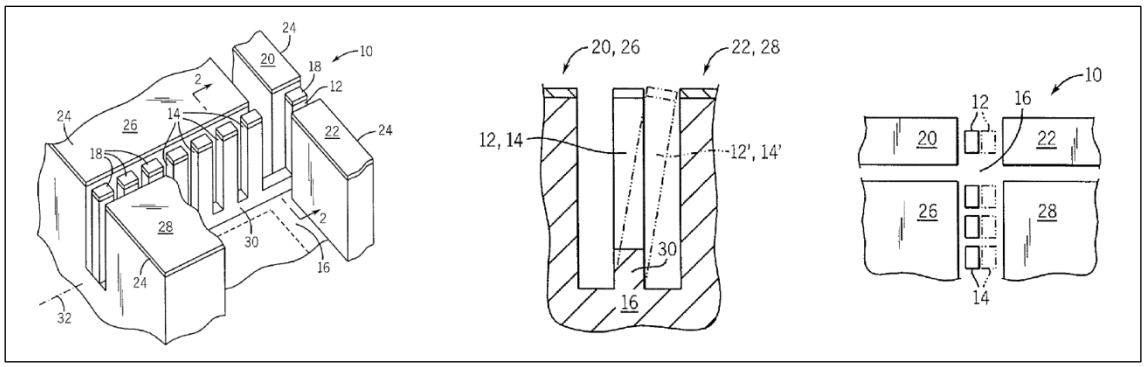

Figure IX: *Images taken from* [77] (*United States Patent 7414437B1 – 2008).*

The working principle described in the patent is briefly summarized as follows. When a sufficient DC voltage is applied on the gate, it triggers the self-excited shuttle regime of the drive resonator. Since all the nanopillars are mechanically coupled by the web, under certain resonance conditions the motion can be transmitted to the whole slave set. Thus, depending on the overall vibrational state achieved, such a system can potentially produce a current amplification effect. On the other hand, the electronic switch operation is simply obtained by regulating the voltage of the gate to alternatively reduce or enhance the slave nanopillars vibrations, thus, inhibit or consent the output shuttle current, respectively.

Since this particular embodiment purportedly mimics the electrical behavior of a conventional transistor, in the rest of this thesis we refer to it as the *NanoMechanical Transistor* (NMT).

Noticeably, this working principle has been introduced, in both [60] and [77], with mere qualitative arguments. Up to present day, at Author's knowledge, no theoretical investigations on such NMT systems have been realized, nor experimental evidence of the described phenomenologies to produce the desired functionalities exist.

The entire Part Two of this thesis, is devoted to verify the functionality of such a device, proposing a set of equation to numerical investigate its dynamical and functional behavior. In particular, the desired functionalities of a NMT are: i) electric switch, ii) current amplification.

It has be remarked that the amplification feature, in Blick's opinion, is crucial to realize the "mechanical computer", since each NMT which composes a logical circuit has to provide a certain *fan-out* †, when connected to the following element. In fact, from the article [60]: *"Key to any computing machine are logic elements. These require gain to provide a noise margin. It seems that gain might be achieved in a NEMSET ‡ by mechanically coupling two sets of pillars. One set, the input set, puts the output set in motion. Gain is achieved if the input set consumes less charge than the output set delivers to the load. This is implemented when the input set contains fewer pillars or if each pillar transfers less charge than a pillar in the output set."*

Again, from the patent [77]: *"Greater charge transfer may occur between the second opposed electrodes than between the first opposed electrodes for each cycle of flexure of the pillars. It is thus an object of one embodiment of the invention to provide for gain or amplification as is necessary to allow adequate "fan-out" for the practical interconnection of logical devices".*

However, we anticipate here that, while the switching operation (analyzed in Sections 10.1 and 11.1) is evident to test in a numerical model; the actual feasibility of the amplification process, mechanically controlled by resonant dynamics of the nanopillars, is not trivial at all (Sections 10.2 and 11.2). In particular, in the conclusion of this thesis, we demonstrate that there is no clear convenience in increasing the number N of slave pillars to obtain a larger current gain.

† Fan-out means a (at least small) current amplification effect to compensate electrical dissipations.

‡ Blick uses this abbreviation for NanoElectroMechanical SET.

Resume: overview of the thesis contents

In this – necessarily substantial – Introduction, we presented all the fundamental concepts around electron shuttle which the rest of the work will deal with. In fact, as the thesis title hints, we are going to deal with the theoretical study of nanomechanical resonators, finalized to design a nanotransistor characterized by a mechanical working principle: the electron shuttle. In this sense, it is clear the thesis concept originated from the conjunction of a theoretical research by L. Y. Gorelik (on nanoscale shuttle, such as [25,27]) and a practical application by R. H. Blick (on the mechanical transistor, [60,77]). The structure of the thesis inherits this dichotomy as well.
In fact, in Part One – "Theory of Mechanical Electron Transport" – theoretical investigations on Quantum Shuttle Modules are carried out, whereas in Part Two – "Application to the NanoMechanical Transistor" – a preliminary design of the NanoMechanical Transistor is attempted.
Consequently, this work denotes a dual nature. As a first step, the approach of a theoretical physicist is employed, investigating Quantum Shuttle Modules as mere dynamical systems whose stability properties depend on the values assumed by of a set of parameters. Then, instead, the feasibility of motion regimes is critically assessed: equation parameters are constrained to measurable properties of a real device, leading to an exquisite design stage on the NanoMechanical Transistor, aimed to correctly reproduce its main functionalities – current switching and amplifications. Follows a brief overview of the thesis contents.

Part One begins by analyzing some nanoscale electron transport devices. Then, a prototypal architecture of Quantum Shuttle Module is presented. A concentrated parameters model is proposed to describe the system by using a couple of lagrangian coordinates: the shuttling element position and charge. Conductive and dynamical features are investigated with both analytical and numerical approaches. A systematic study of Quantum Shuttle Modules is attempted by considering two kinds of symmetry breaking mechanisms. Notice how, all the historical examples of macroscale or nanoscale shuttle devices presented in this Introduction make use of the same symmetry breaking effect: a DC voltage applied between the two fixed electrodes. Instead, a different kind of symmetry breaking is proposed in Part One, in which the oscillator vibrates under a parametric resonance triggered by an AC voltage, and a shuttle current can be established between two electrodes maintained at the same voltage. This is an interesting point, since the black-box conductance of such Quantum Shuttle Module is infinite.

Part Two opens with an analysis of the NanoMechanical Transistor patent, more detailed with respect to the previous Section. Follows the selection of the characteristic scales of the device and the typology of Quantum Shuttle Module to be the best candidate as NanoMechanical Transistor subsystem. An high flexible set of equations is obtained, allowing to carry out a large number of numerical experiments. First, a single Quantum Shuttle Module is considered: a predictive model inspired to a Turing machine is proposed, relating the bias voltage applied to the motion regimes consequently established. Then, more Quantum Shuttle Modules are arranged to realize the NanoMechanical Transistor: a functional analysis of the whole device is presented, its peculiar dynamical regimes are investigated, and a set of strategies aimed to correctly reproduce switching and amplification functionalities is proposed. Last, the electrical characterization of the NanoMechanical Transistor is outlined, together with an estimation of its current amplification properties.

Summarizing, Part One constitutes the theoretical foundation for a more applicative Part Two: once the theoretical properties of electron shuttle have been investigated, the Quantum Shuttle Module which is more appropriate to build a NanoMechanical Transistor can be chosen.

Part One

THEORY OF MECHANICAL ELECTRON TRANSPORT

In the following Chapters the theoretical analysis of mechanical charge transport – namely *electron shuttle* – is carried out, with particular emphasis on the different QSM architectures and the possible working principles able to achieve a form of shuttle mechanism.
In Chapter 1, a number of nanoscale charge transport devices is investigated: after the Tunnel Junction and the Single-Electron Transistor, the Quantum Shuttle Module is definitely analyzed.
In Chapter 2, a detailed description of Quantum Shuttle Modules is attempted: first a prototypal architecture is suggested, then the definition of their main features, the general terminology and the classifications are presented in detail. In particular, the following arguments are discussed: shuttle and tunnel current contributions, distinction between soft and hard shuttle, transport factor, autonomous or induced oscillations, electromechanical coupling, current-voltage hysteresis, effects of Coulomb blockade. In particular, two kinds of shuttle mechanism are discerned, depending on the voltage boundary conditions used: *direct shuttle* and *inverse shuttle*. The first one is characterized by self-excited vibrations, the second one relies on parametric resonance.
In Chapter 3, an overview of the feasible analytical models and approximations is proposed.
In Chapter 4, a direct shuttle Quantum Shuttle Module is investigated with numerical simulations, and the occurrence of a current-voltage hysteresis, peculiar of hard systems is discussed.
In Chapter 5, analytical and numerical approaches are used to study inverse shuttle Quantum Shuttle Modules. First, a "wide-gate" is used to investigate soft shuttle regimes, for which a more exquisitely "quantum" approach is preferred; then, the general case is investigated by using a "semi-classical" model. In both cases, similar results are obtained. Specifically, the chance to realize an AC shuttle current is analyzed and highlighted with numerical simulations.
In Chapter 6, *hybrid shuttle* – the combination between direct and inverse shuttle – is suggested.
To conclude, a general framework reassumes the conduction mechanisms treated in the thesis.

Chapter 1

Charge transport devices at nanoscale

1.1 Quantum Tunneling in a Tunnel Junction

A first description of Quantum Tunneling (QT) has been presented in the Introduction.
QT refers to a quantum mechanical effect which allow a particle to surpass a potential barrier also in the case the laws of classical mechanics would not allow so.

Consider a rectangular potential barrier U and a particle with energy E. In the classical frame, only a particle with $E > U$ can surmount the barrier. In quantum mechanics, a non-zero probability to find the particle over the barrier exists, also in the case $E < U$. A simplistic, though useful interpretation of QT is that the particle "borrows" missing energy $U - E$ from its surroundings, and this is repaid making the other reflected particles more energetic than they otherwise would have been [78]. A more strict explanation relies the wave-particle duality, which involve the Heisenberg uncertainly principle, from which follows a particle position cannot be predicted nor excluded with absolute certainty. Quantum scenario also involves the particle does not strictly transit through the barrier, but simply "appears" – *tunnels* – on the other side. Therefore, the "duration time" of QT is an highly debated argument, and produced some interesting results on the apparent superluminal "tunneling speed" [79,80].

The tunneling problem consists in solving the Schröedinger equation and integrate the wave function in the positions over the barrier to provide the probability for a particle to tunnel over barrier: this provides the QT *transmission coefficient.* Historically, the first important result was that of Fowler-Nordheim tunneling [81], referred to triangular barriers. For rectangular or piecewise barriers exact analytical solutions exist [82]. Corrections for parabolic potential are long known also [83]; while, for arbitrary shapes of practical interests, approximated solutions, mainly based on the WKB method, have been proposed [84,85].

When QT is referred to electrons, it is called *electron tunneling*, and its study is of particular interest in electronic devices. The most simple system exhibiting electron tunneling is a *Tunnel Junction* (TJ). A TJ is constituted by a couple of electrodes separated by a thin insulating layer. The dielectric produces a potential barrier electrons can tunnel through to reach the other conductor. Since the architecture of a TJ is similar to a plate capacitor, the circuital equivalent of a TJ is formed by a resistor and a capacitor in parallel (Fig.1.1). The capacitance C_t may be calculated as usual. Instead, the current-voltage characteristic is peculiar of QT and highly non-linear, and different approaches are used in literature to model the TJ conductance G_t .

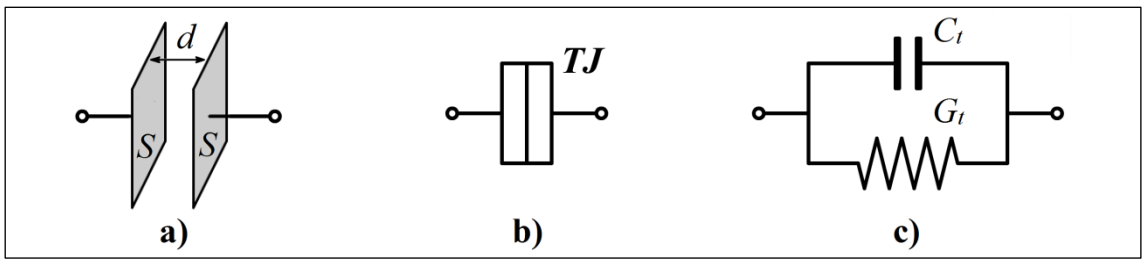

Figure 1.1 – *(a) Architecture, (b) circuital symbol and (c) circuital equivalent of a TJ.*

The standard approach is that of assuming a conductance with a negative exponential dependence from the insulator thickness:

$$G_t{}^{V^*}(d) = G_c \mathrm{e}^{-\frac{d}{\lambda}} \tag{1.1a}$$

where G_c represents the *contact conductance* and λ is the *tunnel length*. Both parameters can be determined by experiments by assuming a known, constant, potential difference V^*: typical values reported in literature are $G_c = 10^{-6}\sim 1\ S$ and $\lambda = 0.05\sim 0.3\ nm$ [25]. Physically, these values depend on the electrodes average surface S and work function ϕ .
In order to take into account the dependence from the applied voltage, more accurate formulae are also available (see Appendix A). Such models (see Fig.1.2) can be useful to calculate QT equivalent conductances in the case one of the parameter (usually, the distance d) varies in time.

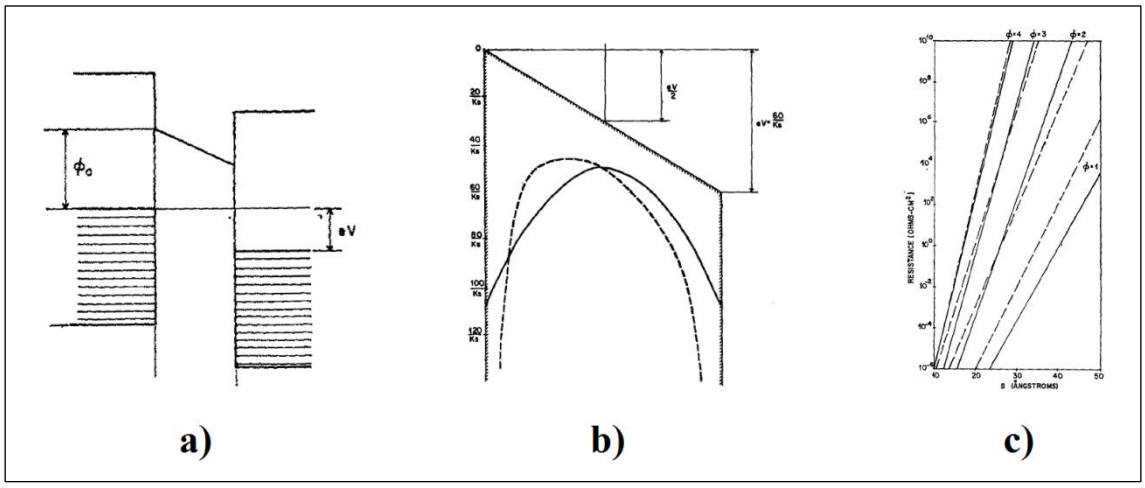

Figure 1.2 – *Images from article* [86]*. (a) Rectangular barrier. (b) Hyperbolic correction. (c) Some exemplificative curves represent equivalent QT conductances as a function of voltage and distance.*

One can fit the standard formulation (1.1a) with one of these approaches, in order to obtain a more neat relation in which the dependence from voltage is included within the tunnel length:

$$G_t(d,V) = G_c \mathrm{e}^{-\frac{d}{\lambda(V)}} \tag{1.1b}$$

where $\lambda = \lambda(V)$ is calculated for a system of known geometry and materials. Notice this formulae are referred to a *normal-conducting* TJ †.

1.2 Coulomb Blockade in a Tunnel Junction

A brief comment on Coulomb Blockade (CB) effects has been presented in the Introduction.
This name originates from an obsolete way to refer to electrostatic energy, as "Coulomb energy", however, since CB is the manifestation of the discrete nature of charge in presence of QT, it is sometimes referred as *quantized charge tunneling* or *single electron charging effect*.

† Therefore, not *super-conducting* (in which Cooper pairs tunnel), nor *semiconducting* (when the transmission coefficient highly depends on temperature).

The term CB was originally introduced to indicate the increase of resistance in a TJ around very small voltages; however, it is now used extensively to group a number of CB-related effects which can be exhibited by NEMS devices comprising at least a TJ. In this paragraph, we start our analysis on CB by considering its effects on a single (normal-conducting) TJ.

Consider a TJ exhibiting QT, characterized by a capacitance C_t . An interpretation of the CB phenomenon is provided as follows (refer to Fig.1.3). Due to the discrete nature of charge, QT can be considered as a series of events in which exactly one electron tunnels from the low-biased electrode to the high-biased one, producing a discrete decrement of the potential difference $dV = e/C_t$. Assume in a time t_{i-1} the potential difference between the electrodes is $V_{i-1} > 0$. The event "tunnel of the i-th electron", would produce a voltage drop to $V_i = V_{i-1} - dV$. In the case V_{i-1} and/or C_t are very small, V_i could result negative, and in this case the QT of the i-th is inhibited. The black-box effect is that of an increase of the TJ resistance around very small voltages: a *blockade* which indeed summarizes the CB effect. This increment in resistance cannot provided by formulae and, if present, it has to be introduced in a theoretical model by using a discrete-charge approach (see Section 2.3).

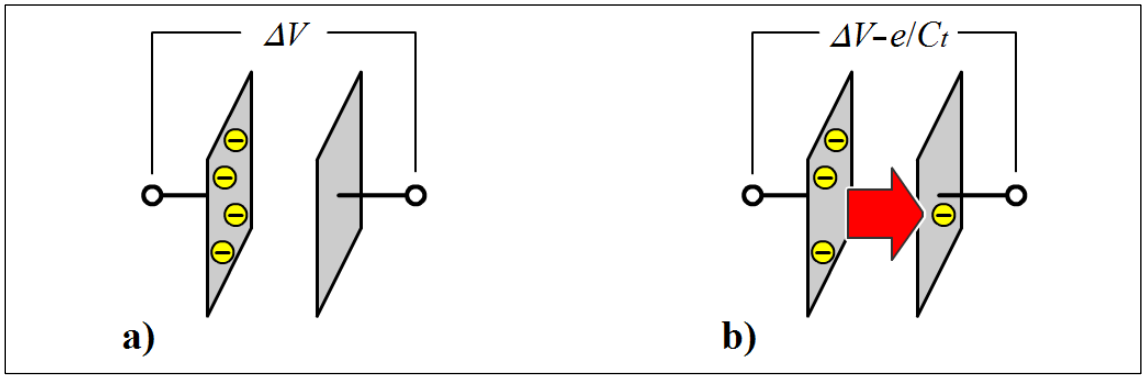

Figure 1.3 – *Explanation of CB due to the QT of a single electron in a TJ: (a) before, (b) after the event.*

However, to detect CB, some requirements have to be met. First, electrons receive energy not only from the electric field induced by an applied voltage, but also from thermal excitation. A *temperature* θ, differently from the directional effect of an electric field, excites electrons *randomly*, producing fast, back-and-forth tunneling episodes between the two electrodes. Consequently, at relatively high temperatures, effects of charge discreteness on the time scale of current measurement are not revealable. Second, one needs the TJ potential barrier is sufficiently opaque that the electrons are actually "located somewhere" (in either the electrodes). This condition involves the Heisenberg uncertainty principle and requires a TJ resistance $R_t = 1/G_t$ which allows a limited number quantum fluctuations over the time scale of the measurement.
Therefore, in order to observe CB in a TJ, the following conditions have to subsist [21,87]:

$$\frac{e^2}{C_t} \gg k_B \Theta \tag{1.2a}$$

$$R_t \gg \frac{e^2}{h} \tag{1.2b}$$

where k_B and h are the Boltzmann and the Planck constants, respectively. Sometimes, (1.2a) is very restrictive: a TJ with $C_t = 1 \times 10^{-15}\ F$ requires a temperature $\Theta \ll 1\ K$. Thus, the chance to observe CB in a NEMS is constrained to miniaturization technological limits.

† We are excluding the *co-tunneling* occurrence. Actually, this assumption is not feasible if the applied voltage is relatively high.

1.3 Coulomb Blockade in a Double Junction: the Single-Electron Transistor

By coupling two TJ, the presence of CB can be more relevant and produces interesting effects. Consider the device depicted in Fig.1.4: the element in the center labeled with I is called *island*. The island is separated from both the electrodes L and R, by a thin layer of dielectric. Therefore, a system characterized by this architecture is a *Double Tunnel Junction* (DTJ).

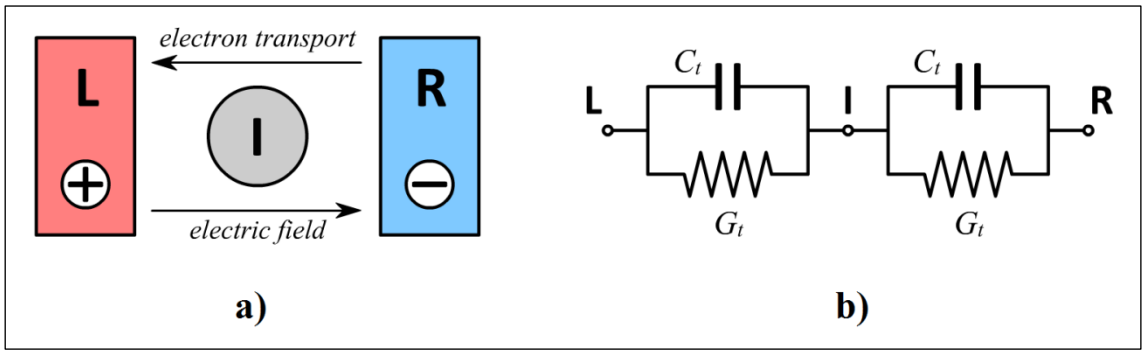

Figure 1.4 – *Two-terminals system representing a DTJ: (a) architecture, (b) circuital equivalent.*

In a DTJ, the interpretation of CB involving the discrete QT of electrons is still valid. The novel effect is that the application of a sufficiently small voltage between L and R, definitely prevents the contemporary tunneling of two or more electrons on the island (*co-tunnel*). Electrons are transferred one-by-one, since only when the first one has finished to tunnel from I to R (or L) a second electron can tunnel from L (or R) to I. This phenomenology is called *single electron tunneling*. Introduce the total capacitance of the island $C_I = 2C_t$ (being C_t the capacitance of either two specular TJ), then, conditions (1.2a,b) generalize into:

$$\frac{e^2}{C_I} \gg k_B\Theta \tag{1.3a}$$

$$R_t \gg \frac{e^2}{h} \tag{1.3b}$$

A DTJ in which both (1.3a) and (1.3b) hold, exhibits, consequently to the behavior explained above, a peculiar step-like shape of the current-voltage curve, called *Coulomb staircase* (Fig.1.5). Specifically, single electron tunneling occurs in correspondence of the first step of the curve. By applying increasing voltages, multiple electrons start to co-tunnel, towards/from the island and this leads to a progressive smearing of the steps of the Coulomb staircase.

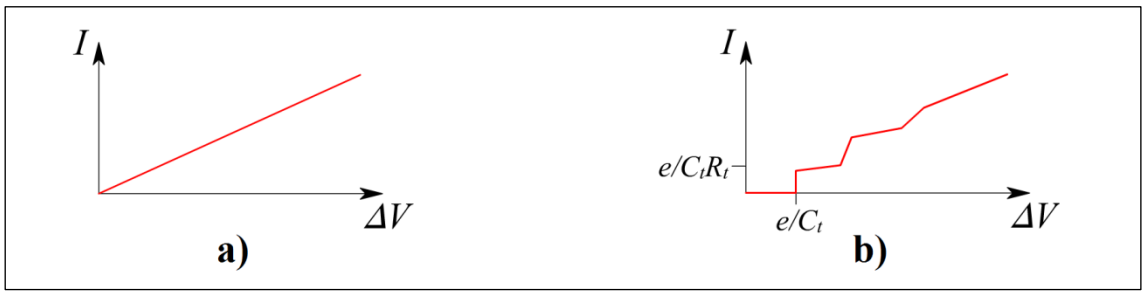

Figure 1.5 – *Effect of Coulomb Blockade on the I-V curve of a DTJ: (a) without CB, (b) with CB. In the second case, the Coulomb staircase is visible.*

However, the *two-terminals* system depicted in Fig.1.4 requires relatively high voltages $\Delta V \sim e/C_I$, to produce QT. This may prejudice the thermal equilibrium of the system: in order to overcome this inconvenient, a *three-terminals* device as that in Fig.1.6a can be proposed.
A third electrode, the *gate* G , is capacitively coupled with the island I: now the gate voltage V_G allows to regulate the electrostatic potential V_I , thus, to control the presence of CB in the system. In presence of CB, this three-terminal geometry can exhibit single-electron tunneling, therefore we refer to it a *Single Electron Transistor* (SET). In such system, electrodes L and R act as a conventional transistor *drain* D and *source* S.

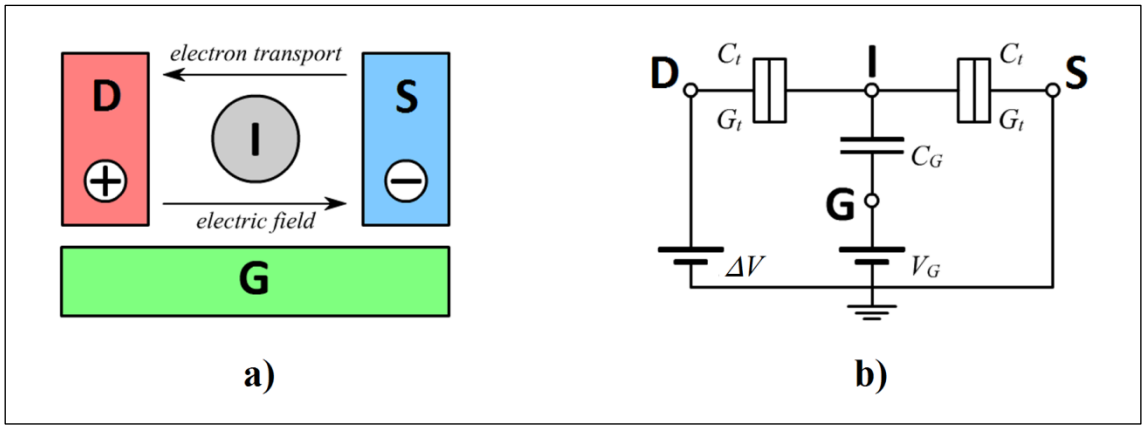

Figure 1.6 – *Three-terminals system representing a SET: (a) architecture, (b) circuital equivalent.*

In a SET, a relatively a small gate voltage V_G can switch the device from the insulating to the conducting state (or vice versa): if correctly designed, a single electron is sufficient to consent/prevent the one-by-one source-to-drain electron tunnel.
Therefore, a SET requires an additional condition on the bias voltage, which needs to be as small as the first step of the Coulomb staircase:

$$\Delta V < \frac{e}{C_I} \tag{1.3c}$$

Triplet (1.3a,b,c) constitute the set of requirements to realize a working SET.

The SET represents the most important application of CB. Its concept was first suggested by in 1986 [15], and was first successfully tested in a cryogenic environment [17] †. This is bacause condition (1.3a) imposes a temperature relatively small with respect to the capacitance C_I . The cryogenic limitation represented for many years a main concern about the technological feasibility of a SET device. However, with the recent improvements of nanotechnology, in mid 90s, the first SETs operating at room temperature were realized by progressively reducing the size of the island and by using different bottom-up approaches.
Another issue in SETs is related to the co-tunnel leakage failures, which may be prevented by using multiple-TJ geometries [87,88,89] instead of a simple pair of TJs.

In a more general context, the fundamental importance of the SET as the basic component of a less energy-consuming information technology ‡ have been theoretically investigated in a number of works [90,91,92] but commercial (more stable) applications are yet to come and represents one of the most exciting challenges for future NEMS research.

† In this work, Fulton and Nolan noticed the high sensitivity of a SET current to the charge on the gate (*Coulomb oscillations*), and proposed an alternative use of the device as a *single electrometer*.

‡ In a conventional MOSFET (Metal-Oxide-Semiconductor Field-Effect Transistor) over one thousand electrons are needed to perform the same transistor functionality of a SET.

1.4 Technological feasibility of Coulomb Blockade: the Quantum Dot

Pioneers of CB investigated its effects by measuring anomalies in the conductive properties of granular thin films [11,12]. In their first SET prototype, dated 1987, Fulton and Nolan [17] made use of an aluminum structure to produce CB. In the following years, the advent of the STM promoted a renewed interest for small grains [93], in particular single electron devices whose island consisted of a single nanocrystal [20,69]. In 1996, single-electron tunneling was successfully exhibited at room temperature in self-assembled molecular nanostructures by Andres et al. [18], further explored by Soldatov [19,94,95] and recently reviewed by Joachim [96]. In particular, interest focused towards carbon structures, from the versatile C60 molecules [97,98], to the recent realizations of SETs using carbon nanotubes, started in 2001 by Postma et al. [99] and whose research continues today producing interesting results [100,101].

All these examples constitute different ways to overcome the same technological needs: miniaturization of a (semi)conductor element in order to observe CB at room temperature, giving the chance to realize SET devices suitable for commercial electronic applications.
There is no formal difference in the physics of most cases cited above: each of them represents a confined structure containing a small amount of electrons which exemplifies the concept of *Quantum Dot* (Q-dot). Although, strictly speaking, this term properly refers to a semiconductor nanostructure, such phenomenology is substantially similar to that of a cluster, a metallic particle, a grain, or a molecule. Both orthodox – i.e. realized in silicon – and not Q-dot devices have been proved to show CB effects [102], and can work as a SET [103,104,105].
A rather complete review on Q-dots can be found in [106].

The peculiar conductive behavior of a Q-dot can be understood by using the band theory, which, how it is well-known, describes the behavior of electrons in solids by postulating the existence of energy bands in a material. Electrons, according to their fermionic nature and the Pauli exclusion principle (no more than one fermion can occupy the same state), occupy the available energy states by starting from the lowest one, following – under the "many-electrons approximation" – the *Fermi-Dirac* distribution. The *Fermi level* is the energy of the highest occupied energy level in a system of fermions (i.e. electrons) when $\Theta = 0\,\mathrm{K}$. In the case of electrons only two states are present in each energy level.

Referring to Fig.1.7, different possibilities arise, depending on the nature of the material.
In metals (we are only interested with *solid* conductors), regardless temperature, a band partly empty and partly filled exists. In these material electrons have an high mobility.
In insulators or semiconductors, the lowest almost fully occupied band is the *valence band* while the highest almost unoccupied band is the *conduction band* . Distance between these two bands is the *bandgap*. In insulators, such bandgap is large, in semiconductor is thin.

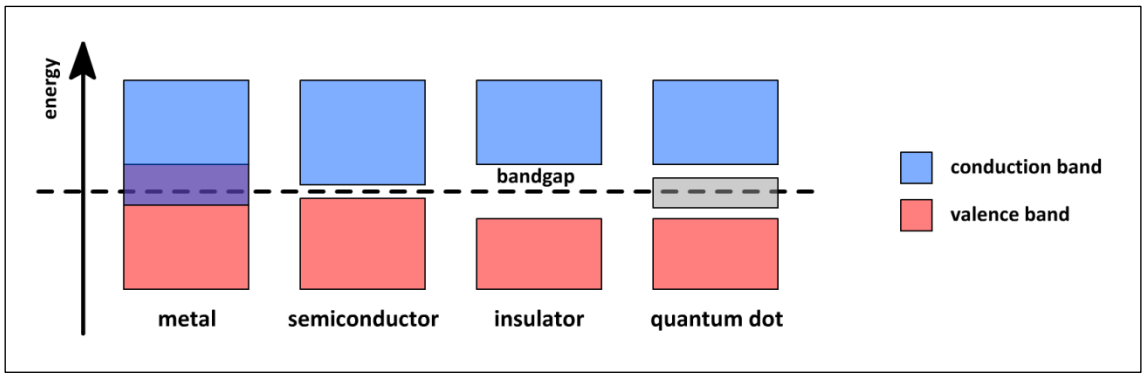

Figure 1.7 – *Band theory representation of different materials.*

Since only the electrons excited to the conduction band can concur to electric current, in insulators only a few electrons are found there and their electrical conductivity is lower. On the other hand, semiconductors can exhibit a more or less conductive behavior depending on the temperature, the required excitation of electrons coming from thermal energy.

Up to here, this is matter of basic solid-state physics. Introduce now to the concept of Q-dot in the context of band theory. In a macroscopic object ("bulk material" model), the discreteness of energy bands is not detectable (Fig.1.8a). However, the more the scale is reduced, the more the size of the bands increase. When the diameter of the objects of the order of nanometer ("nanoparticle" model) the bandgap becomes dependent on the size of the object. An electron behaves as if it were free when the dimension of the confining material is large respect to its De Broglie wavelength. Otherwise, a *n*-dimensional *potential well* due to the small material scale is observed: an effect called *quantum confinement*. Depending on the typology of the quantum confinement, different nomenclatures are used. A *quantum well* (Fig.1.8b) is a one-dimensional quantum confinement. A *quantum wire* (Fig.1.8c) is a two-dimensional quantum confinement †. Finally, if all three dimensions are confined, it is the case of a *quantum dot* (Fig.1.8d).

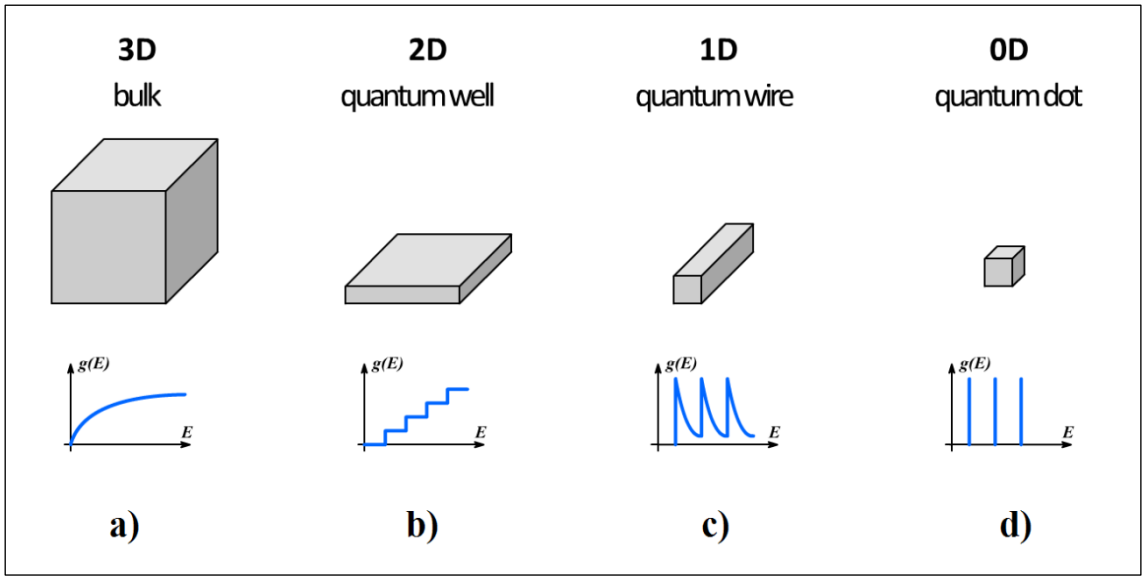

Figure 1.8 – *Distribution of energy levels in different cases of quantum confinement.*

Summarizing, a Q-dot is obtained when an inclusion of a semiconductor material of the dimensions of its De Broglie wavelength – thus, exhibiting quantum confinement – is included within a larger semiconductor characterized by a larger bandgap (refer to Fig.1.7). The conductive behavior a Q-dot is therefore an hybrid between bulk conductors and discrete molecules: consequent to this it is often referred as an "artificial atom". Since, due to an high extinction coefficient, their optical properties deviate from the bulk materials, Q-dots are often used in optical applications. Last, semiconductor Q-dots can be easily connected to electrodes, differently from molecular clusters.

To conclude, two main Q-dots categories exist: *little* Q-dots (i.e. nanocristalline semiconductors in colloidal solutions), which have a characteristic diameters of a few nanometers and are composed $10^2 \div 10^5$ atoms; and *self-assembled* Q-dots, over 10 nanometers.

† Carbon nanotubes constitute an optimal embodiment to realize quantum wires, as first demonstrated in [107].

1.5 Double Junction with an oscillating island: the Quantum Shuttle Module

In 1998, Gorelik [25] first suggested to consider a DTJ system in which the island was free to oscillate between leads. In its article, the feasibility for such a device to exhibit a conduction mechanism based on the vibrational state of the island was theoretically demonstrated. This peculiar form of charge transport was named *shuttle*. A similar mechanism was already exhibited by some macroscale devices (see the Introduction), but this was the first time such a concept was explored in a NEMS, in presence of both QT and CB effects. In its paper, he suggests a minimal *two-terminals* geometry, composed by fixed electrodes L and R, and a shuttling element S (Fig.1.9a). Years later, Isacsson [29] introduced a *three-terminals* shuttle device, more similar to a SET, in which a gate G is present also (Fig.1.9b).
Both configurations have been later investigated in theoretical and experimental works, whose a detailed review have been already presented in the Introduction.

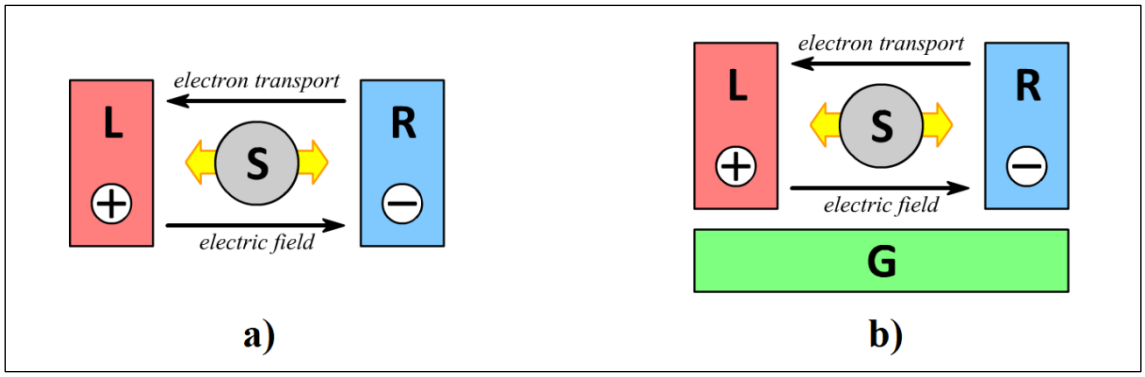

Figure 1.9 – *Schematic representation of a QSM: (a) two-terminals, (b) three-terminals configuration.*

Different terminologies are used in literature to indicate devices which can be schematized by one of the geometries in Fig.1.9, or, by extension, which exhibit a similar phenomenology: *nanomechanical charge shuttle*, *quantum electron shuttle*, *shuttle junctions*.
In this thesis, we univocally refer to them as *Quantum Shuttle Modules* (QSMs), whereas analogous macroscale devices are simply named *Shuttle Modules* (SMs), to underline the strict connection between these two categories and simultaneously remind their differences.

The dynamics and conductive properties exhibited by a QSMs differ from those of a SMs primarily for the presence of QT, while CB plays a secondary role (Introduction, Tab.I). This fact states an important difference with SETs (whose working principle *relies* indeed on CB): *a QSM does not require any CB-related condition to operate*. More specifically, the missing demand for condition (1.3a) bears a pair of advantages for QSMs.
First, the working principle of a QSM not only is adapt to operate at room temperatures, but is refractory to high temperatures not compatible with conventional semiconductor electronics: this fact was often highlighted by Blick as a strong point of an information technologies based on QSMs instead of SETs [60]. Second, the absence of a condition on having a maximum capacitance, loosens the miniaturizing constraints of a QSM: in particular the shuttling element of a QSM can be realized with a certain versatility by using different shapes and technologies: from small silicon Q-dots transferring single electrons [108], to larger metallic Q-dots [109], metallic clusters in organic links [68], or even larger embodiments consisting in a metallic cap on the tip of a nanocantilever as preferred by Blick [26,31,32,36,37,41,42,52].

Chapter 2

Approaching the Quantum Shuttle Module

2.1 Prototypal architecture of a Quantum Shuttle Module

The most general architecture of a QSM is represented by the three-terminals configuration in Fig.1.9b. The left and right *electrodes* L and R and the *gate* G are the fixed terminals, whereas a fourth conductor body, the *shuttling element* S , is free to oscillate between L and R . As usual in literature, QSMs are theoretically investigated by using a concentrated parameters model.

In the following considerations, refer to Fig.1.10 for the mechanical part of the system and to Fig.1.10b for its electrical counterpart.

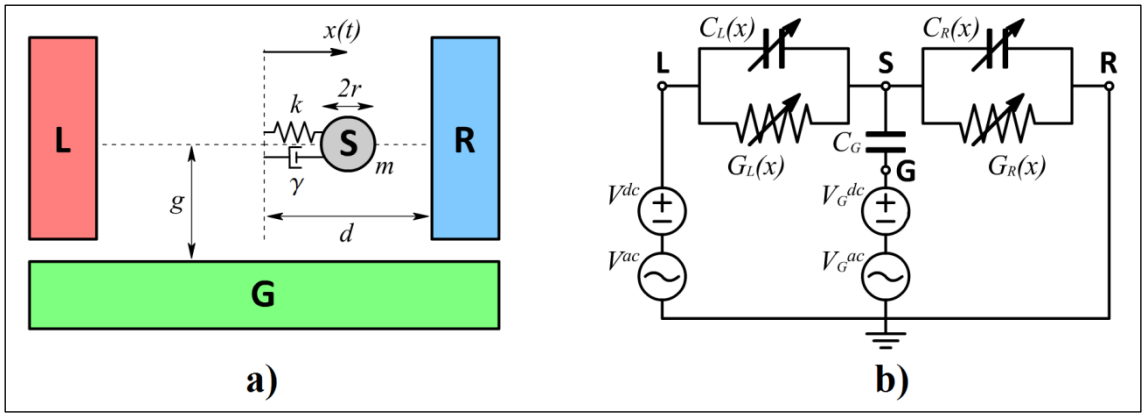

Figure 1.10 – *Prototypal QSM architecture: (a) geometrical and (b) electrical schemes.*

In this simple model, the evolution of a QSM can be described by using only two lagrangian coordinates: one mechanical, the position $x(t)$, and one electrical. The choice of the electrical coordinate is more subtle: first of all, one can alternatively choose the shuttling element voltage or electric charge. Secondly, different analytical models arise depending from the use of a *discrete-* or a *continuous-charge* model. The approach proposed in this paragraph strictly refers to the latter case, however, with a certain abuse of notation, it can be adapted to a discrete-charge model. When not conversely specified, in this thesis we prefer the continuous-charge approach which uses $Q_S(t)$ as the electrical lagrangian coordinate. The simple relation $Q_S(t) = eN_S(t)$ can be used, if needed, to switch between the two approaches.

In Fig.1.10a, (mechanical scheme) the shuttling element S is modeled as a single-DOF oscillator with mass, damping and stiffness respectively m , γ and k . Being $2r$ the characteristic size of S and d the half-distance between L and R, in a symmetrical embodiment, S can occupy positions $x(t) \in [-d + r, +d - r]$. Last, we assume the distance g between S and G is constant.

In Fig.1.10b, (electrical scheme) the shuttling element S is capacitively coupled with L, R and G by the means of position-dependent capacitances $C_L(x)$ and $C_R(x)$ and a constant C_G † .

† Equivalent circuit in Fig.1.10b considers only nearest neighbors capacitances. Analyses carried out in Part One use this approximation. In Part Two, a more accurate electrostatics involving a capacitance matrix is considered.

Other capacitive effects are neglected, so that the shuttling element self-capacitance is:

$$C_S(x) \triangleq C_L(x) + C_R(x) + C_G \tag{1.4}$$

Depending on the position x, the pairs L-S and S-R can alternatively form a TJ, thus exhibiting non-null equivalent tunnel conductances $G_L(x)$ and $G_R(x)$, which, in this Part †, will be calculated by making use of simple formulae (1.1a,b) ‡

Voltages of the three terminals are directly controlled by both DC and/or AC signals, so that:

$$V(t) = V_L(t) - V_R(t) \triangleq V^{dc} + V^{ac}\cos(\omega_{LR}t) \tag{1.5a}$$

$$V_G(t) \triangleq V_G^{dc} + V_G^{ac}\cos(\omega_G t) \tag{1.5b}$$

The selection of the six values V^{dc}, V^{ac}, ω_{LR}, ${V_G}^{dc}$, ${V_G}^{ac}$, ω_G sets the boundary conditions. Electrostatics of the whole system influences the shuttling element voltage, so that in general, one can calculate its potential by using the following formula:

$$V_S(t) = \frac{Q_S(t)}{C_S(x)} + \alpha(x)V(t) + \beta(x)V_G(t) \tag{1.6}$$

where $\alpha(x)$ and $\beta(x)$ are appropriate positive quantities ‡†. Depending on the actual values of voltages and conductances, currents I_L and I_R are established, their instant value being:

$$I_L(t) = G_L(x)[V_L(t) - V_S(t)] \tag{1.7a}$$

$$I_R(t) = G_R(x)[V_S(t) - V_R(t)] \tag{1.7b}$$

In this thesis the following convention is used for current directions: I_L is positive from L to S and I_R is positive from S to R . These currents are the only ones included in this model ‡‡ .
Conductances G_L and G_R rely on QT effect. Thus, they are calculated by making use of one of the relations (1.1a,b), dependent from position and potential differences:

$$G_L(x) = G_t(d - r + x, |V_L - V_S|) \tag{1.8a}$$

$$G_R(x) = G_t(d - r - x, |V_R - V_S|) \tag{1.8b}$$

Since the schemes in Fig.1.10 constitute the most general case of QSM, in the following Chapters of this Part we'll refer to it as the *prototypal architecture*. In fact, every specific embodiment of a QSM differentiates from this most-general architecture only by the power relationships between its constitutive elements and the different choices on boundary conditions.

† In Part Two, more accurate models taking into account the voltage effects are introduced, by making use of Simmons formulae.

‡ Except when a more exquisite quantum approach is attempted to determine QT. Here we refer to a quantum approach when the discrete nature of electric charge is considered. In this sense, QT cannot be modeled by the means of equivalent conductances, but with different approaches.

‡† This is an approximated, although effective relation often used in literature [27] and, in this thesis, only in Part One.

‡‡ Here, we only consider QT currents since we are not interested in apparent currents coming from the charging of capacitors. Also, since QT between S and G is not included in the model, the geometrical properties and voltage boundary conditions of the system may to be selected appropriately. Again, in Part One we neglect long tunnel between L and R with respect to short tunnel between L and S or S and R : in Part Two, it is reintroduced as well.

2.2 General concepts on electron shuttle

2.2.1 Shuttle and tunnel contributions to the macroscopic current

Referring to the QSM prototypal architecture in Fig.1.10, the only currents are $I_L(t)$ and $I_R(t)$. They represent *microscopic currents*, whose instant values – calculated by using relations (1.7a,b) – do not generally match. However, when averaged over an appropriate period of time Δt †, their values coincide ‡, and a QSM exhibits a *macroscopic current*:

$$\bar{I} \triangleq \frac{1}{\Delta t}\int_{t_0}^{t_0+\Delta t} I_L(t)\,dt \equiv \frac{1}{\Delta t}\int_{t_0}^{t_0+\Delta t} I_R(t)\,dt \tag{1.9}$$

When a QSM is considered as a black-box, current $\bar{I}$ represents the serviceable output consequent to the electrodes and the gate voltage applications ‡† . To achieve the electrical characterization of the device, one can plot, for example, a family of I-V curves referred to the current (1.9) as a function of the (maintained constant: $\omega_{LR} = 0$) bias voltage (1.5a), and by using stepped values of the ($\omega_G = 0$) gate voltage (1.5b).

Since, from (1.7a,b), both currents $I_L(t)$ and $I_R(t)$ rely on the equivalent QT conductances $G_L(x)$ and $G_R(x)$, in a QSM the form of charge transport wherewith the shuttling element S produces a macroscopic current $\bar{I}$ is the QT. This fact states a first fundamental difference with a SM, where electrons are transferred, instead, by contact. The second difference is that in a QSM the current can be considered as the sum of two contributions, corresponding to as many distinct physical mechanisms: the *shuttle current* I_s and the *tunnel current* I_t , while in a SM only the first contribution is present, since QT is not present at macroscale. The term I_s represents the part of current which relies on the vibrational state of the shuttling element, while I_t is the part of current which is present also when the shuttling element is at rest. We already discussed the consequences related to this dichotomy in the Introduction (Tab.I). However, in this sub-Paragraph we study in deep some last considerations.

Consider an experimental setup in which three device: a SM, a TJ and a QSM are present. In the SM, there is no QT effect, and the whole current is produced by the shuttle mechanism. On the contrary, in a TJ the island is at rest and the only contribution is from the tunnel current. In a QSM, the island (shuttling element) is free and QT effect is present: thus, there is a combination of both shuttle and tunnel currents. Summarizing, we are in front of this situation:

$$I(t) = I_s(t) \tag{1.10a}$$

$$I(t) = I_t(t) \tag{1.10b}$$

$$I(t) = I_s(t) + I_t(t) \tag{1.10c}$$

where (1.10a,b,c) respectively refer to a SM, a TJ and a QSM.

† Usually it is sufficient to average over a single period of oscillation T_s to make quantities $\overline{I_L}$ and $\overline{I_R}$ coincide. However, this is not true in general: exotic cases of a QSM in which a longer averaging time $\Delta t \gg T_s$ is required, exist indeed. A procedure to determine the appropriate Δt will be presented in the Section 2.2.2.

‡ An heuristic, but effective argument to demonstrate this statement is presented ahead. Consider a QSM achieving a certain periodic motion regime: since S cannot accumulate electrons indefinitely, a stationary condition, in which $\overline{I_L}$ and $\overline{I_R}$ are going to match, has to be eventually reached. Such an asymptotic common value of the current can be either null or not.

‡† This fact is analogous to a SET. On the other hand, whereas a SET can easily work as a transistor (i.e. the gate voltage modulates the current passage between a source and a drain), this is not straightforward in the case of a QSM, as has been anticipated in the Introduction, and as will be widely argued in the following Chapters of the thesis.

Relations (1.10a,b,c) seem to suggest the intuitive fact a QSM is a combination of a TJ and a SM: however this vision is misleading, since the definition of the tunnel current in (1.10b) for a TJ *is different* from that in (1.10c) for a QSM. In fact, the following relation holds for a TJ:

$$I_t(t) = G_t V(t) \tag{1.11}$$

where closed-form formulae like (1.1a,b) can be profitably used to calculate the tunnel conductance G_t . One could conclude it is possible to do the same to estimate the tunnel contribution to current in a QSM in (1.10c), but *this is wrong*, because a QSM more resembles a DTJ, and there is no chance to use (1.11), which applies to a mere TJ. In conclusion, the instantaneous contributions to current cannot be discerned (both theoretically or experimentally) in a QSM.

There is, however, the chance to distinguish the shuttle current from the tunnel one if considered as time-averaged quantities. Experimentally, the only possibility relies on realize two *twin* embodiments of the same system. In the first one, the shuttling element is free to oscillate; in the second, it is fixed in some way. A similar approach has been attempted in literature in at least one case [41]. Clearly, this approach gives rather poor estimations of current contributions. The scenario is in fact more clear in a theoretical context. In the Introduction, relying on heuristic arguments , we already derived (formula (IVI), an operative relation for the shuttle current:

$$\bar{I}_s = eN_s f_s \tag{1.12a}$$

In this, f_s is the shuttling frequency and N_s the number of (positive) charge carriers shuttled in a cycle. Relation (1.12a) was first introduced by Gorelik when, in 1998 [25], he first suggested the archetype of a nanoscale QSM. However in (1.12a) the meaning of N_s needs to be further specified. Again in [25], Gorelik rigorously introduced the shuttle current as:

$$\overline{I_s} = \frac{1}{\Delta t}\int_{t_0}^{t_0+\Delta t} I_{mech}(0,t)\, dt \quad , \quad I_{mech}(x^*,t) = \delta\left(x(t)-x^*\right)\dot{x}(t)Q_S(t) \tag{1.12b}$$

In this formula, $I_{mech}(x^*,t)$ is the *mechanically mediated current*, referred to a cross-section x^* ($\delta(\circ)$ is the *Dirac delta* function). Therefore, due to the symmetry, the shuttle current has been defined as the mechanically mediated current in $x^* = 0$ averaged over a period of oscillation T_s. Definition (1.12b) matches the more generic (IV). Notice these relations are general and apply to both a SM or a QSM. Last, the tunnel current can be introduced in a residual way as:

$$\overline{I_t} = \bar{I} - \overline{I_s} \tag{1.13}$$

where $\overline{I_s}$ is calculated using one of (1.12a,b), while the total current $\bar{I}$ comes from (1.9) †.
In Tab.1.1 the overall scenario involving shuttle and tunnel current contributions is summed up.

Table 1.1 – *Determination of shuttle and tunnel currents in different devices.*

Device	Current Contribution	Experimental Setup		Theoretical Model	
		instant	time-averaged	instant	time-averaged
SM	shuttle	(1.10a)		no	(1.12a,b)
TJ	tunnel	(1.10b)		(1.1a,b)	
QSM	total	(1.10c)		no	(1.9)
	shuttle	no	"twin" devices	no	(1.12a,b)
	tunnel	no	"twin" devices	no	(1.13)

† Clearly, in order to apply (1.13), both currents $\overline{I_s}$ and $\bar{I}$ have to be averaged on the same period of time Δt .

2.2.2 Phase plot representation: feasibility of the shuttle current

Consider the prototypal QSM architecture in Fig.1.10. Assume the shuttling element undergoes a certain periodic motion regime $\mathcal{X} = x(t)$, in presence of some voltage boundary conditions $\mathcal{B}$ compatible with (1.5a,b), periodic as well. From (1.7a,b), the evolution of charges $\mathcal{Q} = Q_S(t)$ only relies on $I_L(t)$ and $I_R(t)$, in turn depending on $x(t)$, $V_L(t)$, $V_S(t)$, $V_R(t)$. Notice that, if both $\mathcal{X}$ and $\mathcal{B}$ are known, $\mathcal{Q}$ is univocally determined, since $\mathcal{Q} = \mathcal{Q}(\mathcal{X}, \mathcal{B})$.
Let T_s the period of $\mathcal{X}$, and T_q the period $\mathcal{Q}$. Then, the pair $\{\mathcal{X}, \mathcal{Q}\} = \{x(t), Q_S(t)\}$ generates a trajectory on the phase plane x-Q_S which is completely travelled in a time:

$$T_{QSM} \triangleq \mathrm{LCM}\left(T_s, T_q\right) \tag{1.14}$$

where $\mathrm{LCM}(\circ)$ is the *least common multiple*. Now introduce the ratio:

$$\Psi \triangleq \frac{T_s}{T_q} \tag{1.15}$$

and postulate a QSM whose dynamics is compatible with equations:

$$\begin{cases} x(t) = A\,\widetilde{\cos}\left[\dfrac{1}{\Psi}\left(\dfrac{2\pi}{T_q}t + \Phi\right)\right] \\ Q_S(t) = eN^*\,\widetilde{\cos}\left(\dfrac{2\pi}{T_q}t\right) \end{cases} \quad , \quad \begin{matrix} \Psi \in \mathbb{N} \\ \Phi \in (-\pi, +\pi] \end{matrix} \tag{1.16}$$

Strict sinusoidal functions are not required, thus the symbol $\widetilde{\cos}$, which represents any waveform characterized by a null average value. Consequently, equations (1.16) exemplify a QSM characterized by a somehow symmetric behavior. Limit our analysis to equations (1.16) may seem a rather reductive assumption; however, most systems behave in such a symmetric way †.

Characteristic parameters Ψ and Φ are respectively called *characteristic ratio* and *characteristic phase*, and directly control the topology and shape of the phase curve. Also, in a QSM for which (1.16) hold, Ψ and Φ play a fundamental role in determining the conduction properties of the system, specifically, they give strong hints on the magnitude of its shuttle current $\overline{I_s}$ ‡.

When $\Phi \sim 0$ or $|\Phi| \sim \pi$, the phase curve is diagonal and very narrow; whereas if $|\Phi| \sim \pi/2$, the curve encloses a larger area and is symmetric with respect to both axes. Also, the sign of Φ determines the direction of the phase curve. This direction determines the sign of $\overline{I_s}$: compatibly with the convention used in Section 2.1, $\overline{I_s} > 0$ (L to R current, which is R to L electron shuttle) if $\Phi \in (-\pi, 0)$, and vice versa if $\Phi \in (0, +\pi)$. Last, the curve presents $\Psi - 1$ self-crossings ‡† . From (1.12a), $\overline{I_s} \propto N_s$, but, compatibly with (1.12b) and from the symmetry constraints given by (1.16), $N_s = 2N^* \mathrel{\widetilde{\propto}} \left|Q_{S,0}\right|$, being $Q_{S,0} \triangleq \delta\big(x(t)\big)Q_S(t)$ the number of charge carriers (positive or negative depending on the motion direction) on the shuttling element S when it intersects the central cross-section (Fig.1.11). If Ψ is an even number, the phase curve presents a crossing in the origin, thus $Q_{S,0} = 0$ and $\overline{I_s} = 0$; instead, if Ψ is odd, the area (with sign) enclosed within the phase curve is roughly proportional to the shuttled electrons per cycle, so that $\mathcal{A} \mathrel{\widetilde{\propto}} N_s$ ‡‡.

† The QSMs presented in Chapters 3 and 4 follow, for example, (1.16). This point will be better disclosed in Section 2.2.7.

‡ Since, by definition, only the shuttle current depend on the motion regime, while the tunnel one is independent from it.

‡† An orbit in a phase plane cannot cross itself. Anyway, we are not dealing with orbits: since the state of a QSM is described by a triplet $\{x(t), \dot{x}(t), Q_S(t)\}$, we are merely considering its projection on a plane x-Q_S. This is a usual approach in QSM literature.

‡‡ Further details on this proportionality will be discussed in Section 2.2.8.

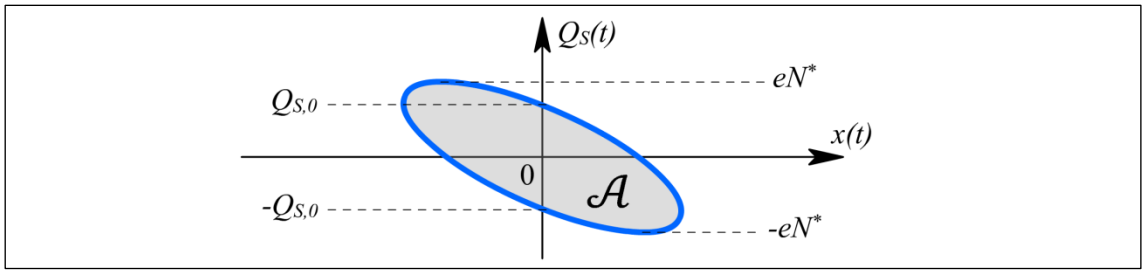

Figure 1.11 – *Qualitative representation of a QSM orbit shuttling $2eN^*$ electrons per cycle.*

In conclusion, this analysis can be used to compare systems characterized by the same oscillation period T_s and characteristic ratio Ψ. Consider two QSMs labeled with "1" and "2". Since $\mathcal{A} \approx N_s$ and, from (1.12a), $\overline{I_s} \propto N_s/T_s$, one obtains the following proportionality:

$$\frac{(\overline{I_s})_1}{(\overline{I_s})_2} \approx \frac{\mathcal{A}_1}{\mathcal{A}_2} \tag{1.17}$$

Relation (1.17) is very useful, since it allows to estimate the relative magnitude of the shuttle current $\overline{I_s}$ of two *isoperiodic* QSMs with a quick look at their phase plots.
In conclusion, Tab.1.2 summarizes the concepts described above with some examples.

Table 1.2 – *Overview of the shape of phase curves and magnitude of the shuttle current in correspondence of different combinations of parameters Ψ and Φ in formulae (1.16), with a sinusoidal waveform. Curve direction and self-crossings are highlighted in red.*

Φ \ Ψ	**1**	**2**	**3**	**4**
0	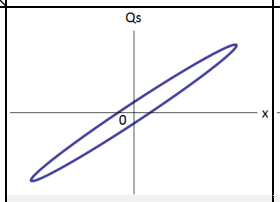 $\overline{I_s} \approx 0$	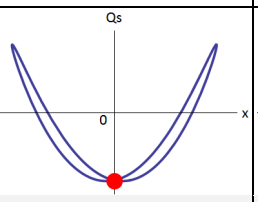 $\overline{I_s} = 0$	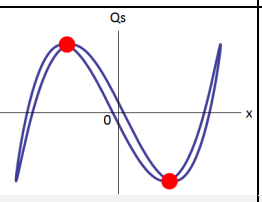 $\overline{I_s} \approx 0$	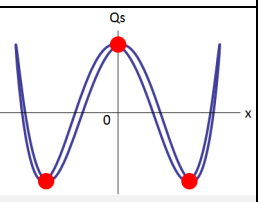 $\overline{I_s} = 0$
$\pi/2$	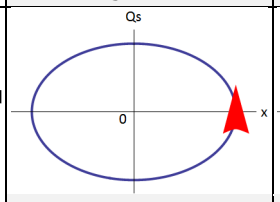 $\overline{I_s} < 0$	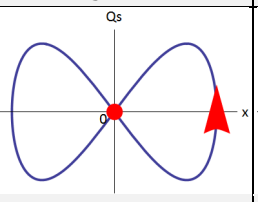 $\overline{I_s} = 0$	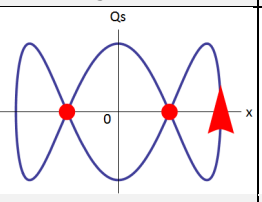 $\overline{I_s} < 0$	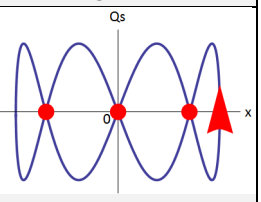 $\overline{I_s} = 0$
$\pm\pi$	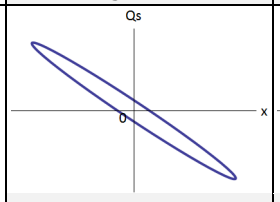 $\overline{I_s} \approx 0$	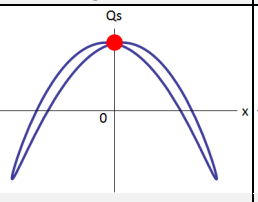 $\overline{I_s} = 0$	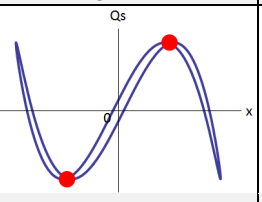 $\overline{I_s} \approx 0$	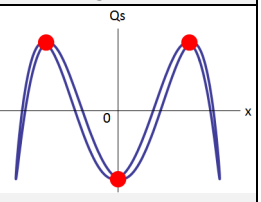 $\overline{I_s} = 0$
$-\pi/2$	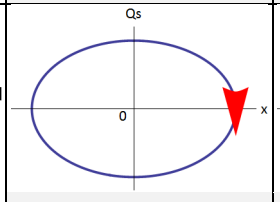 $\overline{I_s} > 0$	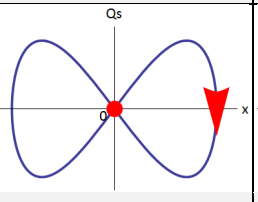 $\overline{I_s} = 0$	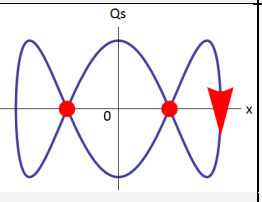 $\overline{I_s} > 0$	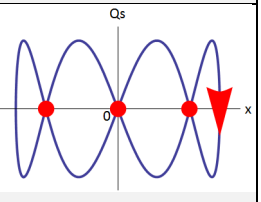 $\overline{I_s} = 0$

2.2.3 Induced and autonomous shuttle

Imagine the shuttling element of the prototype in Fig.1.10 with initial conditions $x(0) = A$ and $\dot{x}(0) = 0$. In the case $k > 0$, after a single oscillation, $\Delta\mathcal{E}_{out} \propto \gamma$ is the mechanically dissipated energy and $\Delta\mathcal{E}_{in}$ the work done on the shuttling element. Trivially, a competition $\Delta\mathcal{E}_{in} \lesseqgtr \Delta\mathcal{E}_{out}$ determines the increase or decrease of oscillations amplitude. When equilibrium is reached:

$$\Delta\mathcal{E}_{in} \equiv \Delta\mathcal{E}_{out} \tag{1.18}$$

and a permanent oscillating regime $\mathcal{X}$ is reached. It has to be remarked the existence of a shuttle current wholly relies on the chance to maintain in motion the shuttling element †.
Depending on how the energy $\Delta\mathcal{E}_{in}$ is supplied, the considered QSM is characterized by:

- *induced shuttle:* if $\Delta\mathcal{E}_{in}$ comes from a power source exterior to the scheme in Fig.1.10;
- *autonomous shuttle:* if $\Delta\mathcal{E}_{in}$ comes from the voltage boundary conditions $\mathcal{B}$.

These definitions match with the more generic ones given in the Introduction.
In turn, induced shuttle can be produced by:

- *forced oscillations:* $\mathcal{X}$ is partly determined;
- *controlled oscillations:* $\mathcal{X}$ is completely determined.

We anticipate here (from Section 2.2.6) that autonomous shuttle can either refer to:

- *self-excited oscillations*: limit-cycle oscillations with a periodic $\mathcal{X}$ can be established;
- *parametric resonance*: in a linear resonator, $\mathcal{X}$ can diverge.

Both induced and autonomous shuttle have been investigated in recent QSM literature. Shortly after the theoretical feasibility of self-excitation was demonstrated by Gorelik in 1998 [25], this was experimentally confirmed by Tuominen [68] using a metallic cluster shuttling element. The first autonomous device with a nanopillar geometry, due to the intrinsic larger size, was realized only in recent times by Blick [67]. Prior to this, Blick [26,31,32] and others [53] explored the shuttle mechanism by using a RCF (Resonant Coulomb Force) approach. They used a QSM characterized by a more complex architecture with respect to the prototypal one. A first pair of electrodes excite the shuttling element at half its height with an AC voltage, while the charge transport is operated at its tip between a second pair of electrodes, DC-biased instead (Fig.1.12).

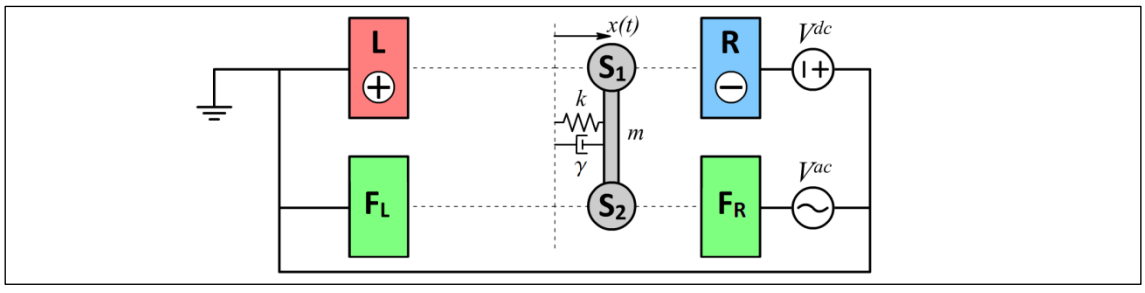

Figure 1.12 – *Circuital scheme of a shuttle device working using RCF.*

The dynamics of a QSM is described by the pair $\{\mathcal{X}, \mathcal{Q}\} = \{x(t), Q_S(t)\}$. In Section 2.2.2, we discussed how, if (1.16) hold, it is possible to obtain information on the shuttle current from $\mathcal{X}$ and $\mathcal{Q}$. However, in general, the conductive behavior $\mathcal{I}$ of a QSM is fully determined only if the boundary conditions $\mathcal{B}$ are also known: $\mathcal{I} = \mathcal{I}(\mathcal{X}, \mathcal{Q}, \mathcal{B})$. Thus, depending on the role $\mathcal{X}, \mathcal{Q}, \mathcal{B}$ play in (1.18), a subtler induced/autonomous definition can be introduced. Consider $\mathcal{I}$ the output of a QSM. Then, in the case of autonomous shuttle, the only input is $\mathcal{B}$, while in induced shuttle both $\mathcal{X}$ and $\mathcal{B}$ are the inputs. From now on, in this thesis, we'll focus on autonomous shuttle.

† In fact, if the shuttling element is at rest, only the tunnel current is present, and a QSM regresses in a DTJ.

2.2.4 Electromechanical coupling

Consider an autonomous QSM reaching a (stable) limit-cycle oscillation with amplitude A. The energy related to the vibrational state of the shuttling element is $\mathcal{E}_{mech} \triangleq kA^2/2$. Introduce:

$$\mathrm{K} \triangleq \frac{\Delta\mathcal{E}_{in}}{\mathcal{E}_{mech}} \tag{1.19}$$

Since, in autonomous shuttle, $\Delta\mathcal{E}_{in} = \Delta\mathcal{E}_{in}(\mathcal{B})$, then K is the ratio between an electrical and a mechanical energies. Consequently, of a QSM device, the value of K returns the magnitude of its *electromechanical coupling*. This is the complete casuistic:

- $\mathrm{K} = 0$ (*free oscillations*): all voltages are null, $V^{dc} = V^{ac} = V_G^{dc} = V_G^{ac} \equiv 0$.
- $\mathrm{K} \ll 1$ (*weak coupling*): damping ratio $\zeta = \gamma/2\sqrt{km} \ll 1$. Sinusoid-like oscillations.
- $\mathrm{K} \sim 1$ (*strong coupling*): $\zeta \sim 1$. Saw-tooth shape oscillations.
- $\mathrm{K} = \infty$ (*ballistic motion*): the restoring mechanical force is not present, $k = 0$.

Cases $\mathrm{K} = 0$ and $\mathrm{K} = \infty$ represent degenerate systems we are not going to deal with. Excluding them, having a weak coupling is important to develop approximated analytical solutions †.

2.2.5 Symmetry breaking and continuative oscillations

In autonomous shuttle the chances for a QSM to produce a macroscopic shuttle current relies on the feasibility of *limit-cycles*. In turn, a limit-cycle leads to a stable orbit characterized by a finite amplitude $A > 0$ whose existence requires two conditions:

- the presence of a certain *symmetry breaking* effect, to select the current sign;
- the chance to achieve *continuative oscillations*, depending on the energy balance (1.18).

We investigate the physical origin of both conditions, limiting the analysis to autonomous QSM.

In Section 2.2.2, by postulating a dynamics compatible (1.16), the curve direction sets the sign of the shuttle current, and both rely on the sign of Φ. Since, in autonomous QSMs, the only input is the set of boundary conditions $\mathcal{B}$, the symmetry of voltages application with respect to the cross-section in $x = 0$, plays a fundamental role in determining the sign of Φ:

$$\mathrm{sign}(\Phi) = \begin{cases} f(\mathcal{B}_{skew}) & \text{if } \mathcal{B} \text{ are not symmetric} \\ f(\mathcal{X}_0, \mathcal{Q}_0) & \text{if } \mathcal{B} \text{ are symmetric} \end{cases} \tag{1.20}$$

where $\mathcal{B}_{skew} = V^{dc}$ is the not symmetric part of $\mathcal{B}$; and $\mathcal{X}_0 = \{x(0), \dot{x}(0)\}$ and $\mathcal{Q}_0 = Q_S(0)$ the *initial conditions* of the system. In turn, the sign of Φ sets the *direction* of the shuttle current. On $\mathcal{B}$ also relies, in a less apparent way, the *magnitude* of the shuttle current.

In Section 2.2.3 we stressed the importance of the energy balance (1.18). In an autonomous QSM, the higher is the damping ratio ζ, the more the mechanical dissipation is huge, and in the balance (1.18), the term $\Delta\mathcal{E}_{out}$ is large. Therefore, the chance to achieve a continuative oscillations with finite amplitude $A > 0$ requires the injected energy $\Delta\mathcal{E}_{in}$ is large as well, thus, as stated in Section 2.2.4, on an appropriate voltage boundary conditions $\mathcal{B}$.

Summarizing the discussion above, in an autonomous QSM, the choice of the voltage boundary conditions $\mathcal{B}$ has a crucial role in determining both its *conductive properties* $\mathcal{I}$ (direction of current) and *dynamics* $\{\mathcal{X}, \mathcal{Q}\}$ (vibrational state and evolution of charges).

† In Section 4.1 we are going to deal with analytical averaging methods for which having a small electromechanical coupling guarantees for a better approximated solution.

2.2.6 Boundary conditions: direct and inverse shuttle

In Section 2.2.5, we discussed how the boundary conditions $\mathcal{B}$ influence the symmetry breaking in a QSM. Actually, depending on the kind of symmetry breaking provided by the applied voltages, the prototypal system in Fig.1.10 differentiates in two main kinds of QSM families:

- *Direct (ordinary) shuttle* ($V^{dc} \neq 0$, $V^{ac} = V_G^{dc} = V_G^{ac} = 0$): self-excitation
- *Inverse shuttle* ($V_G^{ac} \neq 0$, $V^{dc} = V^{ac} = 0$): parametric resonance

The just introduced classification is fundamental in the whole thesis. Terms "direct" and "inverse" arise from the relative role the shuttling element voltage V_S plays in determining the microscopic currents $I_L(t)$ and $I_R(t)$ in (1.7a,b). In the first case, a DC voltage $V \equiv V^{dc} \lesseqgtr 0$ is directly applied to L and R electrodes and the shuttling element maintains an intermediate voltage $V_L \lesseqgtr V_S(t) \lesseqgtr V_R$ whichever is its dynamical behavior: the value of V_S having a *passive* role. In the second case, an AC voltage $V_G^{ac} \lesseqgtr 0$ is applied to the gate G, directly modifying the voltage $V_S(t)$ also when it is in center position: since $V_L \equiv V_R = 0$, the role of $V_S(t)$ is *active*.

The definitions given above also state the chance to achieve continuative oscillation, in direct shuttle, is univocally provided by self-excitation (triggered by the DC bias voltage); and, in the case of inverse shuttle, it relies on parametric resonance (produced by the AC gate voltage). This situation is better explained by the schemes in Fig.1.13.

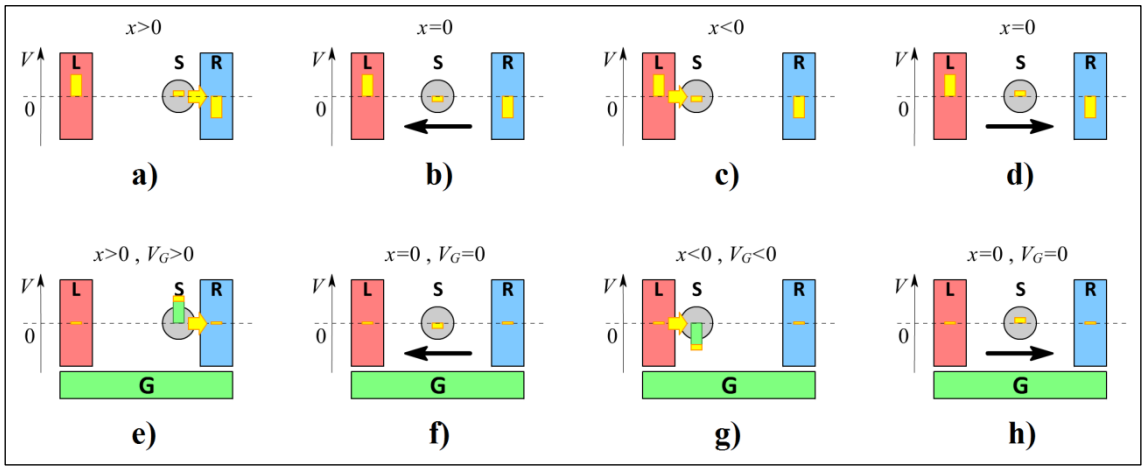

Figure 1.13: *Schematics of the different symmetry breaking effect in the case of direct shuttle (a-d) and inverse shuttle (e-h). In the first case (a-d), the current direction does not depend on the initial conditions, but only on the boundary conditions. The converse is for the second case (e-h).*

Another consideration discussion is related to (1.20). In direct shuttle, since $V^{dc} \neq 0$, the boundary conditions are asymmetric and the direction of electron shuttle depends on sign of $\mathcal{B}_{skew} = V^{dc}$ itself. In this case the current direction is trivially predictable, since a positive V^{dc} produces a positive $\overline{I_s}$ and vice versa. On the other hand, in the case of inverse shuttle, since the gate is at the center of the system, V_G^{ac} nor V_G^{dc} do not de-symmetrize the system and the current sign depends from initial conditions $\mathcal{X}_0 = \{x(0), \dot{x}(0)\}$ and $Q_0 = Q_S(0)$. Clearly, this dependence is more subtle and the shuttle current has a direction which is not trivially predictable.

Last, it is possible to conceive a combination of direct and inverse shuttle:

- *Hybrid shuttle:* $V^{dc} \neq 0$, $V_G^{ac} \neq 0$ (both *self-excitation* and *parametric resonance*)

In Chapter 3, the case of self-excited oscillations (direct shuttle) is analyzed, whereas in Chapter 4 parametric resonance (inverse shuttle) is considered. Finally, in Chapter 5 the possibility of achieving hybrid shuttle is outlined.

2.2.7 Shuttle mechanism: load/unload and oscillating transients

In previous sub-Paragraphs, the compatibility of a QSM to a dynamics as (1.16) was postulated. Here, we suggest with qualitative arguments how equations like (1.16) arise from the peculiar boundary conditions $\mathcal{B}$ in (1.5a,b) and the symmetry inherent to the schemes in Fig.1.10a,b.

Begin by considering *controlled* oscillations. Thus, one has $\mathcal{Q} = \mathcal{Q}(\mathcal{X}, \mathcal{B})$, being the electrodynamics of the system wholly determined by mechanical oscillations and voltage boundary conditions. Assume a "symmetric" $\mathcal{X} = x(t)$ compatible with the first of equations (1.16). Regarding the boundary conditions $\mathcal{B}$, analyze distinctly direct shuttle and inverse shuttle.

In the case of direct shuttle, $V^{dc} \neq 0$. The following discussion refers to $V^{dc} > 0$, but analogous arguments are valid with the converse sign. For the leads and shuttling element voltages, generally holds: $V_L = +V^{dc}/2 > V_S(t) > V_R = -V^{dc}/2$. Consider the following initial conditions: $x(0) = A > 0$ and $Q_S = eN^* > 0$. Referring to formulae (1.7a,b), the electrodynamics occurring in a single oscillation of period T_s can be schematized in four steps:

I) *Load transient*. Since $V_S < V_R$, a S-to-R current $I_R > 0$, relying on QT, is established, progressively rising the value of V_S. The current stops when $V_S = V_R$. During this transient, $-N_s = -2N^*$ electrons are "loaded" on S.

II) *Oscillating transient*. S moves towards L and reaches the same amplitude $x = -A < 0$.

III) *Unload transient*. Since $V_S > V_L$, a L-to-S current $I_L > 0$, relying on QT, is established, progressively reducing the value of V_S. The current stops when $V_S = V_L$. During this transient,$-N_s = -2N^*$ electrons are "unloaded" by S.

IV) *Oscillating transient*. S moves towards R and reaches the same amplitude $x = +A > 0$.

Consider now the case of inverse shuttle: $V_G^{ac} > 0$. The voltage of the shuttling element is capacitively influenced by the gate voltage and, in regime of small oscillations, one has $V_S(t) \approx V_G^{ac} \cos(\omega_G t)$. Instead, for the leads, $V_L = V_R \equiv 0$. Again, let the initial condition $x = A > 0$, $Q_S = eN^* > 0$. As it is detailed in Fig.1.14, one can notice that, under the assumption $\omega_G \approx 2\pi/T_s$, the electrodynamics for a QSM exhibiting inverse shuttle follows the same phenomenology described above in the case of direct shuttle, summarized by steps I-IV.

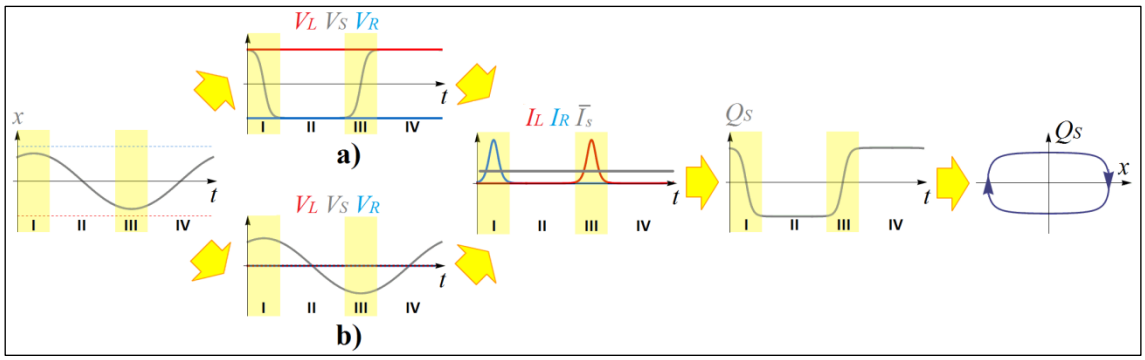

Figure 1.14 – *A self-excited (a) and a parametric resonant (b) QSMs exhibit similar shuttle mechanism if, in the second case,* $V_G(t) = V_G^{ac} \cos(\omega_G t)$ *with* $\omega_G \approx 2\pi/T_s$.

By now, we considered controlled oscillations in which a law $\mathcal{X} = x(t)$ was imposed. Now refer to autonomous oscillations: as detailed in Section 2.2.5, the requirement to maintain continuative oscillations in presence of a damping $\gamma > 0$, is that the shuttling element receive an energy $\Delta\mathcal{E}_{in}$ sufficient to compensate a mechanical dissipation $\Delta\mathcal{E}_{out}$. Such energy is supplied by the boundary conditions $\mathcal{B}$ and guarantees a constant amplitude A. This holds since, after every load/unload transient, the shuttling element tends to reach the same voltage of the close electrode. Thus, neglecting induction attraction, it receives an impulse due to the electrostatic repulsion. This guarantees the existence of stable orbits representing continuative oscillations.

Summarizing, we analyzed with qualitative arguments how the phenomenology exemplified by steps I-IV can produce microscopic currents $I_L(t)$ and $I_R(t)$ which, integrated over a cycle of oscillation, establish a not null macroscopic current $\bar{I}$. We underlined the not trivial fact that, QSMs in which the continuative oscillation are produced by different phenomenologies – self-excitation or parametric resonance – share this peculiar electrodynamics in at least some cases.

One can be interested to discern which part of the macroscopic current $\bar{I}$ comes from the shuttle contribution. The answer is that it is completely due to the shuttle part $\bar{I}_s$, since the described phenomenology comprises two steps which rely on the motion of the shuttling mass. Therefore, steps I-IV are called *shuttle mechanism*. It has to be remarked the shuttle mechanism is not a prerogative of nanoscale QSMs, but it also applies, with minor differences, to macroscopic SMs. In fact the scheme introduced in Fig.IIIa,b,c,d to depict the working principle of a SM can refer as well to the transients I,II,III,IV of a QSM. The only difference is that, in a SM, during load (I) and unload (III) transients, the charge transfer between the shuttling element and the leads physically relies on *contact*, while in a QSM it usually † depends on QT (Tab.I).

In Fig.1.14, the evolution of Q_S as a consequence of an autonomous oscillating motion and the imposed boundary conditions in shown, so that a relation $\mathcal{Q} = \mathcal{Q}(\mathcal{X}, \mathcal{B})$, leading to motion equations of the kind of (1.16) is no more postulated, but demonstrated as *feasible*. Referring to such equations, the first phase plot in Fig.1.14 corresponds to the curve sketched in Tab.1.2 in correspondence of $\{\Psi, \Phi\} = \{1, -\pi/2\}$. From the discussion above, in the case of direct shuttle (self-excited QSM) a characteristic ratio $\Psi = 1$ is *the only* possibility, whereas inverse shuttle (parametric resonant QSM) is compatible with *every* $\Psi \in \mathbb{N}$, depending on the choice of ω_G.
A last difference involves the chance of *quadrature* between $x(t)$ and $Q_S(t)$, which corresponds to a characteristic phase $\Phi = \pm\pi/2$: this condition is important since, as it is clear from Tab.1.2 and relation (1.17), it *maximizes* the value of the shuttle current. Notice that, in direct shuttle, the establishment of a limit-cycle *automatically* tends to $\Phi \approx \pm\pi/2$; instead, in inverse shuttle, the situation is more complex and will be analyzed in detail in Chapter 4.

To conclude, Tab.1.3 is a summary table of the QSMs classifications introduced up to this sub-Paragraph, and the conductive properties they give on such systems.

Table 1.3 – *Overview of the main QSMs classifications.*

Kind of QSM	**Nature of oscillations**	**Symmetry breaking provided by…**	**Energy to the shuttling element coming from… [×: required, ∘: optional]:**						**Allowed values of characteristic parameters (if small K) [$n \in \mathbb{N}$]**		**Chance to produce shuttle current**
			voltage boundary conditions ($\mathcal{B}$)				**external source**				
			V^{dc}	V^{ac}	V_G^{dc}	V_G^{ac}	F_S	x	**Θ**	**Φ**	
autonomous	*self-excited*	$\mathcal{B}_{skew}$	×						1	$\pm\frac{\pi}{2}$	yes
	parametric resonance	$\mathcal{X}_0, \mathcal{Q}_0$			×	∘			$2n+1$	$f(\mathcal{B})$	yes
									$2n$	$f(\mathcal{B})$	no
induced	*forced*	-	∘	∘	∘	∘	×		n	$f(\mathcal{B}, F_S)$	yes
	controlled	-	∘	∘	∘	∘		×	n	$f(x)$	yes
at rest		-	∘	∘	∘	∘			-	-	no

† Actually, collisions between the shuttling element and the electrodes may occur, and occasionally the charge transfer relies on contact also in the case of a QSM. Collisions are usually present in a strong electromechanical coupling.

2.2.8 Soft and hard shuttle regimes

In Section 2.2.1, we introduced to the concepts of shuttle and tunnel current, and underlined how the macroscopic current (1.9) in a QSM is in general the sum of these two contributions.
In Section 2.2.2 we discussed how a dynamics described by equations (1.16) leads to a shape of the phase curves x-Q_S which are compatible, in principle, with the existence of a shuttle current.
Last, in Section 2.2.7 we argued how the shuttle mechanism I-IV can produce, in autonomous QSMs, a dynamics like (1.16), and thus we highlighted the actual feasibility of a shuttle current.
On the other hand, the presence of a tunnel current cannot be directly recognized from phase curves x-Q_S . Since it is defined as the part of current not relying on the oscillating motion of the shuttling element, the tunnel current can be imagined as the current which can pass from L to S and from S to R in a time scale small compared to that of the oscillation of the shuttling element. In this scenario, one could relate the ratio between shuttle and tunnel current contributions to a ratio between the period of oscillation and the characteristic time of the QT.
The first one is provided by relation (1.12a) $\overline{I_s} \propto f_s = 1/T_s$. Introducing $\overline{I_t} \propto 1/T_t$, we also need a relation for the QT time scale T_t. In analogy with an RC circuit it is: $T_t = C_S(0)/G_{L,R}(0)$ which represents the time constant of the DTJ constituted by a QSM with the shuttling element at rest in the center, $C_S(0)$ calculated from (1.4) and $G_{L,R}(0) \triangleq G_L(0) \equiv G_R(0)$ from (1.8a,b). Thus, a raw but effective estimation of the ratio between tunnel and shuttle currents is:

$$\frac{\overline{I_t}}{\overline{I_s}} \propto \frac{T_s}{T_t} = \frac{G_{L,R}(0)}{f_s C_S(0)} \tag{1.21}$$

This formula suggests to introduce a distinction among QSMs depending on such ratio. Consider the following definitions:

- *Soft shuttle regime:* $G_{L,R}(0) > f_s C_S(0)$
- *Hard shuttle regime:* $G_{L,R}(0) < f_s C_S(0)$

This classification was first suggested by Isacsson and Gorelik [27] and is largely used in electron shuttle literature. Originally, the soft/hard distinction – whose names arise from the theory of oscillations [110] – was introduced to underline the different transition from a stable rest condition a stable orbit by increasing the applied voltage V_{dc}. It is a fundamental point, but, since it exclusively applies to the case of self-excited QSMs, it is discussed in Section 2.2.11 and validated in Chapter 3. Here, we limit our analysis on the soft/hard distinction by considering the consequences produces in *both* self-excited and parametric resonant cases.

First of all, in this thesis, we often refer to hard regime by stretching a little the definition and considering $G_{L,R}(0) \ll f_s C_S(0)$. In this way, it is possible to introduce an *hard regime approximation* consisting in the assumption $\overline{I_t} = 0$, which means only the shuttle current $\overline{I_s}$ is present. By relating formulae (1.9) and (1.12a), a useful relation is obtained:

$$\bar{I} \triangleq \frac{1}{\Delta t}\int_{t_0}^{t_0+\Delta t} I_L(t)\,dt \equiv \frac{1}{\Delta t}\int_{t_0}^{t_0+\Delta t} I_R(t)\,dt \approx eN_s f_s \triangleq \bar{I}_s \tag{1.22}$$

Referring to the prototypal schemes in Fig.1.10, analyze which physical properties of a QSM influence terms f_s, $C_S(0)$ and $G_{L,R}(0)$. Oscillation frequency f_s and shuttling element capacitance $C_S(0)$ are respectively inversely and directly proportional to the scale of the device d, making their product $f_s C_S(0)$ independent from d and roughly of the order of $10^{-9}\,S$. Therefore, the soft/hard regimes distinction relies on having a tunnel conductance larger or smaller than a threshold value $G^* \approx 10^{-9}\,S$. In the term $G_{L,R}(0) = G_t(d - r, \Delta V)$, ΔV is alternatively

given by the magnitude of the bias voltage V^{dc} (if direct shuttle) or the AC signal from the gate V_G^{ac} (if inverse shuttle). From Fig.1.2, the typical G^* corresponds to distances and voltages of a few *nanometers* and *volts*, respectively. Assuming constant voltages, soft QSMs are characterized by smaller scales whereas hard ones are larger (but still NEMS). Also, the dependence from V makes the soft/hard distinction not connate with the specific QSM embodiment, and a system in hard regime can, in principle, undergo a soft regime and vice versa.

The two limit cases of soft and hard regimes delimit the range of existence of a proper QSM. The soft limit $G_{L,R}(0)/f_s C_S(0) \to \infty$ is represented by a DTJ , since the island is at rest and $f_s = 0$. On the other hand, a SM exemplifies the hard limit $G_{L,R}(0)/f_s C_S(0) \to 0$ since, in it, d is macroscopic and $G_{L,R}(0) = 0$. Notice how, even when the hard regime approximation (1.22) can be applied to a QSM, it still not similar to a SM, since charge transport still relies on QT (although inopportune collisions with the leads are more frequent than in soft QSM).

A QSM in soft regime can be characterized, from (1.21), by a considerable tunnel contribution to the overall current (1.9). However, the presence of such current does not affect the phase plot, since, by definition, it does not depend on oscillations. The tunnel current physically relies on the chance of having short tunnel from L to S and from S to R (or vice versa), that is a stationary current $I_t(t) \approx \min[I_L(t), I_R(t)]$ which does not produce any increment nor decrement of the shuttling element charges $Q_S(t)$. Therefore, in a QSM characterized by soft regime, the shuttle mechanism discussed in Section 2.2.7 is not directly influenced by the tunnel current.

However, the typical evolution of $Q_S(t)$ and the shape of phase curves on the plane x-Q_S are distinguishable in the soft/hard cases, since differences arise by a more or less sharp occurrence of the microscopic currents (1.7a,b). In particular, the competition between mechanical and electrodynamical characteristic times and the peculiar QT dependence from distance together manifest by differentiate the power relationships among durations of the shuttle mechanism steps. Let introduce them as T_I, T_{II}, T_{III}, T_{IV}, respectively referred to steps I,II,III,IV, being T_s the whole the period of oscillation. Respectively referring to a soft QSM, hard QSM and the hard limit exemplified by a macroscopic SM, the following casuistic stands:

$$T_I = T_{III} \approx T_s \tag{1.23a}$$

$$T_I = T_{III} \ll T_s \tag{1.23b}$$

$$T_I = T_{III} \approx 0 \tag{1.23c}$$

In (1.23c), the charge transfer relies on contact. Trivially, in each case, $T_{II} = T_{IV} \approx T_s/2$.

A concept strictly related to the transients duration is that of tunneling region. Referring to Fig.1.11, the region $\mathcal{O}$ in which S oscillates is delimited by L and R, thus, for a stable orbit, $x(t) \in \mathcal{O}$. Directly from the definition, in soft regime, the tunneling conductance G_t is relevant even when $x(t) \approx 0$: this means the load/unload regions *overlap*, since there's a region of space around $x = 0$ interested by *both* load and unload transients. In hard regime, instead, load/unload regions do not overlap, and in the hard limit (SM), these regions degenerate in a pair of points. Introduce the *tunneling region* $\mathcal{T}$ as the region of space where either load or unload transients happen. Then the following casuistic respectively refers to soft QSM, hard QSM and SM †:

$$\mathcal{T} \equiv \mathcal{O} = [-d + r, d - r] \tag{1.24a}$$

$$\mathcal{T} = \mathcal{O} \setminus [-A_t, A_t] \tag{1.24b}$$

$$\mathcal{T} = \{-d + r, +d - r\} \tag{1.24c}$$

† A certain abuse of notation is used in (1.24c), since in a SM, the charge transport does not rely on QT but on contact.

The effect of relations (1.23a,b,c) on the duration of the shuttle mechanism steps are qualitatively highlighted in Fig.1.15, where the different shapes in a stable orbits phase curve are highlighted in the case of hard and soft oscillations.

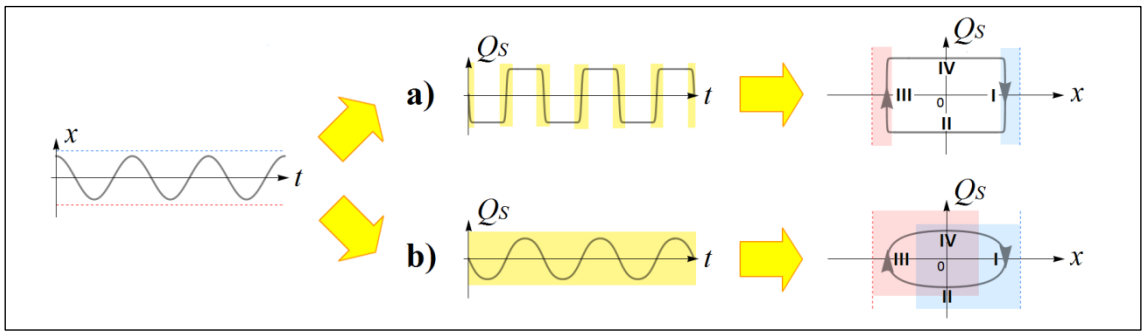

Figure 1.15 – *Qualitative scheme depicting the phase plot representation of stable orbits in the case of: (a) hard and (b) soft oscillations. In the soft case, the load and unload transients partly overlap.*

Similarly, the effect of relations (1.24a,b,c) on the width of the tunneling region is qualitatively highlighted in Fig.1.16, again in the case of hard and soft oscillations.

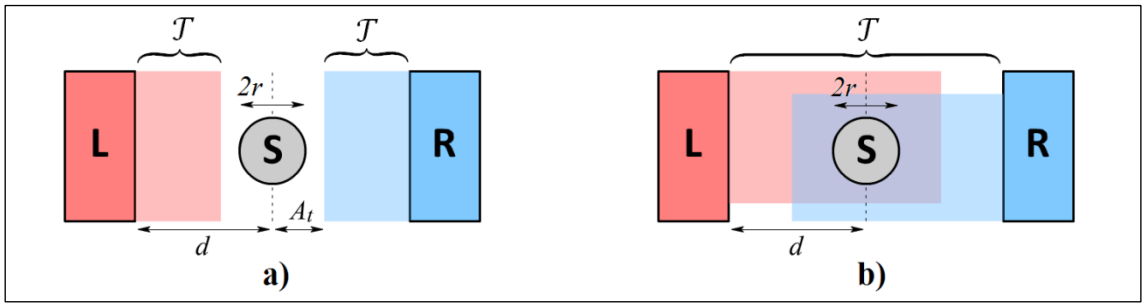

Figure 1.16 – *Qualitative scheme showing the tunneling region $\mathcal{T}$ in: (a) hard and (b) soft oscillations.*

In general, the electrodynamics $\mathcal{Q} = Q_S(t)$ of a QSM depends from the vibrational state $\mathcal{X} = x(t)$ and the voltage boundary conditions $\mathcal{B}$: thus $\mathcal{Q} = \mathcal{Q}(\mathcal{X}, \mathcal{B})$. However, assuming a strict validity of relations (1.24) a powerful approach for the analytical study of a QSM is proposed, in which a simplified dependence $\mathcal{Q} = \mathcal{Q}(\mathcal{B})$ holds. It is called *two-states approximation*. First, take into account the following approximations †:

$$\begin{cases} \forall\ t^*/x(t^*) \in \mathcal{T} & \Longrightarrow \quad Q_S(t^*) \approx C_S(0)\left[V_S(t^*) - V_{L,R}(t^*)\right] \\ \forall\ t^*/x(t^*) \notin \mathcal{T} & \Longrightarrow \quad \dot{Q}_S(t^*) \approx 0 \end{cases} \tag{1.25}$$

In other words, we are assuming that, when $x \in \mathcal{T}$, the characteristic QT frequency is much larger than the mechanical one ($G_{L,R}(x)/C_S(x) \gg f_s$), and vice versa ($G_{L,R}(x)/C_S(x) \gg f_s$) if $x \notin \mathcal{T}$. This means a QSM behaves in a "very soft" way inside the tunneling region, and "very hard" outside. This vision is not in contradiction with the definition of soft/hard regimes. In fact, it refers to the quantities $G_{L,R}(0)$ and $C_S(0)$, thus giving an "average" softness/hardness of a QSM; whereas (1.25) deals with the instantaneous soft/hard behavior of a QSM, which depends on $G_{L,R}(x)$ and $C_S(x)$. A simple interpretation of (1.25) is that the charge on the shuttling element $Q_S(t)$ follows the voltage boundary conditions *where possible*, that is in correspondence of the region in which the electrodynamical time scale is small compared to the mechanical one.

† The term $V_{L,R}$ can alternatively refer to one of the electrodes L or R depending on the load/unload transient considered.

The approach consists in assuming a neat alternation ("two states") of formulas (1.25), in place of the real physics, which clearly relies on a smooth transition between the two limit considered cases. Though, this approximation is rather effective in many cases.

Refer to the symmetric dynamics given by equations (1.16), and start by considering a QSM in soft shuttle regime. From (1.24a), the tunneling region $\mathcal{T}$ coincides with the whole oscillation volume $\mathcal{O}$, so that the first condition of (1.25) applies $\forall\, t \in \mathbb{R}$. Consequently, the system dynamics is described by equations:

$$\begin{cases} x(t) = A\,\widetilde{\cos}(\omega t + \Phi) \\ Q_S(t) \approx C_S(0)\big[V_S(t) - V_{L,R}(t)\big] \propto \widetilde{\cos}(\omega t) \end{cases} \tag{1.26}$$

These equations are valid in direct as well inverse shuttle, due to the somehow similarity in their electrodynamics consequent to the different voltage application, as has been highlighted in Fig.1.14. In particular, in direct shuttle, V_L and V_R are constant and $V_S(t)$, due to the peculiar electrostatics of the QSM, oscillates with a radian frequency *constrained* by the mechanical $\omega = 2\pi f_s$: thus $Q_S(t)$ and $x(t)$ are necessarily *synchronized*, meaning $\Psi = 1$. Instead, in inverse shuttle, by applying (1.6), one has $V_S(t) \propto V_G(t) = V_G^{ac}\cos(\omega_G t)$, while $V_L = V_R \equiv 0$; thus, $Q_S(t)$ oscillates with a *free* frequency depending on the choice of ω_G . As highlighted in both Section 2.2.2 and Tab.1.2, only the cases $\omega_G = \Psi\omega$ with Ψ an odd number can produce a macroscopic shuttle current $\bar{I}_s$; otherwise, the microscopic currents $I_L(t)$ and $I_R(t)$ exist, but the net charge transport in a cycle is *null*. This discussion confirms the qualitative analysis performed at the end of Section 2.2.7 on the allowable values of Ψ in direct and inverse shuttle.

Now consider a QSM in hard shuttle regime. This time, from (1.24b), both options of (1.25) distinctly apply during each cycle of oscillation, thus the second equation of (1.26) is valid only when $x(t) \in \mathcal{T}$; otherwise, when the shuttling element passes near the center in the zone $x(t) \in (-A_t, A_t)$, one has $\dot{Q}_S(t) \approx 0$. An interesting consequence of this fact holds in the case of inverse shuttle. In fact, by choosing $\omega_G = \Psi\omega$ with $\Psi = 3$ (or larger odd numbers, depending on how much the tunneling region is wide), the electrodynamics $\mathcal{Q}$ exhibited by the system is the same of the case $\Psi = 1$, because the further oscillations of voltage happen when $x(t) \notin \mathcal{T}$ and $Q_S(t)$ remains substantially fixed. This curious phenomenology is explained in Fig.1.17.

Last, approach (1.26) applies as well to the hard limit case (exemplified by a SM). In this, (1.24c) hold, and the situation is complementary to the case of a soft QSM, since the second option of (1.26) never applies except when the shuttling element hits the leads. In that instant, its charge level is refreshed to a value proportional to the voltage of the leads $V^{dc} = V_L - V_R$ (due to the device scale, it is not possible to consider the inverse shuttle phenomenology).

In conclusion, the shuttle mechanism requires oscillations for which $A \in \mathcal{T}$. Therefore, in order to exhibit a shuttle current, a QSM has to reach the tunneling region (*activation problem*).

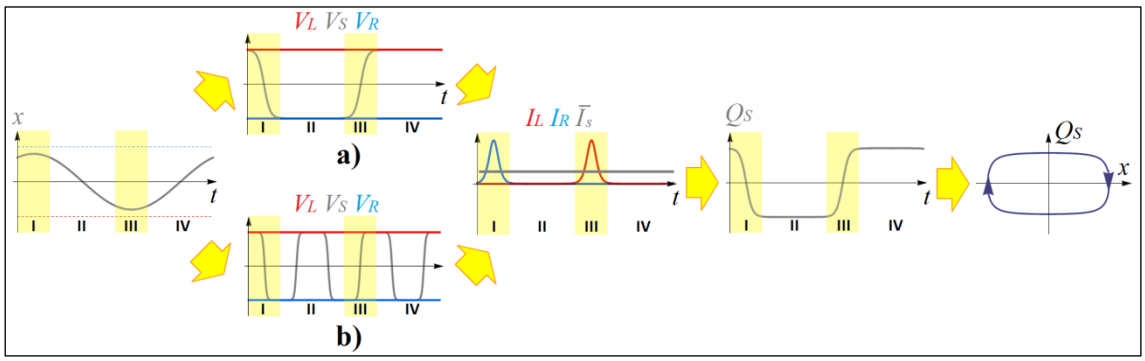

Figure 1.17 – *A QSM subjected to hard oscillations for which (a)* $\Psi = 1$ *, exhibits a dynamics similar to that with odd topology indexes, like (b)* $\Psi = 3$ *.*

2.2.9 Capacitance of the shuttling element and transport factor

The self-capacitance C_S of the shuttling element S is an important feature in a QSM. Since C_S is directly related to the amount of charge carriers N^* which S can contain †, when other parameters are fixed, it returns an estimation of the maximum shuttle current obtainable:

$$\max(\bar{I}_s) \propto N^* \propto C_S \tag{1.27a}$$

Actually, being calculable from formula (1.4), C_S is a function of the position $x(t)$ ‡, and has to be referred to a value $\bar{A}$ corresponding to the average of amplitudes weighted on the magnitude of microscopic currents flowing, thus $\bar{A} \in \mathcal{T}$. However, due to the exponential dependence of QT from distance, one can say $\bar{A} \approx A$. From this, (1.27a) can be written in a more precise form:

$$\max(\bar{I}_s) \propto eN^*(A) \approx C_S(A)\left|V_S(t) - V_{L,R}(t)\right|_{t\to t^*/x(t^*)=A} \tag{1.27b}$$

This relation can be put into relation with the formula (1.12a) for the actual shuttle current $\bar{I}_s$. Blick, in [37], introduced the *transport factor* η as the ratio between these two quantities:

$$\eta \triangleq \frac{\bar{I}_s}{\max(\bar{I}_s)} = \frac{N_s}{N^*(A)} \leq 1 \tag{1.28}$$

This definition assumes an evident engineering importance since η can be considered as a sort of *efficiency* of the shuttle mechanism. In general, the flux of electrons on/from the shuttling element would continue until a potential difference $\left|V_S - V_{L,R}\right| \to 0$. If this is the case, the dynamics is maximal efficient and S shuttles the maximum amount of electrons it could contain per cycle, leading to $\eta = 1$. Otherwise, mechanical limitations do not allow the potential difference to vanish, and S shuttles only a fraction $\eta < 1$ of the electrons it could contain.

The strict relation between N_s and $N^*(A)$ is more clear by collecting formulae (1.12a), (1.12b) and using definition (1.28)

$$\bar{I}_s = \frac{1}{T_s}\int_{t_0}^{t_0+T_s} \delta\big(x(t)\big)\dot{x}(t)Q_S(t)\,dt \approx eN_s f_s = 2\eta eN^*(A)f_s \tag{1.29}$$

It has to be remarked the proposed definition (1.28) for η is rather operative. Obtain an accurate prediction of η is often problematic, as stressed in [37]. An analytical estimation of η arises by comparing the charge carriers transferred during a load/unload transients, $N_{I,III}$, with $N^*(A)$. Consequently, if $N_{I,III} \approx 2N^*(A)$, then $\eta = 1$; whereas if $N_{I,III} < 2N^*(A)$, one has $\eta < 1$.

Consider a QSM in hard shuttle. In this case, the load and unload tunneling regions do not overlap, thus, one can calculate $N_{I,III}$ by integrating either (1.7a,b):

$$N_{I,III} = \frac{1}{e}\int_{T_{I,III}} G_{L,R}(x)\left|V_{L,R}(t) - V_S(t)\right| dt > 0 \tag{1.30a}$$

† The quantity N^* was first defined in the Introduction and used in both relations (III) and (IV) as $N^* = 2Srn^*$, being $2Sr$ the shuttling element volume. Here, we refer to a more strict meaning.

‡ In the regime of small oscillations, C_S can be considered constant and posed equal to $C_S(0)$, this value roughly proportional to the diameter of the shuttling element $2r$. However, directly from (1.24a,b), small oscillations for which $A \ll d - r$ are compatible with a shuttle mechanism producing a shuttle current $\bar{I}_S \neq 0$ only in the case of soft shuttle, where charge transfer occurs also when $x(t) \approx 0$. Therefore, assuming $C_S \approx C_S(0)$ in (1.27a) is, in general, not allowed.

The tendency to have an inefficient shuttle, thus, from (1.30a), a relatively small $N_{I,III}$, relies on: i) brief transients $T_{I,III} \propto 1/f_s$, ii) small conductances $G_{L,R}(x)$, iii) small bias voltage $|V_S - V_{L,R}| \approx V/2$. On the other hand, from (1.27b), a large $N^*(A)$ depends on: iv) large $V/2$, v) large self-capacitance $C_S(A)$. Summarizing, the following estimation holds for η in hard QSMs:

$$\eta \propto \frac{N_{I,III}}{2N^*(A)} \propto \frac{G_{L,R}(A)}{f_s C_S(A)} \approx \frac{G_{L,R}(0)}{f_s C_S(0)} e^{\frac{A}{\lambda(V)}} \tag{1.31}$$

where, in the last passage, relation (1.1b) has been used. Formula (1.31) makes clear that, comparing two hard QSMs characterized by the same ratio $G_{L,R}(0)/f_s C_S(0)$, inefficient shuttle is more feasible for smaller tunneling lengths $\lambda(V)$, which, in turn (Appendix A) relies on having a small bias voltage V. When this condition occurs, it is called *hard inefficient shuttle*.

Now consider a QSM in soft shuttle. This time, the load and unload tunneling regions partly overlap, therefore the expression for $N_{I,III}$ combines both (1.7a,b):

$$N_{I,III} = \frac{1}{e}\int_{T_{I,III}} |G_L(x)[V_L(t) - V_S(t)] - G_R(x)[V_S(t) - V_R(t)]|\, dt > 0 \tag{1.30b}$$

In (1.30b), it is not trivial relate a small $N_{I,III}$ with quantities $G_{L,R}(0)$, f_s, $C_S(0)$ and λ. However, if $\lambda > d$, load/unload tunneling regions completely overlap, and, in the soft limit $\lambda \gg d$, load and unload transients are completely merged, thus $N_{I,III}$ vanishes. Since λ depends on the applied voltage, the tendency $\lim_{V\to\infty} \eta = 0$ holds. In conclusion, in soft QSMs, a $\eta < 1$ depends on having an extremely large bias voltage V: this is called *soft inefficient shuttle*.

In Fig.1.18, the qualitative comparison between efficient ($\eta = 1$) and inefficient ($\eta < 1$) phase curves in the case of soft and hard QSMs is shown.

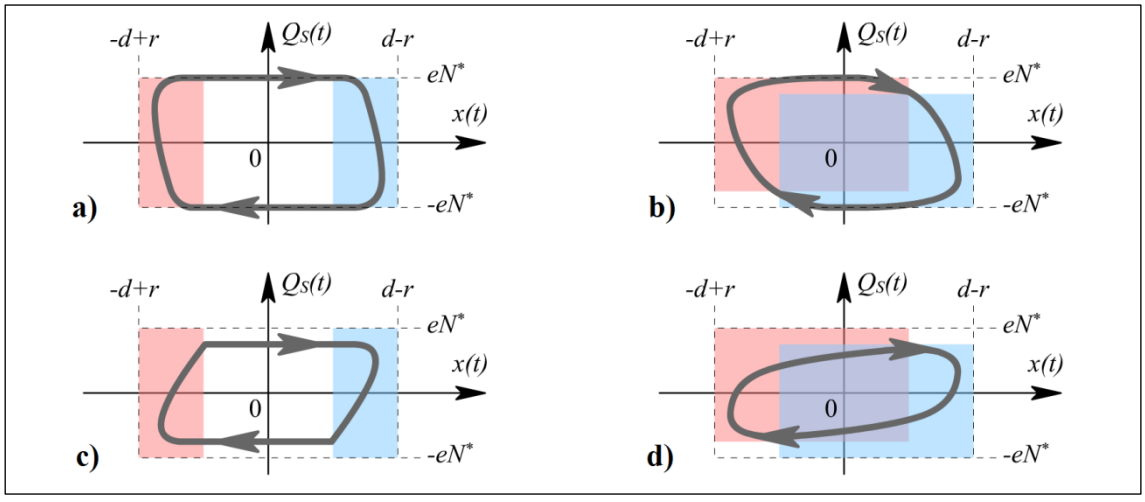

Fig.1.18 – *Typical phase plots for: (a) hard, (b) soft efficient shuttle; (c) hard, (d) soft inefficient shuttle.*

In conclusion, when $\eta < 1$, the continuity of oscillations can be prejudiced. Specifically, the power supply on the shuttling element can be no more sufficient to sustain the current vibrational state (energy balance (1.18)) and the amplitude of oscillation is reduced due to a low transport factor. When η is smaller than a certain threshold, a *saturation* of the shuttle mechanism occurs, and both the vibrational state and shuttle current stop. In the case of *hard saturation*, this risk depends on a small bias voltage V, and the amplitude abruptly reduces from A_t to 0. Instead, *soft saturation*, may occur at extremely high V, and the amplitude smoothly goes to 0.

2.2.10 Effects of Coulomb Blockade

In Sections 1.1.2 and 1.1.3 the effect of CB respectively in a TJ and a DTJ, have been analyzed. Since the architecture of a three-terminal QSM is analogous to a DTJ in which the island can move, relations (1.3a,b,c) directly generalize † into:

$$\frac{e^2}{C_S(x)} \gg k_B\Theta \tag{1.32a}$$

$$\frac{h}{e^2} \gg G_{L,R}(x) \tag{1.32b}$$

$$\left|V_S - V_{L,R}\right| < \frac{e}{C_S(x)} \tag{1.32c}$$

The dependence of QT conductances and shuttling element capacitance from the position $x(t)$ states an important point. In a QSM, differently from a TJ or a SET, once the physical parameters are fixed, the presence of CB is no more a general feature of the system, but it is a property exhibited in some portions of the oscillation region. In fact, from (1.32a,b,c) directly follows the definition of an amplitude $A_{CB} \in [0, d-r]$ for which, when $x(t) \in [0, A_{CB}]$, one has $I_L(t) = I_R(t) \equiv 0$. Therefore, in presence of CB, the abstract concept of the tunneling region $\mathcal{T}$ introduced in (1.24a,b,c) can be redefined in a more physically reasonable manner, assuming $A_t = A_{CB}$, so that $\mathcal{T} = \mathcal{O} \setminus [-A_{CB}, A_{CB}]$, being $\mathcal{O} = [-d+r, d-r]$. By referring conditions (1.25) to this new definition for $\mathcal{T}$, the approximated analytical approach (1.26) is far more feasible to return accurate estimations of the actual system dynamics. In fact, in presence of CB, the second equation of (1.25) become *exact*, since current is actually inhibited.

Clearly, as in a TJ or a SET, the troublesome CB requirement is (1.32a), for which only QSMs relatively small (with respect to temperature) are characterized by a value $A_{CB} > 0$. Notice that, also when a QSM has a relevant CB effect, it does not affect its working principle.

Consider a QSM. Assume we are interested to the electrical characterization of the device considered as a black-box. Analyze direct (or inverse) shuttle, vary the voltage V^{dc} (or V_G^{ac}) and detect the consequent L-to-R macroscopic current. In this, both shuttle $\overline{I_s}$ and tunnel $\overline{I_t}$ contributions exist and, from the arguments made in Section 2.2.1, these two parts are experimentally undistinguishable. Plotting the *I-V* curve, one of the following behaviors are detected:

I) if $A < A_{CB}$, no current passes;
II) if $A > A_{CB} > 0$ then a Coulomb staircase effect appears;
III) if $A > A_{CB} = 0$ the *I-V* curve is smooth.

Notice that the interpretation of points I),II) and III) is not trivial at all. In fact, since in general A_{CB} is a function of the voltage boundary conditions $\mathcal{B}$ and the system geometry $\mathcal{G}$, one has $A_{CB} = A_{CB}(\mathcal{B}, \mathcal{G})$, and the same system can be characterized a single *I-V* curve in which more behaviors among I)-II)-III) are exhibited, depending on the applied voltage V.

First, consider a system in which at least one of (1.32a,b) do not hold in $x = 0$. In this case, the *I-V* curve presents a behavior III) for every boundary condition, even when low values of the applied voltages accomplish condition (1.32c). In this case, CB effects do not manifest at all.

† This generalization of the CB requirements from relations (1.3a,b,c) for a DTJ to position-dependent (1.32a,b,c) is somehow analogue to the less strict definition of the soft/hard character of a QSM involving the instantaneous ratio $G_{L,R}(x)/f_sC_S(x)$, compared to of the conventional, less general definition $G_{L,R}(0)/f_sC_S(0)$. Like in such case, in fact, by referring (1.32a,b,c) to the center position $x = 0$, (1.3a,b,c) are obtained.

Then, consider a system in which both (1.32a,b) hold in $x = 0$. A more composite situation arises. Near the origin, (1.32c) is surely achieved, and the I-V curve exhibits the behavior I) . In autonomous QSMs, the applied voltage affects the amplitude of oscillation, usually in a monotonic way, with V^{dc} (or V_G^{ac}) related with requirement (1.32c), and A with (1.32b) and, less strictly, with (1.32a). By increasing V^{dc} (or V_G^{ac}), the first condition which ceases to be accomplished is (1.32c), then behavior ii) appears and, if amplitude of oscillation is monotonic with the voltage, behavior iii) is definitely reached. Instead, in the case the first requirement to be ceased is one of (1.32a,b), then the system transits *directly* from I) to III).

In Fig.1.19 the described scenario, in which zero, one or two threshold values for the voltage appear in the I-V curve, corresponding to so much transitions, is summarized.

Clearly, CB effects discussed here are not accounted – as for a TJ or a SET – by current relations (1.9) or (1.29). In order to take into account charge discreteness effect in a QSM, continuous-charge models has to be substituted by discrete-charge models (see Section 2.3).

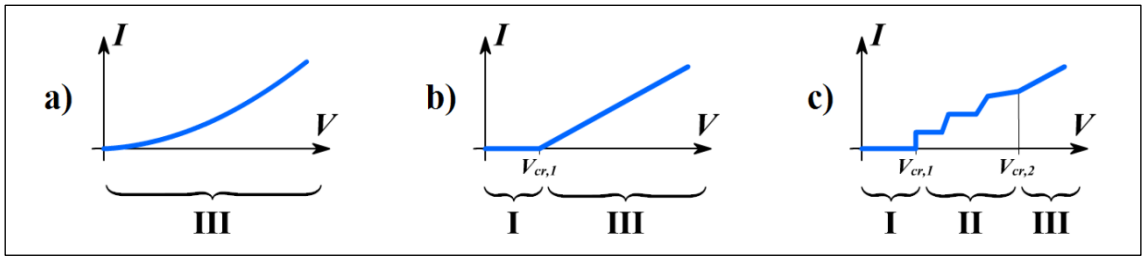

Figure 1.19 – *Different qualitative shapes of the I-V curve with behaviors I), II), III) highlighted.*

2.2.11 Hysteresis of the I-V curve and mechanical advantage

Curves in Fig.1.19 can refer to autonomous or induced shuttle as well. However, from a mechanical point of view, some interesting considerations arise in the second case.

First, how was hinted by some authors, behavior II) is particularly interesting, since somehow leads to have a "quantized" set of limit-cycles, because of discrete attractors corresponding to discrete amplitudes A_i and bias voltages V_i. Each of these threshold corresponds to a surpass of the *i*-th step of Coulomb staircase. This feature can be useful to modulate oscillations.

Second, limiting our analysis to the case of direct shuttle, the vibrational state of the shuttling element relies on self-excitation. Thus, referring to I-V curves in Fig.1.19b,c when $V^{dc} < V_{cr,1}$, the shuttling element cannot oscillate and remains in *static regime*. When $V^{dc} > V_{cr,1}$, in a soft QSM the transition from a static to a *shuttle regime* is indeed "smooth", whereas in a hard QSM in "sudden". In fact, in the latter case, for $V^{dc} > V_{cr,1}$ a tunnel current starts to flow, but the shuttling element remains in static regime, since the center position is still a stable condition. Only by applying a value $V^{dc} > V_{act} > V_{cr,1}$ a limit-cycle is triggered and the shuttle mechanism is abruptly activated, producing a clearly detectable "macrostep" in the I-V curve. This step *is not* related with CB and/or Coulomb staircase effects (in fact, it persists in continuous-charge models): it depends on the stability properties of the hard QSM, for which an orbit of amplitude A is stable only when $A \geq A_{min}$, with A_{min} corresponding to the application of a voltage V_{act} . This fact discloses an even more interesting behavior: if the voltage is lowered, the system returns in static regime *only* by applying a voltage $V^{dc} < V_{deact} < V_{act}$, leading to an apparent *hysteretic behavior*, clearly visible by plotting two times the I-V curve, alternatively increasing and reducing V^{dc} (Fig.1.20a). This fact was explained in [27] with both numerical simulations and stability analyses, which prove the presence of hysteresis in hard QSM.

A last consideration arises from the fact that, in hard systems, the activation of the shuttle mechanism is quite detectable: all the current obtained for voltages $V^{dc} < V_{act}$ comes indeed from the only tunnel contribution. Notice how, in a hard QSM (Fig.1.20b), such tunnel current is very small (or completely absent, if CB conditions occur). In a soft system the current gradually rises and no neat activation voltage is present (Fig.1.20c). In a very soft QSM, one has the tunnel contribution for small voltages is even more considerable than the shuttle current to be established when $V^{dc} > V_{act}$: in this condition, a gradually decrease of the overall current is obtained in correspondence to the soft oscillations triggering. This is because the tunnel current is interfered by the presence of mechanical oscillations, since, from Section 2.2.8 and due to the exponential QT dependence from distance, the term $I_t(t) \approx \min[I_L(t), I_R(t)]$ is maximal when the shuttling element is at rest in the center (1.20d).

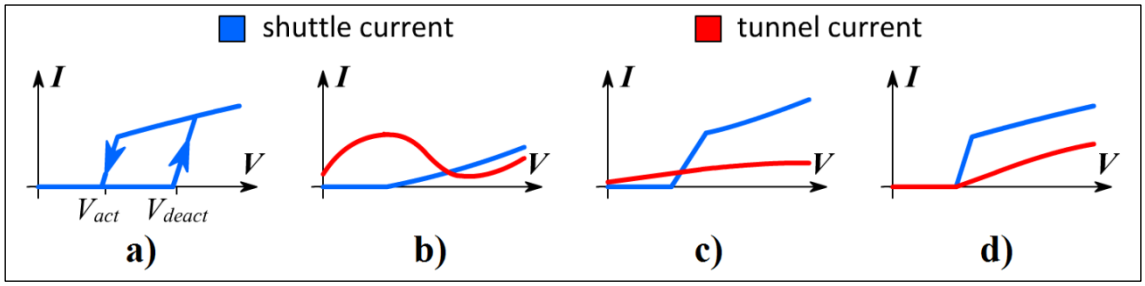

Figure 1.20 – *(a) Hysteresis of the shuttle current in a hard QSM, with voltage thresholds V_{act} and V_{deact} highlighted. Comparison between shuttle and tunnel current contributions in: (b) hard, (b) soft, (c) very soft systems. All I-V curves are smooth, thus either CB is absent or a continuous-charge model is used.*

A deep understanding of qualitative plots in Fig.1.20 is required when approaching to the study of QSM. In fact, in an experimental setup, there is a certain difficulty in directly detect oscillations, so that the standard scenario common to many authors (see the Introduction for a list of articles), is that of an *indirect estimation* of the vibrational state, in which the vibrational regime of the shuttling element is *supposed* by only knowing the *I-V* curve. First, one measures the overall current I when a bias voltage V is applied; second, one estimates which part comes from the shuttle contribution I_s; and, last, one uses formula (1.12a) to estimate the vibrational frequency. It is clear a preliminary theoretical study of these systems is really necessary in order to correctly interpret the conduction mechanism occurring in a QSM device.

Conductive properties of a QSM are, in general, a function of the voltage boundary conditions and the system geometry, so that $\mathcal{I} = \mathcal{I}(\mathcal{B}, \mathcal{G})$. Consider the overall current $\mathcal{I}_0$ generated in a system in which the shuttling element is fixed ($f_s = 0$) in the center ($A = 0$), and the current $\mathcal{I}$ the same system exhibits when a stable orbit characterized by $f_s > 0$ with $A > 0$ is established. The ratio between these two currents is the *mechanical advantage* M:

$$\mathrm{H} \triangleq \frac{\mathcal{I}(\mathcal{B},\mathcal{G})}{\mathcal{I}_0(\mathcal{B},\mathcal{G})} = \frac{\bar{I}|_{f_s>0,A>0}}{\bar{I}|_{f_s=0,A=0}} \tag{1.33}$$

From an engineering point of view, H is an important parameter, since it states the convenience of establishing the shuttle mechanism by undergo mechanical vibrations in a QSM, with respect to a DTJ in which the central element is at rest. Notice how it is not straightforward obtaining $\mathrm{H} > 1$ in any working condition for a QSM. For example (Fig.1.20b), in very soft systems there is often no practical advantage in activating the shuttle mechanism, with respect to the rest condition. Usually, more hard is the system, the more the mechanical advantage is high, since the presence of the tunnel current reduces when the scale of the device is increased.

2.3 Analytical models and feasible approximations

Various approaches are used in literature to model the dynamics of a QSM. A priori, none of them can be considered the most appropriate. In Fig.1.10a,b, for example, we made use, for the mechanical part, of a single-DOF oscillator; and, for the electrical part, of a circuital equivalent. The decision to use such a "classical-oriented" approach comes from the analyses to be presented in Part Two of this thesis, where, since more QSM will be coupled together, a simple and practical modeling for any of its components is required. Nonetheless, the choices made for the models in Fig.1.10a,b are not straightforward. In this Paragraph, we indeed discuss how, in general, the selection of the most feasible theoretical approach to model a QSM depends on a preliminary analysis of the main features of the system, in particular: its characteristic scales, its soft/hard nature, and the presence of CB effects.

In general, in every concentrated parameters models, the QSM is schematically distinguished in two parts, due to its dual nature: the mechanical and the electrical part. Each of them refers to a set of concentrated parameters and one or more lagrangian coordinates. Some additional, environmental parameters, as (for example) the temperature, can be included as well.

From the mechanical point of view, a first choice comes from modeling the shuttling element as either a classical or a quantum oscillator. The latter case could apply when the scale of the device is exceptionally reduced, in particular if the total energy of the oscillator is comparable with the quantized packets $\Delta\mathcal{E} = hf_s$. Such an approach is used, for example, in [51]. However, these models refer to a sub-nm size of the shuttling element: although atomic-scale quantum dots have been recently realized [111], model a QSM as a quantum oscillator can be still considered too much "exotic" to be profitably applied to the study of a real system. Then, one has to decide to model the system as a linear oscillator or not. Usually, non-linearities are negligible when a regime of small oscillation can be assumed; however, in the case of hard shuttle, the shuttle mechanism does require large amplitudes, and, especially in the case of cantilever resonators, hardening non-linear oscillators should be considered [26]. Again, in the case of a cantilever realization, one can take into account more vibrational modes or only the first one, respectively leading to 1 or N_{mech} mechanical lagrangian coordinates.

A more compelling issue is related to the part of oscillation which is due to stochastic thermal vibrations. Actually, this problem directly involves the design of the device, in addition to its theoretical modeling. Prior model a QSM, one should check which is the minimal amplitude of oscillations which is comparable with the expected value of thermal vibrations. By using the Fluctuation Dissipation Theorem (FDT) (see for example, [112]), a simple estimation gives: $\sigma_x \approx \sqrt{k_B\Theta/k}$. A concentrated parameters model can deterministically describe only oscillations for which $A \gg \sigma_x$. It has be remarked that the presence of thermal vibrations, as highlighted in [41], could be actually considered useful to activate the shuttle mechanism.

The feasibility of a classical circuital scheme is much more questioned in literature, with respect to the use of a classical oscillator. Solving the equivalent circuit does not guarantee an accurate description of the electrodynamics of a QSM at a nm-scale, mainly due to the "macroscopic" concepts of capacitance and conductance. Thus, in QSM literature, the dependence of the shuttling element capacitance C_S from its position $x(t)$ is not always considered (differently from formula (1.4)). In these works, it is calculated as $C_S = 4\pi\varepsilon r$ (self-capacitance of a spherical conductor). Now consider the equivalent QT conductances between the electrodes and the shuttling element, G_L, G_R. Closed-form relations as (1.1a,b) exist to estimate their values. However, this is only an abstraction which constraints the true nature of QT (a residual probability for an electron to surpass a certain potential barrier) to a classic concept (the conductance) by applying the ergodic hypothesis to a large population of electrons. Then, the tunneling probabil-

ity (*tunneling rate*, indicated with Γ) is put into relation with their ensemble behavior. If the number of electrons on the shuttling element is low, a more correct approach has to directly deal with the tunneling rates (for example, [25] and [27]). Also, in this model, the effect of temperature Θ has to be considered by the means of the *Fermi-Dirac distribution*.

The number of electrical lagrangian coordinates to be used is strictly related to the concept of charge discreteness. If the number of shuttled electrons is high and/or CB requirements (1.32a,b,c) – which depend on capacitances and conductances – on are not met, a continuous-charge model is appropriate [29]. Otherwise, one can use a discrete-charge model in which the probability for any electron to undergo QT is related to the tunneling rates. In this case, the number of electrical lagrangian coordinates is that of the quantity of electrons N_{elec} which can occupy the shuttling element. Two main strategies can be used. In the first one, N_{elec} equations in terms of discrete variables $N_i(t) = \{0,1\}$ are used. Simulation results can be postprocessed, using Montecarlo algorithms in order to get the ensemble behavior of a group of systems [25,27]. In the second one, the discrete nature of charges is not completely considered, since it is assumed the QT fluctuation of electrons are very fast with respect to the mechanical time scale. Under this assumption, a Master equation can be used, in which N_{elec} equations in terms of the *occupation probability of states* $P_i(t) = \langle N_i(t) \rangle \in [0,1]$ are considered. This approach is widely used in theoretical works such as [25,27].

The mechanical and electrical parts of the system are mainly coupled by the forcing term acting on the shuttling element F_S. Consequently, a central role is played by the model used in order to take it into account. In general, the coupling is electromagnetic. However, magnetism is neglected in most models, except when the effects of a Lorentz force arising from an applied magnetic field are deliberately introduced in the system. The remaining part is electrostatic, produced by the distribution of charges in the whole system. Different models can be used. The most simple assumes a constant electric field in the whole oscillating region [25,27,29], so that $F_S \propto VQ_S$. This approach does not include the electrostatic induction, which sometimes plays a central role, especially when $r/d \sim 1$. If this is the case, a considerable force acts on the shuttling element also when no net charge is present on it. To introduce such effects in the model, the force has to be attained as the derivative of the electrostatic potential energy $F_{es} = -\partial \mathcal{U}/\partial x$.

A summarizing overview of possible analytical approaches and feasible approximations is given respectively in Tab.1.4 and Tab.1.5.

Table 1.4 – *Analytical approaches*

System part	Description	Equations	Nature	Lagrangian Coordinates	Number of Coordinates
Mechanical	Quantum	Schroedinger	-	$\mathcal{E}_i$	energy levels
	Classical	Newton's	continue	x_i	modes
Electrical	Quantum	Montecarlo algorithm	discrete	N_i	states
		Master equation	continue	$P_i = \langle N_i \rangle$	states
	Semi-classical	Ohm's law	continue	Q_i or V_i	conductors

Table 1.5 – *Feasible approximations*

System part	Description	Model used	Quantity	Approximation feasibility
Mechanical	Oscillator nature	linear	kx	small oscillations
		non-linear (hardening)	$k_i x^i$	(general case)
Electrical	Quantum tunneling	equivalent conductances	G	large conductors
		tunneling rates	Γ	(general case)
Electro-mechanical	Shuttling element force	constant-field	$\propto VQ_S$	small ratio d/r
		accurate (electrostatic	$-\partial \mathcal{U}/\partial x$	(general case)

Chapter 3

Direct shuttle: a self-excited Quantum Shuttle Module

3.1 Architecture and boundary conditions

On the basis of the classifications and nomenclatures introduced in Chapters 1 and 2, let us consider an *autonomous* QSM, characterized by a *two-terminals* architecture, and exhibiting *direct shuttle*. Consequently, the shuttling element capacitance (1.4) and the set of voltage *boundary conditions* (1.5a) respectively specify into:

$$C_G = 0 \quad \longrightarrow \quad C_S(x) \triangleq C_L(x) + C_R(x) \tag{1.34a}$$

$$\begin{cases} V^{dc} \neq 0 \\ V^{ac} = 0 \end{cases} \quad \longrightarrow \quad V = V_L - V_R = V^{dc} \tag{1.34b}$$

Whereas (1.5b) do not appear since the gate is not present in the system.
To investigate such a system, refer to the mechanical and electrical schemes in Fig.1.21a,b, which represent a particular case of the prototypal architecture introduced in Section 2.1.

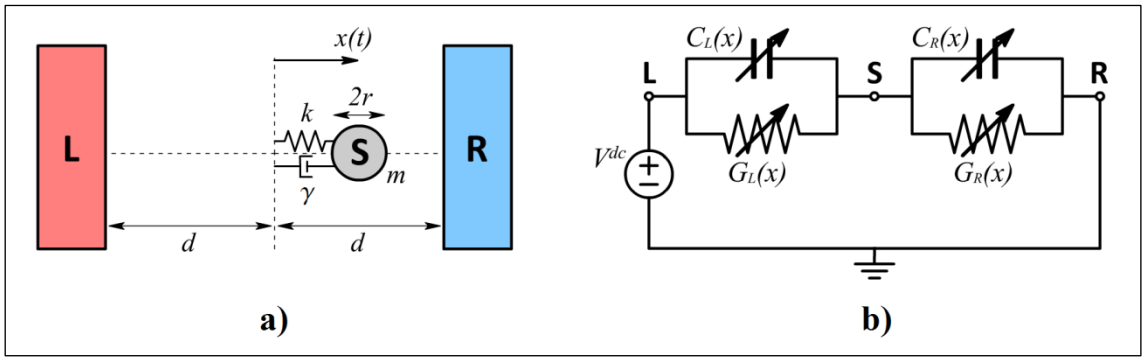

Figure 1.21 – *Two-terminals QSM exhibiting direct shuttle: (a) mechanical and (b) electrical schemes.*

Consequently to the arguments discussed in Section 2.2, we expect such a QSM is feasible to achieve motion regimes characterized by *self-excited* oscillations, establishing a macroscopic current whose direction is univocally determined by the *symmetry breaking* coming from the application of an appropriate bias voltage V.
In this Chapter, numerical simulations are aimed to quantitatively verify these qualitative analyses. Specifically, we are interested to highlight that: i) closed orbits on the phase plane x-Q_S , representing stable motion regimes, can be described by equations (1.16) with characteristic parameters $\Psi = 1$ and $\Phi \approx \pm\pi/2$; ii) an hysteresis of the I-V curve can be experienced only in the case of hard shuttle, whereas in the case of soft shuttle is not possible.

3.2 Equations

Referring to the analytical models and approximations discussed in Section 2.3, and compatibly with the schemes in Fig.1.21a,b, the equations used in this Chapter make use of a classical single-DOF mechanical model and a semi-classical continuous-charge circuital equivalent.

Let the first lagrangian coordinate the position $x(t)$ of the shuttling element, then, the mechanical part of the system in Fig.1.21a is described by the Newton equation:

$$m\frac{d^2x}{dt^2}+\gamma\frac{dx}{dt}+kx=F_S \tag{1.35}$$

On the other hand, let the electrodynamics of the system described by the lagrangian coordinate $Q_S(t)$, representing the shuttling element total charge. From Ohm's law, the second equation is:

$$\frac{dQ_S}{dt}=G_L(V_L-V_S)-G_R(V_S-V_R) \tag{1.36}$$

In (1.35) and (1.36), terms V_L , V_R , V_S , G_L , G_R , F_S require to be further specified.
Directly from (1.34b), the left/right electrodes voltages are constant and respectively equal to:

$$V_L=+\frac{V^{dc}}{2} \quad , \quad V_R=-\frac{V^{dc}}{2} \tag{1.37a, b}$$

The voltage of the shuttling element V_S depends on both $x(t)$ and $Q_S(t)$. By applying (1.35a) and (1.37a,b) to the relation $Q_S=C_L(V_S-V_L)+C_R(V_S-V_R)$, one obtains:

$$V_S=V_S(x,Q_S)=\frac{Q_S+[C_L(x)-C_R(x)]\frac{V^{dc}}{2}}{C_S(x)} \tag{1.38}$$

which specifies the general expression (1.6) with constants $\alpha=(C_L-C_R)/2C_S(x)$ and $\beta=0$.
The QT equivalent conductances are calculated by applying (1.8a,b) to (1.1a), so that:

$$G_{L,R}=G_{L,R}(x)=G_c\mathrm{e}^{-\frac{d-r\pm x}{\lambda}}=G_c\mathrm{e}^{\frac{r-d}{\lambda}}\mathrm{e}^{\mp\frac{x}{\lambda}}=G_0\mathrm{e}^{\mp\frac{x}{\lambda}} \tag{1.39a, b}$$

where $G_0\triangleq G_c\mathrm{e}^{(r-d)/\lambda}$. For the electrostatic force on the shuttling element F_S, we choose a simple model in which electrostatic induction effects are not included (E is the electric field):

$$F_S=EQ_S\approx\frac{V^{dc}}{2d}Q_S \tag{1.40}$$

Substituting relations (1.37)-(1.40) into equations (1.35)-(1.36), the dynamics of the QSM in Fig.1.21 is described by the pair of coupled equations (time dependencies are omitted):

$$\begin{cases} m\dfrac{d^2x}{dt^2}+\gamma\dfrac{dx}{dt}+kx=\dfrac{V^{dc}}{2d}Q_S \\ \dfrac{dQ_S}{dt}+2G_0\cosh\left(\dfrac{x}{\lambda}\right)\dfrac{Q_S}{C_S(x)}=-G_0\left[\sinh\left(\dfrac{x}{\lambda}\right)+\cosh\left(\dfrac{x}{\lambda}\right)\dfrac{C_L(x)-C_R(x)}{C_S(x)}\right]V^{dc} \end{cases} \tag{1.41}$$

We assume the electrostatics of the scheme in Fig.1.21 is analogous to that of a sphere between two plates. Therefore, we model the capacitance terms C_L and C_R in the following way:

$$C_{L,R}(x) = 4\pi\varepsilon r\left(1 + B\frac{r}{d - r \pm x}\right) \tag{1.42a, b}$$

A value $B = 0.165$ can be calculated by best fitting curves coming from:

$$C(r, D) = 4\pi\varepsilon r\sum_{h=1}^{\infty}\frac{\sinh\left[\ln\left(\frac{D}{r} + \sqrt{\frac{D^2}{r^2} - 1}\right)\right]}{\sinh\left[h\ln\left(\frac{D}{r} + \sqrt{\frac{D^2}{r^2} - 1}\right)\right]} \tag{1.43}$$

which represents a closed-form relation to calculate the capacitance of a sphere-plate capacitor, with r the sphere radius and $D \geq r$ the plate-to-center distance †.
Now, let the mechanical frequency $\omega \triangleq \sqrt{k/m}$ and introduce the non-dimensional quantities:

$$\begin{gathered}\tau \triangleq \omega t \quad , \quad \xi(t) \triangleq \frac{x(t)}{d - r} \quad , \quad N_S(t) \triangleq \frac{Q_S(t)}{e} \\ \zeta \triangleq \frac{\gamma}{2\sqrt{km}} \quad , \quad \tilde{d} \triangleq \frac{d}{\lambda} \quad , \quad \tilde{r} \triangleq \frac{r}{d} \\ v_{dc} \triangleq \frac{C_S(0)V^{dc}}{e} \quad , \quad v_S \triangleq \frac{C_S(0)V_S}{e} \quad , \quad \tilde{G}_0 \triangleq \frac{G_0}{\omega C_S(0)} \quad , \quad \tilde{\epsilon} \triangleq \frac{e^2}{2d(d - r)m\omega^2 C_S(0)}\end{gathered} \tag{1.44}$$

Plugging (1.44) into (1.41) the dimensional equations are:

$$\begin{cases}\dfrac{d^2\xi}{d\tau^2} + 2\zeta\dfrac{d\xi}{d\tau} + \xi = \tilde{\epsilon}v_{dc}N_S \\ \dfrac{dN_S}{d\tau} + 2\tilde{G}_0[1 - a(\xi)]\cosh\left(\tilde{d}\xi\right)N_S = \tilde{G}_0\left[b(\xi)\cosh\left(\tilde{d}\xi\right) - \sinh\left(\tilde{d}\xi\right)\right]v_{dc}\end{cases} \tag{1.45}$$

$$a(\xi) \triangleq \frac{B\tilde{r}\xi^2}{(1 - \tilde{r})(1 - \xi^2) + B\tilde{r}} \quad , \quad b(\xi) \triangleq \frac{B\tilde{r}\xi}{(1 - \tilde{r})[(1 - \tilde{r})(1 - \xi^2) + B\tilde{r}]}$$

Referring again to Fig.1.21, the microscopic currents (1.7a,b), are:

$$I_{L,R}(\tau) = \frac{G_0}{C_S(x)}\mathrm{e}^{\mp\frac{x}{\lambda}}\left[C_{R,L}(x)V^{dc} \mp Q_S\right] \tag{1.46a, b}$$

and their dimensionless counterpart:

$$i_{L,R}(\tau) \triangleq \frac{I_{L,R}(\tau)}{\omega e} = \tilde{G}_0\mathrm{e}^{\mp\tilde{d}\xi}[1 - a(\xi)]\left[c_{L,R}(\xi)v^{dc} \mp N_S\right] \tag{1.47}$$

$$c_L(\xi) \triangleq \frac{(1 - \xi)(1 - \tilde{r}) + B\tilde{r}}{2(1 - \xi)(B\tilde{r} + 1 - \tilde{r})} \quad , \quad c_R(\xi) \triangleq \frac{(1 + \xi)(1 - \tilde{r}) + B\tilde{r}}{2(1 + \xi)(B\tilde{r} + 1 - \tilde{r})}$$

† Relations (1.42a,b) are the simplest in which limits $\lim_{x\to\mp(d-r)} C_{L,R}(x) = +\infty$ and $\lim_{x\to\pm\infty} C_{L,R}(x) = 4\pi\varepsilon r$ distinctly hold.

In conclusion, the macroscopic non-dimensional current is defined, similarly to (1.9), by averaging $i_L(\tau)$ or $i_R(\tau)$ on a single (dimensionless) period of oscillation $\tilde{T}_s \triangleq \omega T_s$:

$$\bar{\imath} \triangleq \frac{1}{\tilde{T}_s}\int_{\tau_0}^{\tau_0+\tilde{T}_s} i_L(\tau)\,d\tau \approx \frac{1}{\tilde{T}_s}\int_{\tau_0}^{\tau_0+\tilde{T}_s} i_R(\tau)\,d\tau = \frac{\bar{I}}{\omega e} \tag{1.48}$$

and its shuttle and tunnel contributions can be obtained, like in (1.12b) and (1.13), as follows:

$$\bar{\imath}_s \triangleq \frac{1}{\tilde{T}_s}\int_{\tau_0}^{\tau_0+\tilde{T}_s} \delta\big(\xi(\tau)\big)\dot{\xi}(\tau)N_S(\tau)\,d\tau = \frac{\bar{I}_s}{\omega e} \tag{1.49}$$

$$\bar{\imath}_t \triangleq \bar{\imath} - \frac{1}{\tilde{T}_s}\int_{\tau_0}^{\tau_0+\tilde{T}_s} \delta\big(\xi(\tau)\big)\dot{\xi}(\tau)N_S(\tau)\,d\tau = \frac{\bar{I}_t}{\omega e} \tag{1.50}$$

3.3 Numerical results and discussion

In this Paragraph we show the results of a set of numerical simulations characterized by the same initial conditions but in which different bias voltages v_{dc} are applied. An *I-V* curve, reassuming the conductive black-box behavior of the QSM depicted in Fig.1.21, is produced. Actually, we investigated a pair of systems exemplifying the soft/hard shuttle phenomenology. Both cases share the following set of parameters: $\lambda = 0.2\ nm$, $G_c = 1\ S$, $\zeta = 0.01$.

The first QSM is characterized by a relatively small scale:

$$d = 4\,nm \quad , \quad r = 1\,nm \quad , \quad m = 10^{-22}\,kg \quad , \quad \omega = 10^{11}\,Hz \tag{1.51a}$$
$$C_S(0) = 2.35\times 10^{-19}\,F \quad , \quad G_0 = 3.06\times 10^{-7}\,S$$

which corresponds to the following values for dimensionless quantities defined in (1.44):

$$\tilde{d} = 20 \quad , \quad \tilde{r} = 1/4 \quad , \quad \tilde{\epsilon} = 4.55\times 10^{-3} \quad , \quad \tilde{G}_0 = 13.0 \tag{1.51b}$$

In this case, $\tilde{G}_0 = G_0/\omega C_S(0) > 1$, therefore, compatibly with definitions given in Section 2.2.8, this choice of parameters individuates a QSM exhibiting a *soft* shuttle regime. Numerical results representing the dynamics and the *I-V* curve for such a system are shown in Fig.1.22.

The second investigated system is characterized by a relatively larger scale:

$$d = 12\,nm \quad , \quad r = 3\,nm \quad , \quad m = 10^{-21}\,kg \quad , \quad \omega = 10^{10}\,Hz \tag{1.52a}$$
$$C_S(0) = 7.04\times 10^{-19}\,F \quad , \quad G_0 = 2.86\times 10^{-20}\,S$$

corresponding to:

$$\tilde{d} = 60 \quad , \quad \tilde{r} = 1/4 \quad , \quad \tilde{\epsilon} = 1.69\times 10^{-3} \quad , \quad \tilde{G}_0 = 4.06\times 10^{-12} \tag{1.52b}$$

This QSM, since $\tilde{G}_0 = G_0/\omega C_S(0) \ll 1$, exhibits a (very) *hard* † shuttle regime. In this case, results of numerical simulations are shown in Fig.1.23.

† In a system like this, the "two-states approximation" (1.25) holds with a rather good precision, and equations (1.26) lead to an accurate estimation of the dynamics of this QSM.

All results in Fig.1.22 and Fig.1.23 refer to the same choice of initial conditions:

$$\xi(0) = \dot{\xi}(0) = 0 \quad , \quad N_S(0) = 30 \tag{1.53}$$

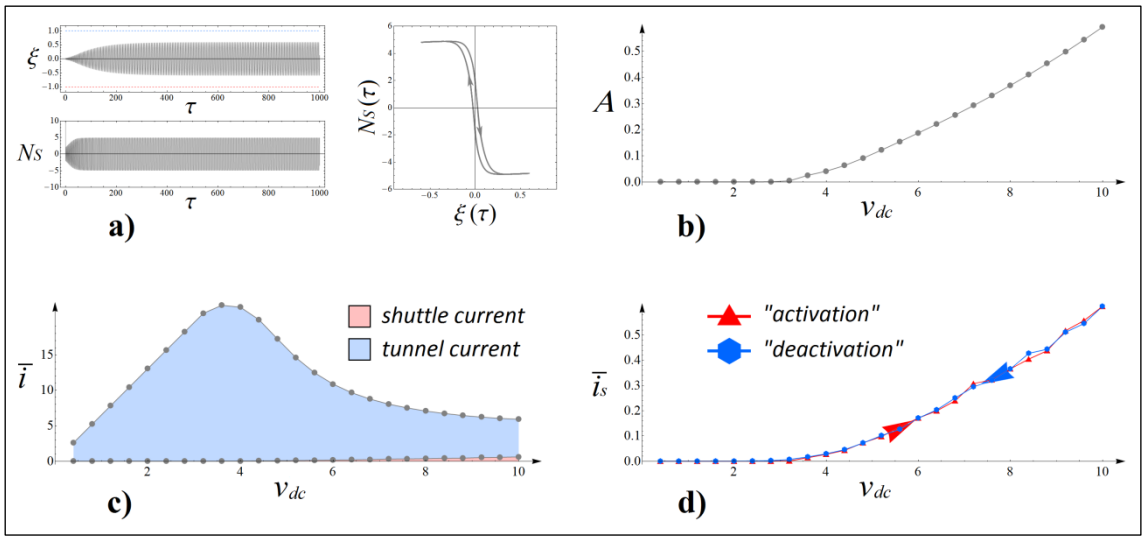

Figure 1.22 – *Results of numerical simulations for a soft QSM characterized by parameters (1.51a,b) and initial conditions (1.53), obtained by integrating equations (1.45). (a) evolution of shuttling element position $\xi(t)$ and charges $N_S(t)$ with $v_{dc} = 10$; the phase curve is plotted also. (b) amplitude of oscillation A as a function of v_{dc}. (c) I-V curve obtained by varying v_{dc} , with $\bar{\imath}$ calculated from relation (1.48): the shuttle (red curve, formula (1.49)) and tunnel (blue, (1.50)) contributions to the macroscopic current per cycle $\bar{\imath}$ are highlighted. (d) I-V curve obtained by increasing voltage from $v_{dc} = 0$ (red curve) or decreasing from $v_{dc} = 10$ (blue), and considering the only shuttle part $\bar{\imath}_s$.*

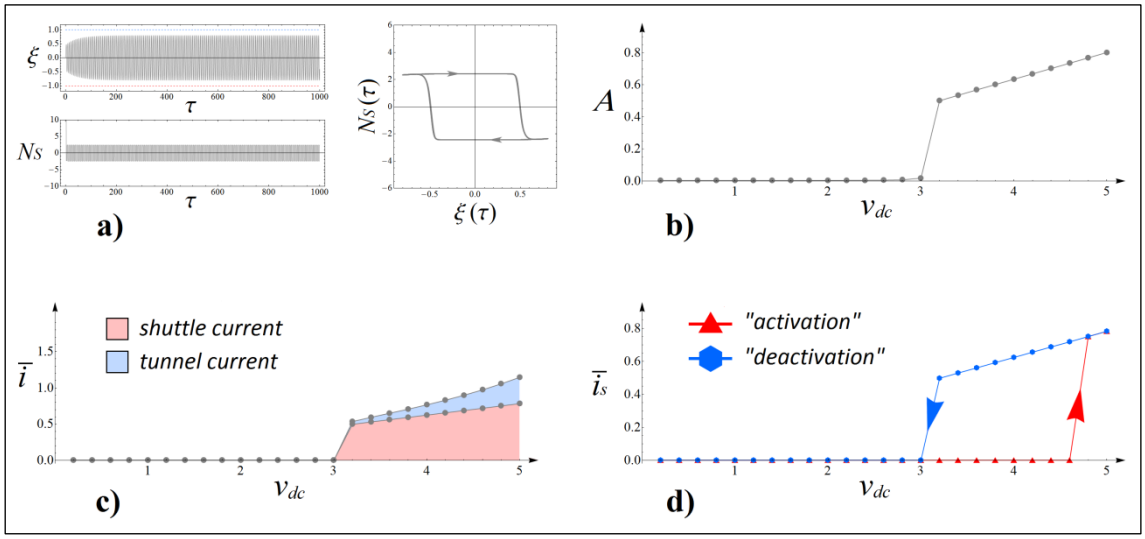

Figure 1.23 – *Plots (a), (b), (c), (d) are analogous to those in Fig.1.22 except they refer to a (very) hard QSM characterized by parameters (1.52a,b). Here, the voltage in (a) is $v_{dc} = 5$.*

A discussion on the results in (Fig.1.22) and (Fig.1.23), in particular a comparative analysis of the mechanical and electrical properties exhibited by soft and hard QSMs, is presented.

From a mechanical point of view, the different transition from a rest condition to self-excited oscillations is well observable by comparing Fig.1.22b and Fig.1.23b: in the first plot amplitude smoothly increases with v_{dc} , whereas in the second one the distinction between the rest and shuttle regimes is more neat.

From the electrical point of view, in Fig.1.22c,d and Fig.1.23c,d some *I-V* curves are plotted, by using the activation/deactivation procedures explained here. The keyword "activation" indicates the case in which the system starts with a null voltage (compatible with a rest condition), and then a larger value v_{dc} is applied to reach the shuttle mechanism. Instead, "deactivation" refers to a system starting with a voltage which guarantees the shuttle mechanism, and later a smaller value v_{dc} is applied which stops the motion of the shuttling element. Fig.1.22b,c and Fig.1.23b,c, refer to the deactivation procedure, whereas Fig.1.22d and Fig.1.23d compare results coming from activation and deactivation. In Fig.1.22c and Fig.1.23c it is clearly visible that in soft QSM the tunnel current represents the main contribution, whereas in the hard case the current is quite inhibited until the shuttle contribution appears. By comparing plots in Fig.1.22d and Fig.1.23d, in the first case (soft system), the activation/deactivation curves match, whereas in Fig.1.23d (hard system) they don't, producing an *hysteresis* of the *I-V* curve.

These differences between soft and hard regimes were already anticipated in Section 2.2.11 and are here a confirmation through numerical simulations is provided. The simple, continuous-charge model proposed in this chapter, highlights the fact that the main features related to the soft/hard distinction and, in particular, the chance of observing an hysteresis on the *I-V* curve, do not rely on the discrete nature of charge. Therefore, under the hypothesis CB-related effects are not present (formulae (1.32a,b,c) not accomplished) a continuous-charge model is feasible to provide an accurate description of the shuttle dynamics, also at nanoscale. Notice that all the properties discussed above are well-known in literature. In particular, a first analyses of the stability properties of a QSM in soft and hard regimes was first given by Isacsson and Gorelik [27], and results provided in this Chapter are according with this article.

A last, important fact has to be remarked: hysteresis of the *I-V* curve *is not* a constant feature in hard QSMs. This means the hard regime is a required but not sufficient condition in order to observe such hysteretic behavior. Instead, it depends on the choice of the initial conditions. In order to demonstrate this statement, in Fig.1.24a, different *I-V* "activation" curves are plotted for the same system, the only difference being the initial number of electrons on the shuttling element $N_S(0)$. These curves are indeed different, and present a step (in correspondence to the emergence of the shuttle mechanism) on different thresholds $v_{dc} = v_{act}(N_S(0))$. In particular, the larger is the number of electrons, the more activation is favored and is exhibited for low values of v_{act} . Instead, from Fig.1.24b, the deactivation curve is unique and v_{deact} does not depend on $N_S(0)$. From a comparison between Fig.1.24a and Fig.1.24b follows that, when $N_S(0) \geq 50$, then $v_{act} \approx v_{deact}$, and the hysteretic behavior is no more present.

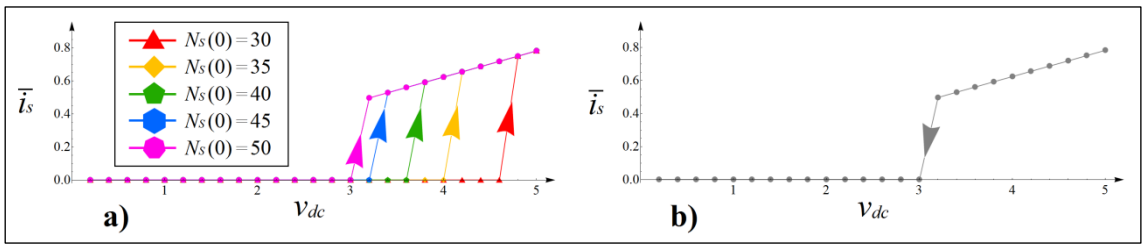

Figure 1.24 – *(a) activation curves for a hard system with parameters (1.52a,b) and different initial conditions. (b) deactivation curve for the same system, independent from the initial conditions*.

The fact the *I-V* curve hysteresis "disappears" by simply choosing appropriate initial conditions hints to the fact the activation/deactivation transient does not involve any physical phenomenon which is intrinsically *hysteretic*; thus, hysteresis is only *apparent*. Consequent to this, in Section 9.2 , an engineering satisfying interpretation of this behavior will be proposed. The subtle nature of hard QSM hysteresis is, at Author's knowledge, not enough pointed up in literature.

Chapter 4

Inverse shuttle: a parametric resonant Quantum Shuttle Module

4.1 Architecture and boundary conditions

Let us investigate an *autonomous* QSM, this time in the case of *inverse shuttle*, thus feasible to trigger a parametric resonance. In order to do this, we consider a particular case of the prototypal scheme in Fig.1.10, where the boundary conditions (1.5a,b) respectively specify into:

$$\begin{cases} V^{dc} = 0 \\ V^{ac} = 0 \end{cases} \quad \longrightarrow \quad V = V_L - V_R = 0 \tag{1.54a}$$

$$\begin{cases} V_G^{dc} \neq 0 \\ V_G^{ac} \neq 0 \end{cases} \quad \longrightarrow \quad V_G = V_G^{dc} + V_G^{ac}\cos(\omega_G t) \tag{1.54b}$$

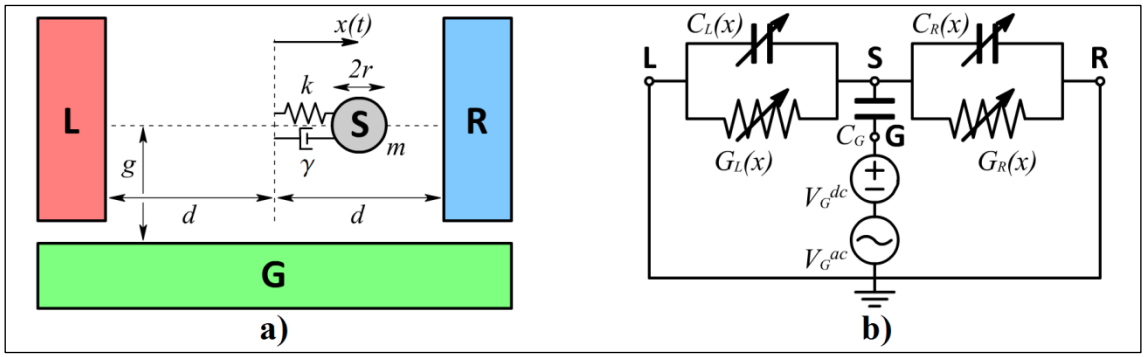

Figure 1.25 – *Three-terminals QSM exhibiting inverse shuttle: (a) mechanical and (b) electrical schemes.*

Referring to Fig.1.25 and compatibly with (1.6) and (1.54a), the shuttling element potential is:

$$V_S(x,t) = Q_S(t)/C_S(x) + \beta(x)V_G(t) \tag{1.55}$$

Let g the distance between the gate G and the shuttling element S. If $g \gg d$ (*wide-gate* approximation), G envelops around S an electric field almost uniform in the whole oscillating region, thus β does not depend on x, i.e. $\beta = \text{const}$ (Fig.1.26a). Conversely, the gate influence is local and a term $\beta(x)$ has to be included (Fig.1.26b). In this Chapter, different analytical approaches are used. In Section 4.2 the wide-gate approximation is treated, in Section 4.3 the general case.

Figure 1.26 – *Qualitative shape of the electric field in the: (a) wide-gate approximation, (b) general case.*

4.2 Wide-gate approximation: "quantum" analytical approach

4.2.1 Introduction

The "wide-gate" approximation is a very strong hypothesis on the structure of V_S , but is useful to carry out a preliminary analysis of inverse shuttle. Also, it leads to consider the following cascading consequences:

i) In the qualitative scheme in Fig.1.26a, to maintain the miniaturization of the device, the design requirement $g \gg d$ leads to consider a relatively small d instead of a large g .
ii) By maintain a relatively small d, the system is probably in regime of *soft shuttle*, thus the QT characteristic frequency is larger than the mechanical frequency.
iii) The limited oscillating space leads to consider a *Q-dot* realization of the shuttling element, instead that, for example, a *nanopillar* geometry, compatible with larger devices. Following this, the shuttling element, in this Paragraph, is represented with the letter "D".
iv) Due to the small scale, the presence of CB in the system is probable. To obtain a more accurate description of the system dynamics, we use a *discrete-charge model* and a description of QT based on the *Fermi-Dirac distribution*. Thus, with respect to Chapter 3, a more exquisite *"quantum" analytical approach* is used to describe the electrical part.
v) The use of a "quantum" approach makes the circuital scheme in Fig.1.25 partly misleading.

The following sub-Paragraphs refer to these preliminary points in order to: obtain equations for the system dynamics, estimate its conductive properties, produce numerical results, develop an approximated analytical solution, to the study QSM of interest.

4.2.2 Equations and simplifying hypotheses

By assuming the *wide-gate approximation*, the voltage of the Q-dot is, from (1.55):

$$V_D(x,t) = \frac{Q_D(t)}{C_D(x)} + \beta V_G(t) \tag{1.56}$$

From this, the total energy can be calculated as (time dependences are omitted):

$$\mathcal{E}_D(x) = \frac{Q_D V_D}{2} + \mathcal{K}_q = \frac{{Q_D}^2}{2C_D(x)} + Q_D\frac{\beta}{2}V_G + \mathcal{K}_q \tag{1.57}$$

The term $\mathcal{K}_q$ represents the quantum kinetic energy. Here we assume, for simplicity's sake, $\beta/2 = 1$ † . It is possible to develop a Taylor expansion of $1/C_D(x)$ around $x = 0$, up to the quadratic term. Since, for a symmetric realization of the device, $C_L(x) = C_R(-x)$, linear terms disappear, and one finally obtains:

$$\frac{1}{C_D(x)} = \frac{1}{C_D(0)\left[1 + \frac{1}{2C_D(0)}\frac{d^2C_D(x)}{dx^2}\Big|_{x=0}x^2\right]} \approx \frac{1 - \frac{1}{2C_D(0)}\frac{d^2C_D(x)}{dx^2}\Big|_{x=0}x^2}{C_D(0)} \tag{1.58}$$

In the last passage, the binomial approximation $1/(1+\varepsilon) \approx 1 - \varepsilon$ has been used.

† In general, $0 < \beta < 1$. Assume a value for $\beta \neq 1$ leads to the consequence all plots that will be obtained here has to be simply scaled of a factor $1/\beta$ on the V_G axis. Thus, assuming $\beta = 2$ doesn't introduce any further physical approximation.

Finally, the energy is:

$$\mathcal{E}_D(x) = \frac{{Q_D}^2}{2C_D(0)} - \epsilon {Q_D}^2 x^2 + Q_D V_G + \mathcal{K}_q \quad , \qquad \epsilon \triangleq \frac{1}{4C_D(0)^2}\frac{d^2 C_D(x)}{dx^2}\bigg|_{x=0} \tag{1.59a}$$

Similarly to Chapter 3, the mechanical descriptor of the system is a continuous coordinate $x(t)$, however, this time, we have a discrete-charge electrical model. Let $Q_D(t) = eN_D(t)$, so that:

$$\mathcal{E}_D(x) = \frac{e^2 {N_D}^2}{2C_D(0)} - \epsilon e^2 {N_D}^2 x^2 + eN_D V_G + \mathcal{K}_q \tag{1.59b}$$

The quantity $N_D(t)$ physically represents – in absolute value – the number of electrons on the Q-dot in a certain time. Every electron has a certain probability to tunnel from/towards it in a certain time, therefore a set of equations is needed, in general, to describe the electrodynamics of the system: this leads to use one of the "quantum" approaches discussed in Section 2.3 Here, we select the *Master equation* approach, and assume the system is in CB regime, so that *only one* electron can occupy the Q-dot: $N_D(t) = \{0,1\}$. In this case, the Master equation includes only the evolution for the occupation probability of a single electron:

$$P_1(t) \triangleq \langle N_D(t) \rangle \tag{1.60}$$

Consequently, the system is still described by a pair of equations: one mechanical, in terms of the continuous coordinate $x(t)$; and one electrical, in terms of the (continuous) ensemble $P_1(t)$ of the (discrete) number of electrons $N_D(t)$. In this context, as highlighted in point v) of Section 4.2.1, the circuital scheme in Fig.1.25 is no more valid, the evolution of $P_1(t)$ given by relation:

$$\frac{dP_1}{dt} = i_{in} - i_{out} = \left(i_{in,L} + i_{in,R}\right) - \left(i_{out,L} + i_{out,R}\right) \tag{1.61}$$

whose terms, as conventional in NEMS literature, are modeled as follows (Fig.1.27):

$$i_{in,L} \triangleq (1 - P_1)\Gamma_L(x) f\left(\mathcal{E}_D|_{N_D=1} - \mu_L\right) \tag{1.62a}$$

$$i_{in,R} \triangleq (1 - P_1)\Gamma_R(x) f\left(\mathcal{E}_D|_{N_D=1} - \mu_R\right) \tag{1.62b}$$

$$i_{out,L} \triangleq P_1 \Gamma_L(x)\left[1 - f\left(\mathcal{E}_D|_{N_D=1} - \mu_L\right)\right] \tag{1.62c}$$

$$i_{out,R} \triangleq P_1 \Gamma_R(x)\left[1 - f\left(\mathcal{E}_D|_{N_D=1} - \mu_R\right)\right] \tag{1.62d}$$

Electron rates $i_{in,L}$, $i_{in,R}$, $i_{out,L}$, $i_{out,R}$ play a role analogous to the microscopic currents I_L, I_R , however, differently from them, ohmic-equivalent relations like (1.7a,b) do not hold anymore.

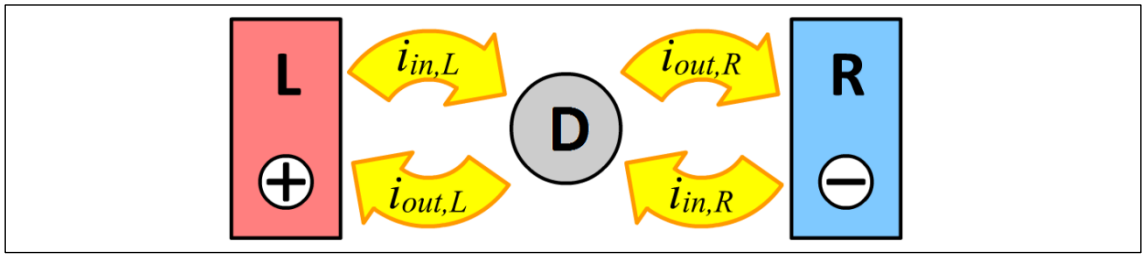

Figure 1.27 – *Evolution of the occupation probability of the Q-dot. Gate electrode not represented.*

Instead, in equations (1.62a,b,c,d), equivalent QT conductances G_L and G_R are substituted by dimensionless *tunneling rates* Γ_L and Γ_R . They are calculated similarly to formulae (1.39a,b):

$$\Gamma_{L,R}(x) = \Gamma_0 \mathrm{e}^{\mp\frac{x}{\lambda}} \qquad (1.63\text{a, b})$$

where Γ_0 is the *charge fluctuation frequency*.
Last, the ohmic relations (1.7a,b) used to calculate the microscopic currents in the semi-classical case, are here substituted by formulae involving the *Fermi-Dirac distribution* f :

$$f(\mathcal{E}_D|_{N_D=1} - \mu_{L,R}) \triangleq \frac{1}{1 + \mathrm{e}^{\frac{\mathcal{E}_D|_{N_D=1} - \mu_{L,R}}{k_B\Theta}}} \qquad (1.64\text{a, b})$$

In these, $\mathcal{E}_D|_{N_D=1}$ is the energy of the Q-dot, calculable from (1.59b) by posing $N_D = 1$, while μ_L and μ_R are respectively the *chemical potentials* of the left and right electrodes. Then, k_B is the Boltzmann constant, and Θ the temperature. Since the system is symmetric and L and R are maintained at the same (null) voltage, we can profitably assume $\mu_R \equiv \mu_L \triangleq \mu_0$, so that, taking into account (1.62a,b,c,d) and (1.63a,b), equation (1.61) becomes:

$$\frac{dP_1}{dt} = 2\Gamma_0 \cosh\left(\frac{x}{\lambda}\right)\left[f\left(\mathcal{E}_D|_{N_D=1} - \mu_0\right) - P_1\right] \qquad (1.65)$$

Let us introduce the chemical potential of the Q-dot as:

$$\mu_D \triangleq \frac{e^2}{2C_D(0)} + \mathcal{K}_q \qquad (1.66)$$

Then, the explicit form of the argument of the Fermi-Dirac distribution is, from (1.59b):

$$\left(\mathcal{E}_D|_{N_D=1} - \mu_0\right) = (\mu_D - \mu_0) - \epsilon e^2 x^2 + eV_G \qquad (1.67\text{a})$$

Now, in the place of the gate boundary conditions (1.54b), use the following relation:

$$V_G = V_{G,0}^{dc} + V_G^{dc} + V_G^{ac}\cos(\omega_G t) \qquad , \quad V_{G,0}^{dc} \triangleq -\frac{\mu_D - \mu_0}{e} \qquad (1.54\text{c})$$

The physical meaning of using (1.54c), is clear: we are assuming the chemical potentials of the Q-dot and the left/right electrodes have been preliminary "put on a par" by applying an additional static voltage on the gate $V_{G,0}^{dc}$. Consequently to the use of (1.54c), (1.67a) simplifies into:

$$\left(\mathcal{E}_D|_{N_D=1} - \mu_0\right) = -\epsilon e^2 x^2 + e\left[V_G^{dc} + V_G^{ac}\cos(\omega_G t)\right] \qquad (1.67\text{b})$$

and the explicit form of the Fermi-Dirac distribution appearing in (1.65) is:

$$f\left(\mathcal{E}_D|_{N_D=1} - \mu_0\right) \triangleq \frac{1}{1 + \mathrm{e}^{-\frac{\left[\epsilon e^2 x^2 + eV_G^{dc} + eV_G^{ac}\cos(\omega_G t)\right]}{k_B\Theta}}} = f(x) \qquad (1.68)$$

In conclusion, equation (1.65) where (1.68) holds, describes the electrical part of the system.

For the mechanical equation, as in Chapter 3, we consider a simple single-DOF resonator:

$$m\frac{d^2x}{dt^2}+\gamma\frac{dx}{dt}+m\omega^2x=F_D \tag{1.69}$$

with $\omega^2=k/m$. However, in this Chapter, the electrostatic force F_D cannot be modeled in a simple way as in (1.40). In fact, regardless of having a term $V^{dc}/2d=0$, the term F_D is not null, since electrostatic induction effects – neglected in Chapter 3 – are present here. In order to take into account electrostatic induction in a simple way, calculate the force F_D as:

$$F_D=-\frac{\partial \mathcal{U}_D}{\partial x}=-\frac{\partial}{\partial x}\left[\frac{e^2{N_D}^2}{2C_D(0)}-\epsilon e^2{N_D}^2x^2+eN_DV_G\right]=2\epsilon e^2{N_D}^2x \tag{1.70}$$

where only potential part of the energy (1.59b), $\mathcal{U}_D=\mathcal{E}_D-\mathcal{T}_q$, have been used, obviously. Notice formula (1.70) depends on the actual number of electrons $N_D(t)$, whereas we are using $P_1=\langle N_D\rangle$ as lagrangian coordinate for equation (1.65). In general, it is not possible directly substitute the term ${N_D}^2$ with any function of P_1 . To proceed, we need to introduce a further assumption (in addition to the flat-gate approximation), this one being a direct consequence of consideration ii) in Section 4.2.1. In fact, in this system, due to the relatively small scale, we can assume the charge fluctuation frequency is much larger than the mechanical one, thus:

$$\Gamma_0\gg\omega \tag{1.71}$$

In the hypothesis (1.71) holds we are investigating a *soft* QSM †, and this leads to the following considerations. Since the mechanical time scale is slow, one can, in the mechanical equation (1.69), use an average force, neglecting faster electron fluctuations described by (1.65), so that:

$$F_D\approx\overline{F_D}=\overline{2\epsilon e^2{N_D}^2x}=2\epsilon e^2\overline{{N_D}^2}x=2\epsilon e^2\overline{N_D}x \tag{1.72a}$$

The last passage is possible since, in this particular case, N_D can assume only the values $\{0,1\}$. Last, assuming the *ergodic hypothesis* holds, one can match a time average with an ensemble:

$$\overline{F_D}=2\epsilon e^2\overline{N_D}x\approx2\epsilon e^2\langle N_D\rangle x \tag{1.72b}$$

Therefore, by using definition (1.60) and consequently to (1.72a,b), the mechanical equation is:

$$m\frac{d^2x}{dt^2}+\gamma\frac{dx}{dt}+m\omega^2x=2\epsilon e^2P_1x \tag{1.73}$$

which requires condition (1.71) is satisfied. Reassuming, equations (1.65) and (1.73) describe the dynamics of the whole system in Fig.1.25 if the shuttling element bears only one electron:

$$\begin{cases}m\dfrac{d^2x}{dt^2}+\gamma\dfrac{dx}{dt}+m\omega^2x=2\epsilon e^2P_1x\\[2ex]\dfrac{dP_1}{dt}=2\Gamma_0\cosh\left(\dfrac{x}{\lambda}\right)[f(x)-P_1]\end{cases},\quad f(x)\triangleq\frac{1}{1+\mathrm{e}^{-\frac{[\epsilon e^2x^2+eV_G^{dc}+eV_G^{ac}\cos(\omega_Gt)]}{k_B\Theta}}} \tag{1.74}$$

† Terms Γ_0 and $G_0/C_D(0)$ physically represent the same phenomenon, thus their values coincide, though they refer to a quantum and a semi-classical approach, respectively. From this follows that, compatibly with the definitions given in Section 2.2.8, in the case $\Gamma_0/\omega=G_0/\omega C_D(0)>1$, we are in soft regime.

Equations (1.74) can be non-dimensionalized by introducing a set of dimensionless parameters:

$$\tau \triangleq \omega t \quad , \quad \xi(t) \triangleq \frac{x(t)}{d-r}$$
$$\tilde{\gamma} \triangleq \frac{\gamma}{m\omega} = 2\zeta \quad , \quad \tilde{\epsilon} \triangleq \frac{2e^2\epsilon}{m\omega^2} \quad , \quad \tilde{d} \triangleq \frac{d-r}{\lambda} \quad , \quad \tilde{\Gamma}_0 = \frac{\Gamma_0}{\omega} \tag{1.75}$$
$$\theta \triangleq \frac{\epsilon e^2 d^2}{k_B \Theta} \quad , \quad v_{dc} \triangleq \frac{eV_G{}^{dc}}{k_B \Theta} \quad , \quad v_{ac} \triangleq \frac{eV_G{}^{ac}}{k_B \Theta} \quad , \quad \tilde{\omega} \triangleq \frac{\omega_G}{\omega}$$

In conclusion, a pair of non-dimensional equations is obtained:

$$\begin{cases} \dfrac{d^2\xi}{d\tau^2} + \tilde{\gamma}\dfrac{d\xi}{d\tau} + \xi = \tilde{\epsilon}P_1\xi \\ \dfrac{dP_1}{d\tau} = 2\tilde{\Gamma}_0 \cosh\left(\tilde{d}\xi\right)[f(\xi) - P_1] \end{cases} \quad , \quad f(\xi) = \frac{1}{1 + \mathrm{e}^{-[\theta\xi^2 + v_{dc} + v_{ac}\cos(\tilde{\omega}\tau)]}} \tag{1.76}$$

and the electron rates (1.62a,b,c,d), expressed in terms of dimensionless parameters, become:

$$i_{in,L} = (1 - P_1)\tilde{\Gamma_0}\mathrm{e}^{-\tilde{d}\xi} f(\xi) \tag{1.77a}$$
$$i_{in,R} = (1 - P_1)\tilde{\Gamma_0}\mathrm{e}^{+\tilde{d}\xi} f(\xi) \tag{1.77b}$$
$$i_{out,L} = P_1\tilde{\Gamma_0}\mathrm{e}^{-\tilde{d}\xi}[1 - f(\xi)] \tag{1.77c}$$
$$i_{out,R} = P_1\tilde{\Gamma_0}\mathrm{e}^{+\tilde{d}\xi}[1 - f(\xi)] \tag{1.77d}$$

Thus, the net left/right instant electron rates, similarly to the dimensionless microscopic currents introduced in (1.47) and with sign convention compatible with that defined in Section 2.1, are:

$$i_L(\tau) \triangleq i_{in,L} - i_{out,L} = \tilde{\Gamma_0}\mathrm{e}^{-\tilde{d}\xi}[f(\xi) - P_1] \tag{1.78a}$$
$$i_R(\tau) \triangleq i_{out,R} - i_{in,R} = \tilde{\Gamma_0}\mathrm{e}^{+\tilde{d}\xi}[P_1 - f(\xi)] \tag{1.78b}$$

The macroscopic non-dimensional current, analogously to (1.48), is obtained by averaging over a (dimensionless as well, and taken from formula (1.14)) time $\tilde{T}_{QSM} = \omega \cdot \mathrm{LCM}(T_s, T_q)$:

$$\bar{\imath} \triangleq \frac{1}{\tilde{T}_{QSM}} \int_{\tau_0}^{\tau_0 + \tilde{T}_{QSM}} i_L(\tau)\, d\tau \approx \frac{1}{\tilde{T}_{QSM}} \int_{\tau_0}^{\tau_0 + \tilde{T}_{QSM}} i_R(\tau)\, d\tau = \frac{\bar{I}}{\omega e} \tag{1.79}$$

The same is for the shuttle current contribution, calculable as in (1.49):

$$\bar{\imath}_s \triangleq \frac{1}{\tilde{T}_{QSM}} \int_{\tau_0}^{\tau_0 + \tilde{T}_{QSM}} \delta\big(\xi(\tau)\big)\dot{\xi}(\tau) N_D(\tau)\, d\tau = \frac{\bar{I}_s}{\omega e} \tag{1.80}$$

An important point is that, differently from direct shuttle, in inverse shuttle no tunnel current appears and $\bar{\imath} \equiv \bar{\imath}_s$. In fact, since the bias voltage V^{dc} is absent, when the Q-dot is at rest, no net current flows between L and R. The only chance to achieve a macroscopic current is matching a parametric resonance condition so that a limit-cycle performs the usual shuttle mechanism.

4.2.3 Parametric resonance conditions

Compatibly with hypothesis (1.71), consider the limit: $\tilde{\Gamma}_0 = \Gamma_0/\omega \to \infty$ into (1.76). Then, from the electrical equation, we directly obtain the relation:

$$P_1(\tau) \approx f(\xi, \tau) \tag{1.81}$$

Which, substituted in the mechanical one, returns (time dependences are omitted):

$$\frac{d^2\xi}{d\tau^2} + \tilde{\gamma}\frac{d\xi}{d\tau} + \xi = \tilde{\epsilon} f(\xi)\xi \tag{1.82}$$

Now write the Fourier series of the Fermi-Dirac distribution in $\xi = 0$ up to the first harmonic:

$$f(0,\tau) = \frac{1}{1 + \mathrm{e}^{-[0+v_{dc}+v_{ac}\cos(\tilde{\omega}\tau)]}} \approx a_0 + a_1\cos(\tilde{\omega}\tau) \tag{1.83}$$

In regime of small oscillations ($\xi \approx 0$), expression (1.83) can be plugged into (1.82), obtaining:

$$\frac{d^2\xi}{d\tau^2} + \tilde{\gamma}\frac{d\xi}{d\tau} + (1 - \tilde{\epsilon}a_0)\left[1 - \frac{\tilde{\epsilon}a_1}{1 - \tilde{\epsilon}a_0}\cos(\tilde{\omega}\tau)\right]\xi \approx 0 \tag{1.84}$$

The constant term a_0 produces a frequency shift of the oscillator, which is softened due to the presence of electrostatic induction and whose actual natural frequency is $\omega\sqrt{1 - \tilde{\epsilon}a_0}$. Consequently, a parametric resonance is obtained when the value of $\tilde{\omega}$ matches one of the:

$$\tilde{\omega}_h \triangleq \frac{2}{h}\sqrt{1 - \tilde{\epsilon}a_0} \qquad , \quad h \in \mathbb{N} \tag{1.85}$$

As it is well-known from the classical theory of parametric resonance (see for example, [113]) the strongest (and orthodox) parametric excitation corresponds to the choice $h = 1$, whereas the cases $h > 1$ correspond to less evident resonance peaks. Therefore, the best mechanically-wise parametric resonance condition arises by accomplishing condition:

$$\tilde{\omega} = \frac{\omega_G}{\omega} \equiv \tilde{\omega}_1 = 2\sqrt{1 - \tilde{\epsilon}a_0} \approx 2 \tag{1.86a}$$

From a conductive point of view, however, applying (1.86a) is not appropriate. In fact, since the investigated system is in *soft* regime, formula (1.26) can be profitably used to estimate the system dynamics. In this, relation (1.86a) leads to consider a characteristic ratio $\Psi \approx 2$, which, from Tab.1.2, would lead to "8-shaped" orbits on the ξ-P_1 plane. These, how has been widely discussed in Chapter 2, are not compatible with a net shuttle current: microscopic currents $i_L(\tau)$ and $i_R(\tau)$ appear as well, but the net effect when integrating over a time $\tilde{T}_{QSM}$ is a null macroscopic current. Summarizing, in order to actually achieve a shuttle current, a less mechanically-effective parametric resonance condition has to be suggested. For example, using $h = 2$:

$$\tilde{\omega} = \frac{\omega_G}{\omega} \equiv \tilde{\omega}_2 = \sqrt{1 - \tilde{\epsilon}a_0} \approx 1 \tag{1.86b}$$

In this case, the characteristic ratio is $\Psi \approx 1$ and, from Tab.1.2, this condition corresponds to an optimal shape of the phase curve ξ-P_1, with no crossings and with a maximal the shuttle current. Therefore, in the following analyses, we use the condition (1.86b) to select the value for $\widetilde{\omega}$ †. Consequently to this choice, $T_s \equiv T_q$ and, in (1.79) and (1.80), $\tilde{T}_{QSM} = \omega \cdot \mathrm{LCM}(T_s, T_q) = \omega T_s$. Also, it has be remarked the parametric resonance peak, is usually rather narrow. Again from [113], the following estimation can be obtained for the case $h = 2$:

$$\sqrt{1-\tilde{\epsilon}a_0} - \frac{1}{8}\left(\frac{\tilde{\epsilon}a_1}{1-\tilde{\epsilon}a_0}\right)^2 \lesssim \widetilde{\omega} \lesssim \sqrt{1-\tilde{\epsilon}a_0} + \frac{1}{8}\left(\frac{\tilde{\epsilon}a_1}{1-\tilde{\epsilon}a_0}\right)^2 \tag{1.87}$$

Some conclusive remarks. If the stationary part of the gate voltage v_{dc} is null, $a_0 = 1/2$. This comes from the shape of the Fermi-Dirac distribution evolution $f(0,\tau)$, which is characterized by an average value $1/2$ for any choice of v_{ac}. In Fig.1.28, some curves $f(0,\tau)$ are plotted, corresponding to different combinations of v_{dc} and v_{ac}; and, from (1.86b), with $\widetilde{\omega} = 1$.

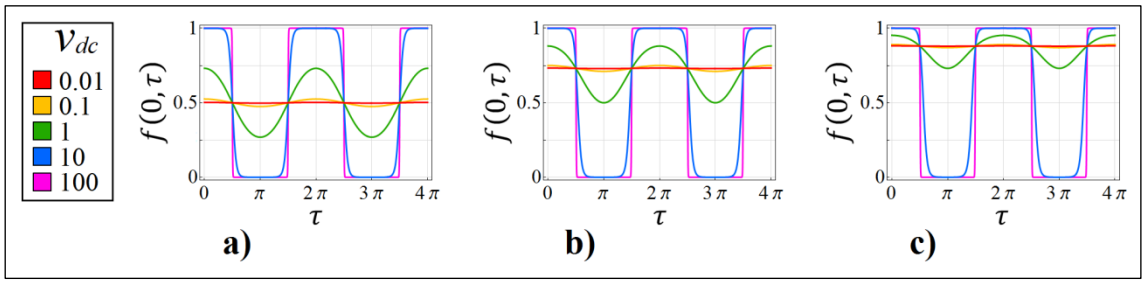

Figure 1.28 – A number of $f(0,\tau)$ curves from formula (1.83) are plotted in the case $\widetilde{\omega} = 1$, by step-varying v_{ac} and for: (a) $v_{dc} = 0$, (b) $v_{dc} = 1$, (c) $v_{dc} = 2$. Negative v_{dc} produce the same plots of positive v_{dc} except they are symmetrical with respect to the horizontal line $f = 1/2$.

From Fig.1.28 it is clear the larger are v_{dc} , v_{ac} , the more the shape of the distribution deviates from that of a sinusoid since the presence of higher harmonics becomes considerable. Consequently, since the whole procedure to estimate the parametric resonant matching conditions (1.86a,b) is based on the only contribution of the first harmonic, an accurate prediction of parametric resonance is possible only for relatively small values of the applied voltages V_G^{dc} and V_G^{dc} with respect to the temperature Θ, which is, indeed, having small v_{dc} and v_{ac} .

Last, it has to be remarked conditions (1.86a,b) match the parametric resonance only for small oscillations, since, from (1.83), we assumed $\xi = 0$ in the Fermi-Dirac distribution. The more ξ increases, the more presence of the term $\theta\xi^2$ in $f(\xi,\tau)$ is not negligible and pushes the system out from the resonant peak. Notice that the chance of reaching stable orbits relies on having a certain positive θ. In fact, in the limit case $\theta \to 0$, the oscillator is linear, and parametric resonance (as it is well-known and differently from conventional resonance) leads oscillations to diverge. In conclusion, the effect of θ is that of stabilize the Q-dot oscillations by progressively shift out the system from the resonant condition (1.86b) the more $\overline{\xi^2}$ is increases.

† Different numerical simulations, not reported in the thesis, have been carried out using condition (1.86a) as well. In these cases, as predicted, the system underwent a stronger parametric resonance, i.e. smaller values of voltages are sufficient to overcome a certain mechanical damping. However, the drawback anticipated here is confirmed, and those simulations showed no net current flowing between the L and R electrodes. Then, an interesting solution has been also attempted, by considering a double signal applied to the gate, $V_G = V_G^{dc} + V_G^{ac,I}\cos(\omega_G t) + V_G^{ac,II}\cos(\omega_G t/2)$, the harmonic $V_G^{ac,I}$ providing for an effective parametric resonance, while $V_G^{ac,II} \neq 0$ guaranteed a de-symmetrization of the "8-shaped" orbit, in order to allow a non-zero shuttle current was exhibited by the system. In conclusion, in such simulations, both (1.86a,b) were accomplished at different weights: by varying the ratio $V_G^{ac,II}/V_G^{ac,I}$ it was possible to regulate the QSM conductive behavior. For example, if $V_G^{ac,II}/V_G^{ac,I} \ll 1$ a small current passed but a strongest resonance was obtained, whereas $V_G^{ac,II}/V_G^{ac,I} \gg 1$ the converse conditions were met.

4.2.4 Approximated analytical methods

The existence of stable orbits for a system described by equations (1.76) can be analytically demonstrated by using again the soft regime assumption (1.71), for which the second equation of (1.76) is completely determined since relation (1.81) holds. One only equation remains:

$$\frac{d^2\xi}{d\tau^2} + \tilde{\gamma}\frac{d\xi}{d\tau} + \xi = \frac{\tilde{\epsilon}\xi}{1 + e^{-[\theta\xi^2 + v_{dc} + v_{ac}\cos(\tilde{\omega}\tau)]}} \tag{1.88}$$

For this, assume a solution in the form $\xi(\tau) = \tilde{A}(\tau)\cos[\tilde{\omega}\tau + \chi(\tau)]$ †. The "slowly varying approximation" for variables $\tilde{A}(\tau)$ and $\chi(\tau)$ can be assumed in case of weak electromechanical coupling, corresponding to both $\tilde{\gamma} \ll 1$ and $\tilde{\epsilon} \ll 1$ ‡, which leads to introduce the constraint:

$$\dot{\tilde{A}}\cos(\tilde{\omega}\tau + \chi) - \tilde{A}\dot{\chi}\sin(\tilde{\omega}\tau + \chi) = 0 \tag{1.89}$$

Thus, one can employ an averaging method which, after some calculations, leads to the following pair of equations in terms of $\tilde{A}(\tau)$ and $\chi(\tau)$:

$$\begin{cases} \dot{\tilde{A}} + \dfrac{\tilde{\gamma}\tilde{A}}{2} = +\dfrac{\partial\mathcal{H}}{\partial\chi} \\ \dot{\chi} = -\dfrac{\partial\mathcal{H}}{\partial\tilde{A}} \end{cases} \tag{1.90}$$

In these, $\mathcal{H}$ is the Hamiltonian, whose expression (after a change of variables $\psi \triangleq \tilde{\omega}\tau + \chi$) is:

$$\mathcal{H}(\tilde{A}, \chi) = -\frac{(1-\tilde{\omega}^2)}{2\tilde{\omega}}\tilde{A}^2 + \frac{\tilde{\epsilon}}{2\theta\pi\tilde{\omega}}\int_{-\pi}^{+\pi} \ln\left[1 + \mathrm{e}^{\theta\tilde{A}^2\cos^2\psi + v_{dc} + v_{ac}\cos(\psi-\chi)}\right] d\psi \tag{1.91}$$

Therefore, the explicit form of (1.90) is the following integro-differential set of equations:

$$\begin{cases} \dfrac{d\tilde{A}}{d\tau} + \dfrac{\tilde{\gamma}\tilde{A}}{2} + \dfrac{\tilde{\epsilon}\tilde{A}}{2\pi\tilde{\omega}}\displaystyle\int_{-\pi}^{+\pi} \frac{\sin\psi\cos\psi}{1 + \mathrm{e}^{-[\theta\tilde{A}^2\cos^2\psi + v_{dc} + v_{ac}\cos(\psi-\chi)]}} d\psi = 0 \\ \dfrac{d\chi}{d\tau} - \dfrac{(1-\tilde{\omega}^2)}{2\tilde{\omega}} + \dfrac{\tilde{\epsilon}}{2\pi\tilde{\omega}}\displaystyle\int_{-\pi}^{+\pi} \frac{\cos^2\psi}{1 + \mathrm{e}^{-[\theta\tilde{A}^2\cos^2\psi + v_{dc} + v_{ac}\cos(\psi-\chi)]}} d\psi = 0 \end{cases} \tag{1.92}$$

Notice equations (1.92) completely describe the system dynamics, since we previously assumed $P_1(\tau) \approx f(\xi, \tau)$ and $\xi(\tau) = \tilde{A}(\tau)\cos[\tilde{\omega}\tau + \chi(\tau)]$. Also, they represent the direction field of a dynamical system which can be investigated by using standard methods.

First, individuate the stationary points. By posing $\{\dot{\tilde{A}}, \dot{\chi}\} = \{0,0\}$ in (1.92), it happens that solutions always occur in pairs: to any stationary point $S_i = \{\tilde{A}_i, \chi_i\}$ corresponds a conjugated one $\overline{S_i} = \{\tilde{A}_i, \chi_i - \pi\}$. Then, the total number of stationary points $2i$ depends on the values assumed by v_G^{dc} and v_G^{ac} . Four stationary solutions, $S_1 = \{0, \pi/4\}$, $S_2 = \{0, 3\pi/4\}$, and their conjugates $\overline{S_1}$ and $\overline{S_2}$, appear for any value of the parameters and represent a rest condition. An additional pair of solutions $S_3 = \{\tilde{A}_3, \chi_3\}$ and $\overline{S_3}$, with $\tilde{A}_3 > 0$, correspond to periodic regimes and appear only when $v_{ac}^* < v_{ac} < v_{ac}^{**}$, with $v_{ac}^*(v_{dc}) > 0$ and $v_{ac}^{**}(v_{dc}^*) > 0$.

† Notice that this is the same form introduced in Chapter 2 in both (1.16) and in (1.26), for somehow similar reasons.

‡ Since $\tilde{\gamma}$ represents the damping and $\tilde{\epsilon}$ is the electrically-normalized forcing term, from the definition of electromechanical coupling proposed in Section 2.2.4, both conditions are required in order to have $K \ll 1$.

As a second task, a stability analysis can be performed by calculating the eigenvalues of the Jacobian matrix in correspondence to the stationary solutions. If S_3 appears, it is stable and both S_1 and S_2 are unstable. In the case S_3 is not present, two situations arise: if $v_{dc} > 0$, S_1 and S_2 are respectively stable and unstable, whereas if $v_{dc} < 0$, then S_1 and S_2 are unstable and stable. In every case, conjugate pairs of points share the same stability properties.

In Fig.1.29, phase portraits on the plane $\tilde{A}$-χ of systems characterized by certain parameters combinations are depicted, highlighting separatrices and basins of attraction of stable solutions. Also, the loci of stable stationary points when varying v_{dc} and v_{ac} is shown.

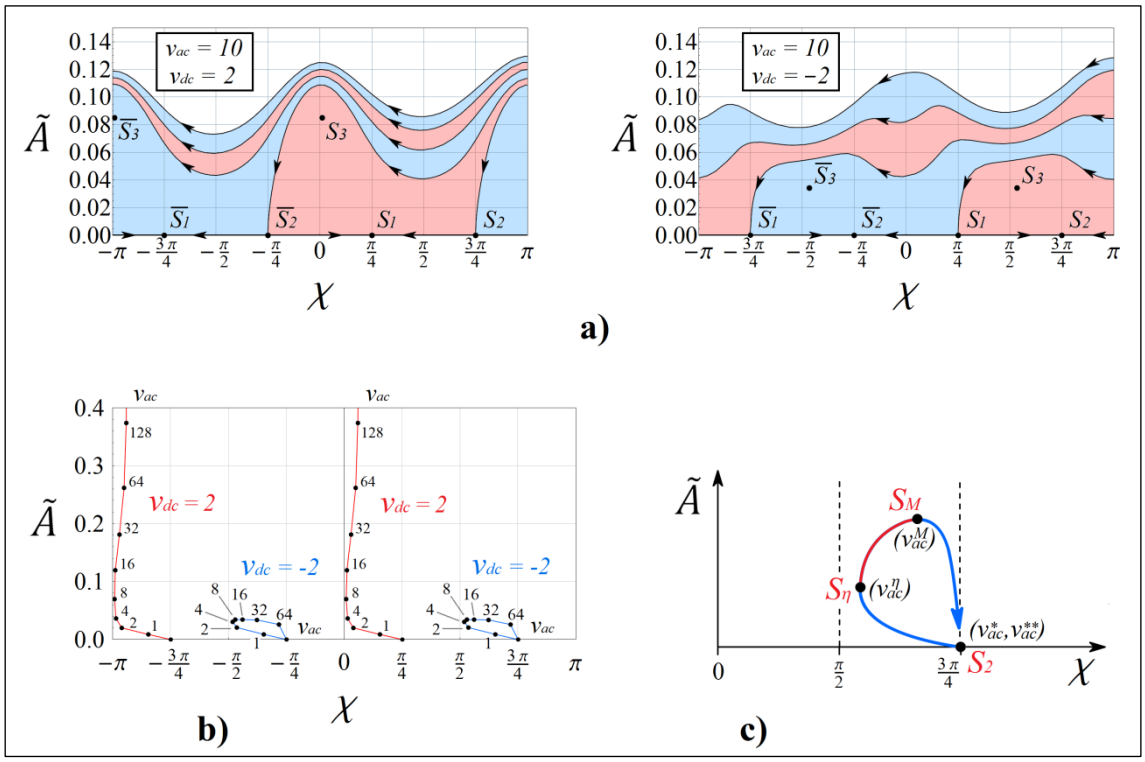

Figure 1.29 – *Stability analysis of the dynamic system described by equations (1.92) and fulfilling resonance condition (1.86b). In (a), the phase portraits for a system with parameters* $\tilde{d} = 20$, $\theta = 837$, $\tilde{\gamma} = 0.001$, $\tilde{\epsilon} = 0.1$, $a_0 = 0.56$, $v_{ac} = 10$, $v_{dc} = +2$ *(left plot) and* $v_{dc} = -2$ *(right) are shown. In both cases,* $v_{ac}^* \leq v_{ac} \leq v_{ac}^{**}$, *stable points* S_3 *and* $\bar{S}_3$ *are present, their basins of attractions respectively colored in red and blue. In both phase diagrams,* S_1 , $\bar{S}_1$, S_2 , *and* $\bar{S}_2$ *are unstable. In general, separatrices originate from* S_2 *and* $\bar{S}_2$ *when* $v_{dc} > 0$ *and from* S_1 *and* $\bar{S}_1$ *if* $v_{dc} < 0$. *Arrows indicate the separatrices direction. Trivially, the portraits are* 2π*-periodic for the phase* χ. *In (b), the position of the stable point* $S_3 = \{\tilde{A}_3, \chi_3\}$ *is plotted as a function of the applied voltages, in a QSM characterized by the same parameters choices as in (a). Curves are obtained by increasing* v_{ac} *from* v_{ac}^* *to* v_{ac}^{**} . *In the case* $v_{dc} = 2$ *(blue curve), one has* $v_{ac}^{**} \sim 100$, *while if* $v_{dc} = -2$ *(red), then* v_{ac}^{**} *appears to be infinite. In general, if* $v_{dc} > 0$, *one has* $0 < \chi_3 < \pi/4$, *whereas if* $v_{dc} < 0$, *then* $\pi/2 < \chi_3 < 3\pi/4$ *; again, when* $v_{dc} > 0$, *one has* $v_{sup} \to \infty$, *with* S_3 *originating from* S_1 , *while if* $v_{dc} < 0$, *then* v_{sup} *has a finite value, and* S_3 *both originates from and terminates in* S_2 . *In (c), one of the curves obtained for* $v_{dc} = -2$ *is magnified in a qualitative plot. Its trajectory is particularly important, since two additional characteristic conditions for* S_3 *can be individuated. A first point,* S_η , *obtained by applying a value* $v_{ac}^\eta = v_{ac}^\eta(v_{dc})$, *corresponds to the minimal distance from the phase* $\chi_3 \approx \pi/2$ *and represents an orbit which exhibits a maximally efficient shuttle mechanism (see Chapter 2). The second characteristic point,* S_M , *is obtained for* $v_{ac}^M = v_{ac}^M(v_{dc})$ *and corresponds to an orbit with the maximal amplitude, thus, maximal current, due to the exponential dependence of QT conductances from distance. In conclusion, the part of curve between* S_η *and* S_M , *in neat analogy to the power band in an engine, the loci of the best "working points" for a QSM operating in inverse shuttle.*

One can be interested to calculate the macroscopic current established by the system when it achieves a stable orbit corresponding to a stationary point S_3. Since (1.71) leads to $\tilde{\Gamma}_0 \to \infty$, relation (1.79) is not feasible to do that. Therefore, to obtain a current estimation compatible with equations (1.92), a perturbative method has to be used for the second equation:

$$P_1 = P_1{}^{(0)} + \left(\frac{1}{\tilde{\Gamma}_0}\right) P_1{}^{(I)} + \left(\frac{1}{\tilde{\Gamma}_0}\right)^2 P_1{}^{(II)} + \ldots \tag{1.93}$$

In this, compatibly with (1.71), $1/\tilde{\Gamma}_0 \ll 1$ is the perturbation parameter. The zero order approximation corresponds to the case $P_1(\tau) = f(\tau)$, already discussed in Section 4.2.3 and not viable to obtain a current estimation. Consequently, a first-order approach $P_1(\tau) = f(\tau) + \delta P_1$ is attempted, which, after some calculations, leads to an expression for the instant (left) current:

$$i_L(\tau) = \tilde{\omega} \mathrm{e}^{-\tilde{d}\tilde{A}\cos\psi} B_1(\psi) B_2(\psi) \tag{1.94a}$$

$$B_1(\psi) = \frac{\mathrm{e}^{-\left[\theta\tilde{A}^2\cos^2\psi + v_{dc} + v_{ac}\cos(\psi-\chi)\right]}}{\left\{1 + \mathrm{e}^{-\left[\theta\tilde{A}^2\cos^2\psi + v_{dc} + v_{ac}\cos(\psi-\chi)\right]}\right\}^2} \quad , \quad B_2(\psi) = \frac{2\theta\tilde{A}^2\sin(2\psi) + v_{ac}\sin(\psi-\chi)}{2\cosh\left(\tilde{d}\tilde{A}\cos\psi\right)}$$

From this, by applying (1.79), the macroscopic current can be finally obtained:

$$\bar{\imath} = \bar{\imath}\left(\tilde{A}, \chi\right) = \frac{1}{\tilde{T}_S}\int_{\tau_0}^{\tau_0+\tilde{T}_{QSM}} i_L(\tau)\, d\tau = \frac{\tilde{\omega}}{2\pi}\int_{-\pi-\chi}^{+\pi-\chi}\left[\mathrm{e}^{-\tilde{d}\tilde{A}\cos\psi} B_1(\psi) B_2(\psi)\right] d\psi \tag{1.94b}$$

Since we used $1/\tilde{\Gamma}_0$ as a small parameter, this formula is independent from the choice of $\tilde{\Gamma}_0$, and can be profitably used to calculate the current $\bar{\imath}$ established by stable orbits corresponding to any stationary point S_3 . Notice that, from the structure of (1.94a,b), conjugate orbits $S_3 = \{\tilde{A}_3, \chi_3\}$ and $\overline{S_3} = \{\tilde{A}_3, \chi_3 - \pi\}$ produce currents about equal in absolute value but different in sign †.
This fact is clearly visible in Fig.1.30, where a pair of contour plots for the current $\bar{\imath} = \bar{\imath}\left(\tilde{A}, \chi\right)$ are shown for different choices of v_{dc} and v_{ac} . In any case, these plots are symmetric with respect to the value $\chi = 0$, present a maximum current, in absolute value, around $\chi = \pm\pi/2$, and a null current for $\tilde{A} = 0$ and/or $\chi = 0 \pm h\pi$, with $h \in \mathbb{N}$.

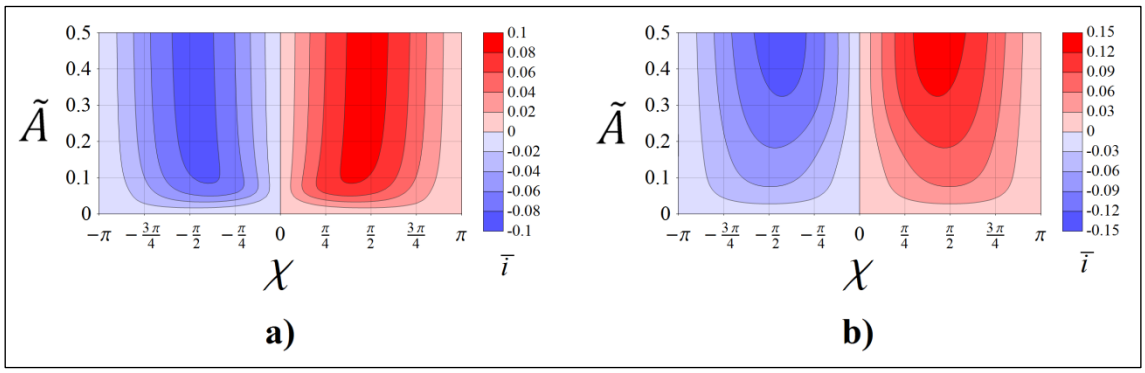

Figure 1.30 – *Dimensionless macroscopic current $\bar{\imath}$ as a function of the amplitude $\tilde{A}$ and the phase χ . Contour plots obtained from (1.94b), by matching resonance condition (1.86b), and with the following parameters: $\tilde{d} = 20$, $\theta = 837$, $\tilde{\epsilon} = 0.1$, $a_0 = 0.81$. In (a) $v_{ac} = v_{dc} = 2$, in (b) $v_{ac} = 2$ and $v_{dc} = -2$.*

† This fact confirms the anticipation made in Chapter 2, for which a QSM characterized by the same phase plot of another one, but walked in different direction (conjugate orbits with phases χ_3 and $\chi_3 - \pi$), produces the same current, but with different sign.

4.2.5 Results comparison and discussion

A series of numerical simulations have been carried out by integrating dimensionless equations (1.76) and accomplishing parametric resonance condition (1.86b). In every case, the established macroscopic current has been calculated by using formula (1.80).
Results in this Paragraph refer to the following choices of *fixed* dimensionless parameters:

$$\tilde{d} = 20 \quad , \quad \tilde{\gamma} = 0.001 \quad , \quad \tilde{\Gamma}_0 = 10 \quad , \quad \tilde{\epsilon} = 0.1 \tag{1.95a}$$

corresponding to the set of physical properties of the system:

$$(d - r) = 2\ nm \quad , \quad \lambda = 0.1\ nm \quad , \quad r \approx 4\ nm \tag{1.95b}$$
$$m \approx 5 \times 10^{-21}\ kg \quad , \quad \omega = 10^{10}\ Hz \quad , \quad \Gamma_0 = 10^{11}\ Hz$$

These numbers appear realistic for a quantum Q-dot realized with a gold nanoparticle (values for d, ω, r are compatible with [109], λ with [27] and Γ_0 gives a resistance according with [27]. Last, the relation $\tilde{\epsilon}_{[\mathrm{CGS}]} \sim (d - r)^{-3}_{[\mathrm{CGS}]}$, valid in CGS units, individuates a correct device scale).
We considered a pair of sensible values for the temperature: $\Theta = \{10, 300\}\ K$. These choices respectively correspond to the non-dimensional parameter:

$$\theta = \{837, 28\} \tag{1.95c}$$

The dimensionless quantities related to the applied voltages, v_{dc} and v_{ac} , have been treated as *free* parameters. We considered them within the following ranges:

$$v_{dc} \in [-8, +8] \quad , \qquad v_{ac} \in [0, +8] \tag{1.95d}$$

which correspond to voltages of the order of $0.1 \div 0.005\ V$, depending on the value of Θ (or θ).

It has be remarked that, compatibly with the single-electron assumption made at the beginning of Section 4.2.2, the CB requirements (1.32a,b,c), have to be fulfilled. In particular, by using relation $C_D = 4\pi\varepsilon_0 r$ †, such entire triplet of inequalities is largely verified for any combination of the fixed parameters and the allowable choices for v_{dc} , v_{ac} , θ .

An analysis of the numerical simulations, specifically the time histories for $\xi(\tau)$ and $P_1(\tau)$ under different initial conditions, provides a preliminary scenario of parametric excitation under the wide-gate assumption. We expect if $\xi(0) = 0$ the Q-dot remains at rest: $\xi(\tau) \equiv 0$. In this static regime, not only the shuttle current is null, but also the tunnel one, since no bias voltage is applied ‡. Consequently, the macroscopic current $\bar{\imath}$, calculated from (1.95), is null as well.
On the other hand, if $\xi(0) \neq 0$, a parametric excitation can be triggered. When a stable orbit is reached, the current flows in either direction depending on initial conditions, specifically the initial phase $\chi(0)$ between mechanical oscillations $\xi(\tau) = \tilde{A}(\tau)\cos[\tilde{\omega}\tau + \chi(\tau)]$ and gate voltage $v_G(\tau) = v_{dc} + v_{ac}\cos(\tilde{\omega}\tau)$. This point makes clear that it is not engineering feasible to foresee (and set) the direction of the current established by a QSM under parametric resonance. In an experimental setup, every time the signal is switched-on, the system undergoes a transient which, compatibly with the analyses in Fig.1.29, leads to a stable orbit with expected amplitude $\tilde{A}_3$ but a phase randomly χ_3 or $\chi_3 - \pi$, representing the conjugated stationary points S_3 and $\overline{S_3}$.

† This is the formula for the self-capacitance of a sphere of radius r, conventionally used in the QSM literature to calculate the capacitance of a Q-dot shuttling element. Also, we couldn't use formula (1.4), since it holds only in semi-classical models.

‡ Another explanation is that, in a symmetrical system, the application of an AC voltage on the gate cannot break the symmetry. This result is expected, since in parametric resonance the central position is a stationary (though unstable) point (see Fig.1.29).

In Fig.1.31a,b, the results of a couple of simulations obtained by integrating equations (1.76) with initial conditions $\xi(0) = \pm 0.01$ are shown (the trivial case $\xi(0) = 0$ is not reported here). In both cases, the behavior of the system confirms the discussion presented above, in particular, stable orbits characterized by the same amplitude but opposite phase produce phase portraits which are symmetrical with respect to the vertical axis and (not reported) opposite currents.

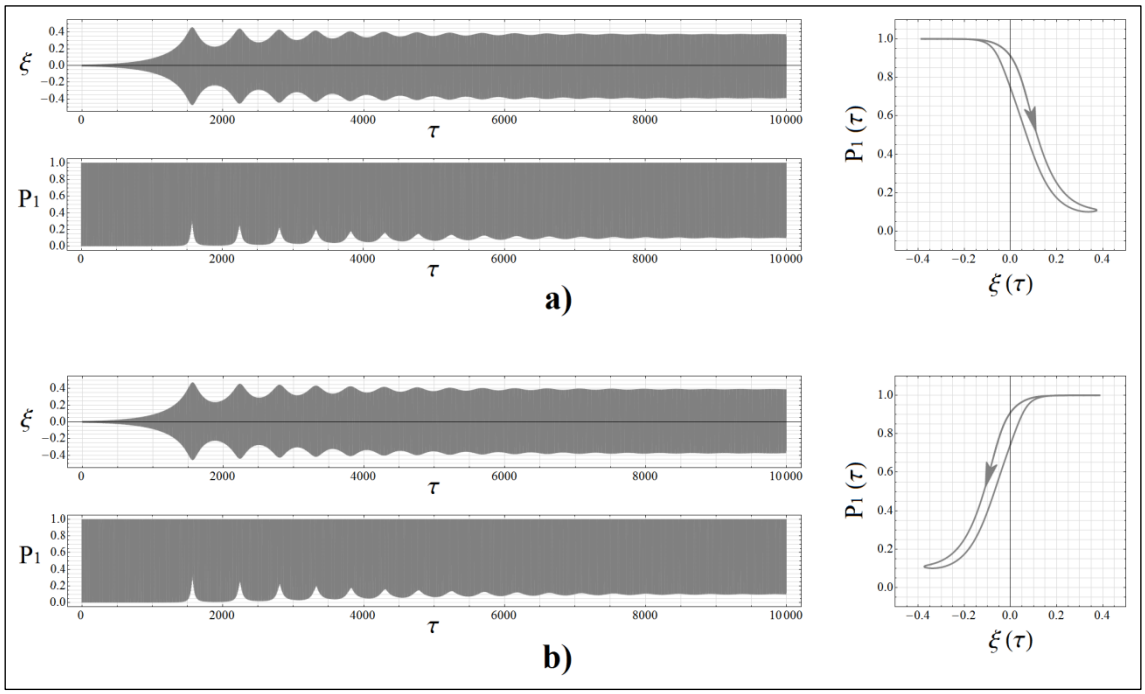

Figure 1.31 – *Inverse shuttle produced by accomplishing parametric resonance condition (1.86b). Time histories for $\xi(\tau)$ and $P_1(\tau)$ obtained by integrating equations (1.76) with initial conditions $P_1(0) = 0$ and (a) $\xi(0) = -0.01$, (b) $\xi(0) = 0.01$. Fixed parameters as in (1.95a), free parameters $v_{dc} = 2$, $v_{ac} = 8$, $\theta = 28$. Closed orbits representing stable periodic regimes are depicted on a phase plane ξ-P_1.*

Numerical results in Fig.1.31 correspond to the parametric resonance condition (1.86b), for which $\tilde{\omega} \approx 1$. As glimpsed in Section 4.2.3, the orthodox parametric resonance (1.86a) for which $\tilde{\omega} \approx 2$ establishes stable orbits characterized by a characteristic ratio $\Psi = 1$ (see Section 2.2.2), and this (from Tab.1.2) is not feasible to produce a shuttle current. In Fig.1.32, these considerations are confirmed with a numerical simulation in which the same system in Fig.1.31 undergoes a parametric resonance (1.86a) in the place of (1.86b). This time, a faster transient leads to an "8-shaped" orbit compatible with instant charge transfer but that, independently from the initial conditions, produces a null macroscopic current when averaged over a time $\tilde{T}_{QSM}$.

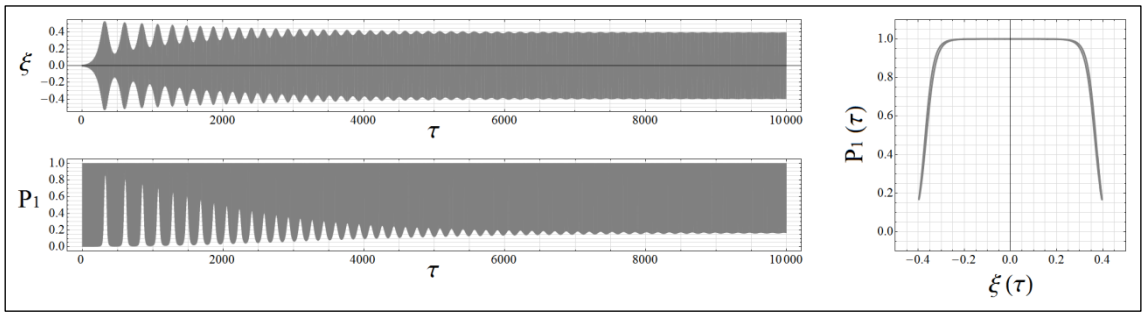

Figure 1.32 – *Inverse shuttle produced by accomplishing parametric resonance condition (1.86a). Parameters as in Fig.1.31, and initial conditions $P_1(0) = 0$ and $\xi(0) = +0.01$. Time histories for $\xi(\tau)$ and $P_1(\tau)$ establish a stable orbit on phase plane ξ-P_1 unable to produce a net current.*

By now, focus our attention only on the case of parametric resonance (1.86b), that is $\tilde{\omega} \approx 1$. We carried out a series of numerical simulations similar to those in Fig.1.31 in order to systematically investigate the properties of the stable orbits reached in inverse shuttle.
In particular, in Fig.1.33, curves representing the asymptotic values for the amplitude $\tilde{A}$ and phase χ, are plotted as a function of v_{ac}, for a fixed value of v_{dc} and different temperature. These results refer to permanent regimes established in numerical simulations obtained by integrating equations (1.76) with initial conditions $\xi(0) = +0.01$ and parameters as in (1.95a).

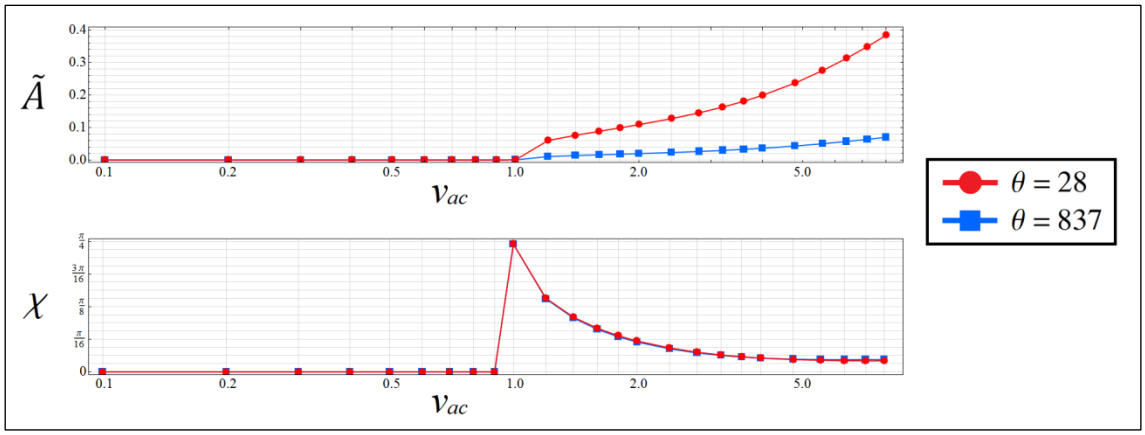

Figure 1.33 – *Curves $\tilde{A}(v_{ac})$, $\chi(v_{ac})$ plotted for $v_{dc} = +2$ and parameters (1.95a), obtained from a set of numerical simulations by integrating (1.76) with $P_1(0) = 0$, $\xi(0) = +0.01$, and fulfilling (1.86b). The cases of room ($\theta = 28$, red lines) and cryogenic ($\theta = 837$, blue) temperatures are compared.*

A quick look to plots in Fig.1.33 confirms two facts respectively glimpsed in Sections 4.2.4 and 4.2.3: i) the parametric instability is triggered for voltages $v_{ac} \geq v_{ac}^*$, whereas, for $v_{ac} < v_{ac}^*$ the system remains at rest; ii) the parameter θ has a stabilizing effect on the parametric excitation, reducing the amplitude of oscillation $\tilde{A}$, but does not influence the phase χ nor v_{ac}^*.
Consequently, once parameters (1.95a) are set, the threshold voltage v_{ac}^* remains a function of v_{dc} only, and the curve $v_{ac}^*(v_{dc})$ plays a crucial role, because it separates a plane v_{dc}-v_{ac} into two regions: $\tilde{A} = 0$ and $\tilde{A} > 0$. It is therefore clear the estimation of the function $v_{ac}^*(v_{dc})$ represents an exceptional instrument to foresee the dynamics of a QSM in inverse shuttle.

Here, we can obtain the relation $v_{ac}^*(v_{dc})$ by using two somehow complementary criteria. The first one, "numerical", produces a series of confidence intervals based on the results of a collection of numerical simulations, obtained by integrating equations (1.76) similarly to Fig.1.33, by choosing an appropriate initial conditions $\xi(0) \neq 0$. The second approach, called "analytical", is based on a closed-form estimation similar to the approximated methods seen in Section 4.2.4. In particular, by using a perturbative analysis of the generatrix Hamiltonian (1.91) with a small parameter $\tilde{A}^2$, it is possible to develop the following criterion of instability:

$$\frac{\tilde{\gamma}}{\tilde{\epsilon}} \leq \frac{\sin(2\chi^*)}{2\pi\tilde{\omega}} \int_{-\pi}^{+\pi} \frac{\cos(2\psi)}{1 + \mathrm{e}^{-[v_{dc} + v_{ac}\cos(\psi - \chi)]}} d\psi \tag{1.96}$$

In this, χ^* represents the phase of stationary solutions compatible with an incipient parametric instability, thus, from the stability analysis discussed in Fig.1.29, $\chi^* = \pi/4 \pm h\pi/2$, $h \in \mathbb{N}$.
Then, once the values for $\tilde{\gamma}$, $\tilde{\epsilon}$, $\tilde{\omega}$, χ^* are set, relation (1.96) can be profitably solved for v_{ac} with the sign "=", providing an analytical estimation of the curve $v_{ac}^*(v_{dc})$.
In Fig.1.34, the *numerical* and *analytical* methods are used to determine the function $v_{ac}^*(v_{dc})$, for a system with parameters (1.95a), in the cases of cryogenic and room temperatures.

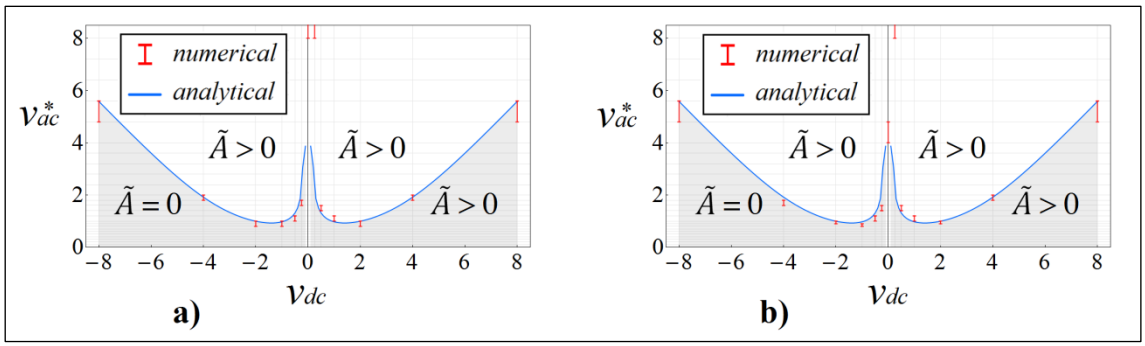

Figure 1.34 – *Threshold voltage v_{inf} as a function of v_{dc} for a system with parameters (1.95a) and fulfilling (1.86b), individuates the region (in grey). The red curve comes from numerical simulations from equations (1.76) with $\xi(0) \neq 0$; the blue curve by solving the instability criterion (1.96) for v_{ac} with sign "=". A comparison between: (a) room ($\theta = 28$), and (b) cryogenic ($\theta = 837$) temperature, is shown.*

The red and blue curves † in Fig.1.34 show a very good agreement in the whole considered range of v_{dc}: this validates all of perturbative methods exposed in Section 4.2.4. However, by applying larger voltages (results not shown here), the validity of these analytical approaches worsens, since the presence of higher order harmonics in the forcing term becomes more relevant, and the parametric resonance condition (1.86b) is less accurate. This is also the reason for which only the investigation of the threshold voltage v_{ac}^* is feasible, whereas v_{ac}^{**} not.

Last, one is interested to understand the overall conductive performances of the system. To achieve this goal, in Fig.1.35, contour plots showing the absolute value of the current $\bar{\imath} = \bar{\imath}(v_{dc}, v_{ac})$, are obtained by using the numerical approach (same set of simulations to which the red intervals in Fig.1.34 are referred) with parameters (1.96a) and different values of θ .

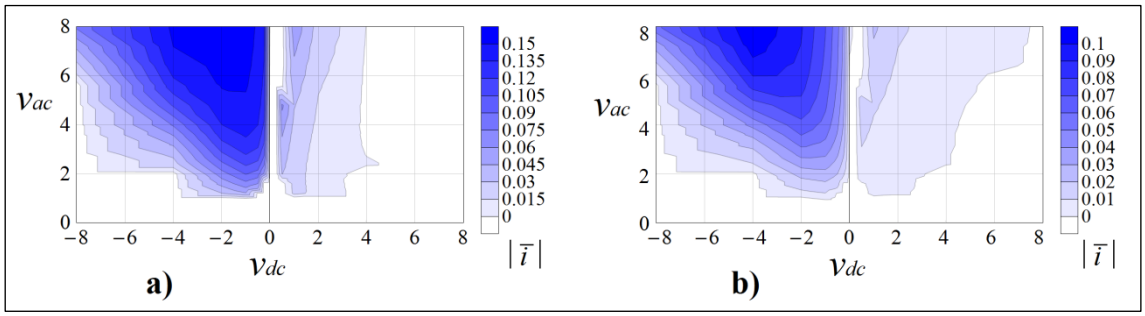

Figure 1.35 – *Absolute value of the dimensionless current $\bar{\imath}$ as a function of applied voltages v_{dc} and v_{ac}. Results refer to a collection of numerical simulations based on equations (1.76) with $\xi(0) \neq 0$. System parameters as in (1.95a) and accomplishing resonance condition (1.86b). A comparison between: (a) room ($\theta = 28$), and (b) cryogenic ($\theta = 837$) temperature, is shown.*

Plots in Fig.1.35 are highly non-symmetric with respect to the application of the voltage v_{dc} . This unusual behavior is explained with a comparative analyses with the previous results. From Fig.1.29b, the sign of v_{dc} has a strong influence on the phase χ: negative v_{dc} are more feasible to produce limit-cycles with a phase around $\chi \approx \pm\pi/2$; this, from Fig.1.30, corresponds to the maximizing condition for the current. In conclusion, use a negative value for v_{dc} is profitable. Again, the current $\bar{\imath}$ in Fig.1.35 is depicted in absolute value, since its sign depends on the initial conditions of the system, which, in an experimental setup, are not controllable. Last, the effect of decreasing θ (that is, increasing Θ) was that (from Fig.1.33) to increase the amplitude of oscillations $\tilde{A}$: this fact is inherited by the current $\bar{\imath}$, which (from Fig.1.35) is indeed promoted.

† Actually, the blue curve is the same in both Fig.1.34a,b, since formula (1.96) is independent from the parameter θ.

4.3 Generic gate distance: "semi-classical" analytical approach

4.3.1 Introduction

In this paragraph, a generalization of the results obtained in Section 4.2 is considered. This comes by considering the dependence of the shuttling element voltage V_S from its position $x(t)$, thus, in relation (1.55), the term $\beta(x)$ is no more a constant.
Since in the model in Fig.1.25, we assumed no QT occurs between S and G †, the characteristic gate distance g has to be considerably larger than the tunneling distance λ. Follow that, if one is interested to investigate the effect of a relevant dependence $\beta(x)$, then has to consider a system for which $\lambda \ll g \leq d$. The latter condition justifies the choice, made indeed in this Paragraph, to investigate an inverse QSM in the *hard* regime, differently from Section 4.2, which was referred to the *soft* case. This leads to the following general considerations:

i) The scale of the device is now sufficient to consider a nanopillar realization of the shuttling element. Thus, in this Paragraph, the shuttling element is indicated with the letter "P".
ii) Due to the larger scale, we are not in CB regime. Therefore, a continuous-charge model is acceptable and is here used. In particular, the circuital scheme in Fig.1.25 is again valid. According to Section 2.3 and similarly to Chapter 3, the electrodynamics of the system is indeed described by equivalent QT conductances calculated with one of relations (1.1a,b).
iii) As in Chapter 3, the external force on the pillar is due to electrostatic induction, and an assumption like (1.70) is used. However, the averaging procedure (1.72a,b) based on the hypothesis (1.71) is no more required here. Also, it would be not feasible, because, in the hard regime, the electrodynamics/mechanical frequency ratio is less than unity.
iv) In this system it is not trivially possible to consider a small oscillations regime $A \ll d - r$ (which would allow to neglect again the dependence $\beta = \beta(x)$). In fact, due to the classical model used, no stabilizing effect is present in the system: a term θ, in Section 4.2.3, provided for this, but here is not present, since we are using a semi-classical electrical model, and there is no role for the Fermi-Dirac distribution (from which θ physically arouse). However, in a linear system (without the hardening effect of θ), a resonator under parametric resonance would increase its oscillations amplitude indeterminately.
v) Consequently, to avoid a divergence of the system, we have to take into account some nonlinear effects introduced *ad hoc* and which could be neglected in Section 4.2.3, also because we were under the hypothesis of small oscillations.

4.3.2 Equations

Since the circuital model in Fig.1.25 is now valid, equations refer to the same general form of (1.36a,b). In these, terms V_L , V_R , V_S , G_L , G_R , F_P have to updated to the present case.
First, from (1.54a), the leads voltages are identically null: $V_L = V_R \equiv 0$. Then, the instant voltage of the pillar V_P has the general structure (1.55). In this case, it specifies into:

$$V_P = V_P(x, Q_P) = \frac{Q_P + C_G V_G}{C_P(x)} \tag{1.97}$$

since $\alpha = C_P(x)$ and $\beta = C_G/C_S(x)$. This confirms that $\beta = \beta(x)$, differently from Section 4.2.

† This condition is analogous to a SET, but different, for example, from a more general architecture investigated by Isacsson [29] and comprising, indeed *three* TJ. That article demonstrates in such case, a chaotic dynamics can be exhibited by the system.

Then, QT is introduced by using equivalent conductances $G_{L,R}(x)$ modeled as in Chapter 3:

$$G_{L,R}(x) = G_c \mathrm{e}^{\frac{r-d}{\lambda}} e^{\mp\frac{x}{\lambda}} = G_0 \mathrm{e}^{\mp\frac{x}{\lambda}} \tag{1.98a, b}$$

From point iii) of Section 4.3.1, follows that the external force on the pillar has to be calculated from the electrostatic potential energy $\mathcal{U}$. Actually, one has to subtract the effect of the voltage application on the gate. Thus:

$$\tilde{\mathcal{U}} = \mathcal{U} - Q_G V_G = \frac{(Q_P + C_G V_G)^2}{2C_P(x)} - \frac{C_G {V_G}^2}{2} \tag{1.99a}$$

$$F_P = -\frac{\partial \tilde{\mathcal{U}}}{\partial x} = -\frac{(Q_P + C_G V_G)^2}{2} \frac{\partial}{\partial x}\left[\frac{1}{C_P(x)}\right] \tag{1.99b}$$

Now, similarly to (1.58), we develop a Taylor expansion of the forcing term around the center position, obtaining a linearized forcing term:

$$F_{P,lin} = 2\epsilon(Q_P + C_G V_G)^2 x \quad , \qquad \epsilon \triangleq \frac{1}{4{C_P}^2(0)} \left.\frac{d^2 C_P(x)}{dx^2}\right|_{x=0} \tag{1.100}$$

Then, to take into account the hardening effects which are neglected in $F_{P,lin}$, we deliberately add a non-linear term in the mechanical equation, obtaining a non-linear *Duffing oscillator* with $\kappa > 0$, so that a relation $F_P = F_{P,lin} - \kappa x^3$ holds. This approach (separation between a linear electrostatic force and an *ad hoc* non-linear term) has been used because: i) differently from Section 4.2.3, we now have to (this is explained in point v) of Section 4.3.1) include non-linear effects in our model; ii) an expression in which the coupling parameter ϵ appears is still useful to calculate the parametric resonance condition.
In conclusion, collecting relations (1.98)-(1.100), the whole QSM is described by equations:

$$\begin{cases} m\dfrac{d^2x}{dt^2} + \gamma\dfrac{dx}{dt} + kx + \kappa x^3 = 2\epsilon(Q_P + C_G V_G)^2 x \\ \dfrac{dQ_P}{dt} = -2\dfrac{G_0}{C_P(x)} \cosh\left(\dfrac{x}{\lambda}\right)(Q_P + C_G V_G) \end{cases} \tag{1.101}$$

in these, from (1.54b) the gate voltage is further specified in $V_G \triangleq {V_G}^{dc} + {V_G}^{ac} \cos(\omega_G t)$.

The electrostatics of the system can be modeled similarly to Chapter 3. In this case, referring to the scheme in Fig.1.36, the fixed electrodes can be considered as *plate* conductors, whereas the cap of the pillar (representing the shuttling element), is a *spherical* one.

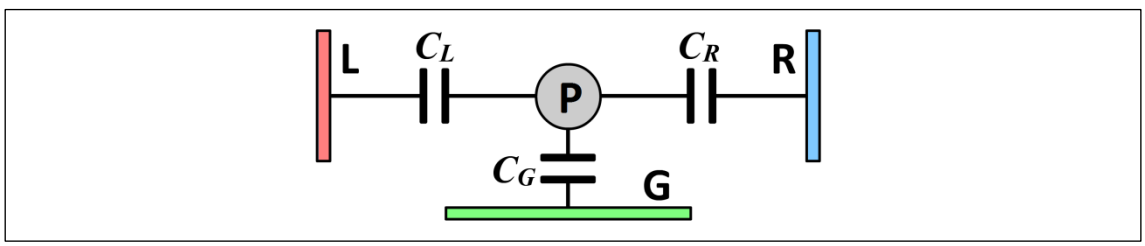

Figure 1.36 – *Electrostatic scheme of the QSM depicted in Fig.1.25, in the case of generic gate distance. Terminals L , R , G are modeled as plate conductors, while the cap of the pillar P is considered a sphere.*

Then, the capacitances of the system are calculated as follows (a value $B = 0.165$, which best fits relation (1.43), is used for them):

$$C_P(x) = C_L(x) + C_R(x) + C_G = 4\pi\varepsilon r\left[3 + Br\left(\frac{1}{d-r+x} + \frac{1}{d-r-x} + \frac{1}{g-r}\right)\right]$$

$$C_{L,R}(x) = 4\pi\varepsilon r\left(1 + B\frac{r}{d-r\pm x}\right) \quad , \quad C_G = 4\pi\varepsilon r\left(1 + B\frac{r}{g-r}\right) \qquad (1.102)$$

Define the following set of non-dimensional parameters:

$$\tau \triangleq \omega t \quad , \quad \xi(\tau) \triangleq \frac{x(\tau)}{d} \quad , \quad N_P(\tau) \triangleq \frac{Q_P(\tau)}{e}$$

$$\tilde{d} \triangleq \frac{d}{\lambda} \quad , \quad \tilde{g} \triangleq \frac{g}{d} \quad , \quad \tilde{r} \triangleq \frac{r}{d} \quad , \quad \tilde{\gamma} \triangleq \frac{\gamma}{m\omega} \quad , \quad \tilde{\kappa} \triangleq \frac{\kappa d^2}{m\omega^2} \qquad (1.103a)$$

$$v_{dc} \triangleq \frac{C_G {V_G}^{dc}}{e} \quad , \quad v_{ac} \triangleq \frac{C_G {V_G}^{ac}}{e} \quad , \quad \tilde{G}_0 \triangleq \frac{G_0}{\omega C_P(0)} \quad , \quad \tilde{\epsilon} \triangleq \frac{2e^2\epsilon}{m\omega^2} \quad , \quad \tilde{\omega} \triangleq \frac{\omega_G}{\omega}$$

and introduce the non-dimensional function:

$$c_P(\xi) \triangleq \frac{3 + B\tilde{r}\left(\frac{2}{1-\tilde{r}} + \frac{1}{\tilde{g}-\tilde{r}}\right)}{3 + B\tilde{r}\left(\frac{1}{1-\tilde{r}+\xi} + \frac{1}{1-\tilde{r}-\xi} + \frac{1}{\tilde{g}-\tilde{r}}\right)} \qquad (1.103b)$$

Then, a dimensionless set of equation is obtained (time dependencies omitted):

$$\begin{cases} \dfrac{d^2\xi}{d\tau^2} + \tilde{\gamma}\dfrac{d\xi}{d\tau} + \xi + \tilde{\kappa}\xi^3 = \tilde{\epsilon}[N_P + v_{dc} + v_{ac}\cos(\tilde{\omega}\tau)]^2\xi \\ \dfrac{dN_P}{d\tau} = -2\tilde{G}_0 c_P(\xi)\cosh\left(\tilde{d}\xi\right)[N_P + v_{dc} + v_{ac}\cos(\tilde{\omega}\tau)] \end{cases} \qquad (1.104)$$

The dimensionless microscopic currents are:

$$i_{L,R}(\tau) \triangleq \frac{I_{L,R}(\tau)}{\omega e} = \mp\tilde{G}_0 e^{\mp\tilde{d}\xi(\tau)} c_P(\tau)[N_P(\tau) + v_{dc} + v_{ac}\cos(\tilde{\omega}\tau)] \qquad (1.105\text{a, b})$$

From these, the macroscopic non-dimensional current and its part due to the shuttle contribution are calculated similarly to (1.79)-(1.80) by averaging over the dimensionless time $\tilde{T}_{QSM}$:

$$\bar{\imath} \triangleq \frac{1}{\tilde{T}_{QSM}}\int_{\tau_0}^{\tau_0+\tilde{T}_{QSM}} i_L(\tau)\,d\tau \approx \frac{1}{\tilde{T}_{QSM}}\int_{\tau_0}^{\tau_0+\tilde{T}_{QSM}} i_R(\tau)\,d\tau = \frac{\bar{I}}{\omega e} \qquad (1.106)$$

$$\bar{\imath}_s \triangleq \frac{1}{\tilde{T}_{QSM}}\int_0^{\tilde{T}_{QSM}} \delta\big(\xi(\tau)\big)\dot{\xi}(\tau)N_P(\tau)\,d\tau = \frac{\bar{I}_s}{\omega e} \qquad (1.107)$$

4.3.3 Parametric resonance conditions

Due to the different structure of the voltage of the pillar V_P , and to the multiple-electron shuttle exhibited by the considered system, the electrostatic forcing term in equations (1.104) is formally different from that analyzed in Section 4.2.3 †. In fact, the first equation produces:

$$\frac{d^2\xi}{d\tau^2}+\tilde{\gamma}\frac{d\xi}{d\tau}+\left(1-\frac{\tilde{\epsilon}{v_{ac}}^2}{2}-\tilde{\epsilon}{v_{dc}}^2\right)\left\{1-\frac{2\tilde{\epsilon}}{2-\tilde{\epsilon}{v_{ac}}^2-2\tilde{\epsilon}{v_{dc}}^2}\times\right. \tag{1.108}$$

$$\left.\times\left[{N_P}^2+2N_Pv_{dc}+2N_Pv_{ac}\cos(\tilde{\omega}\tau)+\frac{{v_{ac}}^2}{2}\cos(2\tilde{\omega}\tau)+2v_{dc}v_{ac}\cos(\tilde{\omega}\tau)\right]\right\}\xi+\tilde{\kappa}\xi^3=0$$

In such situation, the study of parametric resonance is more complex with respect to Section 4.2. In fact, as much as *five* oscillating terms appear: those in the square brackets in formula (1.108).

Start our analysis by considering a regime of small oscillations ($\xi\sim 0$). In this case, charge transport is not activated ‡ and $N_P=\text{const}$: thus, oscillating terms which depend on the $N_P(\tau)$ cannot play a role in the parametric excitation, and the nonlinear term $\tilde{\kappa}\xi^3$ can be neglected. Therefore, the mechanical equation (1.108) simplifies into:

$$\frac{d^2\xi}{d\tau^2}+\tilde{\gamma}\frac{d\xi}{d\tau}+\left(1-\frac{\tilde{\epsilon}{v_{ac}}^2}{2}\right)\left\{1-\frac{2\tilde{\epsilon}}{2-\tilde{\epsilon}{v_{ac}}^2}\left[\frac{{v_{ac}}^2}{2}\cos(2\tilde{\omega}\tau)+2v_{dc}v_{ac}\cos(\tilde{\omega}\tau)\right]\right\}\xi=0 \tag{1.109}$$

On the other hand, the prototypical equation for a standard parametric resonance is:

$$\ddot{X}(t)+\Omega^2\left[1\pm A\cos\left(\frac{2\Omega}{h}t\right)\right]X(t)=0 \qquad , \quad h\in\mathbb{N} \tag{1.110}$$

Let us investigate under which requirements (1.109) is compatible with the general structure (1.110), by taking into account that: i) in equation (1.109), condition $\tilde{\omega}\approx 1$ is necessary to have a system whose stable orbits are able to produce a macroscopic current (see Section 2.2.2); ii) in equation (1.110), condition $h=1$ achieves the most effective excitation (see Section 4.2.3). Focus our attention on equation (1.109): two terms, depending on the choice of $\tilde{\omega}$, can trigger the parametric resonance. The overall casuistic is summarized in Tab.1.6.

Table 1.6 – *Parametric resonance conditions achievable by a system described by equations (1.109).*

Condition	**Dimensionless forcing frequency**	**Parametric resonance achievable by the term:**	
		$\boldsymbol{{v_{ac}}^2\cos(2\tilde{\omega}\tau)/2}$	$\boldsymbol{2v_{dc}v_{ac}\cos(\tilde{\omega}\tau)}$
I	$\tilde{\omega}>2$	no	no
II	$\tilde{\omega}\approx 2$	no	yes, $h=1$
III	$\tilde{\omega}\approx 1$	yes, $h=1$	yes, $h=2$
IV	$\tilde{\omega}\approx 1/2$	yes, $h=2$	yes, $h=4$
…	$\tilde{\omega}\approx 1/N$	yes, $h=N$	yes, $h=2N$

Although *two* terms are feasible to trigger a parametric instability in the system, from a design point of view, it is preferable optimize the system to reach resonance with only one of them. Only in such case, in fact, the structure of (1.109) can resemble (1.110), and an univocal resonant condition (similar to (1.86a,b)), to accomplish by selecting an appropriate $\tilde{\omega}$, is obtained.

† Notice how, in particular, here it is not possible to assume $1/\tilde{G}_0\to 0$ as in the perturbative approaches carried out Section 4.2.

‡ This is because since we are in hard regime (from Section.4.3.1), then (from Section 2.2.8) one has $\tilde{A}_t>\xi\approx 0$.

In order to do this, introduce the following constraints †:

$$\frac{v_{ac}}{|v_{dc}|} \gg 4 \quad , \qquad 0 < \frac{v_{ac}}{|v_{dc}|} \ll 4 \tag{1.111a, b}$$

Consider (1.111a): in the limit case $v_{dc} = 0$, only the first term in (1.109) remains. Then, from Tab.1.6, a parametric resonance can be obtained with conditions III, IV, or the consequent ones. Neatly, the best choice is condition III, because it fulfills both $h = 1$ (the most effective parametric excitation for the first term) and $\widetilde{\omega} \approx 1$ (feasibility of a net macroscopic current). Substituting $h = 1$ in equation (1.109), the following resonant matching condition is obtained:

$$\widetilde{\omega} = \sqrt{1 - \tilde{\epsilon}\frac{{v_{ac}}^2}{2}} \approx 1 \tag{1.112a}$$

Now consider (1.111b). In this case, only the second term in the square brackets of (1.109) is important, and parametric resonance can be obtained, referring to Tab.1.6, by using conditions II, III, IV, and so on. One could select again condition III by fulfilling (1.112a): this is compatible with a macroscopic current (since $\widetilde{\omega} \approx 1$); but, this time, corresponds to a less effective excitation and more narrow resonant peak (because, for the second term, $h = 2$). Otherwise, one could select condition II, which is unfeasible to produce a current (since $\widetilde{\omega} \approx 2$); but produces the most effective parametric resonance for the second term (for which $h = 1$). Condition II is achieved by matching the following resonance:

$$\widetilde{\omega} = 2\sqrt{1 - \tilde{\epsilon}\frac{{v_{ac}}^2}{2}} \approx 2 \tag{1.112b}$$

The situation is summarized as follows. If constraint (1.111a) holds, condition III in Tab.1.6 is the best from both the conductive and mechanical points of view, and is obtained by fulfilling (1.112a). Instead, constraint (1.111b) leads to select among condition III or condition II, respectively achieving the conductive or mechanical goals, and obtained with (1.112a) or (1.112b).
Last, if none of (1.112a,b) holds, no clear resonance condition can be obtained.
In conclusion, from a design point of view, constraint (1.111a) seems straightforwardly preferable , thus, the limit case $v_{dc} = 0$ is taken into account in the next sub-Paragraph numerics.

Up to here, our analysis was limited to a regime of small oscillations. This was useful to understand better the incipient dynamics of the system. However, once a parametric excitation has been triggered, the amplitude of oscillations grows indefinitely. When the assumption $\xi \sim 0$ does not hold anymore, the system cannot be further described by the equation (1.109), and its complete form (1.108) should be considered: this produces two main physical consequences.
The first one is that the hardening effects of the nonlinear term $\tilde{\kappa}\xi^3$ are now relevant, gradually shifting the system out from the resonant peak and stabilizing the amplitude of oscillation.
The second effect is that, over a certain amplitude threshold $\tilde{A}_t$ (we are in *hard* shuttle regime), QT phenomena become important, the shuttle mechanism is activated, and the effect of the oscillating terms which contain $N_P(\tau)$ "dirties" the (standard) parametric resonance, producing not predictable effects on the system dynamics and conductive properties. These phenomena will be disclosed in the following sub-Paragraph.

† In (1.111b), the limit case $v_{ac} = 0$ should be avoided, since in such condition both oscillating terms disappear, making a parametric excitation unfeasible.

4.3.4 Numerical results and discussion

The structure of equations (1.104) does not allow analytical approaches based on perturbative methods which assume $1/\tilde{G}_0$ as a small parameter, as it was the case of Section 4.2.4. Thus, inverse shuttle is investigated with direct numerical simulations based on equations (1.104).
Also, as anticipated in the previous sub-Paragraph, the parametric resonance situation is now more various than in Section 4.2, and generalizes the results obtained under the "wide-gate" assumption, which constituted, in this sense, a special case of the results presented here.

Compatibly with the larger device scale (Section 4.3.1), consider the physical quantities:

$$d = g = 30\,nm \quad , \quad r = 10\,nm \quad , \quad m = 1 \times 10^{-18}\,kg \quad , \quad \omega = 1 \times 10^{8}\,Hz \tag{1.113a}$$

Select a tunneling length $\lambda = 0.5\,nm$; then, respectively from (1.198a,b) and (1.102):

$$G_0 \approx 4.2 \times 10^{-15}\,S \quad , \quad C_P(0) \approx 3.6 \times 10^{-18}\,F \quad , \quad C_G \approx 1.2 \times 10^{-18}\,F \tag{1.113b}$$

Therefore, the following values for the non-dimensional parameters in (1.103a) are set:

$$\tilde{d} = 60 \quad , \quad \tilde{g} = 1 \quad , \quad \tilde{r} = 3 \quad , \quad \tilde{\gamma} = 10^{-3} \quad , \quad \tilde{\kappa} = 0.1 \quad , \quad \tilde{G}_0 = \tilde{\epsilon} = 10^{-5} \tag{1.114a}$$

The only free parameters are v_{ac} and v_{dc} , which are considered within in the intervals:

$$v_{ac} \in [0{,}50] \quad , \qquad v_{dc} \in [-50, +50] \tag{1.114b}$$

These ones correspond to applied voltages ${V_G}^{dc}$ and ${V_G}^{dc}$ with values of the order of some *volts*. Last, referring to Tab.1.6, we choose the parametric instability condition III: the exact value for $\tilde{\omega}$ is calculated from (1.112a) to match the resonant peak. Settings (1.114a,b) and resonance condition (1.112a) are used to carry out all the numerical simulations in this sub-Paragraph.

To achieve a preliminary understanding of the dynamics, postulate oscillations in the form:

$$\xi(\tau) = \tilde{A}\cos(\tilde{\omega}\tau + \chi) \tag{1.115}$$

where $\tilde{A} \triangleq A/d$ and χ is the phase with respect to the voltage signal $v(\tau) = v_{dc} + v_{ac}\cos(\tilde{\omega}\tau)$. Then, in a first set of simulations, plug the ansatz (1.115) into the second equation of (1.104) and integrate it for $N_P(\tau)$. Such approach tests the electrodynamical response of a system to a motion regime determined by a given combination $(\tilde{A}, \chi)$, using relation (1.106) to calculate the corresponding macroscopic current $\bar{\imath}$. In Fig.1.37, some charts $\bar{\imath} = \bar{\imath}(\tilde{A}, \chi)$ are shown.

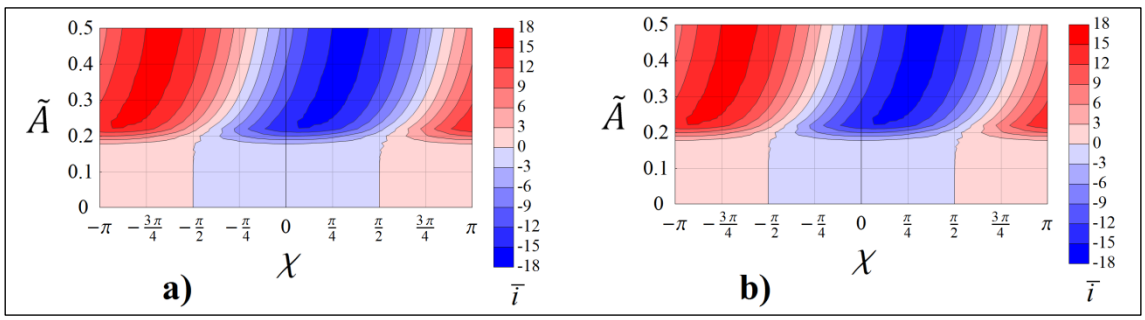

Figure 1.37 – *Current $\bar{\imath}$ as a function of $\tilde{A}$ and χ from (1.115), plugged in the second equation of (1.104), solved for $N_P(\tau)$, with $N_P(0) = 0$. Contour plots obtained using relation (1.106), by matching resonance condition (1.112a), and parameters as in (1.114a). In (a) $v_{ac} = 50$ and $v_{dc} = 0$, in (b) $v_{ac} = v_{dc} = 50$.*

It has be remarked the existence of mechanical oscillations like (1.115) requires the weak electromechanical coupling assumption (already used in Section 4.2.4), then (from the definition given in Section 2.2.4) relatively low values for $\tilde{\gamma}$ and $\tilde{\epsilon}$, coherent with the choices in (1.114a).
Analyze the contour plots in Fig.1.37. First of all, they are substantially identical, meaning the presence of a stationary voltage on the gate does not perturbate the electrodynamics of a system characterized by a known vibrational regime. Second, these plots, at small amplitudes, present a macroscopic current which is maximum, in absolute value, in correspondence of $\chi = 0$ (negative in sign), and $\chi = \pm\pi$ (positive). This states a different behavior with respect to Section 4.2.4, in particular Fig.1.30, in which the maximum absolute current is around $\chi = \pm\pi/2$. Such contrast arises from the different structure of the forcing term in the mechanical equation of (1.76) versus (1.104), due to the single-electron hypothesis introduced in Section 4.2. Last, contour plots in Fig.1.37 states an orbit with parameters $(\tilde{A}, \chi)$ exhibits the same macroscopic current, with different direction, of an orbit $(\tilde{A}, \chi - \pi)$. This resembles the discussion around the conjugated stable solutions S_3 and $\overline{S_3}$, in Section 4.2.4 as well: in turn, it suggests that, also in this case, initial conditions have a role in selecting which specular asymptotic behavior $(\tilde{A}, \chi)$ or $(\tilde{A}, \chi - \pi)$ is achieved, and, consequently, which is the direction of the macroscopic current.
To conclude the analysis of Fig.1.37, notice that, while in Fig.1.30 the emergence of the current is gradual when the amplitude is increased, since the system was *soft*; this is not the case of Fig.1.30, where, due to the *hard* nature of the investigated QSM, a considerable current appears only when a certain threshold amplitude $\tilde{A}_t$ is reached. Notably, this fact could produce a proper "transition" among two different vibrational states: in order investigate this possibility, we require a *tout court* analysis of the QSM dynamics, in which $\xi(\tau)$ is not imposed as in (1.115).

Consequently, consider another series of numerical simulations coming from the simultaneous integration of *both* mechanical and electrodynamical equations in (1.104). We again refer to the parameters (1.113a,b) and (1.114a,b). In Figg.1.38-1.41, the results of some exemplificative numerical simulations are shown, corresponding to different combinations of the gate voltages v_{dc} and v_{ac} and equations solved with opposite initial conditions $\pm\xi_0$ with $\xi_0 = \xi(0) > 0$. In all plots, time histories for pillar position $\xi(\tau)$ and electrons $N_P(\tau)$ are shown, together with the post-processed phase and macroscopic current †, showed in both cases of initial conditions.
In Fig.1.38, $v_{ac} = 25$ and $v_{dc} = 0$: these boundary conditions are sufficient to trigger a parametric instability and a conventional shuttle mechanism characterized by amplitude $\tilde{A} \approx 0.1$ is definitely achieved. Depending on the initial conditions selected, the phase χ establishes around 0 ($\xi(0) = +0.1$) or π ($\xi(0) = -0.1$). This, compatibly with the discussion around Fig.1.37, produces a macroscopic current $\bar{\imath}$ flowing in either directions but equal in absolute value.
In Fig.1.39, $v_{ac} \equiv v_{dc} = 25$: the system dynamics and conductive properties are the same of Fig.1.38, except for average value of electrons on the pillar, which oscillates around a value $N_P(\tau) \approx 25$. Since, in Fig.1.38, the mean value was $N_P(\tau) \approx 0$, one understands that, while establishing a stable shuttle mechanism, the value of N_P tends to the value $-v_{dc}$. Actually, this is the only effect of the presence of a static voltage v_{dc}: in particular, directly from (1.111a,b), in the case $v_{dc} > v_{ac}/4$, the transient duration to make $N_P \to -v_{dc}$ can dramatically increase.
In Fig.1.40, $v_{ac} = 50$ and $v_{dc} = 0$: a parametric instability is again triggered, but a different vibrating regime, corresponding to a *novel* kind of shuttle mechanism, is established. In fact, such a high voltage makes the pillar to surpass the amplitude $\tilde{A}_t$, reaching the tunneling region. The consequent sudden increase in the charge transport phenomena (something not experienced in soft shuttle) produces a phase χ which does not stabilize but *shifts with time*, instead. In other words, *an exotic shuttle mechanism, achieving a macroscopic AC current, is obtained*.
The same arguments hold for Fig.1.41, where $v_{ac} \equiv v_{dc} = 50$, except for the shifted electrons oscillating range $N_P(\tau) \in (-v_{ac} - v_{dc}, v_{ac} - v_{dc})$ (in Fig.1.40 it was $N_P(\tau) \in (-v_{ac}, v_{ac})$).

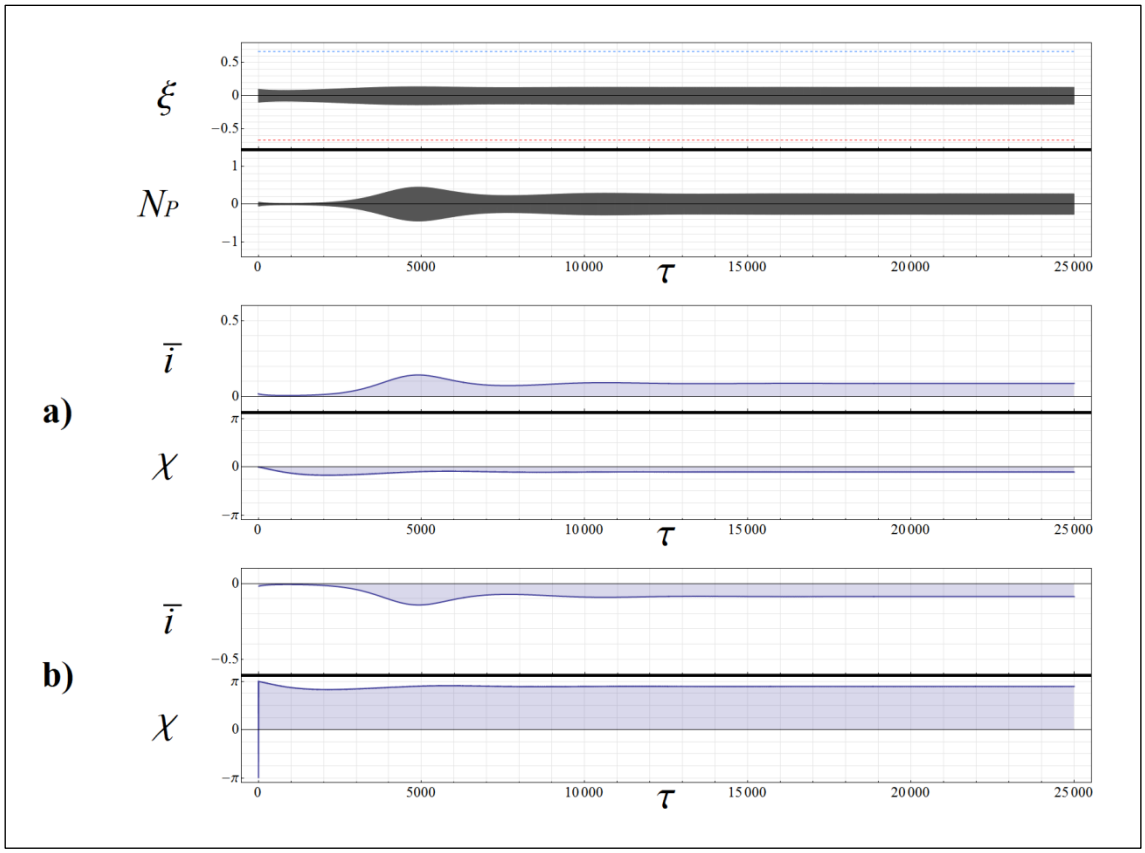

Figure 1.38 – *Time histories of position $\xi(\tau)$ and electrons $N_P(\tau)$ given by integrating equations (1.104). Phase $\chi(\tau)$ and macroscopic current $\bar{\imath}(\tau)$ by using initial conditions: (a) $\xi(0) = +0.1$, (b) $\xi(0) = -0.1$. System parameters as in (1.114a), resonance condition (1.112a), and voltages $v_{ac} = 25$, $v_{dc} = 0$.*

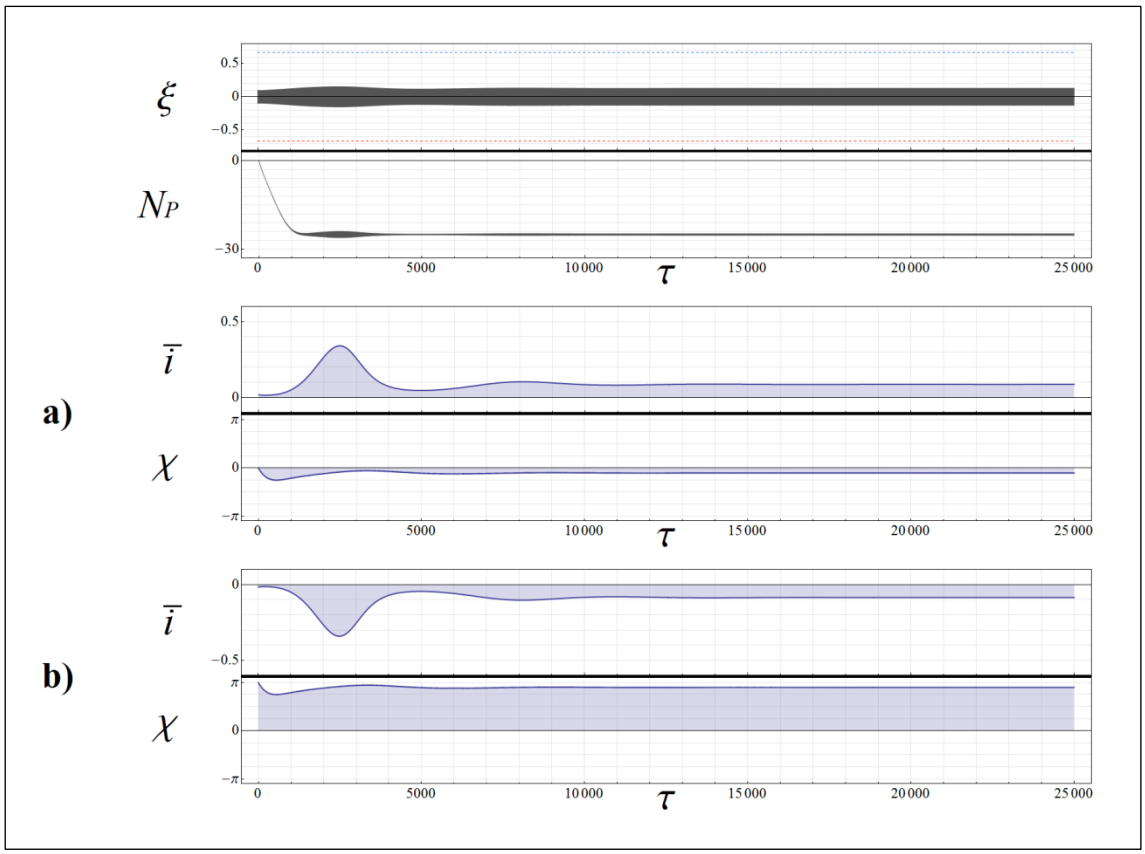

Figure 1.39 – *Same description as in Fig.1.38, except for voltages $v_{ac} \equiv v_{dc} = 25$.*

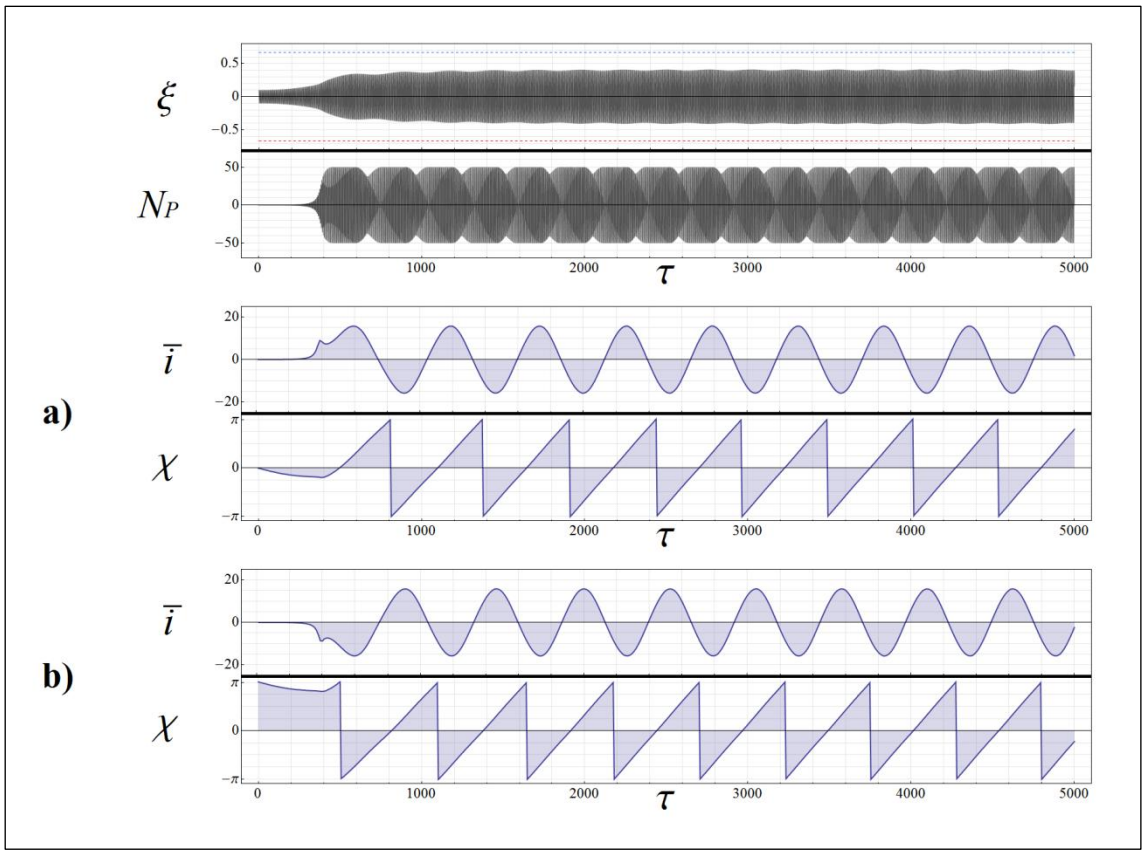

Figure 1.40 – *Same description as in Fig.1.38, except for voltages* $v_{ac} = 50$, $v_{dc} = 0$.

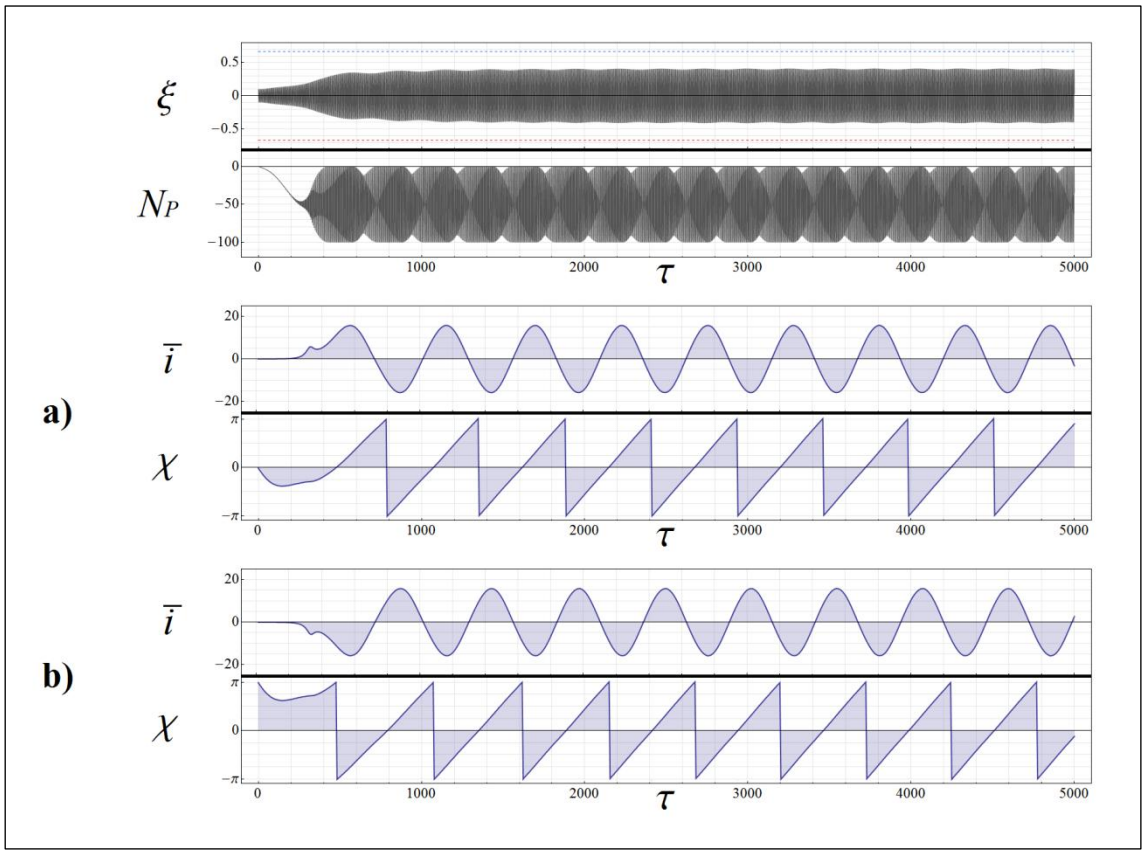

Figure 1.41 – *Same description as in Fig.1.38, except for voltages* $v_{ac} \equiv v_{dc} = 50$.

In conventional situations like those highlighted by Fig.1.38 and Fig.1.39, the shuttle mechanism produces a stationary macroscopic current:

$$\bar{\imath}(\tau) = i_{dc} = \text{const} \tag{1.116a}$$

In both Fig.1.40 and Fig.1.41 current (and, in all the similar simulations performed), a new archetype of shuttle mechanism produces an alternate current whose the waveform highly resembles a sinusoid; therefore, and can be therefore described as:

$$\bar{\imath}(\tau) = i_{ac}\cos(\widetilde{\omega}_I \tau) \tag{1.116b}$$

with $\widetilde{\omega}_I \triangleq \omega_I/\omega$ being its dimensionless frequency. Notice that the frequency $\widetilde{\omega}_I$ is not equal to that of the exciting v_{ac} voltage, $\widetilde{\omega}_G$: instead, it is considerably smaller in any situation, so that a relation $\widetilde{\omega}_I \ll \widetilde{\omega}_G$ always hold. In turn, such "slow" oscillations modulate the oscillations amplitude which cannot stabilize, but slightly oscillates around a mean value. Last, in Fig.1.40 and Fig.1.41, one can notice the phase χ shifts: i) linearly, ii) increasingly; both circumstances being independent from the initial conditions. Such a behavior for the phase shift hints the forced mechanical frequency is constantly slightly slower with respect to the exciting voltage frequency: this means we are in the case the mechanical oscillations are *de-synchronized* from the voltage oscillations. Such desynchronization comes from the huge charge transport dynamics achieved, and definitely explains the existence of such an unusual kind of shuttle mechanism.
In conclusion, we demonstrated that, in some situations, the application of an AC voltage on the gate is sufficient to produce a parametric resonant shuttle mechanism, but may be no more an appropriate way to achieve a symmetry breaking for the system, since, by averaging over a period of time multiple of $2\pi/\widetilde{\omega}_I$, no net charge transfer is achieved between the leads.

Summarizing, equations (1.104) describe a QSM which is able to establish permanent motion regimes which can be classified depending on the kind of shuttle regime performed:

- *no shuttle*: the parametric instability is not triggered and no shuttle regime is possible;
- *DC shuttle*: the parametric instability achieves the usual shuttle mechanism, in turn producing a macroscopic DC current (1.117a);
- *AC shuttle*: the parametric instability achieves an unconventional shuttle mechanism, in turn producing a macroscopic current (1.117b).

In order to systematically investigate the occurrence of these three behaviors, a series of numerical experiments has been carried out, testing a QSM under the same initial conditions and by using different values of v_{ac} (v_{dc} is maintained constant †). Results are collected in Fig.1.42.
Generally, one can notice the occurrence of the three dynamical behaviors listed above occurs at increasing voltages. In particular, similarly to the analysis performed in Section 3.3, it is possible to introduce two threshold values, v_{ac}^{*} and $v_{ac}^{**} \geq v_{ac}^{*}$. In the case $v_{ac} < v_{ac}^{*}$, "no shuttle" is performed; if $v_{ac}^{*} \leq v_{ac} < v_{ac}^{**}$ the conventional "DC shuttle" occurs; whereas, when $v_{ac} > v_{ac}^{**}$ the unconventional "AC shuttle" mechanism producing an alternate current is achieved ‡.
One can notice that, in correspondence to v_{ac}^{*} the amplitude of oscillation $\tilde{A}$ gradually deviates from 0 and the phase χ increases from an incipient value $-\pi/4$, producing a gradually increasing current i_{dc}. Instead, the reach of the threshold v_{ac}^{**} individuates a sudden increase in the amplitude $\tilde{A}$, the disappearance of the stationary current i_{dc} in favor of a larger alternate current whose both amplitude i_{dc} and frequency $\widetilde{\omega}_I$ linearly increases with v_{ac} .

† In fact, from Figg.1.37-1.41, the effect of v_{dc} on the dynamical transients is limited and even null on the conductive features.

‡ Notice how, while the DC shuttle phenomenology intuitively performs the functionality of a *rectifier* (as already stressed by some Authors, such as Pistolesi and Fazio [70]), the AC shuttle casuistic can result in perhaps more interesting applications.

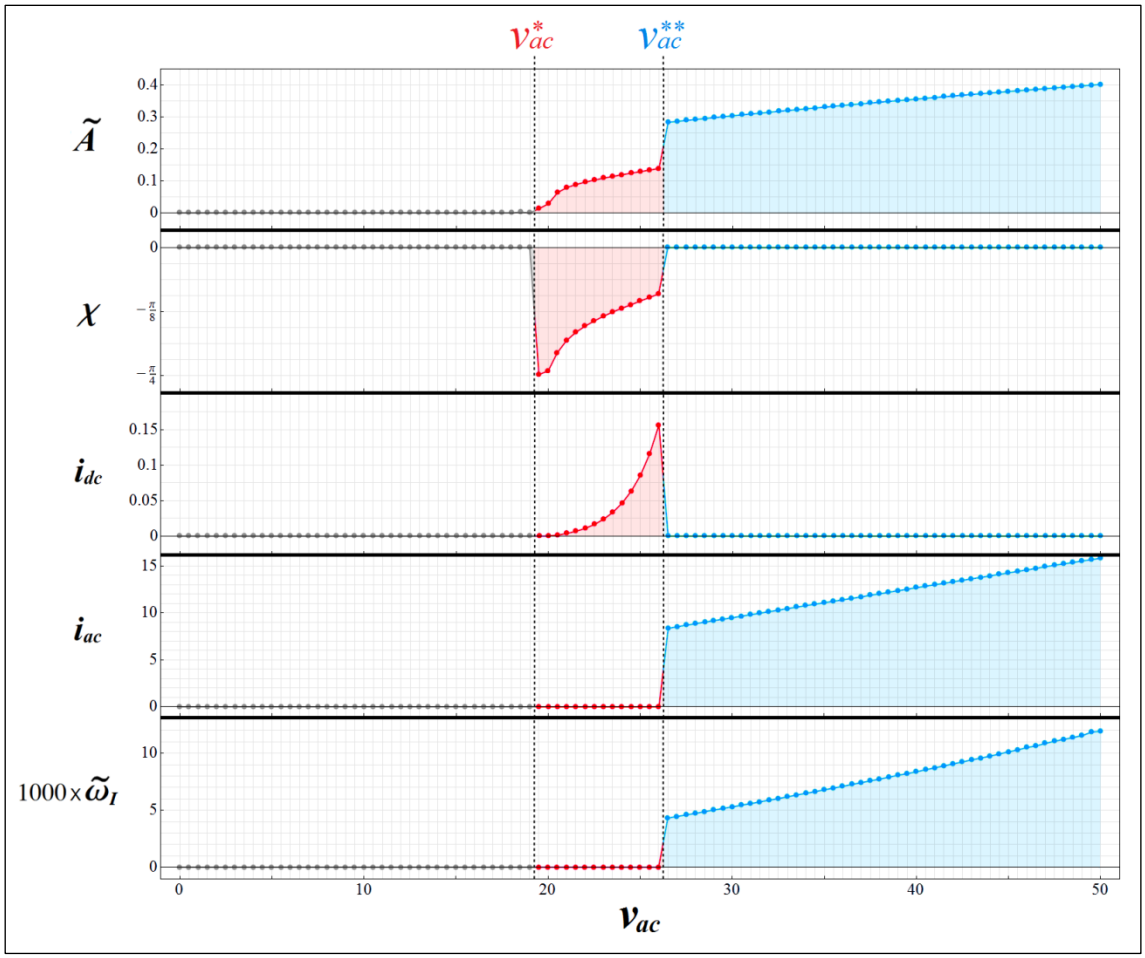

Figure 1.42 – *Curves* $\tilde{A}(v_{ac})$, $\chi(v_{ac})$, $i_{dc}(v_{ac})$, $i_{ac}(v_{ac})$, $\omega_I(v_{ac})$ *plotted for* $v_{dc} = 0$, *obtained from a set of numerical simulations by integrating (1.104) with initial conditions* $N_P(0) = 0$, $\xi(0) = +0.1$, *parameters as in (1.114a) and fulfilling (1.112a). Voltage thresholds* v_{ac}^{*} *and* v_{ac}^{**} *are highlighted.*

In general (again similarly to Section 3.3) the voltage thresholds v_{ac}^{*} and v_{ac}^{**} depend on v_{dc}. This is shown in Fig.1.43, where a graph obtained by collecting a large number of numerical results summarizes the occurrence of "no shuttle", "DC shuttle" and "AC shuttle", by portraying such regions on a v_{dc}-v_{ac} plane and highlighting curves $v_{ac}^{*} = v_{ac}^{*}(v_{dc})$ and $v_{ac}^{**} = v_{ac}^{**}(v_{dc})$.

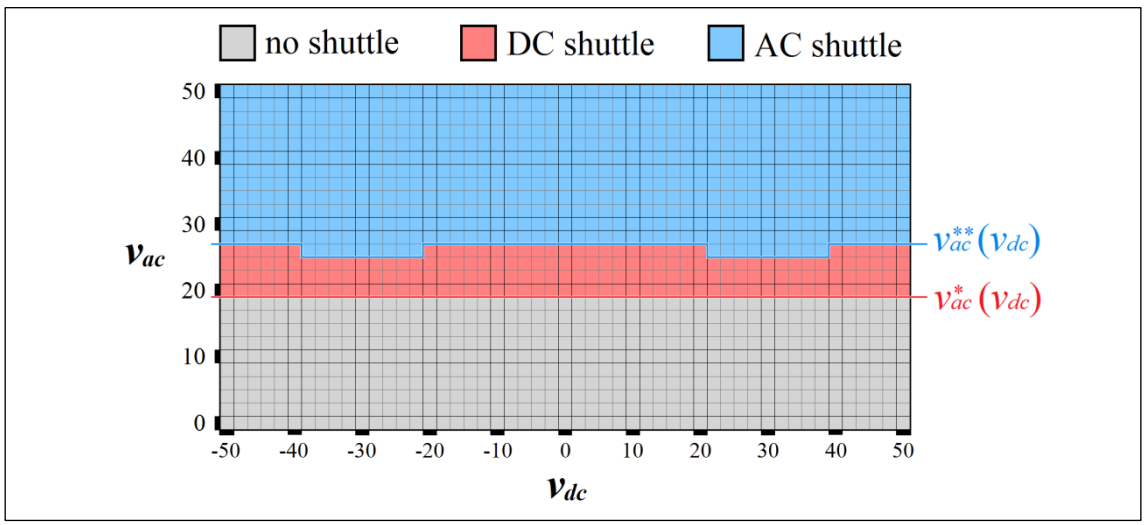

Figure 1.43 – *Curves* $v_{ac}^{*} = v_{ac}^{*}(v_{dc})$ and $v_{ac}^{**} = v_{ac}^{**}(v_{dc})$, *from a set of numerical results by integrating (1.104) with initial conditions* $N_P(0) = 0$, $\xi(0) = +0.1$, *fulfilling (1.112a) and parameters (1.114a).*

First, the graph in Fig.1.43 is horizontally symmetric, meaning the sign of v_{dc} is not important. Second, the dependence from v_{dc} of the voltage thresholds v_{ac}^{*} and v_{ac}^{**} is, differently from Section 3.3, rather small. Actually, by assuming the proper † initial condition $N_P(0) = -v_{dc}$, the effect of v_{dc} on both v_{ac}^{*} and v_{ac}^{**} is completely null, and, on a v_{dc}-v_{ac} plane, the regions corresponding to "no shuttle", "DC shuttle" and "AC shuttle" would be horizontal bands.

Therefore with the experience gained through the whole numerics in this paragraph, one can glimpse the shape of $\tilde{A}$-χ phase plots referred to the investigated systems in applied voltages different conditions. In order to do this, the permanent regime established by a QSM has been tested by using initial conditions $N_P(0) = -v_{dc} < 0$ while varying $\tilde{A}(0)$ and v_{ac} .
The results of this latter series of simulations are in Fig.1.44, together to qualitative portraits of phase plots, partly inspired to those (analytically obtained) in Fig.1.29 of Section 3.3.

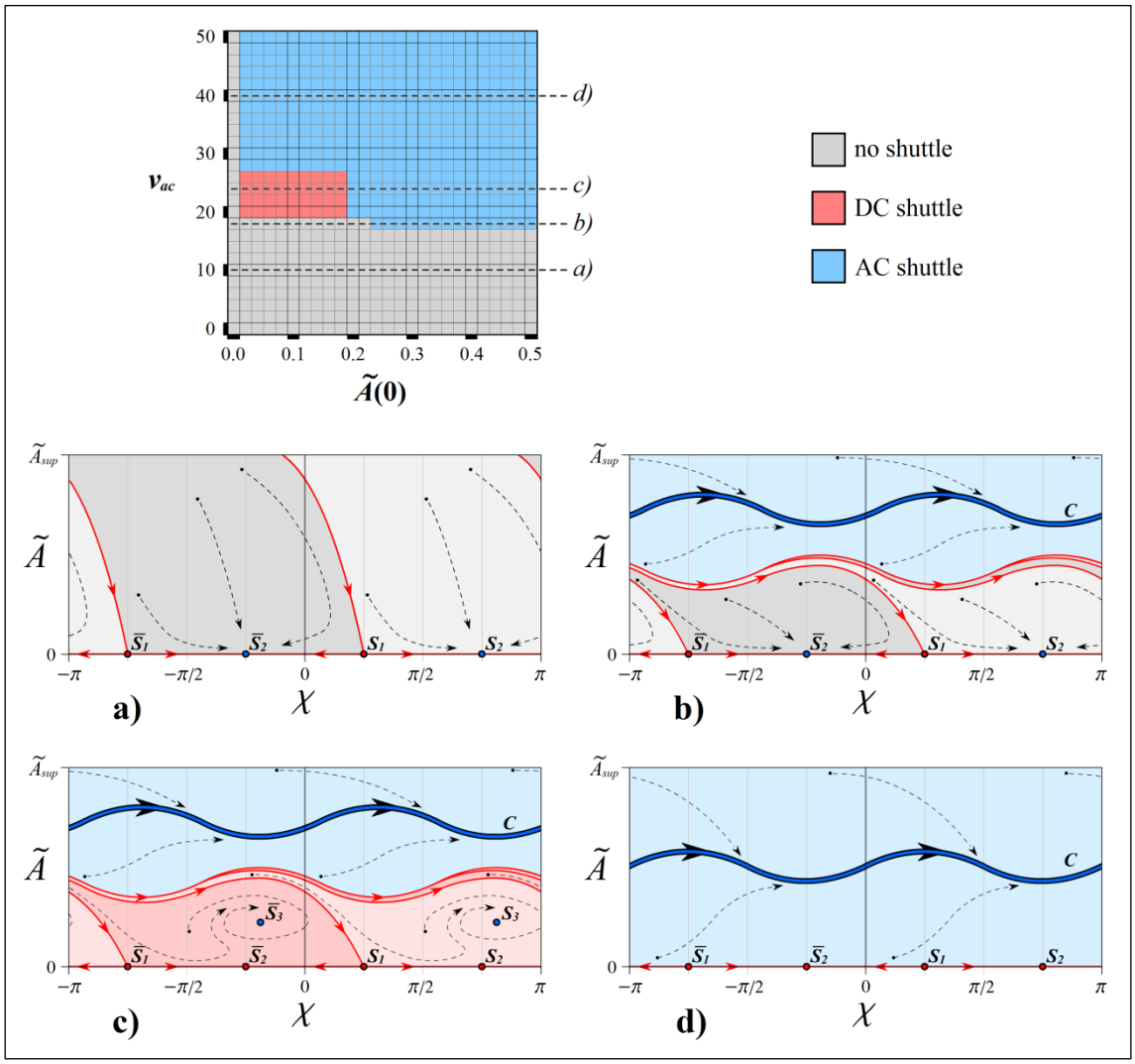

Figure 1.44 – *Induced from a set of numerical experiments on the same system with* $N_P(0) = -v_{dc} < 0$, *phase plots referred to voltage levels (a-d) are qualitatively drawn on a plane* $\tilde{A}$-χ. *Basins of attraction ("no shuttle" in gray, "DC shuttle" in red, "AC shuttle" in blue: different shades for conjugate basins), separatrices (red), stationary points (stable in red, unstable in blue) and exemplificative phase curves (dashed black) are portrayed. As for Fig.1.29, plots are horizontally* 2π-*periodic and conjugated loci are shifted by* π. *The "no shuttle" basins of attraction lead to stationary points* S_1 *and* S_2 *(or conjugates* $\bar{S}_1$ *and* $\bar{S}_2$*), DC shuttle to* S_3 *(or* $\bar{S}_3$*), AC shuttle to a curve* C *(actually a closed orbit, due to the periodicity).*

† Since, as highlighted in Figg.1.38-1.41, the application of a static voltage v_{dc} stabilizes, after a sufficient period of time, an amount of electrons on the pillar N_P just equal to the quantity $-v_{dc}$.

Chapter 5

Hybrid shuttle: some general considerations

Let us consider a QSM characterized by the combination of the voltage boundary conditions (1.34a) (used in Chapter 3) and (1.54a,b) (Chapter 4). Consequently, relations (1.5a) specify into (for simplicity's sake, we assume here $V_G^{dc} = 0$ and $\omega_G \equiv \omega$ †):

$$\begin{cases} V^{dc} \neq 0 \\ V^{ac} = 0 \end{cases} \quad \longrightarrow \quad V = V_L - V_R = V^{dc} \tag{1.117a}$$

$$\begin{cases} V_G^{dc} = 0 \\ V_G^{ac} \neq 0 \end{cases} \quad \longrightarrow \quad V_G = V_G^{ac} \cos(\omega_G t) \tag{1.117b}$$

Then, compatibly with (1.117a,b), refer to the three-terminals architecture in Fig.1.45a,b.

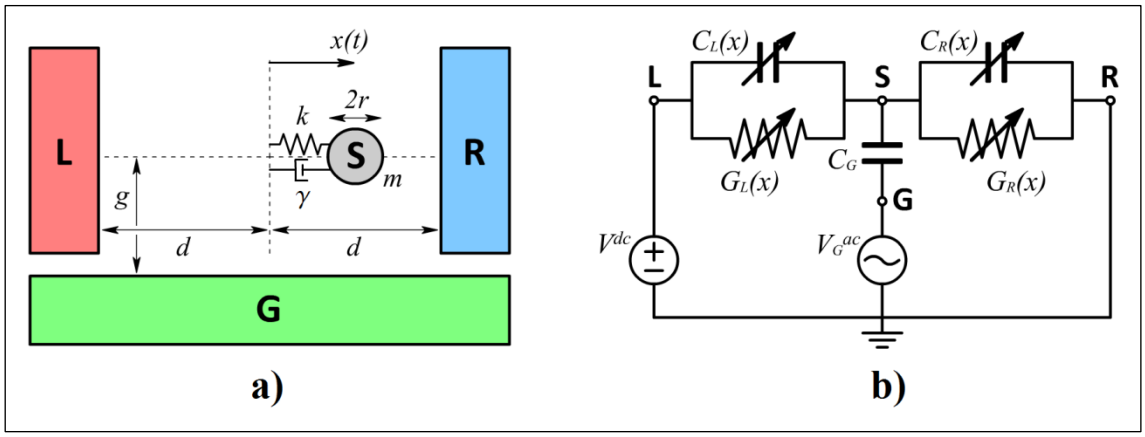

Figure 1.45 – *Three-terminals QSM able to exhibit both direct and inverse shuttle phenomenologies: (a) mechanical and (b) electrical schemes.*

From the analyses carried out in Chapter 2, one can expect a QSM individuated by boundary conditions (1.117a,b), could experience both the self-excited and parametric resonance shuttle mechanisms, somehow constituting a combination of the direct and inverse shuttle phenomenologies. The term *hybrid shuttle* refers to such scenario. Actually, in this thesis, we are not going to deal with a theoretical (nor analytical or numerical) investigation of hybrid shuttle, and this Chapter is only devoted to suggest some general considerations.

Suppose the hybrid QSM portrayed in Fig.1.45 undergoes stable oscillations characterized by amplitude A and frequency f_s. This motion regime is feasible to establish a macroscopic shuttle current I_{HYBR} , which can be assumed to be the linear combination of two terms:

$$I_{HYBR} = \varphi_{DIR} I_{DIR} + \varphi_{INV} I_{INV} \tag{1.118}$$

† In the analyses carried out in Chapter 4, we demonstrated a stationary voltage on the gate is unessential (it does not influence the conductive behavior) and an exciting signal with the same frequency of the mechanical oscillations is preferred (since $\Psi = 1$).

In formula (1.118a), symbols I_{DIR} and I_{INV} represent the shuttle currents achieved by a direct and an inverse QSMs, respectively, achieving the same dynamics of the hybrid QSM (amplitude A and frequency f_s), whereas φ_{DIR} and φ_{INV} are appropriate constants.

From the analyses carried out in Section 2.2.2, one understands that, independently from the physical mechanism guaranteeing the continuity of oscillations (self-excitation for direct shuttle, parametric resonance for inverse shuttle, and both for hybrid shuttle), the conductive behavior $\mathcal{I}$ of a QSM depends only on the electrodynamics $\mathcal{Q}$; this, in turn, is univocally determined by the vibrational regime $\mathcal{X}$ and the voltage boundary conditions $\mathcal{B}$. Summarizing, $\mathcal{I} = \mathcal{I}(\mathcal{X}, \mathcal{B})$.
Follows that, if one considers three QSMs, a direct, an inverse and an hybrid one, all characterized by the same vibrational state $\mathcal{X}$, a relation like (1.118) relates their macroscopic currents, and terms φ_{DIR} and φ_{INV} can be appropriately put in relation with the boundary conditions:

$$\varphi_{DIR} \triangleq \frac{V^{dc}}{V^{dc} + V_G^{ac}} \quad , \qquad \varphi_{INV} \triangleq \pm(1 - \varphi_{DIR}) \tag{1.119a, b}$$

Relations (1.119a,b) are a consequence of the fact that, in a direct shuttle, the macroscopic current I_{DIR} is solely produced by a self-excited mechanism, consequently to the application of a bias voltage V^{dc}; whereas in an inverse shuttle, I_{INV} comes from a parametric excitation triggered by an alternate voltage V_G^{ac}. Thus, the two described phenomenologies are complementary and, the more or less propensity of a system to the first or the second mechanisms only depends on the relative weights of the voltage boundary conditions. Summarizing, every hybrid QSM presents a combination of these two basic forms of shuttle, and its overall current can be estimated by using relations like (1.118) and (1.119). Further notice that, while in direct shuttle the current direction is set by the boundary conditions, in inverse shuttle it depends on the initial conditions: thus, in the definition for φ_{INV} it is not possible foresee the correct sign. As a consequence of this, in an experimental setup comprising a sample of hybrid QSMs characterized by the same voltage boundary conditions, if one measures the macroscopic current produced, the population arranges around two different characteristic values:

$$I_{HYBR}{}^{(I)} \quad , \qquad I_{HYBR}{}^{(II)} = I_{HYBR}{}^{(I)} - \frac{2V_G^{ac}}{V^{dc} + V_G^{ac}} \tag{1.120a, b}$$

To conclude, in Fig.1.46 the hybrid shuttle mechanism is schematized similarly to Fig.1.13, highlighting it is a real *superimposition* of the direct and inverse shuttle basic phenomenologies.

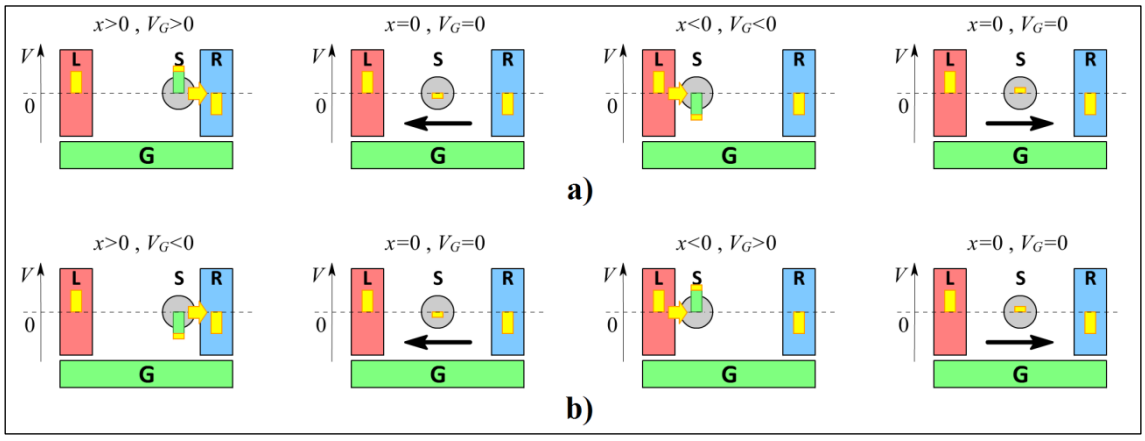

Figure 1.46 – *Schematics of the hybrid shuttle mechanism in the alternative definitions of (1.119b): (a) with a "+" sign, achieving a larger current (1.120a); (b) "−" sign, smaller current (1.120b).*

Conclusions & General framework

Part One opened with a brief overview of charge transport nanoscale devices, up to a detailed study of the conduction mechanism of interest for this thesis: the mechanical electron transport.
In particular, in Chapter 3 we investigated the *direct shuttle* phenomenology exhibited by a two-terminals self-excited QSM; in Chapter 4, it was the case of *inverse shuttle*, achieved by a three terminals QSM triggering a parametric instability. Both configurations originated from the *prototypal architecture* introduced in Section 2.1, and, although oscillations are triggered in a different way, in the case of a characteristic ratio $\Psi = 1$, they are characterized by a similar electrodynamics (as widely demonstrated in Chapter 2 and schematically depicted in Fig.1.13).
The two basic direct and inverse shuttle phenomenologies are somehow complementary, meaning every QSM derived from the prototypal scheme presents a superimposition of such two basic mechanisms. Consequently, in Chapter 5 the concept of *hybrid shuttle* was suggested: in this, we argued the overall current can be considered a linear combination of direct and inverse shuttle contributions, weighted on the basis of the specific boundary conditions used.
Since direct, inverse, and hybrid shuttle complete the scenario of autonomous shuttle devices, the main intent of Part One of the thesis – a theoretical analysis of QSMs – is fulfilled.

Part Two is devoted to a more practical aim: the functional design of a NMT, for which the preliminary study of its constitutive elements – QSMs indeed – was required. Nonetheless, some of the results achieved in Part One are of particular interest, since they are going to constitute the starting point for some analyses to be presented in Part Two. These are listed ahead.
In Chapter 2, the quali-quantitative study on the shuttle mechanism will be useful to perform the functional analysis of a single QSM (Chapter 9), and the whole NMT (Chapter 10), while the definitions and classifications presented will be critically examined in Chapter 7 in order to individuate some preliminary design choices. In particular, the concept of tunneling region and the two-states approximation (formulae (1-25) and (1.26)) will be useful, in Section 9.4, to introduce a neat Turing machine interpretation of the motion regimes established by a QSM.
Related to this, the hysteresis of the *I-V* curve peculiar of the hard shuttle regimes, numerically demonstrated in Chapter 2, will be analyzed in a more deep detail in Section 9.2.3, where a physically satisfying interpretation of is suggested. Also, the coherency of numerical results in Chapter 2 constituted the validation for the semi-classical model to be introduced in Chapter 8, that – with some substantial enhancements – will be diffusely used to describe both the single QSM and the whole NMT. Last, the analytical and numerical quantitative analysis carried out in Chapters 3, 4, respectively for the direct and inverse shuttle, represent the know-how required to understand at a deep detail the electron shuttle phenomenology, and appropriately select the main characteristics of a QSM to be the optimal candidate as a basic element of the NMT.
As a final result, the numerical simulations which are going to be discussed in Part Two, will lead to synthetize a number of so-called "control strategies" for the NMT which constitutes the main achievement of Chapter 10 and of the whole thesis, indeed.

To conclude, the general framework in Tab.1.7 represents a comparison table which summarizes all the charge transport phenomenologies analyzed in Part One.

Table 1.7 – *General framework of conduction mechanisms considered in the thesis.*

Kind of system	Device	Nature of oscillations	Analyzed in the thesis	Shuttle regime	Feasible theoretical approaches	Conduction mechanism	Input signal †	Output currents	Conditions inhibiting conduction	Input signals compatible with CHARGE TRANSPORT	Input signals compatible with NET CURRENT
Continuous Medium	Solid Conductor	-	-	-	classical	free conduction	V	I_f	$G_f = 0$	$V^{dc} \neq 0 \vee V^{ac} \neq 0$	$V^{dc} \neq 0$
Macroscopic Device	AC-driven SM	induced	-	-	classical	shuttle	V , V_E	$I_{s,DIR}$	$\omega = 0$	$V_E{}^{ac} \geq 0$	
	Direct SM	autonomous	theory	-	classical	shuttle	V	$I_{s,DIR}$	$\omega = 0$	$V^{dc} \geq V_{act}$	
NEMS (possibly a metamaterial)	TJ	-	theory	soft	quantum, semi-classical	QT	V	I_t	CB or $G_t = 0$	$V^{dc} \neq 0 \vee V^{ac} \neq 0$	$V^{dc} \neq 0$
	SET	-	theory	soft	quantum	QT	V	I_t	CB	$\lvert V^{dc}\rvert > V_{CB} \vee \lvert V^{ac}\rvert > V_{CB}$	$V^{dc} > V_{CB}$
	AC-driven QSM	induced	-	soft	quantum, semi-classical	shuttle, QT	V , V_E	$I_{s,DIR}$	$\omega = 0$	$V_E{}^{ac} \geq V_{E,act}$	
								I_t	CB or $G_t = 0$	$V^{dc} \neq 0 \vee V^{ac} \neq 0$	$V^{dc} \neq 0$
				hard	semi-classical	shuttle	V , V_E	$I_{s,DIR}$	$\omega = 0$	$V_E{}^{ac} \geq V_{E,act}$	
	Direct QSM	autonomous	theory, numerics, functional analysis	soft	quantum, semi-classical	shuttle, QT	V	$I_{s,DIR}$	$\omega = 0$	$V^{dc} \geq V_{D,act}$	
								I_t	CB or $G_t = 0$	$V^{dc} \neq 0 \vee V^{ac} \neq 0$	$V^{dc} \neq 0$
				hard	semi-classical	shuttle	V	$I_{s,DIR}$	$\omega = 0$	$V^{dc} \geq V_{act}$	
	Inverse QSM	autonomous	theory, numerics, analytical solutions	soft	quantum	shuttle	V_G	$I_{s,INV}$	$\omega = 0$	$V_G{}^{ac} \geq V_{G,act}$	
				hard	semi-classical	shuttle	V_G	$I_{s,INV}$	$\omega = 0$	$V_G{}^{ac} \geq V_{G,act}$	$V_{G,act} \leq V_G{}^{ac} \leq V_\varphi$
	Hybrid QSM	autonomous	concept	soft	quantum, semi-classical	shuttle, QT	V , V_G	$I_{s,DIR}$, $I_{s,INV}$	$\omega = 0$	$V_D{}^{dc} \geq V_{D,act} \quad \vee \quad V_G{}^{ac} \geq V_{G,act}$	
								I_t	CB or $G_t = 0$	$V^{dc} \neq 0 \vee V^{ac} \neq 0$	$V^{dc} \neq 0$
				hard	semi-classical	shuttle	V , V_G	$I_{s,DIR}$, $I_{s,INV}$	$\omega = 0$	to be investigated	

† Consider, for the AC-driven case, an external excitation coming from: $V_E(t) \triangleq V_E{}^{dc} + V_E{}^{ac}\cos(\omega_E t)$.

Part Two

APPLICATION TO THE NANOMECHANICAL TRANSISTOR

The following Chapters focus on the assessment of realizing a NanoMechanical Transistor composed by a set of Quantum Shuttle Modules, correctly reproducing some of a conventional transistor functionalities, such as switching and current amplification.

In Chapter 6, a brief historical introduction on transistors, including some more or less recent proposals involving unconventional (non-electronic) working principles is presented.

In Chapter 7, a detailed analysis of the Blick's NanoMechanical Transistor patent is presented, leading to some preliminary design choices on the Quantum Shuttle Modules composing it.

In Chapter 8, an analytical model for a single Quantum Shuttle Module is suggested, more accurate with respect to Part One, in which electrostatics is modeled by using a capacitance matrix (Appendix A), QT conductances consider the voltage dependence (Appendix B), and electrostatic induction effects are included (Appendix C). Equations are then generalized to the case of an array of coupled Quantum Shuttle Modules realizing the NanoMechanical Transistor.

In Chapter 9, the functional analysis of a single Quantum Shuttle Module is carried out including: the definition of a set of reference parameters, the investigation of transient and permanent motion regimes, a predictive static-machine model, characteristic charts and working points. Also, an engineering satisfying explanation of the current-voltage curve hysteresis is proposed.

In Chapter 10, the functional analysis is extended to the whole NanoMechanical Transistor: a set of control strategies aimed to correctly reproduce both the voltage-driven switch and the current amplifier functionalities are suggested and demonstrated with numerical simulations.

Last, in Chapter 11, the electric performances of the NanoMechanical Transistor are compared with those of electronic devices and a method to estimate the maximal current gain is proposed.

Chapter 6

Transistors: state of the art

6.1 Classifications and main functionalities

Transistors are often considered as the most influential invention of the XX century. This is probably true, since they constitute the fundamental brick for the entire modern information technology: the gadget which put into reality the computing algorithm of a Turing machine, promoting the jump from pioneering analogic calculators towards digital computing †.

Any active circuital element characterized by three *electrodes*, and in which a signal applied on the *input* electrode can control a conveniently larger signal between the *output* ones, is called "transistor" (such signals can be either voltages and/or currents). This generic function can be achieved by devices characterized by different working principles and architectures.

A *Bipolar Junction Transistor* (BJT) is formed by a sandwich of N- and P-type semiconductors (*PNP-* or *NPN-configuration*), separated by two junctions, its working principle involving *two* kinds of charge carriers in a doped semiconductor: electrons and holes. In a BJT, the input electrode is named *Base* (B), and the output ones *Emitter* (E) and *Collector* (C) (see Fig.2.1a).

A *Field-Effect Transistor* (FET), uses *either* electrons or holes (*N-channel* or *P-channel* FET) for conduction, thus it is a *unipolar* transistor. Two FET typologies exist: *Junction* (JFET) and *Insulated Gate* (IGFET, also known as *Metal-Oxide Semiconductor*: MOSFET). In a FET, the input electrode is labeled *Gate* (G), and the output ones *Source* (S) and *Drain* (D) (Fig.2.1b).

BJTs and FETs represent the two main families of conventional (electronic) transistors.

In addition to these, non-conventional transistors involving mechanics-specific concepts have been recently proposed: generally refer to them as *NanoMechanical Transistors* (NMTs). Since NMTs are unipolar and their working principle involves an electric field, their electrodes inherit the same names and symbols used for a FET: *Gate* (G), *Source* (S) and *Drain* (D) (Fig.2.1c).

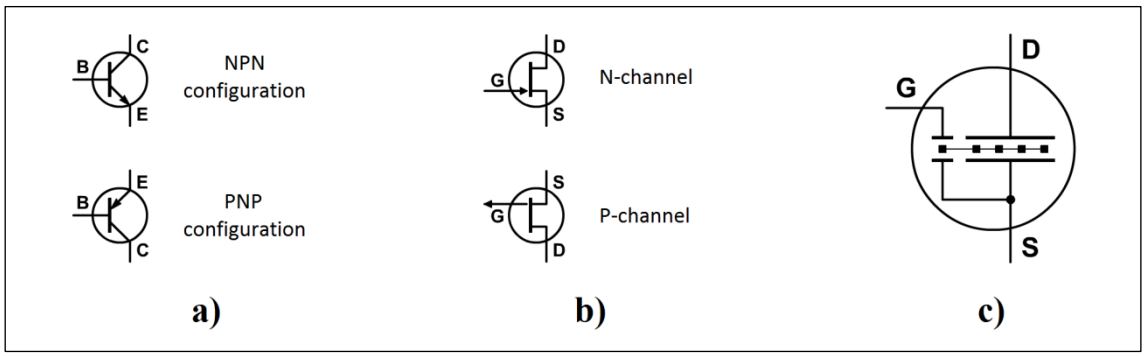

Figure 2.1 – *Circuital symbols for a: (a) BJT, (b) FET, (c) NMT. The NMT symbol, inspired to* [60,77]*, is originally suggested in the thesis and extensively used in the followings.*

† Both logical operations and memory access, in fact, can be achieved by arranging a set of transistors, respectively exemplified by logic gates (*AND*, *NOT*, *OR*, and their combinations) and memory elements (for example *flip-flop* circuits).

Transistors can constitute the central element of circuits specifically designed to achieve the most-representative functionalities of: *voltage-driven switching* and *current amplification*. When an input voltage is used to inhibit/consent an output current, a transistor acts as a *switch*. If the input is used to regulate a proportional output, it works as an *amplifier*. Standard amplifier topologies comprise the common-collector (Fig.2.2a) and common-source (Fig.2.2b,c) ones.

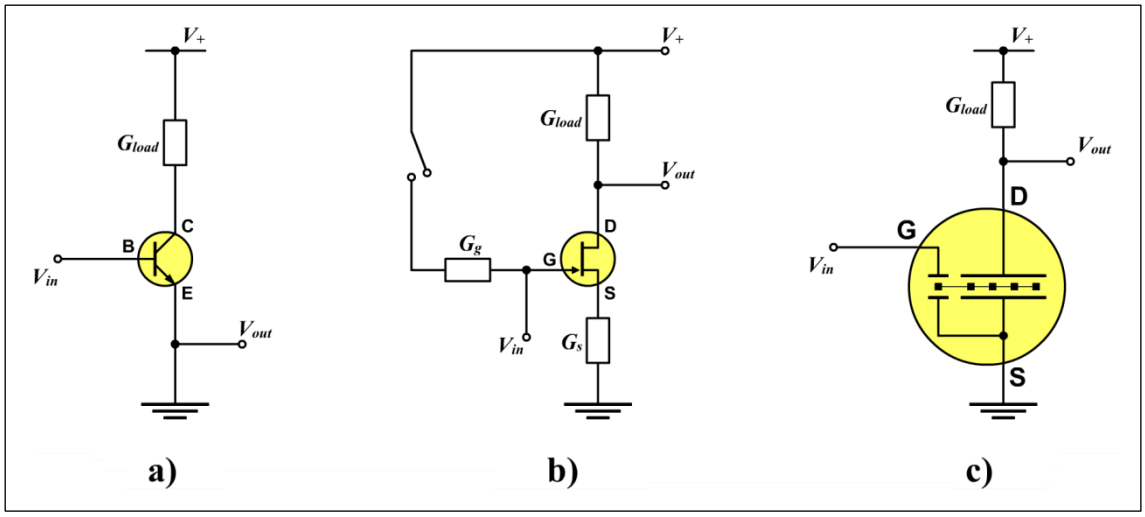

Figure 2.2 – *Standard circuital topologies in which the central element is a transistor: (a) basic NPN BJT common-collector circuit; (b) basic N-channel FET common-source circuit with biasing detail and source degeneration; (c) a NMT plugged into a common-source circuit similarly to conventional devices.*

The (static) conductive behavior of a transistor can be summarized by a series of characteristic curves on a I-V plane. In BJTs, the output is *current-controlled*, thus (referring to the nomenclature presented above) these plots conventionally show a discrete group of collector-to-emitter current curves $I_{CE,i}$ as a function of the output collector-emitter potential difference V_{CE}, for step values of the input base current $I_{B,i}$ (see Fig.2.3a). Instead, FETs are *voltage-controlled*, and a set of drain-to-source output current curves $I_{DS,i}$ as a function of the output drain-source potential difference V_{DS}, for different values of the input gate voltage $V_{G,i}$ are used (Fig.2.3b). An I-V curve in which the current I_{CE} (or I_{DS}) is nearly suppressed for small values of V_B and I_B (or V_G and I_G) is optimal for the switch operation. Instead, in current amplifiers, what plays a central role is the linearity of the I-V curve. Typically, FETs are characterized by a higher switching speed, while BJTs by a good linearity: consequently FETs (especially MOSFET) are conventionally used to produce logic gates, whereas BJTs in amplifying circuits.

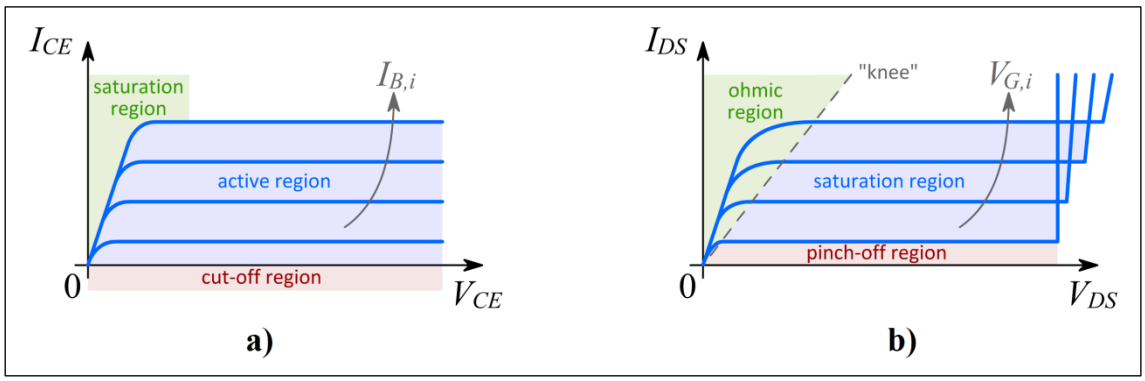

Figure 2.3 – *Typical characteristic I-V curves for a: (a) current-driven BJT, (b) voltage-driven FET.*

6.2 Historical resume of conventional transistors

Although its recent application in computing industry, transistor history is over one century old. A chronological resume of the most important theoretical and technological landmarks for conventional (electronic) transistors is presented in this Paragraph.

In 1906, L. De Forest invented a special thermionic valve, the *audion* (today known as *triode*), realized within a vacuum tube, capable of amplifying signals. American leading company AT&T acquired the De Forest patent and used such a device to solve the main technological issue related to both the emerging (wired) telephony and (wireless) telegraphy: the signal loss due to long-distance transmissions. However, thermionic valves were not a reliable solution: they required too much power to work, thus were characterized by an excessive Joule effect.

Following years, proposals for solid-state replacements for the triode spread. In particular, the physicist J. E. Lilienfeld filed a patent for a FET in 1925 in Canada and, later, in USA, but never published research articles nor produced any working prototype. A somehow similar transistor device was later invented in 1934 by O. Heil in Germany.

In 1940s, at AT&T's Bell laboratories, a *point-contact transistor* was realized. A first, not working prototype, was designed by team's leader W. Shockley in 1945, and was improved and positively tested by J. Bardeen and W. Brattain in 1947. In 1948, Shockley developed the first actual BJT, together with a first comprehensive theory of transistors †. Bell Laboratories demanded for an original name to advertise their new invention: after some initial proposals (such as "semiconductor triode", "surface states triode" and "iotatron"), the term "transistor" was coined in 1948 by J. R. Pierce, joining the words "transfer" and "resistor".

In 1954, Texas Instruments produced the first silicon-based transistor. In 1958-1959, J. Kilby, a Texas Instruments employer, first glimpsed the possibility to produce any circuital component in silicon. He realized and patented the first *Integrated Circuit* (IC).

In 1960, Bell's laboratories produced the first MOSFET, and F. Wanlass patented the *Complementary Metal-Oxide Semiconductor* (CMOS) technology in 1967. MOSFETs slowly substituted BJTs in ICs, which had popularized since decades, and nowadays still constitute the most popular and widespread family of transistor devices.

6.3 Recent proposals involving unconventional concepts

Electronic industry incessantly pulls towards innovation and new concept designs, in order to solve a main need: *miniaturization*. In turn, miniaturization allows lower power consumptions and better performances per volume unit of an IC. This trend is well reassumed by the popular (first) Moore's law, for which "the number of transistors on ICs doubles approximately every five years" ‡. Its prediction revealed unexpectedly accurate also because it is nowadays used in the computer industry to guide long-term planning and set miniaturization landmarks in semiconductor research and production. For example, the International Technology Roadmap for Semiconductors, states that the next target for the average half-pitch of a memory cell will be a 14-*nm* technology node, to be reached within 2013-2014.

† Controversies arouse among Shockley, Bardeen and Brattain when the point-contact transistor was patented. The Shockley's invention overshadowed the work of Bardeen and Brattain, who eventually left Bell Labs. However, they all received the Nobel prize in physics in 1956, accounting for "their researches on semiconductors and their discovery of the transistor effect".

‡ Actually, the first version of Moore's Law [114] cited "18 months". This trend was reformulated in 1970s.

Inevitably, this miniaturization trend is going to decelerate if no step-innovation will be proposed: approaching to *nm*-size transistors introduces undesired quantum effects which limits conventional electronic functionalities. Consequently, industry started to consider new frontiers of computing, in which the presence of quantic phenomena such as *Quantum Tunneling* (QT) or *Coulomb Blockade* (CB) is deliberately used as the working principle of increasingly small transistors which can be considered, in these sense, *unconventional*. Between 1970s and 1980s, the conception of the *Single-Electron Transistor* (SET) (see Section 1.3 for references) was a first step in this sense. Only in recent times room-temperature SETs have been realized. The SETs seem to solve the main needs of electronic industry: miniaturization, low power consumption, and higher performances; however, the main concerns around them, highlighted by some authors [60], are the low robustness and reliability. These issues still relegate SETs to research purposes and, to present day, no SET device has been commercially produced yet.

In order to overcome this impasse, a part of NEMS research is focusing, in recent years, to realize *NanoMechanical Transistors* (NMTs). One of the most notable concepts in this sense was suggested in 2007-2008 by Blick in both an article [60] and a patent [77], and makes use the *shuttle mechanism* (see the Introduction). Blick's proposal consists in properly arrange an array of *Quantum Shuttle Modules* (QSMs) to produce logic gates and memory elements of a so-called "mechanical computer". Since the idea to couple more QSMs to realize a NMT is a matter of interest of this thesis (in particular of Part Two), the Blick's NMT will be analyzed in detail in Chapter 7; in this Paragraph, instead, we briefly list a number of recent alternative proposals of nanotransistors involving mechanical concepts.

For example, the recent enthusiasm around *Carbon NanoTubes* (CNTs) – first, in 1990s – and *graphene* – then, in 2000s – led to some experimental setups in which charge transport is actuated by modifying the mechanical stress conditions of a CNT [115] or by distort graphene sheets [116]. Inspired by these, CNT-based nanotransistors have been conceived [117]. In more recent times, a very high temperature (500°C) working transistor has been produced by simply statically deflect some micrometer-scale silicon carbide levers and cogs [118]; however, this embodiment requires very high activation voltages. In 2011, a Japanese team proposed the novel concept of an *atomic transistor* [119], which works by shuffling individual copper atoms within the device, regulating the conductive path within the source and drain electrodes.

Notice these papers do not make use of a shuttle mechanism. There are, indeed, other proposals which make use of the shuttle mechanism, but in which the shuttling element is excited in a different manner from the Blick's NMT proposal, for example by using a magnetically induced Lorentz force. A brief list of such articles includes [120,121,122,123,124,125]: some of them are analogous to Blick's architectures, others try to be more "single-electron" specific.

A completely different branch of research involves non-mechanical unconventional transistors, namely *Optical Transistors* (OT). They work by using materials characterized by a non-linear refractive index. First conceived in 1976, [126] OTs could be arranged into *optical logic circuits* [127] and, thus, could represent the fundamental brick for *optical* (or *photonic*) *computers*. A first demonstration of optical computing was achieved in 2011 [128].

The SET, NMT and OT research fields are somehow "in competition" to individuate the best NEMS technology to produce faster and more reliable computing devices. Nonetheless, up to the present day, no single embodiment seems to stand out as the best one. Remarkably, all these devices still belong to the classical scenario of *digital computing*. Actually, a further step innovation, that of *quantum computing*, first glimpsed by Richard Feynman in a memorable talk held at MIT in 1981 [129], could represent the ultimate frontier of information technology.

Though, such a topic is wide far from the matter of interest (and pretenses) of this thesis.

Chapter 7

Preliminary design choices

7.1 Analysis of Blick's NanoMechanical Transistor

Robert H. Blick, in the 2007 article "A Nano-Mechanical Computer: Exploring New Avenues of Computing" [60] and in the 2008 US patent: "Nanomechanical Computer" [77], suggests the original architecture for a NMT whose constitutive elements are QSMs †.

The central idea is that of realizing an array of nanopillar-shaped resonators, mechanically coupled through a common basis, the "web", and with a conductive cap on their tip constituting the shuttling elements. A first subgroup of resonators, called "drives" oscillates under the effect of the transistor's input gate voltage among a first pair of biased electrodes; whereas a second subgroup, named "slaves", vibrates among a second pair of electrodes, producing a macroscopic output current, which flows between the drain and source terminals.

In Blick's claims, if such shuttling elements are properly designed and coupled and the electrodes appropriately biased, the described device (see Fig.2.4) could mimic both the voltage-driven switch and current amplification functionalities of a conventional (electronic) transistor.

An detailed analysis of the NMT described above is presented ahead.

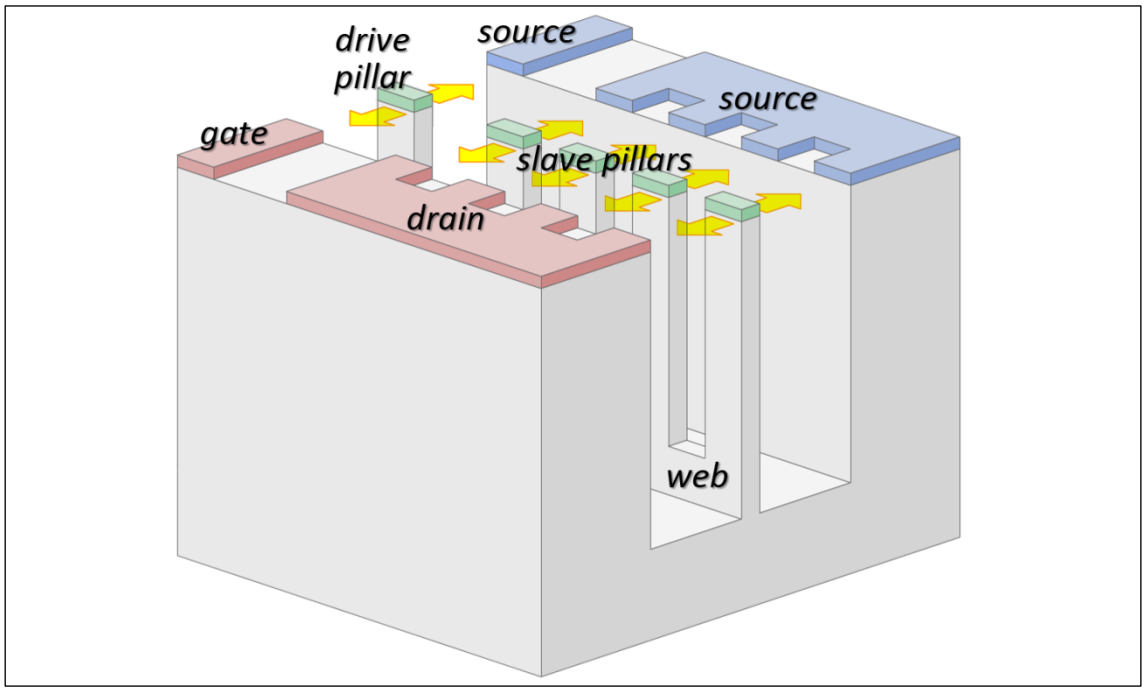

Figure 2.4 – *Architecture of Blick's NMT with main elements highlighted.*
The case of a single drive pillar and a common-source amplifier topology is depicted.

† Some original drawings of the proposed embodiment, from [77] have been reported in Fig.IX of the Introduction.

Consider a NMT characterized by a single drive resonator †, and let N the number of the slave ones. Since every shuttling element oscillates between a pair of fixed electrodes, the whole NMT can be imagined as formed by a set of $N+1$ QSMs, each one similar to the two-terminals device introduced in Section 1.5. Label each conductor of the i-th QSM with a series of increasing subscript numbers $i = 0,1,2,\dots,N$: the *Left* (L_i) and *Right* terminals (R_i) and the *Pillar* resonators (P_i); the same is for any other constant or variable referred to them (see Fig.2.5a).
Compatibly with the conventions used in Part One, let the left electrodes positive-biased, so that $V_{L,i} \geq V_{R,i}$; the macroscopic currents I_i consequently positive when flowing towards right.
The potential difference and the current flowing between the drive electrodes L_0 and R_0 are:

$$V_{dr} \triangleq V_{L,0} - V_{R,0} \quad , \quad I_{dr} \triangleq \overline{I_0} \tag{2.1a}$$

Notice the slave electrodes $\mathrm{L}_{1\dots N}$ and $\mathrm{R}_{1\dots N}$ are connected together and represent a single pair of conductors. Their potential difference and the overall current flowing through them are:

$$V_{sl} \triangleq V_1 \equiv V_2 \equiv \cdots \equiv V_N \quad , \quad I_{sl} \triangleq \overline{I_1} + \overline{I_2} + \cdots + \overline{I_N} \tag{2.1b}$$

Summarizing, the system in Fig.2.5b has a *four-terminals* geometry, in fact two currents, I_{dr} and I_{sl}, distinctly flow through the drive and slave pillars sets. Since a transistor is a *three-terminals* device, an electrical connection between two of these terminals is required, to make this system an actual NMT. Therefore, referring to the standard topologies shown in Fig.2.2, and compatibly with the scheme in Fig.2.4, we conventionally use a *common-source* solution, for which the gate G and drain D are the positive-biased input and output terminals respectively, and the source the (both input and output) negative terminal, usually grounded (Fig.2.5c).
The obtained system properly resembles a transistor, consequently the DC *current gain* can be introduced by using the standard definition:

$$\alpha \triangleq I_{sl}/I_{dr} \tag{2.1c}$$

The nomenclature, definitions, sign conventions and circuital connections presented in this Paragraph will be used extensively in the next Chapters of this thesis.

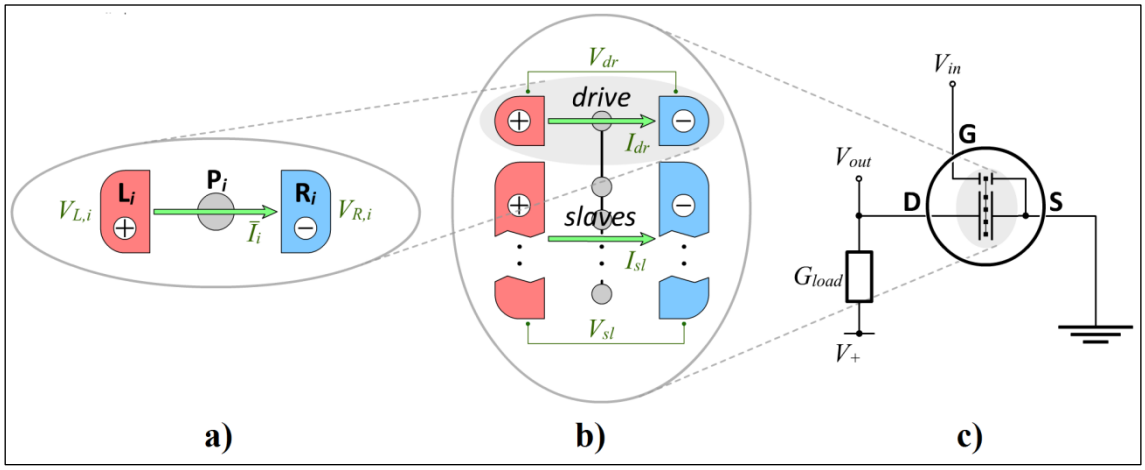

Figure 2.5 – *Zooming out a NMT: (a) i-th two terminals QSM, (b) Blick's NMT, (c) common-source circuital connection of a NMT with the source grounded.*

† In the patent, the non-mandatory chance of using more drive pillars is considered; in this thesis, however we omit such option.

7.2 Selecting the best Quantum Shuttle Module

In the previous Paragraph we highlighted the Blick's NMT is formed by an array of QSMs. Since the goal of this Chapter is to provide a preliminary design for the NMT, a first step in this direction consists in selecting the QSM to be the best candidate to be its fundamental module. Specifically, we are interested to design a NMT system actually able to mimic both the most representative functionalities of a transistor, namely *current switching* and *amplification*.

In Part One, specifically in Chapter 2, we introduced some fundamental QSM classifications. Among the others, the most important were:

- continuative oscillations: *autonomous* VS *induced* oscillations;
- voltage boundary conditions: *direct* VS *inverse shuttle*;
- nature of shuttle mechanism: *soft* VS *hard* shuttle regime;
- force on the shuttling element: *weak* VS *strong* electromechanical coupling.

We consider these options as "preliminary design choices". Analyze them one by one.

The first two choices are rather straightforward. Differently from some of its early experimental setups (see Introduction), Blick, in both [60,77] explicitly indicates the *autonomous* nature of the nanopillar elements motion. Due to the two-terminals geometry for each QSM (Fig.2.5a), the voltage boundary conditions have to be compatible with *direct* shuttle, producing a self-excited mechanism of the shuttling element of the kind investigated in Chapter 3.
The choices between soft/hard shuttle and weak/strong coupling, are rather less trivial.

As widely discussed in Chapter 2, in a QSM the overall current is the sum of two physically different contributions: the shuttle and the current parts. In general, the same feature is inherited by the macroscopic currents (2.1a,b) flowing in a NMT:

$$I_{dr} = I_{dr,s} + I_{dr,t} \tag{2.2a}$$

$$I_{sl} = I_{sl,s} + I_{sl,t} \tag{2.2b}$$

Quantities $I_{dr,s}$ and $I_{sl,s}$ are directly related with the motion regime established by the drive and slave pillars; also, since relations analogous to (1.12a) hold, when the drive and/or slave pillars are at rest, then $I_{dr,s} = 0$ and/or $I_{sl,s} = 0$. On the other hand, tunnel contributions $I_{dr,t}$ and $I_{sl,t}$, in general, continue to flow independently from the pillars motion. Notice that, since in a NMT the slave current is the output, having no control on its inhibition, limits the possibility for the whole system to correctly mimic the voltage-driven switch functionality. In order to be sure a tunnel slave current $I_{sl,t}$ can be partly controlled by the vibrational regime of the slave pillars, one requires the slave QSM are in (very) *hard* regime. In this condition, in fact, when the oscillation of each slave pillar does not reach the *tunneling region* $\mathcal{T}$ (see Section 2.2.8), or (in the limit case) if the slave pillars are at rest, then $I_{sl,s} \approx 0$ and the interrupting state of a switch can be correctly performed by the NMT †. In order to achieve hard shuttle regime, the device scale has to be sufficiently large, that is $d \gg \lambda$.
Schemes in Fig.2.6 highlight the slave oscillations amplitudes compatible with different conductive states of the device. In particular, the first of them represents the output (slave) current interruption state. On the other hand, notice that, when a NMT reproduces the functionality of a current amplifier, the fraction of slave pillars which reach the threshold amplitude A_t gives an information on the magnitude of the current gain α.

† The hard shuttle regime becomes a particularly strict requirement if the NMT is part of a logic circuit.

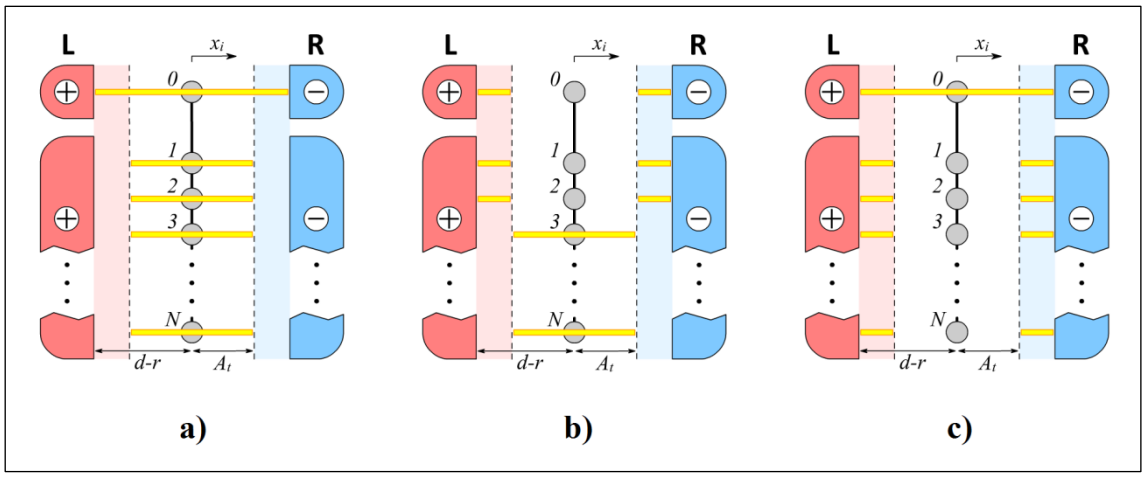

Figure 2.6 – *Qualitative schemes representing a NMT in whose QSMs are in (very) hard regime: (a) interrupting state, (b) partial conduction state, (c) complete conduction state. They respectively correspond to the following casuistic: none, some or all slave pillars reach the tunneling region.*

Provided an appropriate mechanical coupling between different pillars, physically, the number of slaves which reaches a considerable amplitude of oscillation depends on the drive voltage V_{dr}. In the invention description, Blick [77] explicitly mentions the motion regime of the slave set is excited by the drive pillar oscillations by *resonance*. In particular, when the voltage V_{dr}, self-excites the drive pillar to a frequency which does not match the natural frequency of the slave set, their amplitudes remain small and no shuttle current $I_{sl,s}$ (which, in the case of hard shuttle, is the only one contribution) passes (Fig.2.6a). Otherwise, if a resonance condition is matched, the slave pillars reach the maximum amplitude, the tunneling region is reached by some (Fig.2.6b) or all of them (Fig.2.6c), and a conductive state is reached for the NMT.

From the considerations above, follows that, since the vibrational regime of the drive pillar plays a crucial role in enhancing the output current of the NMT, a drive pillar which is more responsive to the voltage V_{dr} is a preferred condition. The relation between applied voltages and mechanical response is given by the electromechanical coupling (see Section 2.2.4). Consequently, the last design choice consists in having (at least) the drive resonator characterized by a strong electromechanical coupling: K∼1 . From its definition (1.19), a large damping is, in turn, required for the drive oscillator, thus, one assumes a large damping is present in the whole NMT. Therefore, we set every QSM is characterized by a strong electromechanical coupling.

In conclusion, Tab.2.1 summarizes the design choices discussed in this paragraph about the fundamental QSM of a NMT.

Table 2.1 – *Preliminary design choices for the fundamental QSM of a NMT.*

Characteristic	Best choice	Design requirement
continuative oscillations	*autonomous*	continuative energy supply
voltage boundary conditions	*direct shuttle*	DC voltage on the leads
nature of shuttle mechanism	*hard regime*	large device scale
Electromechanical coupling	*strong*	large damping

7.3 Shuttling element realization and characteristic size of the system

In this Paragraph we discuss how the actual realization of the shuttling elements influences the order of magnitude of some fundamental quantities of the QSMs in the NMT.
The two main fabrication possibilities for the shuttling element are: a Q-dot embedded within soft molecular links (*metallic grain*, Fig.2.7a) or a cantilever geometry with a conductive cap on its tip (*pillar*, Fig.2.7b). Although the patent [77] explicitly suggests the second realization, here we question this choice by analyzing in in detail the related advantages and disadvantages.

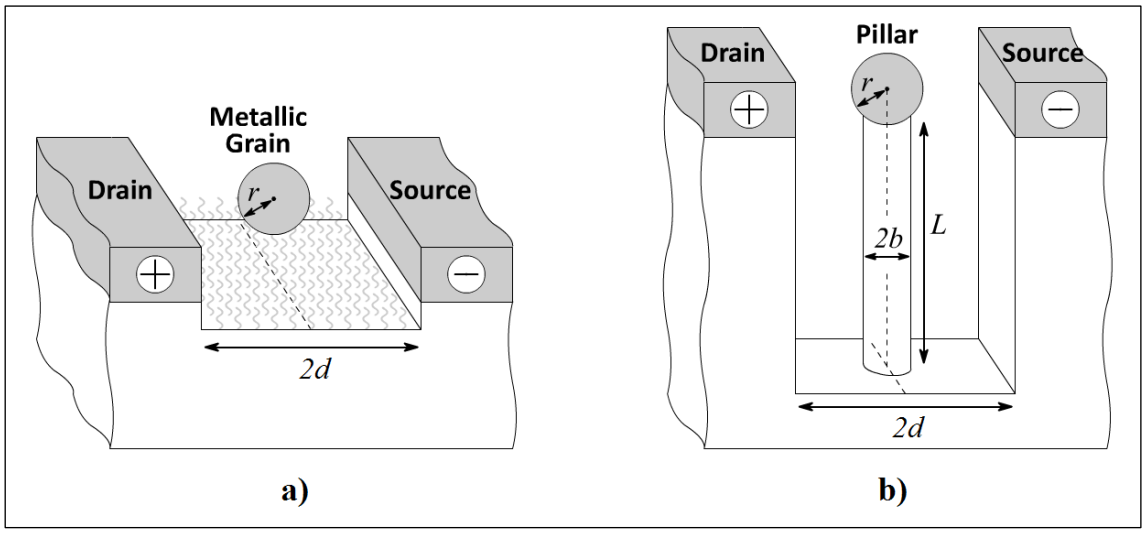

Figure 2.7: *Alternative realization of the shuttling element: (a) metallic grain, (b) pillar.*

The typical diameter $2r$ is, in the case of a metallic grain realizing a Q-dot, of the order of $1\ nm$ [109], whereas the metallic cap of a cantilever geometry is at least one order of magnitude larger (for example, see [41]). Assuming a rather constant value for the ratio $r/d \sim 5$, this leads to the general consideration that the first option is characterized by a smaller scale with respect to the second one. Consequences of this fact have been partly discussed in Sections 4.2.1 and 4.3.1 and are summarized in Tab.2.2.

Table 2.2 – *Preliminary estimations † of system properties related to the shuttling element realization.*

Shuttling element realization	**Characteristic dimensions ($r \ll d$) [nm]**	**Characteristic frequencies [Hz]**	**Kind of shuttle regime**	**Coulomb blockade**	**Max. number of shuttled electrons per cycle**
Quantum dot	$2r = 0.5 \div 10$ $2d = 2 \div 50$	$\omega = 10^9 \div 10^{11}$ $G_0/C(0) = 10^{-53} \div 10^{20}$	soft or hard	present	$N^* = 1 \div 50$
Pillar	$2r = 5 \div 100$ $2d = 20 \div 500$	$10^7 \div 10^{10}$ $G_0/C(0) = 10^{-700} \div 10^{10}$	hard	not present	$N^* = 8 \div 500$

† In this table, mechanical frequencies are referred to Blick's and Gorelik's works, while the charge fluctuation frequency comes from a capacitance calculated from $C(0) = 4\pi\varepsilon r$, and QT conductance from (A.1). These estimations refer to an applied voltage of $5\ V$, a tunneling length $\lambda = 0.3\ nm$, a contact conductance $G_c = 1\ S$, and the shuttling element in center position. Estimations on the number of electrons N^* arise from (1.27b) by assuming $V_S - V_{L,R} = 1\ V$ and using a capacitance $C(A)$ calculated from one of the formulae (1.42a,b), with $x = 0.9(d - r)$. Last, presence of CB refer to the fulfillment of conditions (1.32a,b,c), whereas the soft/hard distinction make use (compatibly with the definitions introduced in Section 2.2.8) of the ratio $G_0/\omega C(0)$.

Since a mandatory design requirements is the presence of *hard* shuttle regime, from Tab.2.2, the *pillar* option is preferred. Also, the pillars set has to be mechanically coupled: this coupling can be realized in a simple (and more proficiently modelable) way by using the "exquisitely mechanical" cantilevers-web realization. In conclusion, each shuttling element is definitely realized as a Pillar (P_i), in agreement with Blick's proposal [77].
Besides, in order to accomplish the design requirement regarding a strong electromechanical coupling, from definition (1.19) follow the estimations †:

$$\mathrm{K} \propto \frac{F_{elec}}{F_{mech}} \approx \frac{eVN^*/2dm}{\omega^2 d} \propto \frac{rV}{\omega^2 d^2 m} \propto \frac{V}{dr} \tag{2.3}$$

In turn, (2.3) states it is convenient to maintain the scale of the device sufficiently small (compatibly with the pillar realization): only in this way, in fact, a large K can be obtained by applying relatively small bias voltages. Consequently to this, and referring to the scheme in Fig.2.7b, a geometrical and mechanical characterization of the pillar is suggested ahead.

The supporting cantilever is realized in silicon ($\rho = 2300\ kg/m^3$), whereas the cap is in gold ($\rho = 19300\ kg/m^3$). Due to the "mushroom-like" mass distribution, we consider only the first mode of vibration. The modal mass m, neglecting that of the silicon cantilever, and using the inferior dimensional limit in Tab.2.2, $2r = 5\ nm$, is assumed to be $m \approx 1 \times 10^{-21}\ kg$. The stiffness, instead, depends only on the silicon cantilever. For a round cross-section and using $L = 40\ nm$, $2b = 2r$, one obtains $k = 3Y\pi r^4/4L^3$ ($Y = 180\ GPa$ for silicon). Such mass and stiffness correspond to a natural frequency $f = \sqrt{k/m}/(2\pi) \approx 2.5\ GHz$ which appears to be a good compromise among Gorelik's and Blick's preferred realization of the resonator element: a metallic grain at $10 \div 100\ GHz$ [25], and a cantilever at $5 \div 300\ MHz$ [26,36,41,67].

It has be remarked the selected cantilever thickness is a only a little beyond some recently proposed sub-10*nm* fabrication techniques [130,131]. However, such a flexural behavior is rather more feasible by using single- or multi-walled CNT [132,133] (which also opens the way to new architectures [131]). Research on nanowires and nanopillars in different boundary conditions (single- or double-clamped) and materials (both silicon and CNTs) is producing in recent years exceptional advances in fabrication techniques and further promising perspectives. One of the most recent and suggestive landmarks is about the direct wiring of CNTs [134].

7.4 Verification of the thermally-induced vibrations

Pillars in a NMT oscillate in air at room temperature. In this condition, they all exhibit a thermal stand-by motion. It is important to verify that this noise vibration regime is sufficiently small with respect to the controlled oscillations. The mean expected displacement can be calculated, as in Section 2.3, with the help of the Fluctuation Dissipation Theorem. Assuming, compatibly with Section 7.3, the following set of parameters: $\Theta = 300\ \mathrm{K}$, $k = 0.25\ N/m$, $d = 10\ nm$, one obtains a ratio $\sigma_x/g \sim 10^{-2}$. This value appears acceptable and allows to neglect thermal vibrations with respect to the forced pillar oscillations.

† In the last passage, it is assumed: $r/d = const$, $\omega \propto r^{-1}$, $m \propto r^3$.

Chapter 8

Modelling the NanoMechanical Transistor

8.1 Suitable analytical approach

Once the characteristic scales of the fundamental QSM have been selected, it is possible to choose the best analytical approach to investigate the whole NMT dynamics.
This decision consists, referring to Section 2.3 and in particular to Tab.1.4, in modeling the mechanical and electrical part of the system by using quantum or (semi)classical approaches.

First, a classical approach for mechanical vibrations is definitely feasible. In fact, for the parameters specified in the last paragraph, the pillar kinetic energy is $\mathcal{K} \approx m(df)^2 \sim 10^{-19}\, J$, quantized in units of $\delta\mathcal{E} = hf \sim 10^{-24}\, J$. The ratio $\mathcal{K}/\delta\mathcal{E} \sim 10^5$ allows to neglect any mechanical quantum effect, even considering exceptionally large forced frequencies $\gg f$.

Secondly, the use of a semi-classical circuital model, which involves capacitances and equivalent QT conductances, depends on the feasibility of a continuous-charge model. Referring to Tab.2.2, this option is suitable for a pillar realization of the shuttling element, since the dimension of the conductive cap allows a relatively large quantity of electrons N^* could be shuttled per cycle. For bias voltages $\gtrsim 1\, V$, $N^* \gtrsim 10 \div 100$: this number is sufficient to neglect any charge quantization effects and justifies the use of a continuous-charge model. In particular, presence of CB effects depend on accomplishing conditions (1.32a,b,c). By using a capacitance $C_P = 4\pi\varepsilon r$ and a conductance $G_{L,R} = 1 \cdot e^{-(d-r)/\lambda}$, (1.32a) is fulfilled at room temperature, whereas the (1.32b) not, and (1.32c) only for voltages $< 0.5\, V$. The fact in both the mechanical and electrical part of the system quantum effects could be neglected causes the discrete set of eigenfrequencies of the pillar can be considered continuous [26].

In conclusion, referring to Tab.1.4, each QSM composing the NMT can be described by a simple pair of equations. The first one is the Newton's law referred to a classical oscillator, the second one the Ohm's law applied to an equivalent circuit. Consequently, the pillar position $x(t)$ and the total charge on the three conductors, $Q_L(t)$, $Q_R(t)$ and $Q_P(t)$ are the lagrangian coordinates: these, under feasible approximations, can be reduced to the pair $x(t)$ and $Q_P(t)$.

8.2 Equations for a single Quantum Shuttle Module

For each of the $N + 1$ QSMs forming the NMT, we refer to scheme in Fig.2.8.
The presented scheme is different from the QSM prototypal architecture introduced in Part One. In particular, more accurate models and feasible approximations are considered for:

- *equivalent QT conductances*: the effect of the potential difference is taken into account;
- *capacitances*: electrostatic effects are calculated using a capacitance matrix approach;
- *force on the pillar*: electrostatic induction effects are included as well.

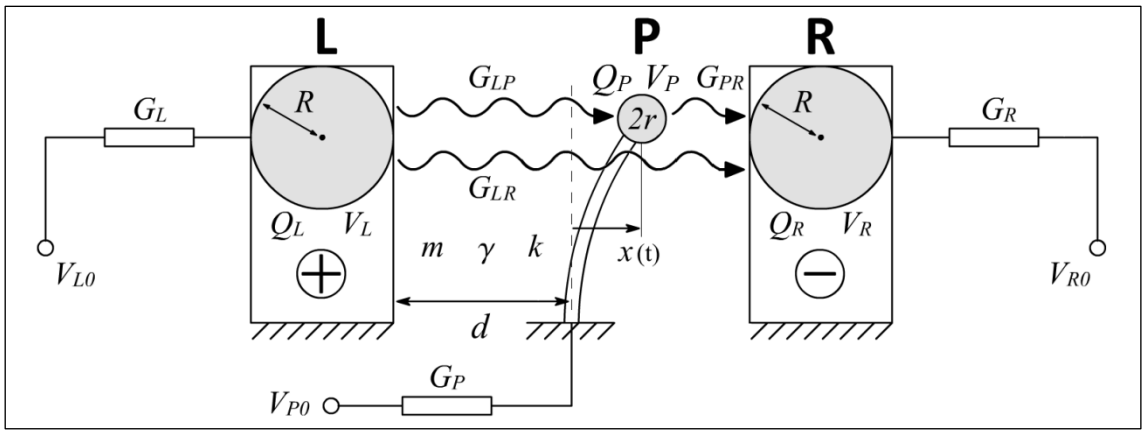

Figure 2.8 – *Schematic representation of a single QSM of a NMT.*

No linearization is considered, except for the pillar motion, which is modeled as a single-DOF linear oscillator †. Last, collisions between the pillar and leads is this time accounted due to the extremely hard nature of shuttle, by using a simple, but numerically efficient model ‡ .
In order to describe the electrical part of the system, it is convenient introduce the arrays:

$$\mathbf{Q} \triangleq \begin{Bmatrix} Q_L(t) \\ Q_P(t) \\ Q_R(t) \end{Bmatrix} \quad , \qquad \mathbf{V} \triangleq \begin{Bmatrix} V_L(t) \\ V_P(t) \\ V_R(t) \end{Bmatrix} \quad , \qquad \mathbf{V_0} \triangleq \begin{Bmatrix} V_{L0} \\ V_{P0} \\ V_{R0} \end{Bmatrix} \quad , \qquad \mathbf{I} \triangleq \begin{Bmatrix} I_{L0}(t) \\ I_{P0}(t) \\ I_{R0}(t) \\ I_{LP}(t) \\ I_{PR}(t) \\ I_{LR}(t) \end{Bmatrix} \tag{2.4}$$

With these definitions, it is possible to write the electrodynamical equations in matrix form:

$$\mathbf{I} = \mathbf{G}\mathbf{V} + \mathbf{G_0}\mathbf{V_0} \quad , \qquad \mathbf{G} = \mathbf{G}[x(t), \mathbf{V}(t)] \tag{2.5}$$

where $\mathbf{G_0}$ and $\mathbf{G}$ are *conductance matrices*. The first one, with constant coefficients, describes classical circuital effects, the second one is indeed specialized to for QT (see Appendix A).
In the most general model, charges and voltages are related by a *capacitance matrix* $\mathbf{C}$:

$$\mathbf{Q} = \mathbf{C}\,\mathbf{V} \quad , \qquad \mathbf{C} = \mathbf{C}[x(t)] \tag{2.6}$$

The three-conductors electrostatics is modeled as that of a system of three spheres or radii r and $R > r$, respectively representing the pillar cap and the fixed electrodes (see Appendix B).
Finally, the relation between currents and charge variations is:

$$\dot{\mathbf{Q}} = \mathbf{D}\,\mathbf{I} \tag{2.7}$$

where $\mathbf{D}$ is a simple matrix of units and zeroes. The mechanical equation is:

$$m\ddot{x} + \gamma\dot{x} + kx = F_P(x, \mathbf{Q}) \tag{2.8}$$

The force on the pillar F_P is calculated by using the electrostatic energy $\mathcal{U}$ (see Appendix C).

† Mechanical nonlinearities are negligible with respect to stronger capacitive and conductance effects when approaching leads.
‡ Collision between the pillar and the fixed electrodes is assumed elastic and modeled by using small and stiff repelling springs.

Eliminating **V** and **I** by combining (2.5)-(2.8), the QSM is described by:

$$\begin{cases} m\ddot{x} + \gamma\dot{x} + kx = F_P(x, \mathbf{Q}) \\ \dot{\mathbf{Q}} - \mathbf{D}\mathbf{G}\mathbf{C}^{-1}\mathbf{Q} = \mathbf{D}\mathbf{G}_0\mathbf{V}_0 \end{cases} \tag{2.9}$$

that is a set of 4 scalar equations in terms of charges $Q_L(t)$, $Q_P(t)$, $Q_R(t)$ and position $x(t)$. This formulation represents the most general description of the system.
However, some simplifications can be introduced in (2.9):

$$G_{LR} \to 0 \quad , \qquad G_{P0} \to 0 \quad , \qquad \begin{cases} G_{L0} \to \infty \\ G_{R0} \to \infty \end{cases} \tag{2.10a, b, c}$$

Conditions (2.10a,b,c) physically correspond to: absence of "long" QT, insulated pillar, bias voltage directly applied on the electrodes. Then, Q_D and Q_S can be expressed in terms of Q_P:

$$Q_L = \frac{(p_{1,3}p_{2,3} - p_{3,3}p_{1,2})Q_P + (p_{3,3} + p_{1,3})V/2}{p_{1,1}p_{3,3} - {p_{1,3}}^2} \tag{2.11a}$$

$$Q_R = \frac{(p_{1,3}p_{1,2} - p_{1,1}p_{2,3})Q_P - (p_{1,3} + p_{1,1})V/2}{p_{1,1}p_{3,3} - {p_{1,3}}^2} \tag{2.11b}$$

where V is the bias voltage, such that $V_{L0} \equiv V_L = +V/2$ and $V_{R0} \equiv V_R = -V/2$, and $p_{i,j}$ are the elements of the elastance matrix $\mathbf{P} = \mathbf{C}^{-1}$. By substituting (2.11a,b) into (2.9), the QSM can be described by using a simple pair of equations (similarly to Chapters 3 and 4):

$$\begin{cases} m\ddot{x} + \gamma\dot{x} + kx = F_P(x, Q_P) \\ \dot{Q}_P + a_1(G_{LP} + G_{PR})Q_P = [a_2(G_{LP} + G_{PR}) + (G_{LP} - G_{PR})]V/2 \end{cases} \tag{2.12}$$

$$a_1 \triangleq \frac{2p_{1,2}p_{1,3}p_{2,3} - p_{3,3}{p_{1,2}}^2 - p_{1,1}{p_{2,3}}^2}{p_{1,1}p_{3,3} - {p_{1,3}}^2} + p_{2,2} \ , \quad a_2 \triangleq \frac{p_{2,3}(p_{1,3} + p_{1,1}) - p_{1,2}(p_{3,3} + p_{1,3})}{p_{1,1}p_{3,3} - {p_{1,3}}^2}$$

8.3 Equations for the whole NanoMechanical Transistor

The NMT device depicted in Fig.2.4 is obtained arranging a set of QSM modeled as in Fig.2.8. Extend the nomenclature presented in the previous Paragraph by considering subscript 0 is for the drive QSM quantities, and $i = 1,2,\dots,N$ for the slave ones. As hinted in Section 7.1, all pillars are mechanically coupled through an elastic web at which their basis are clamped.
Referring to the schemes in Fig.2.9, the whole mechanical part of the NMT can be still described by using a concentrated parameters model. The i-th pillar is characterized by an equivalent mass m_i, a flexural stiffness k_i, and is clamped on a portion of the web with inertia J_i .
The displacement $x_i(t)$ of the cap of the i-th pillar depends on the local rotation of the web $\vartheta_i(t)$ at the pillar clamp and on the flexural deflection $\xi_i(t)$ of its tip, consequently a relation $x_i(t) = L_i\vartheta_i(t) + \xi_i(t)$ holds, being L_i is the clamp-tip height of the pillar.
Finally, neighbor pillars interact by the torsional stiffness of the web represented by κ_i terms. Due to the boundary conditions, notice that $\vartheta_{-1} = \vartheta_{N+1} \equiv 0$.

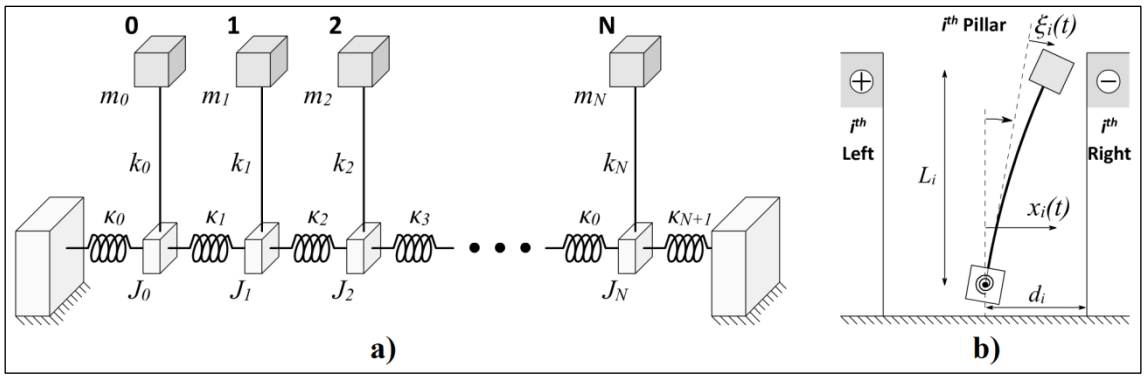

Figure 2.9 – *(a) Concentrated parameters model for the web and pillars, (b) i-th pillar cap deflection.*

The Lagrangian associated to the mechanical part of the system is:

$$\mathcal{L}_{mech} = \left[\sum_{i=0}^{N}\frac{1}{2}m_i\left(L_i\dot{\vartheta}_i + \dot{\xi}_i\right)^2 + \sum_{i=0}^{N}\frac{1}{2}J_i\dot{\vartheta}_i^{\,2}\right] - \left[\sum_{i=0}^{N}\frac{1}{2}k_i\xi_i^{\,2} + \sum_{i=0}^{N+1}\frac{1}{2}\kappa_i(\vartheta_i - \vartheta_{i-1})^2\right] \quad (2.13)$$

that produces a set of $2(N+1)$ equations in terms of ϑ_i and ξ_i , omitted here.

Some particular physical configurations allow to reduce the description of the mechanical vibration of each pillar to a single Lagrangian variable. Qualitative schemes in Fig.2.10 exemplify two particular conditions. In the first case (Fig.2.10a), pillars are clamped on a rigid foundation, allowing to neglect the effect of rotations $\vartheta_i(t)$ on $x_i(t)$; in the second (Fig.2.10b), a large flexural stiffness allows to neglect tip deflections $\xi_i(t)$ on $x_i(t)$. These are the two limit conditions for which torsional and flexural modes are weakly coupled and the system can be still described (as in the previous Section) by using one only mechanical equation per pillar.
In particular, the coordinates x_i now indicate the pillars cap positions, alternatively representing the flexural displacement as in Fig.2.10a, or the torsional angle as in Fig.2.10b.

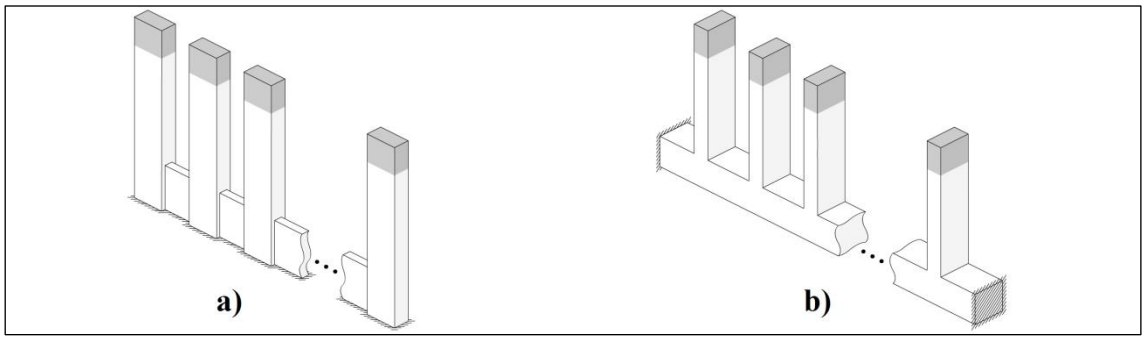

Figure 2.10 – *different realization and boundary conditions of the web geometry: (a) flexural-like coupling between neighbor pillars; (b) torsional-like coupling.*

Then, equations (2.12) (as well parameters $a_{1,i}$, $a_{2,i}$, omitted) generalize into ($i = 0,1,2 \dots, N$):

$$\begin{cases} m_i\ddot{x}_i + \gamma_i\dot{x}_i - k_{i-1,i}x_{i-1} + \left(k_{i-1,i} + k_i + k_{i,i+1}\right)x_i - k_{i,i+1}x_{i+1} = F_P(x_i, Q_{P,i}) \\ \dot{Q}_{P,i} + a_{1,i}\left(G_{LP,i} + G_{PR,i}\right)Q_{P,i} = \left[a_{2,i}\left(G_{LP,i} + G_{PR,i}\right) + \left(G_{LP,i} - G_{PR,i}\right)\right]V_i/2 \end{cases} \quad (2.14)$$

This is a set of $2(N+1)$ equations in terms of $x_i(t)$ and $Q_{P,i}(t)$. The electrical quantities refer to the *i*-th QSM, each one assumed to be electrically decoupled from the others. Last, $V_0 = V_{dr}$ is the voltage on the drive QSM, while $V_1 \equiv V_2 \equiv \cdots \equiv V_N = V_{sl}$ is the common slaves voltage.

Chapter 9

Functional analysis of a Quantum Shuttle Module

9.1 Role of parameters: the reference system

Under assumptions (2.10a,b,c), the evolution of a single QSM is described by equations (2.12), and, at a time t, its configuration is provided by the *coordinates*: $x(t)$, $\dot{x}(t)$, $Q_P(t) = eN_P(t)$. On the other hand, system parameters can be classified depending on the role they play, as:

- *internal parameters:* are constant geometrical, mechanical and electrical quantities which constitute the physical attributes of the device ;
- *external parameters:* are environmental quantities, whose value is subjected to unexpected fluctuations. They are the temperature Θ and the mechanical damping ratio $\zeta \triangleq \gamma/2\sqrt{km}$;
- *control parameters:* are the parameters whose value can be deliberately changed by the observer. The only control parameter is the bias voltage $V(t)$.

Notice that, in principle, disturbances due to the effect of external parameters may be included in the model taking into account a not deterministic system. However, the reduced time scale in which the device operates justifies the assumption to consider both Θ and ζ constant quantities, treating them similarly to internal parameters. Also, pillar thermal fluctuations can be neglected under the estimations made in Section 7.4: this definitely justifies the classical and deterministic approach used here, which assumes one only parameter varies in time, the bias voltage $V(t)$.

The situation is summarized in Tab.2.3 . The variation range is shown for system coordinates, external and control parameters, whereas in the case of internal parameters, a *reference value* (compatibly to the preliminary design choices made in Chapter 7) is specified.

Table 2.3 – *Variables describing a QSM configuration and parameters classification.*

Classifications	**Variable/parameter**		**Reference value or variation range**
	Symbol	***Description***	
system coordinates	$x(t)$	pillar position	$\lvert x(t)\rvert \le d - r$
	$\dot{x}(t)$	pillar velocity	-
	$N_P(t)$	electrons on the pillar	-
internal parameters	$2d$	distance between the fixed electrodes	$20\ nm$
	$2r$	pillar's cap diameter	$5\ nm$
	$2R$	fixed electrodes characteristic size	$50\ nm$
	m	mass of the pillar	$1 \times 10^{-21}\ kg$
	f	natural frequency of the pillar	$2.5 \times 10^{9}\ Hz$
	S	average QT surface	$40\ nm^2$
	ϕ	conductors work function	$5\ eV$
external parameter	ζ	mechanical damping ratio	$10^{-2} \sim 10^{0}$
control parameter	$V(t)$	bias voltage between the fixed electrodes	$V_{CB} \ll V$ †

† The bias voltage has to be larger than the maximum value compatible with CB effect (1.32c), which, for the reference system, is $V_{CB} \approx 0.5\ V$. Otherwise, charge quantization can't be neglected and the semi-classical approach (2.12) is not accurate anymore.

A QSM for which all internal parameters are set to their reference value is the *reference system*.

Since a QSM is finalized to produce a non-zero (averaged over a period) macroscopic current $\bar{I}$, such quantity, in the formalism of *systems theory*, can be considered the *output*, and the voltage application V the *input*. Thus, a black-box conductance $G_{QSM}(t)$ can be introduced as:

$$G_{QSM}(t) \triangleq \frac{\bar{I}}{V(t)} \tag{2.15}$$

This conductance is strictly related with the *transfer function* on the system, whose form is, in turn, determined by the set of internal parameters and expected value for the external one.
Opening the box, the conductive behavior of a QSM depends on the motion regimes established by the pillar, in particular by the possibility to trigger the peculiar shuttle mechanism.

In Part One, we already investigated the electron shuttle dynamics, focusing on the stability analysis of a QSM considered as a dynamical system. This exquisite mathematical vision can be helpful for a first description of the system, but is no more appropriate in a design stage: in this chapter, a more "engineering" approach is used, finalized to investigate the conditions which promote the chance to perform continuative transitions between different motion regimes.

Following the nomenclature suggested in [27], the dynamics of a QSM can refer to a pair of different "classes" of permanent motion regimes:

- *static regimes*: the shuttling element is at rest and no electron shuttle occurs;
- *shuttle regimes*: a stable orbit, achieving the peculiar shuttle mechanism, is established.

Using terms already introduced in Chapter 3, the transitions between these regimes are called:

- *activation transient*: passage from a static to shuttle regime;
- *deactivation transient*: passage from a shuttle to a static regime.

In Paragraph 2, the analysis of transient regimes is carried out, and some considerations lead to a practical (and more effective) interpretation of the *I-V* hysteresis typical of hard shuttle only (see Section 3.3), and to a more deep understanding of the shuttle mechanism itself. Then, in Paragraph 3, we test the dynamical response of a QSM when subjected to different bias voltages $V(t)$, and discuss the consequently established permanent motion regimes. A simple, but neat, predictive model is suggested in Paragraph 4, which interprets such motion regimes as the *states* and the voltages as the input tape of a Turing machine whose evolution depends on a transition function involving some *threshold voltages*. Last, in Paragraph 5, the concepts of *modulability* and *reactivability* are disclosed, together with quantitative definitions.

In conclusion, this Chapter focuses on a single QSM, yet. This will be helpful, in the next Chapter, to carry out a functional analysis for the whole multiple-QSM device: the NMT.

9.2 Transient motion regimes

In general, transitions between the two fundamental permanent motions – *static regime* and *shuttle regime* – can be performed by simply change the level of the bias voltage. In an experimental setup, one is interested to manage the conductive behavior of the QSM (thus, the value of G_{QSM}) by varying the level of V (the only control parameter); then the core practical issue is about *"how to guess" the correct (minimal) voltage required in order to correctly reach a shuttle regime by starting from a static one*. Refer to this statement as the *activation problem* (the *deactivation problem* is instead trivial: it is surely achieved by applying a null bias voltage).

By definition, the soft/hard nature of shuttle (see Section 2.2.8) is strictly related to the way the activation process is achieved. In Chapter 3, it has been highlighted the hard option produces, accordingly with [27], an hysteretic I-V curve. This means, if a hard QSM performs deactivation with any voltage $V < V_{deact}$, activation requires $V \geq V_{act}$, with $V_{act} > V_{deact}$.
We demonstrated with numerical experiments (Fig. 1.24) that the nature of such hysteresis is rather subtle: actually, the value of V_{act} depends on the initial conditions (in particular, $N_P(0)$) so that, if $N_P(0)$ reaches a certain value, the I-V curve hysteresis disappears, and $V_{act} \to V_{deact}$.
On the other hand, soft QSMs do not present any hysteresis, whichever is the initial condition.
The dependence of hard QSM hysteresis from the initial conditions, in Author's opinion, has not been sufficiently investigated in literature yet. Therefore, in this paragraph, an interpretation of the whole activation problem is proposed, which leads to explain the apparent hysteresis and provide a more deep (and physically genuine) comprehension of activation/deactivation process.

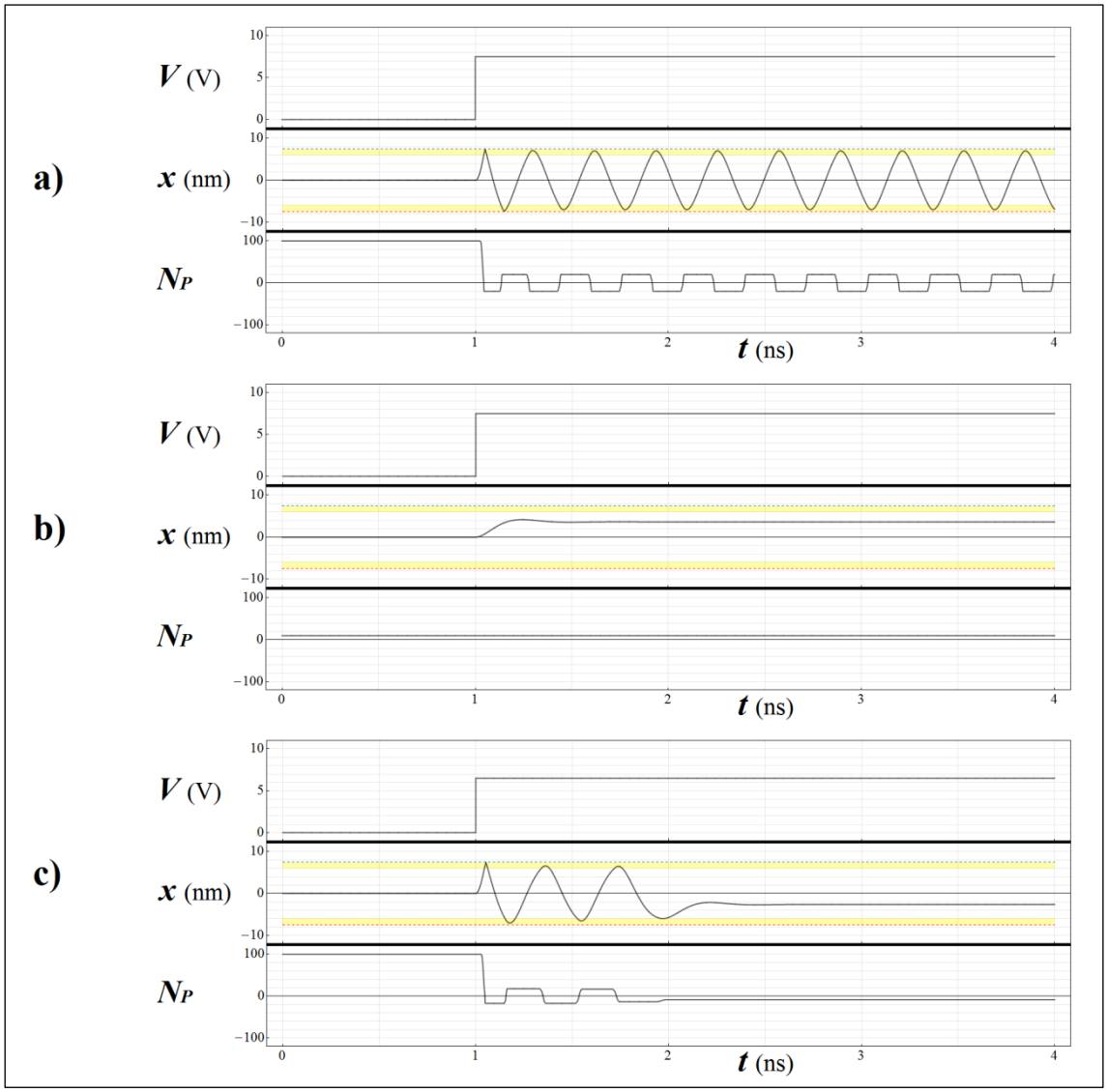

Figure 2.11 –*Three simulations highlight different outcomes of activation transient in a hard QSM. Time histories for bias voltage $V(t)$, pillar position $x(t)$ and electrons $N_P(t)$ are shown. Yellow bands highlight the tunneling region $\mathcal{T}$. Internal parameters as in reference system and damping ratio $\zeta = 0.5$. Results obtained by integrating equations (2.12) and initial conditions: $x(0) \equiv \dot{x}(0) = 0$, $N_P(0) = N_0$. The voltage is maintained null up to a time t^* , then it is raised to a value V^*.*
In (a), $V^* = 7.5\ V$ and $N_0 = 100$. In (b), $V^* = 7.5\ V$and $N_0 = 10$. In (c), $V^* = 6.5\ V$and $N_0 = 100$.

Focus on the numerical results in Fig.2.11, obtained by integrating equations (2.12). The same QSM achieves three activation attempts (internal parameters as in the *reference system*, see Tab.2.3), characterized by different initial conditions and voltage applications. In all cases, the pillar starts in center position at rest, with a number of electrons N_0. Then, the voltage is increased to a value V^*. Combinations of N_0 and V^* determine the activation process outcomes:

- Fig.2.11a: $N_0 = 100$, $V^* = 7.5\ V$ → *successful* activation
- Fig.2.11b: $N_0 = 10$, $V^* = 7.5\ V$ → *failed* activation
- Fig.2.11c: $N_0 = 100$, $V^* = 6.5\ V$ → *failed* activation

In Fig.2.11a, after a brief transient (in which the pillar hits one of the fixed electrodes), a stable orbit characterized by an amplitude A^* is established; therefore, the number of initial electrons and activation voltage are sufficient to trigger and maintain the shuttle mechanism. In Fig.2.11b the pillar deflects, but no microscopic current flows since the distance from the electrodes is too large and is not compatible with QT. In this case, the system returns at rest in a not centered position, since, due to an insufficient number of initial electrons, the shuttle mechanism has not been triggered at all. In Fig.2.11c, the pillar deflects sufficiently to trigger the shuttle mechanism, which is indeed performed for a limited number of oscillations; however, the activating voltage is not sufficient to maintain such self-excited regime, and, after a brief transient, the pillar returns at rest (its final position depending on the details of the last QT episode).

From the analysis of these three exemplificative simulations follows that the activation of a QSM is a process which requires, in general, to accomplish *two distinct* physical requirements:

I) shuttle mechanism *triggering*: a first QT episode has to be performed, that is a first complete electron transfer occurs near one of the fixed electrodes;
II) shuttle mechanism *maintaining*: a limit-cycle is established, leading to a stable orbit whose amplitude and frequency depends on the applied bias voltage.

On the other hand, with no need of any exemplificative simulation, it is straightforward that, the chance for a QSM in shuttle regime to correctly perform a *deactivation process* only relies on not fulfilling (II). Summarizing, the activation and deactivation problems can be summarized as:

$$(I) \wedge (II) \rightarrow activation \quad , \qquad \neg(II) \rightarrow deactivation \tag{2.16a, b}$$

9.2.1 Shuttle triggering: reaching the tunneling region

Since QT has a strong dependence on the distance, (I) is a mere geometrical requirement. Using the symbols introduced in Section 2.2.8, let $\mathcal{O} = [-A_{sup}, A_{sup}]$, with $A_{sup} \triangleq d + r$, the interval where the pillar oscillates, and $\mathcal{T} = \mathcal{O} \setminus [-A_t, A_t]$ the *tunneling region*, in which QT is relevant. Consider a QSM is static regime: the shuttle mechanism is triggered if the pillar deflects up to the tunneling region: in symbols, if $\exists\, t / |x(t)| \geq A_t$. Since the pillar motion depends on the electrostatic force acting on it, accomplish (I) depends on both N_0 and V^* . In particular, a value $V_{act} = V_{act}(N_0)$ exists for which, if the $V^* \rightarrow V_{act}$, then $x \rightarrow A_t$. Reassuming, (I) is fulfilled if:

$$V^* \geq V_{act}(N_0) \tag{2.17}$$

Notice that in a soft QSM, by definition, $\mathcal{T} \equiv \mathcal{O}$. In such case, $A_t = 0$, then $V_{act} = 0$ whichever is the initial condition N_0 . Therefore, condition (I) is sensible only for hard systems.

Some brief arguments to conclude. First, the abscissa A_t can be reached also in a transient overelongation: this means having a small damping ratio generally promotes activation. Last, except for electrostatic induction effects, in the case $N_0 = 0$ activation is not possible, since $V_{act} \rightarrow \infty$.

9.2.2 Shuttle maintaining: energy balance

Once the tunneling region has been reached, the shuttle mechanism is maintained only is the electrostatic pumping on the pillar is sufficient to overcome the mechanical damping. Condition (II) represents such energetic requirement: to analyze which is the corresponding inequality to fulfill, let $\Delta\mathcal{E}_{es}$ the electrostatically energy injected on the pillar per cycle of oscillation, and $\Delta\mathcal{E}_{d}$ the mechanically dissipated one. These terms are respectively calculable as follows:

$$\Delta\mathcal{E}_{es} \triangleq \int_T F_P(V)\dot{x}\,dt \quad , \qquad \Delta\mathcal{E}_{d} \triangleq \gamma \int_T \dot{x}^2\,dt \tag{2.18a, b}$$

being T a single period of oscillation. Assuming the shuttle mechanism is completely *efficient* (compare with the *transport factor* definition in Section 2.2.9), $\Delta\mathcal{E}_{es}$ increases with V. On the other hand, $\Delta\mathcal{E}_{d} \propto \gamma \propto \zeta$. Also, both terms in (2.18a,b) depend in a not trivial way from the amplitude of oscillation, so that $\Delta\mathcal{E}_{es} = \Delta\mathcal{E}_{es}(V, A)$ and $\Delta\mathcal{E}_{d} = \Delta\mathcal{E}_{d}(\zeta, A)$. Consider a QSM in shuttle regime: the amplitude of oscillation evolves depending on the competition among $\Delta\mathcal{E}_{es}$ and $\Delta\mathcal{E}_{d}$: when $\Delta\mathcal{E}_{es} > \Delta\mathcal{E}_{d}$, then A increases; vice versa if $\Delta\mathcal{E}_{es} < \Delta\mathcal{E}_{d}$, A decreases.
Assume a constant voltage V^* is set; then a limit-cycle is established and definitely leads to a stable orbit by amplitude A^* which accomplishes the energy balance (see Section 2.2.3):

$$\Delta\mathcal{E}_{es}(V^*, A^*) \equiv \Delta\mathcal{E}_{d}(\zeta, A^*) \tag{2.19}$$

Since A_t is the minimal amplitude compatible with the shuttle regime, it is possible to define a value V_{inf} that, if $V^* \to V_{inf}$, from (2.19) produces $A^* \to A_t$. Thus, requirement (II) depends on:

$$V^* \geq V_{inf} \tag{2.20}$$

9.2.3 Physical explanation of the activation/deactivation hysteresis

Consider a QSM is static regime: with the aim to correctly perform an *activation transient*, at a time $t = t^*$, the voltage is raised to a value V^*. Then consider the same QSM in shuttle regime: to achieve a *deactivation transient*, at $t = t^{**}$ the voltage is lowered to V^{**}. Consequently, referring to (2.16a,b) and playing a little with propositional logic, the chance to correctly achieve activation/deactivation processes can be related to conditions (2.17) and (2.20):

$$V^* \geq \max\left(V_{inf}, V_{act}\right) \to activation \quad , \qquad V^* < V_{inf} \to deactivation \tag{2.21a, b}$$

At this point, it is straightforward, the I-V curve of a QSM exhibits an hysteretic behavior when $V_{act} > V_{inf}$. In the case of soft shuttle, $\mathcal{T} \equiv \mathcal{O}$ (see Section 2.2.8), thus, from Section 9.2.1, follows $V_{act} = 0$; then, since $V_{inf} \geq 0$, one obtains $V_{act} \not> V_{inf}$ and hysteresis is not possible. This definitely explains why the I-V curve hysteresis only appears in the case of hard QSMs.
In Chapter 3, specifically in Fig.1.24, numerical experiments showed the number of initial electrons has a certain role in the hysteretic behavior of hard QSMs. Since the voltage threshold V_{act} in (2.21a,b) depend on N_0 , one can find a formal relation between N_0 and the hysteresis. Introduce N_{hyst} as the unique value of N_0 for which $V_{act}\left(N_{hyst}\right) \equiv V_{inf}$. Follows that:

$$N_0 \geq N_{hyst} \quad \Leftrightarrow \quad V_{inf} \geq V_{act}(N_0) \tag{2.22}$$

Quantity N_{hyst} plays a crucial role in the design of a hard QSM. At the beginning of an activation process, if $N_0 > N_{hyst}$, *no hysteresis occurs*, since relation (2.22) guarantees $V_{inf} \geq V_{act}$. A last consideration. Since the voltage threshold V_{act} which fulfills (I) is a function of N_0 , one can shift the point of view and use the analogous concept of *electron threshold*, introducing a quantity $N_{act} = N_{act}(V^*)$. An alternative formulation of (2.17) follows, for which, in the case $N_0 \geq N_{act}(V^*)$, shuttle triggering is achieved †. Notice that, in a soft QSM, $N_{act} = 0$.

In conclusion, in this Chapter we demonstrated with simple heuristic arguments that the apparent hysteretic behavior often cited in QSM literature is only *apparent* and does not rely on some intrinsically hysteretic physical phenomena, but is a mere consequence of the not complementary conditions to be accomplished to perform an activation or a deactivation.

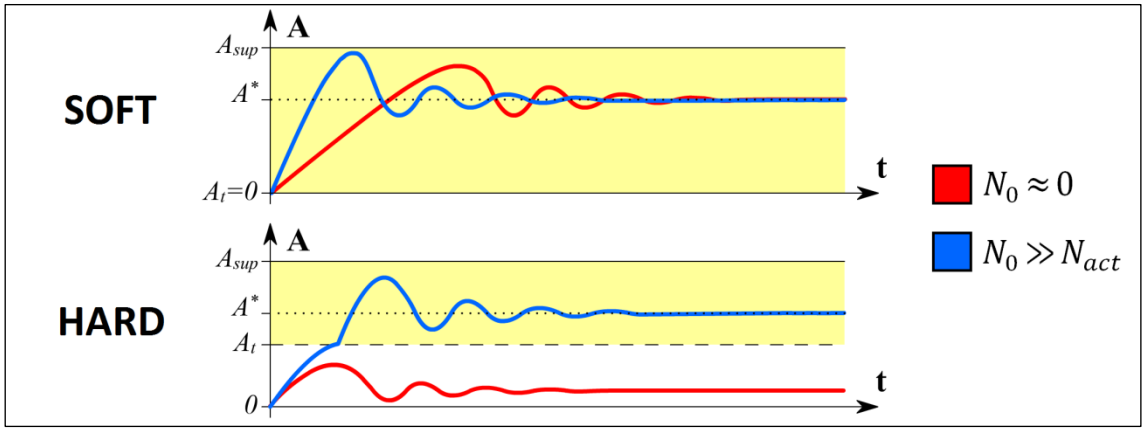

Figure 2.12 – *Qualitative plots $A(t)$ show activation attempts for soft and hard QSMs starting at $A_0 = 0$, achieved with the same voltage $V^* = 0$, and matching energy balance (2.19) for an amplitude A^* . In the soft case the tunneling region $\mathcal{T}$ (in yellow) occupies the whole oscillating space ($A_t = 0$), and activation is always successful. Instead, in the case of a hard QSM, the $\mathcal{T}$ can be reached or not, depending on N_0 . In this sense, the tunneling region behaves as the basin of attraction of the stable orbit with amplitude A^*.*

9.3 Permanent motion regimes

In this Paragraph we test the dynamical response of a QSM at different levels of voltage $V(t)$. In particular, we analyze the established motion regimes and consequent conductive behavior.
A preliminary digress is required. Differently from Part One (and from most theoretical articles [25,27,29]) equations (2.12) take into account the dependence $\lambda = \lambda(V)$ to model the QT (Appendix A). This approach is useful to correctly compute QT conductances when varying the voltage within a single simulation. A direct consequence is that (as hinted in Section 2.2.8) the value assumed by $V(t)$ influences the soft/hard nature of the system. Two possibilities arise:

- if a QSM exhibits a *soft* behavior when $V \approx 0$ it remains soft at increasing voltages ;
- if a QSM is *hard* when $V \approx 0$, it transits towards the *soft* condition when a certain threshold voltage value V_{trans} is surpassed .

For example, the reference system (see Tab.2.3), belongs to the second category of QSMs, and exhibits a hard→soft transition around a value $V_T \approx 35\ V$.

† It has be remarked quantities N_{hyst} and $N_{act}(V^*)$ should not be confused: besides they mean two distinct concepts, N_{hyst} is a peculiar feature of a system with known parameters; while $N_{act}(V^*)$ is a property related to an activation attempt performed at a voltage V^*. Then, any QSM is characterized by a unique N_{hyst}, whereas N_{act} can assume any positive value, depending on V^*.

In Fig.2.13, the numerical results referred to a simulation for the reference system are shown. A number of permanent motion regimes are exhibited, consequent to step applications of the bias voltage $V(t)$, each variation occurring after a period of time sufficient to complete any transient.

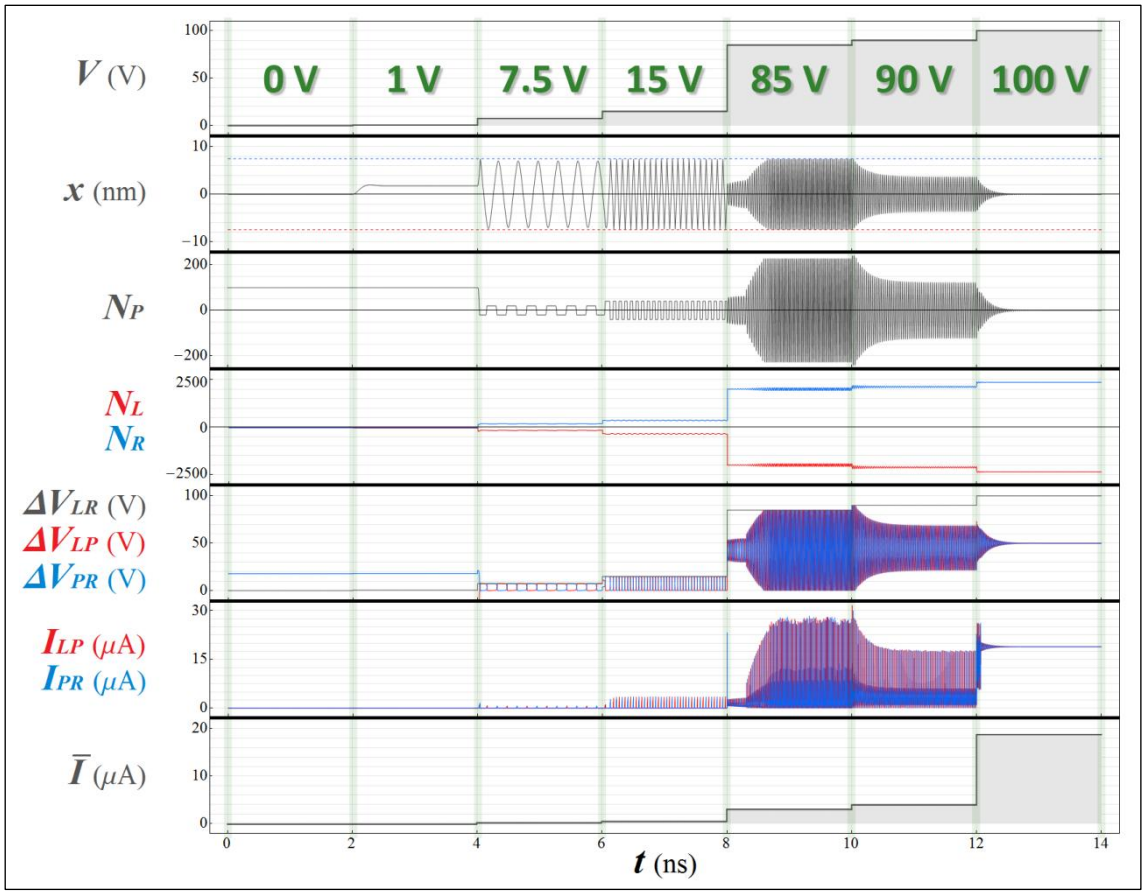

Figure 2.13 – *Numerical results for a single QSM obtained by direct integration of equations (2.12) with initial conditions:* $x(0) \equiv \dot{x}(0) = 0$, $N_P(0) = 100$. *Internal parameters as in the reference system, external parameter (damping ratio)* $\zeta = 0.5$ *and step-variable (voltage) control parameter. Time histories for the following quantities are reported: bias voltage* V *, pillar position* x *, pillar electrons* N_P *, leads electrons* N_L*,* N_R *, potential differences* ΔV_{LR}*,* ΔV_{LP} *and* ΔV_{PR}*, microscopic currents* I_{LP} *and* I_{PR} *, and macroscopic average current* $\bar{I}$.

The permanent motion regimes established by the system are discussed ahead in detail.
At the beginning, the bias voltage is not present: the pillar is at rest in center position and no current passes if (time period labeled with "0 V"). Then, the voltage is raised to a relatively small value (1 V) and the pillar deflects, but activation is not performed and a mere static deflection is obtained, thus, again, $G_{QSM} = 0$. At larger voltage (7.5 V) activation is achieved and the shuttle mechanism is both triggered and maintained, since condition (2.21a) is fulfilled. The self-excited oscillation frequency is usually larger than the natural one; in fact, the larger is the bias voltage, the faster are the oscillations. Thus, V influences not only the oscillations amplitude A (as discussed in Section 9.2.2), but also the frequency f. At last, the reverse point definitely reaches the leads, and a shuttle regime with continuative collisions is performed (15 V).
In this first part of the simulation, $V < V_T$ and the QSM exhibits hard shuttle. When larger voltages are applied, the shuttle nature becomes soft. However, this fact is not trivially detectable if the system remains in shuttle regime (as in Fig.2.13), since the soft/hard distinction is only related to the different properties of the activation transient (as discussed in Paragraph 2).

Clearly, the bias voltage value V affects the pillar oscillation frequency also in the soft range. This trend continues indefinitely, until the shuttle mechanism is no more completely *efficient* (that means $\eta = 1$: see the *transport factor* definition in Section 2.2.9). In fact, for extremely large voltage applications ($85\ V$), the self-excited frequency of the pillar is often one or two order of magnitude larger than the natural one; this definitely leads ($90\ V$) to an *inefficient* shuttle † ($\eta < 1$). The sign of the occurrence of this (rare) condition is in the fifth plot, where it is clearly visible the potential differences ΔV_{LP}, ΔV_{PR} *no more vanish* during each QT episode. For even larger voltage applications ($100\ V$), the shuttle mechanism becomes so much inefficient that the energy pumping is no more sufficient to overcome the mechanical damping, thus condition (II) is no more accomplished, an energetic balance like (2.19) no more holds, and deactivation occurs. Consequently, a new rest condition, due to a somehow "saturative" effect, is obtained. From a mechanical point of view, this situation is completely similar to the rest condition corresponding to null bias voltage; however, from the electrical point of view, they present completely different characteristics, since this new rest condition has occurred after the hard→soft transition ‡. In both cases, the shuttle current contribution is null, but, in the first one ($0\ V$, hard) this is also per the tunnel one, whereas in the second ($100\ V$, soft), a huge current, produced by the tunnel contribution (and even larger than the inefficient shuttle case), is present (look at the last plot). In the latter case, in fact, the tunneling region extends over to central position in which the pillar is at rest, bringing a current independent from its vibrational motion.

Since they range over both the hard and soft nature, plots in Fig.2.13 exemplify the peculiar motion regimes a QSM can establish for different values of the bias voltage. From this point of view, the presented simulation provides a rather complete scenario of the phenomenologies (both dynamics and conductive behavior) for a direct (thus, self-excited) QSM. In the following paragraphs, in order to indicate the archetypical behaviors discussed above, we refer to the tags and keywords listed here (which further specify the static/shuttle regime nomenclature):

- *CENtered* (CEN): *static regime* in centered position ($0\ V$) ;
- *STatic Deflection* (STD): *static regime* in deflected position ($1\ V$) ;
- *Normal SHuttle* (NSH): efficient *shuttle regime* with no collisions ($7.5\ V$) ;
- *Collision SHuttle* (CSH): efficient *shuttle regime* with collisions ($15\ V$ or $85\ V$) ;
- *Inefficient SHuttle* (ISH): inefficient *shuttle regime* ($90\ V$) ;
- *SATuration* (SAT): *static regime* due to severely inefficient shuttle ($100\ V$) .

These motion regimes have been achieved, in Fig.2.13, for the values of the voltage indicated within the parentheses. However, one could be interested to understand *the general* correlation between the applied V and the consequent motion regime established. This would provide an exceptional predictive instrument to foresee the dynamical (and, consequently, the conductive) behaviors of a QSM, giving the chance to govern the pillar motion with targeted voltage applications. This point has been partly disentangled in Paragraph 2, in fact, *activation* and *deactivation* transitions related to the threshold voltages V_{act} and V_{inf} can now be referred to passages from/to a static regime (one of the subgroup: CEN, STD, SAT) to/from a shuttle regime (NSH, CSH, ISH). Nonetheless, to obtain the predictive model suggested above, further transitions – corresponding to any possible passage among CEN, STD, NSH, CSH, ISH, SAT – should be related some additional threshold voltages.

In order to do this, further investigations on the dependence $\Delta\mathcal{E}_{es}(V)$ are required.

† Since the variation of $\lambda(V)$ makes the QT conductance curves $G_{LP}(x,V)$ and $G_{PR}(x,V)$ to tend to be horizontal and match.

‡ Exceptionally, saturative rest regimes occur in the hard region. In this case, the conductive behavior of a static regime with no bias voltage and a saturative static one are undistinguishable. Numerical simulations show most systems behave as in Fig.2.13.

In Section 9.2.2, we said that, if the shuttle mechanism is fully *efficient* ($\eta = 1$), the electrostatically injected energy $\Delta\mathcal{E}_{es}$ monotonically *increases* with V. This fact is indeed true, confirmed by a large set of numerical results (not shown here) and from those in Fig.2.13 as well. However, over a relatively large value of the bias voltage (in Fig.2.13, between 85 V and 90 V), the shuttle mechanism becomes *inefficient* ($\eta < 1$): in such situation, $\Delta\mathcal{E}_{es}(V)$ can *decrease*. Consequently, a new threshold voltage can be introduced, V_η , indicating the transition between efficient and inefficient shuttle. In general, $V_\eta \leq V_M$, the point M indicating the maximum of the curve $\Delta\mathcal{E}_{es}(V)$, also corresponding to the maximal energy pumping on the pillar. Another threshold, V_{sat}, is the highest voltage compatible with inefficient shuttle. For $V > V_{sat}$, the energy pumping is no more sufficient to guarantee the balance (2.19), and a saturative deactivation is performed. These arguments involving V_η , V_{sat} and $\Delta\mathcal{E}_{es}$ are summarized in Fig.2.14.

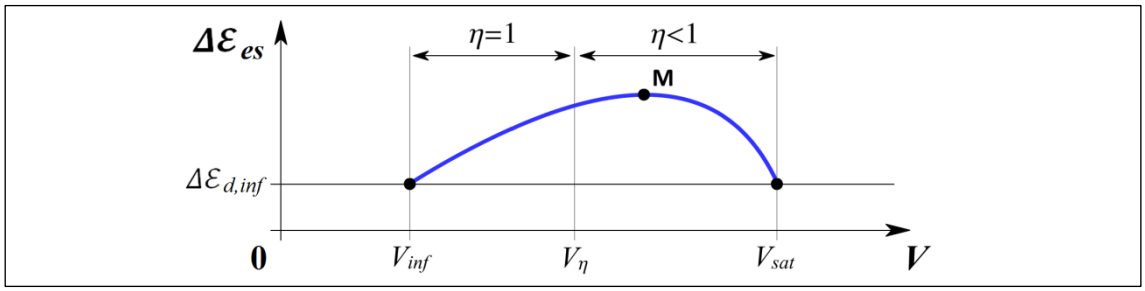

Figure 2.14 – *Qualitative sketch of the curve $\Delta\mathcal{E}_{es}(V)$ with the indication of the shuttle regimes efficiency. The existence of shuttle regimes depends on the possibility to guarantee an energy balance like (2.19). Such energy balance can be achieved only for amplitudes $A \geq A_t$. The line $\Delta\mathcal{E}_{d,inf}$ represents the dissipated energy in correspondence of a shuttle regime with amplitude A_t , consequently, the equivalence $\Delta\mathcal{E}_{es}(V) \equiv \Delta\mathcal{E}_{d,inf}$ individuates the two particular voltages, V_{inf} and V_{sat} , which delimit the range of existence for the shuttle regimes. In turn, the threshold voltage $V_\eta \in [V_{inf}, V_M]$ separates the subregion $[V_{inf}, V_\eta]$, characterized by efficient ($\eta = 1$) shuttle, from the subregion $[V_\eta, V_{sat}]$, inefficient ($\eta < 1$).*

A last voltage threshold, V_{sup}, corresponds to the incipient condition for which the amplitude of the mechanical oscillations reach the maximum amplitude $A_{sup} = d - r$. When $V \geq V_{sup}$, a shuttle regime with continuative collisions occurs.

In conclusion, one can answer the question: "it is possible to foresee the motion regime established by a QSM by only knowing the applied bias voltage V?". The next Paragraph show that, if the voltage thresholds V_{act}, V_{inf}, V_{sup}, V_η and V_{sat} are known, the answer is indeed *yes*.

9.4 Static machine interpretation

A QSM characterized by a set of internal parameters IP, and subjected to the external parameters EP, evolves its coordinates $\mathrm{CO}(t)$ depending on the control parameters $\mathrm{CP}(t)$. This description applies to any deterministic system, and specifically refers to a QSM if (from Section 9.1):

$$\mathrm{CO}(t) \triangleq \{x(t), \dot{x}(t), N_P(t)\}, \quad \mathrm{IP} \triangleq \{d, r, R, m, f, S, \phi\}, \quad \mathrm{EP} \triangleq \{\zeta\}, \quad \mathrm{CP}(t) \triangleq \{V(t)\} \tag{2.23}$$

Besides, one can notice the investigated system presents convenient characteristics, due to the fact the shuttle mechanism is produced by using self-excitation (and not parametric resonance).

First, it is sufficient to apply a constant voltage to have a QSM undergo a certain permanent motion regime. Second, different voltage levels may correspond to one of the peculiar motion regimes listed in the last Paragraph. Last, each transition between different permanent regimes consists in a brief transient regime which lasts a limited number of periods of oscillation.
The situation described above hints to a description of a QSM characterized by the formalism:

- $\mathbb{s}$ *(state):* permanent motion regime exhibited by the system;
- $\mathbb{e}$ *(event):* any imposition in bias voltage;
- $\mathbb{t}$ *(transition):* transient motion regime between two states and induced by an event.

Then, (assuming each bias voltage imposition is separated by an interval of time Δt sufficient to conclude any transient regime), the dynamical behavior of the device can be assimilated to that of a *static machine* receiving as input a succession of events $\mathbb{e}_i$, and producing as output a succession of states $\mathbb{s}_i$, interspersed with transitions $\mathbb{t}_i$ (i potentially goes from 0 to infinity).
By using these definitions, the functionality of a single QSM is formally analogue to the typology of *Turing machine* described in [135]. In this variant, the "events tape" can only advance ($\mathbb{e}_i \rightarrow \mathbb{e}_{i+1}$), and the behavior of the whole system is properly described by the 7-uple:

$$\mathrm{QSM} \triangleq \langle \mathbb{S}, \mathbb{E}, \mathbb{R}, \mathbb{M}, \mathbb{s}_0, \mathbb{F}, \mathbb{T} \rangle \tag{2.24}$$

where:

- $\mathbb{S}$ *(set of states)* → all the possible permanent motion regimes;
- $\mathbb{E}$ *(set of events)* → all the acceptable values for the external voltage;
- $\mathbb{R} \subset \mathbb{E}$ *(subset of regulations)* → events which not produce a change in the current state;
- $\mathbb{M} = \mathbb{E} \backslash \mathbb{R}$ *(subset of maneuvers)* → events which produce a change in the current state;
- $\mathbb{s}_0 \in \mathbb{S}$ *(initial state)* ;
- $\mathbb{F} \subseteq \mathbb{S}$ *(subset of final states)*: permanent regimes refractory to further transitions;
- $\mathbb{T}$: $(\mathbb{S} \backslash \mathbb{F}) \times \mathbb{E} \rightarrow \mathbb{S}$ *(transition function)* → prescribes how the system evolves.

The *extensional* definition of the set of states is:

$$\mathbb{S} \triangleq \{\mathrm{CEN}, \mathrm{STD}, \mathrm{NSH}, \mathrm{CSH}, \mathrm{ISH}, \mathrm{SAT}\} \tag{2.25a}$$

where the abbreviations above correspond to the motion regimes defined in Paragraph 3.
Notice that, among these, no final states exist, therefore such subset is void:

$$\mathbb{F} \triangleq \emptyset \tag{2.25b}$$

The set of events comprises all the acceptable bias voltages. Thus, its *intensional* definition is:

$$\mathbb{E} \triangleq \{V \geq 0\} \tag{2.25c}$$

By using this formalization, states and transitions consequent to an event can be portrayed on a phase plane $\{x, N_P\} \in \left[-A_{sup}, +A_{sup}\right] \times (N_L, N_R)$, with $A_{sup} = d - r$, and N_L and N_R being the number of electrons present on the left and right fixed electrodes, respectively.
In this convention, states $\mathbb{s}$ correspond to points if they refer to one of the static regimes, while are closed trajectories when they portray shuttle regimes (transitions $\mathbb{t}$ could be also represented with curve bows which connect two consequent states representations).
In Fig.2.15 a schematic picture of the possible states is depicted on the phase plane $\{x, N_P\}$.

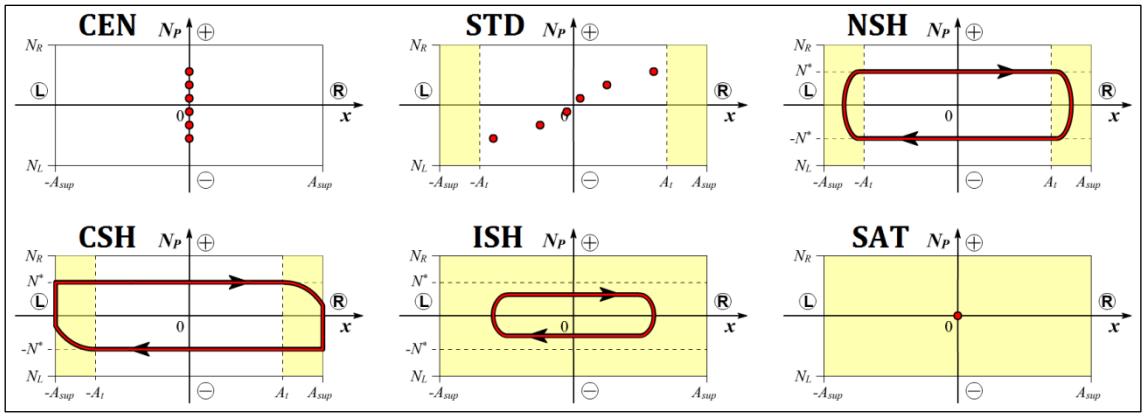

Figure 2.15 – *Points and closed trajectories on the phase plane* $\{x, N_P\}$ *portraying the possible states.*

The formal description of the QSM is completed by an extensive definition of the transition function in Tab.2.4, which involves the voltage thresholds V_{act} , V_{inf} , V_{sup} , V_η , V_{sat} .

Table 2.4 – *Tabular definition of the transition function* $\mathbb{T}$ *for a QSM.*

Current state $(\mathbb{s}_i)$	**Event** $(\mathbb{e}_i)$	**Transition performed** $(\mathbb{t}_i)$	**Consequent state** $(\mathbb{s}_{i+1})$
CEN	$V = 0$	centering	CEN
	$0 < V < \max(V_{act}, V_{inf})$	failed activation	STD
STD	$\max(V_{act}, V_{inf}) \leq V < V_{sup}$	activation	NSH
	$V_{sup} \leq V < V_\eta$	collusive activation	CSH
SAT	$V_\eta \leq V < V_{sat}$	inefficient activation	ISH
	$V \geq V_{sat}$	saturative failed activation	SAT
NSH	$V = 0$	deactivation	CEN
	$0 < V < V_{inf}$	partial deactivation	STD
CSH	$V_{inf} \leq V < V_{sup}$	modulation	NSH
	$V_{sup} \leq V < V_\eta$	collusive modulation	CSH
ISH	$V_\eta \leq V < V_{sat}$	inefficient modulation	ISH
	$V \geq V_{sat}$	saturative deactivation	SAT

In Fig.2.16, a schematic flow-chart representation of a QSM IS SHOWN. States are represented by closed figures, arrows connecting them correspond to transitions consequent to events.

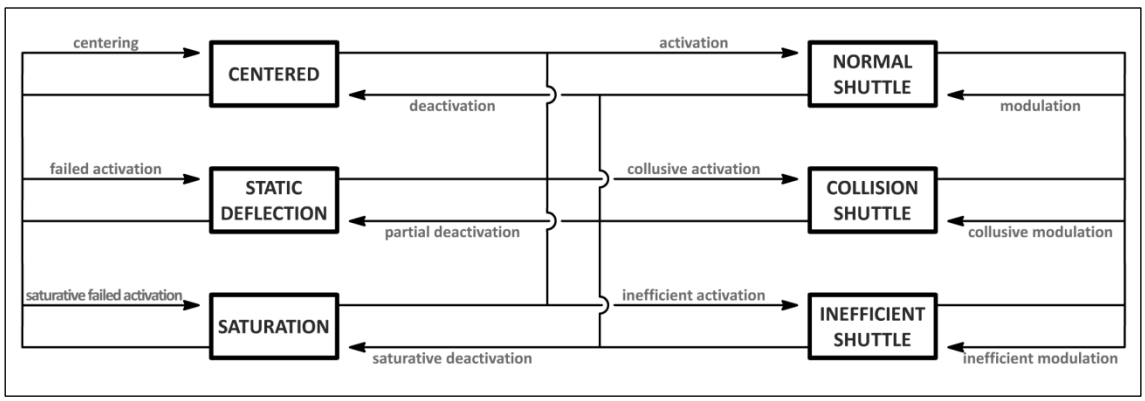

Figure 2.16 – *Flowchart representation of possible states and transitions for a QSM.*

9.5 Role of voltage thresholds: typical attitudes

The transition function defined in Tab.2.4 provides for a *bijective* correspondence between the application of a bias voltage and the consequently established motion regime. However, the usage of such predictive instrument requires the preliminary knowledge of the five voltage thresholds V_{act}, V_{inf}, V_{sup}, V_{η} and V_{sat}. Their values depend on the specific QSM considered; in particular, on both its *internal* and *external parameters* and, only for V_{act}, on its *configuration*:

$$V_{act}(\mathrm{IP},\mathrm{EP},\mathrm{CO}) \quad , \quad V_{inf}(\mathrm{IP},\mathrm{EP}) \quad , \quad V_{sup}(\mathrm{IP},\mathrm{EP}) \quad , \quad V_{\eta}(\mathrm{IP},\mathrm{EP}) \quad , \quad V_{sat}(\mathrm{IP},\mathrm{EP}) \quad (2.26)$$

In particular, V_{act} depends on the number of electrons N_0 precedent to any activation attempt. Remarkably, such peculiarity makes the determination of V_{act} problematic. In fact, N_0 depends on the details of the last deactivation process, and this, differently from other transitions (i.e. activation), is a somehow *aleatory* process. Since the actual value of N_0 is unknown to the observer, one can only obtain a partial estimation of the voltage threshold $V_{act} = V_{act}(N_0)$.
Also, the fact one of the voltage thresholds depends on the initial condition N_0, makes the static machine interpretation introduced in Paragraph 4 conceptually (though not formally) *ill-posed*.

Referring to Section 9.2.3. If one assumes a condition $N_0 \geq N_{hyst}$ holds, from (2.22) follows that $V_{inf} \geq V_{act}$. Consequently, the term V_{act} becomes irrelevant on the success of the activation process (which now depend only on V_{inf}) and does not represent a voltage threshold anymore: in both (2.21a) and Tab.2.16, the term "$\max(V_{act}, V_{inf})$", transforms in "V_{inf}".
In the followings, refer to condition $N_0 \geq N_{hyst}$ as the "convenient deactivation hypothesis" †.
Reassuming, in a QSM under the *convenient deactivation hypothesis* the voltage threshold evolves its states *independently* from V_{act}, so that: i) the estimation of V_{act} is no more required, ii) the static machine interpretation of a QSM is conceptually well-posed. From both i) and ii) follows Tab.2.4 is definitely able to provide a deterministic provisional model.

Assume for now the *convenient deactivation hypothesis* holds ‡. We are in the situation in which only four voltage thresholds determine a QSM dynamics: V_{inf}, V_{sup}, V_{η}, V_{sat}. In principle, since different systems are characterized by a different set of parameters, they could present different relative ratios between the voltage thresholds. Instead, a large number of numerical simulations using realistic (compatible with Section 9.1) values of IP and EP , led to the same casuistic which characterize the reference system (as for the simulation in Fig.2.13):

$$0 < V_{inf} < V_{sup} < V_{\eta} < V_{sat} \quad (2.27a)$$

A QSM for which (2.27a) holds exhibits a *normal attitude*. As it is clear by a quick look to the definition of the transition function in Tab.2.4, such systems are able to perform the entire set of states $\mathbb{S} \triangleq \{\mathrm{CEN}, \mathrm{STD}, \mathrm{NSH}, \mathrm{CSH}, \mathrm{ISH}, \mathrm{SAT}\}$ depending on the applied voltage V .

† Notice how, in particular, the assumption $N_0 \geq N_{hyst}$ is also useful to avoid the most adverse situation in which, at the end of a deactivation transient, exactly zero electrons remain on the shuttle element ($N_0 = 0$). Conversely, in the frame of the rigorously formal scheme introduced in Section 9.4, the state CEN should be further split in two states: a first one, properly tagged CEN, representing the case $N_0 > 0$; and a second one, CEN0, for which $N_0 = 0$. The latter leads to the limit $V_{act} \to \infty$, therefore would correspond to a state refractory to further transitions, the definition (2.25b) becoming $\mathbb{F} \triangleq \{\mathrm{CEN0}\}$. The convenient deactivation hypothesis prevents these complication as well.

‡ The physical requirements promoting the feasibility of the convenient deactivation hypothesis will be analyzed in a more deep detail in Section 9.6.1. In the meantime, we simply postulate it.

Exotic choices of parameters or extremely small device sizes, sometimes produce situations in which the pillar can't reach the maximum amplitude $A_{sup} = d - r$. In these cases, following the definition proposed in Section 9.3, V_{sup} should remain *undefined*; however, let conventionally set $V_{sup} = V_\eta$, so that the definition of the transition function in Tab.2.4 is still valid. Thus:

$$0 < V_{inf} < V_{sup} = V_\eta < V_{sat} \tag{2.27b}$$

In this case, a QSM presents a *diminished attitude*, since no choice V can perform the state CSH.

Reducing a little more the scale can lead to the condition $V_\eta = V_{inf}$, that is no efficient shuttle regime can be achieved. Consequently:

$$0 < V_{inf} = V_{sup} = V_\eta < V_{sat} \tag{2.27c}$$

This condition is called *inefficient attitude*, since the only shuttle regime possible is ISH .

Last, exceptional cases lead to the situation for which no shuttle regime is possible at all; this means V_{inf} is not defined, but can be conventionally posed equal to V_{sat} :

$$0 < V_{inf} = V_{sup} = V_\eta = V_{sat} \tag{2.27d}$$

In Tab.2.5 the overall casuistic is summarized. Clearly, from an engineering point of view, the *typical* or *diminished* attitudes are the preferred conditions for a QSM.

Table 2.5 – *Overview of the typical QSM attitudes under the assumption* $N_0 \geq N_{hyst}$.

Typical attitudes	**Voltage thresholds**											
	0		V_{inf}		V_{sup}		V_η		V_{sat}			
Normal	CEN	STD		NSH		CSH		ISH		SAT		
Diminished	CEN	STD		NSH				ISH		SAT		
Inefficient	CEN		STD				ISH			SAT		
Refractory	CEN				STD				SAT			

Remarkably, each of the typical attitudes can be related to a peculiar qualitative behavior of the curves $\Delta\mathcal{E}_{es}(V)$ and $A(V)$ in the range of voltages compatible with a shuttle regime. Let V_M the voltage corresponding to the maximum point M of the curve $\Delta\mathcal{E}_{es}(V)$, achieving the shuttle regime with the largest energy injection on the pillar. In general, the amplitude of oscillation $A(V)$ is comprised between the superior horizontal line $A_{sup} = d - r$, and the inferior limit $A_{inf} = A_t(V)$, which is a decreasing line † , intersecting the line $A = 0$ in the point T, corresponding to the hard→soft transition voltage V_T . In a system characterized by the *normal attitude* (Fig.2.17a), the shuttle regime is efficient up to a value $V_\eta \approx V_M$, and the hard→soft transition occurs at $V_{sup} < V_T < V_\eta$. In the case of *diminished attitude* (Fig.2.17b), the shuttle mechanism is efficient up to $V_{inf} < V_\eta < V_M$, the hard→soft transition at $V_{inf} < V_T < V_\eta$. In the *inefficient attitude* (Fig.2.17c), shuttle is always inefficient since $V_{inf} = V_\eta$, the transition occurring at $V_T > V_\eta$. Last, a *refractory attitude* QSM has $\Delta\mathcal{E}_{es}(V) - \Delta\mathcal{E}_{d,inf} < 0$ for any V: consequently, shuttle regimes are not possible, and the pillar merely statically deflects up to $V_T = V_\eta$.

† Term $A_t(V)$ indicates the tunneling region lower limit. Its value (due the QT dependence from distance) shifts linearly with V .

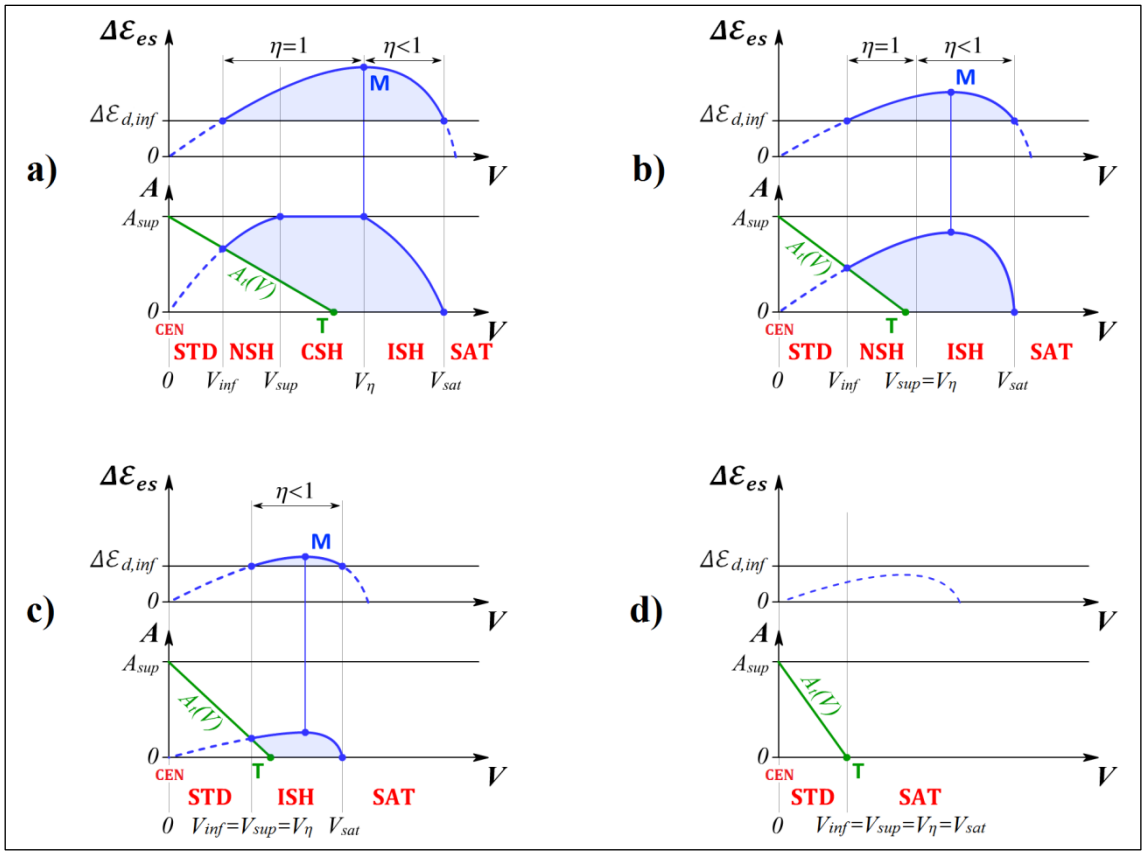

Figure 2.17 – *Qualitative schemes of the curves $\Delta\mathcal{E}_{es}(V)$ and $A(V)$ summarize the different situations peculiar of a QSM with: (a) normal, (b) diminished, (c) inefficient, (d) refractory attitudes.*

9.6 Reactivability and modulability in the hard regime

One of the design requirements discussed in Section 7.2 was about the hard nature of shuttle. Only in such case, the macroscopic current completely vanishes with slave pillars in static regime. In fact, dealing with hard systems has the practical advantage that (see Section 2.2.11) the macroscopic current depends only on the shuttle contribution (no tunnel current is present), so that $I \approx I_s$. Thus, the chance to achieve a not null conductance G_{QSM} uniquely depends on triggering the shuttle mechanism: specifically, the current is proportional to the mechanical frequency (formula (1.12a)). We highlighted in Paragraph 3 how an initially hard system transits towards the soft condition for large bias voltages. From the conductive point of view, the surpass of the voltage V_T corresponds to a *breakdown* of the system, since, over such value, the current interruption is no more guaranteed.

In the most-experienced *normal* and *diminished* attitudes analyzed in the previous Paragraph, $V_T \leq V_\eta$: follows that only QSMs in soft regime ($V > V_T$), can perform a saturative deactivation or establish an inefficient shuttle mechanism. Instead, in this Paragraph we limit our analysis to the hard regime ($V < V_T$), so that increasing bias voltages surely correspond to a larger energy pumping in the system. Then, we will focus on two distinct problems:

- perform continuative transitions between static/shuttle regimes (activation and deactivation);
- modulate the oscillation properties of a system in the NSH state.

These points are respectively related to concepts of *reactivability* and *modulability* of a QSM.

9.6.1 Reactivation index

Set two design voltage levels, V_{ON} and V_{OFF} : the first one to be selected with the aim to correctly perform an activation transient, whereas the second a deactivation one.
The *reactivability* of a QSM can be conceptually introduced as the tendency for a system to perform continuative transitions (both activation and deactivation) between static and shuttle regimes by alternatively apply two voltage levels V_{OFF} and $V_{ON} > V_{OFF}$.
However, in Paragraph 2 we demonstrated the activation ($V_{OFF} \to V_{ON}$) is a more problematic transient with respect to the deactivation ($V_{ON} \to V_{OFF}$). In particular, if one selects $V_{OFF} = 0$, this choice surely fulfills the deactivation requirement (2.21b). Consequently, in order to investigate reactivability, emphasis is given only on the activation process. Directly from (2.21a), follows that an activation attempt is successful when two conditions on V_{ON} are satisfied:

$$V_{ON} > V_{inf} \quad , \qquad V_{ON} > V_{act}(N_0) \tag{2.28a, b}$$

The first condition (2.28a) can be achieved by simply selecting, in a design stage, $V_{ON} \geq V_{inf}$. On the other hand, the second one (2.28b) is particularly subtle, since it depends on the initial number of electrons N_0 . In a succession of static/shuttle regimes, N_0 is a consequence of the details of the last deactivation transient. From a practical point of view, we widely discussed in Paragraph 5 that N_0 is an aleatory quantity: since there is no way to foresee the details for a deactivation transient, there is no way to guarantee the success of any consecutive activation attempt. Nonetheless, in this Paragraph we explain how to obtain some estimations on it.
For example, the deactivation process consequent to a shuttle regime characterized by a number of shuttled electrons per cycle N_{ON} leads to a number of residual electrons $N_0 \leq N_{ON}$. Also notice that, in the case of a QSM with normal or diminished attitudes, shuttle is surely efficient: this means that, by substituting $\eta = 1$ in definition (1.28), $N_{ON} = N^*(V_{ON})$. Using the same nomenclature of Paragraph 2, assume (2.28b) is accomplished for $N_0 \geq N_{act}$. Summarizing, one can say a system for which $N^* < N_{act}$ is never reactivable. Conversely, the more the ratio N^*/N_{act} is large, the higher is the probability of success of the i-th activation attempt.
In conclusion, one can introduce a *quantitative* definition for the reactivability as follows:

$$\mathrm{A} \triangleq \frac{N^*(V_{ON})}{N_{act}(V_{ON})} - 1 \tag{2.29}$$

The quantity A is called *reactivation index*. If the selection of the voltage V_{ON} leads to $\mathrm{A} < 0$, reactivation is not possible; conversely, if $\mathrm{A} > 0$ reactivation is possible, and the higher is a A the more successful reactivations are probable.

From definition (2.29) it is clear that A depends on the design choice of V_{ON}. However, some systems tend to be more "reactivable" than others: which is they are inclined to achieve positive values of A in correspondence to smaller choices of V_{ON}. For example, plots in Fig.2.18 highlight the different outcome of the same system performing a succession of activation/deactivation transients corresponding to a different choice of the external parameter. Remarkably, in the first case ($\zeta = 1$, Fig.2.18a) all the activation (green bands) and deactivation (red) transients are correctly performed, whereas in the second case ($\zeta = 0.1$, Fig.2.18b), only the first activation is successful, and the system remains in static regime after any of the consequent activation attempts (so that, clearly, no deactivation is performed also). These simulations show a larger damping ratio promotes higher values of A. Actually, this is a tendency frequently exhibited by QSMs, confirmed by a large series of numerical simulations (not reported here).

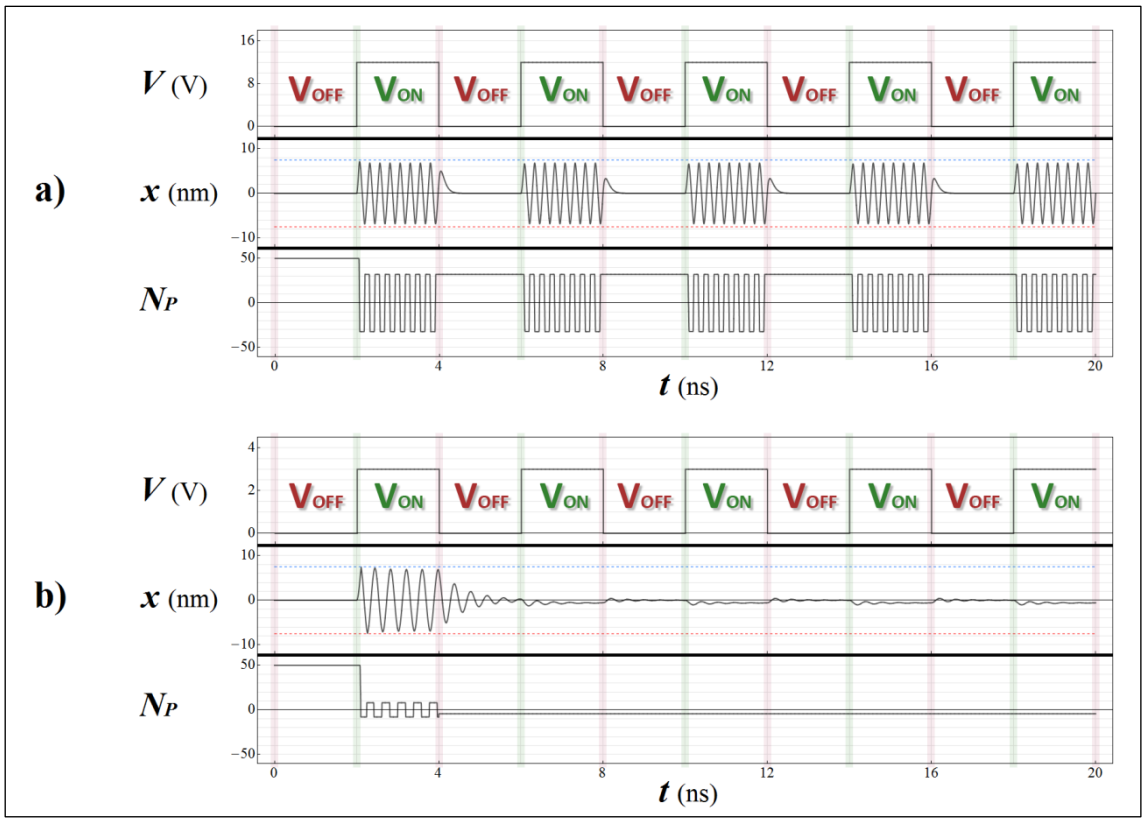

Figure 2.18 –*Two simulations show different outcomes of a series of activation/deactivation attempts for the reference system. Time histories of voltage* $V(t)$*, pillar position* $x(t)$ *and electrons* $N_P(t)$ *are present. Results obtained by integrating equations (2.12) with initial conditions:* $x(0) \equiv \dot{x}(0) = 0$, $N_P(0) = 50$. *In both simulations the voltage is alternatively set to* $V_{OFF} = 0$ *and a* V_{ON} *compatible with* NSH *state. Simulations differ for the damping ratio values: in (a)* $\zeta = 1$ *and in (b)* $\zeta = 0.1$.

One explanation could be that, when ζ is high, a larger voltage V is required to establish a shuttle regime: the term $N^*(V_{ON})$ in (2.29) being larger as well. This argument can be generalized by noticing a larger static deflection occurs in systems for which the electrostatic force is relatively large with respect to the elastic one. Thus, the more a QSM is characterized by a strong electromechanical coupling (Section 2.2.4), the more it is reactivable. In symbols, the general tendency $\mathrm{K} \gg 1 \implies \mathrm{A} \gg 1$ holds. In conclusion, while in Paragraph 5 we *a priori* assumed the *convenient deactivation hypothesis* $N_0 \geq N_{hyst}$ held, here we demonstrated that (for $V_{ON} > V_{inf}$), such hypothesis is far more viable in the case of large K and/or ζ .

9.6.2 Modulation index

In Section 9.2.2 we briefly discussed how the applied voltage V, by the means of an energetic balance of the kind of (2.19), is able to influence the oscillations properties of a pillar performing a shuttle regime. Since, from Section 9.5, hard QSMs in normal and diminished attitudes cannot perform the ISH state, follows the only admitted shuttle regimes are NSH and CSH .
In real systems, collisions between the pillar and the fixed electrodes are inopportune †, and

† There are two main reasons for this. From a theoretical modeling point of view, collisions lead to a more complex dynamical behavior, with huge dependence on initial conditions and weaker stability properties. On the practical perspective, achieving continuative high-frequency collisions may largely prejudice the device integrity. It is difficult to estimate the actual occurrence of the pillar-electrodes collisions, however, there is no clear opinion on how much the system durability is actually prejudiced.

establishing the NSH state is the preferred possibility. In this context, *modulability* of a QSM can be conceptually introduced as the capacity for the bias voltage to vary its shuttle regime oscillation properties (i.e. the amplitude and/or frequency) by modifying the bias voltage.
The modulability can be therefore tested comparing the shuttle performances of a system excited by NSH-compatible voltages $V \in [V_{inf}, V_{sup})$, corresponding to amplitudes $A \in [A_{inf}, A_{sup})$ and (forced) frequencies $f_s \in [f_{inf}, f_{sup})$. In particular, $A_{inf} = A_t$ and $A_{sup} = d - r$.

In Fig.2.19, modulability in the same system, characterized by different choice of the external parameter, is highlighted. One can notice amplitude slightly varies in both cases: it is more interesting (and it is also related to one of the design requirements discussed in Section 7.2), analyze the modulation in frequency. In the first case ($\zeta = 1$, Fig.2.19a), the frequency corresponding to the case $V = V_{sup} - dV$ is approximately twice with respect to the minimal one, obtained when $V = V_{inf}$. In the second plot ($\zeta = 0.1$, Fig.2.19b), this difference is rather small. One can quantitatively relate the modulability of a QSM to the formula:

$$\mathrm{M} \triangleq 1 - \frac{V_{inf}}{V_{sup}} \tag{2.30}$$

in which quantity M is the *modulation index*. In a system for which $\mathrm{M} \approx 1$ the frequency can be largely modulated, whereas this possibility is rather poor when $\mathrm{M} \approx 0$.

The general tendency, confirmed by the simulations in Fig.2.19 as well (and by other ones not reported here), is that systems characterized by a large mechanical damping ζ are more modulable than others. This is because, since the mechanically dissipated energy $\Delta\mathcal{E}_d$ is larger, higher voltages are required to balance it with the term $\Delta\mathcal{E}_{es}(V)$ and establish stable orbits.

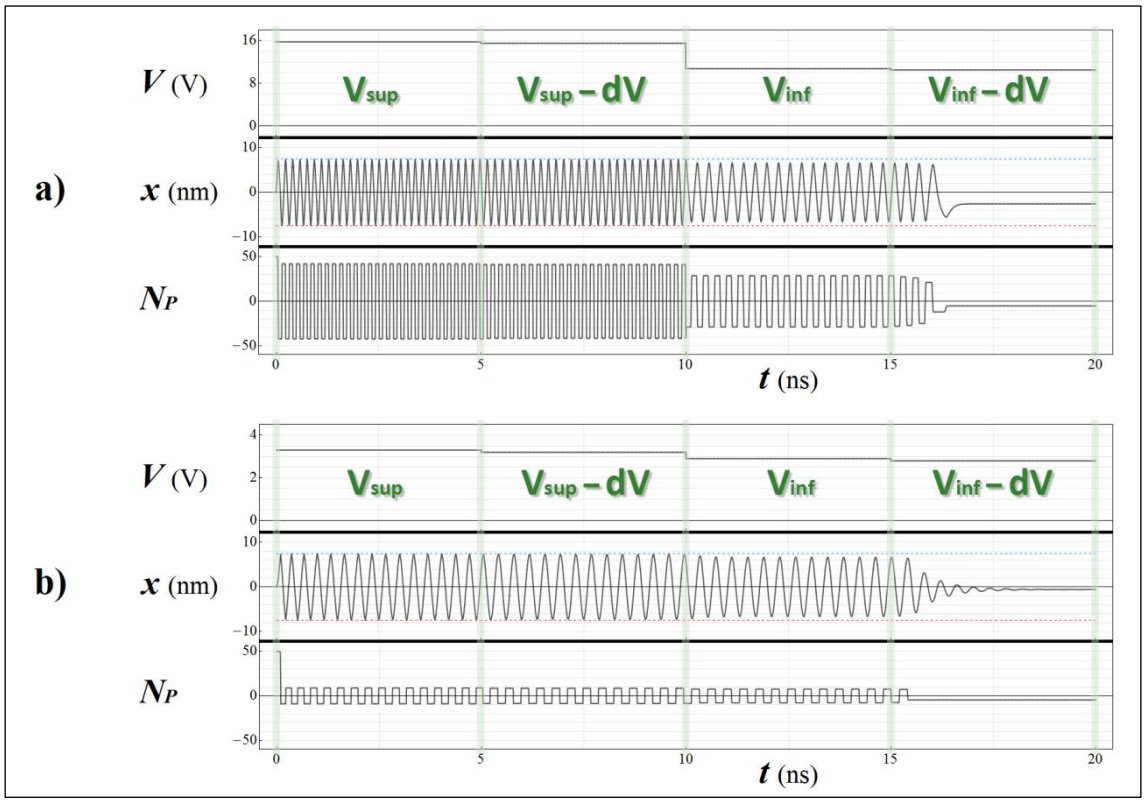

Figure 2.19 –*Two simulations show different modulation features exhibited by the reference system. Time histories, equations used and initial conditions as in Fig.2.18. Simulations differ for the damping ratio values: in (a) $\zeta = 1$ and in (b) $\zeta = 0.1$.*

9.7 Characteristic chart and working points

The analyses performed in this Chapter encourage for a description of a QSM based on the control parameter $\mathrm{CP} = V$ as a function of the external one $\mathrm{EP} = \zeta$. Specifically, every QSM characterized by a certain set of internal parameters IP can be associated to a pair of *characteristic curves* on a V-ζ plane: $V_{inf}(\zeta)$ and $V_{sup}(\zeta)$. These curves separate the plane in three parts:

- $V(\zeta) < V_{inf}(\zeta)$: the STD region ;
- $V_{inf}(\zeta) < V(\zeta) < V_{sup}(\zeta)$: NSH region ;
- $V(\zeta) > V_{sup}(\zeta)$: CSH region .

Any couple $\{V, \zeta\}$ locates a point on the V-ζ plane which belongs to one of these regions. Considering the damping ratio ζ as an environmental quantity, one can use the characteristic curves $V_{inf}(\zeta)$ and $V_{sup}(\zeta)$ as a *characteristic chart* to select the free parameter, the bias voltage V, by using a proper criterion. Since the NSH state represents the optimal "working condition" for a QSM, if one choose V to match the NSH region, the couple $\{V, \zeta\}$ individuates a *working point*.

Consider a working point $\mathrm{P} = \{V_P, \zeta_P\}$. Referring to the scheme Fig.2.20a, introduce:

$$\mathrm{R}(V_P, \zeta_P) \triangleq \left(\frac{V_{P,sup} - V_{P,inf}}{V_{P,sup}}\right)\left(\frac{\zeta_{P,sup} - \zeta_{P,inf}}{\zeta_{P,sup}}\right) \tag{2.31}$$

The quantity $\mathrm{R} = \mathrm{R(P)}$ is the *robustness index* associated to a working point P: in fact, it returns the extension of the NSH region around the point P. A system operating in correspondence of a working point for which $\mathrm{R} \approx 1$ is less refractory to (environmental or control) disturbances on the design values (V_P and ζ_P), with respect to one for which $\mathrm{R} \ll 1$. Characteristic charts in Fig.2.20b,c,d (produced by arranging the results of a set of numerical experiments) show the characteristic curves $V_{inf}(\zeta)$ and $V_{sup}(\zeta)$ for three QSM associated to as much different choices of the IPs. A QSM is correctly designed if such IPs produce characteristic curves that maximize the value $\mathrm{R}(P)$ for the expected value of ζ_P : the proper voltage V_P to be consequently selected.

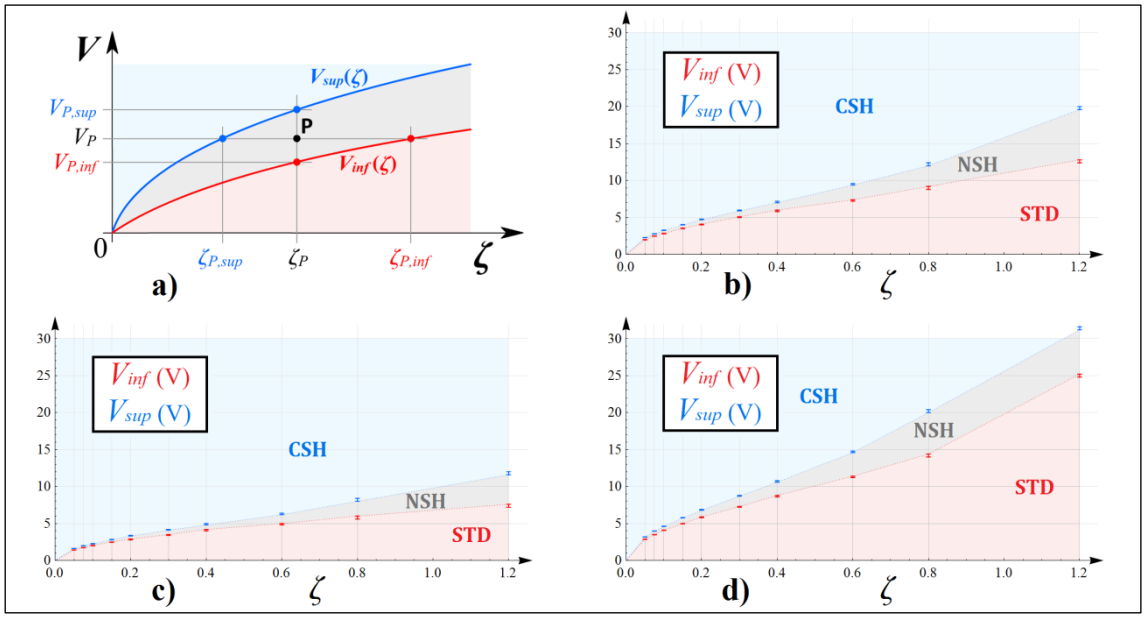

Figure 2.20 – *(a) Qualitative characteristic chart with a working point* P *highlighted. (b-d) Characteristic curves obtained from numerical simulations based on equations (2.12), with reference values: (b) for all parameters, (c) except for* $m = m_{ref}/2$ *and* $k = k_{ref}/2$ *, (d) except for* $m = 2m_{ref}$ *and* $k = 2k_{ref}$.

Chapter 10

Functional analysis of a NanoMechanical Transistor

In this Chapter the possibility of reproducing some features of a conventional transistor by using a multiple-QSM is investigated. All numerical results refer to the equations set (2.14).
By assuming the mechanical coupling among the different pillars is relatively small with respect to the oscillation energy, one can consider, in a first approximation, the dynamics of each resonator is functionally described by using the arguments presented in Chapter 9. Also, we assume each QSM accomplishes the design requirements discussed in Chapter 7, in particular, those listed in Tab.2.1. We make use of these hypothesis in order to delineate a set of control strategies required to make the whole NMT work.
Namely, we consider both the voltage-driven switch and the current amplifier functionalities, distinctly discussed in Paragraph 1 and Paragraph 2, respectively.

10.1 Switch operation

10.1.1 States and commutations

Consider a NMT composed by only two QSMs. This is the simplest architecture able of replicating a voltage-driven switch functionality. The first module is the *drive* (subscript 0) and the second is the only slave (subscript 1). Since N the number of slaves, in this case $N = 1$.
The core working principle for this device has been briefly described in Chapter 6: a bias voltage applied to the drive $V_{dr} = V_0$ could influence the macroscopic current flowing through the slave $I_{sl} = \overline{I_1}$. In a switch, two design voltage levels for V_0 have to be selected, corresponding to as much conductive behaviors for the device †:

$$V_0 = V_{OFF} \quad \rightarrow \quad \overline{I_1} = 0 \quad \forall\, V_1 \geq 0 \tag{2.32a}$$

$$V_0 = V_{ON} \quad \rightarrow \quad \overline{I_1} > 0 \quad \forall\, V_1 > 0 \tag{2.32b}$$

Relation (2.32a) refers to the *OFF state*, instead (2.32b) represents the *ON state*.
Name the transitions between the interrupting and conducting states as:

- *switch-ON* commutation: OFF state → ON state
- *switch-OFF* commutation: ON state → OFF state

In order to correctly reproduce the voltage-driven switch functionality, a NMT has to perform two main tasks: i) correctly reproduce OFF and ON states, ii) be able to perform an indefinite succession of consecutive switch-ON and switch-OFF commutations.

† Notice the current $\overline{I_1}$ is symmetrical with respect to the voltage V_1 (no diode-effect); thus, in the followings, only positive values for voltages and currents are considered.

10.1.2 Control strategies

The experience gained by running a large number of numerical simulations, led to synthesize a set of five thumb rules which allows to realize the voltage-driven switch functionality:

I) *Resonant matching:* $V_{ON} \approx V_R > V_{inf,0}$

II) *Correctly perform the ON state:* $A_1|_{V_0=V_{ON}} \geq A_{t,1}$

III) *Correctly perform the OFF state:* $A_1|_{V_0=V_{OFF}} < A_{t,1}$

IV) *Avoid the switch-ON failure:* $V_{OFF} > V_{inf,0}$

V) *Avoid switch-OFF failure:* $V_1 < V_{lock}$

Since accomplish conditions (I)-(V) is required in order to correctly mimic the functionalities of a switch, they can be considered as the *control strategies* to be paired up with the design requirements discussed in Chapter 7. The physical meaning of (I)-(V) is commented ahead.

First of all, since $f_0 = f_0(V_0)$, one can introduce the resonant voltage V_R as the particular value of V_0 for which the slave reaches resonance, that is $f_0(V_R) \triangleq f_{R,1}$. As a first approximation, one can calculate $f_{R,1}$ in absence of the coupling with the drive pillar:

$$f_{R,1} \approx \frac{\sqrt{1-2\zeta_1^{\,2}}\sqrt{\frac{k_1}{m_1}}}{2\pi} \tag{2.33}$$

Then, condition (I) involves the possibility to match such resonance condition. In order to do this, two requirements have to be fulfilled: one has to select a proper voltage $V_{ON} \approx V_R$ compatible with a shuttle regime for the drive, that is $V_{ON} > V_{inf,0}$. To be simultaneously kept, these conditions require special combinations of parameters m_0 , m_1 , k_0 , k_1 , ζ_0 , ζ_1 and $k_{0,1}$. Notice that, in the case of identical pillars or same electrodes distance, point (I) does not easily hold.

Condition (II) is referred to correctly perform the conducting ON state (2.32a). In this case, $V_0 = V_{ON}$, and the slave pillar, in order to trigger a shuttle regime, has to reach the tunneling region $\mathcal{T}_1 = \mathcal{O}_1 \setminus [-A_{t,1}, A_{t,1}]$. To provide the minimal amplitude A_1, values for m_1 , k_1 , $k_{0,1}$ and ζ_1 have to be selected appropriately.

On the other hand, condition (III) refers to the interrupting OFF state (2.32b). If $V_0 = V_{OFF}$, it is required the slave pillar doesn't reach the tunneling region, so that the current passage is inhibited. Again, m_1 , k_1 , $k_{0,1}$ and ζ_1 have to be selected properly to fulfill this requirement.

In order to correctly reproduce both the OFF and the ON states (conditions (II) and (III)), a certain modulability in frequency for the drive pillar is required (see Section 9.6.2), so that frequencies $f_0(V_{OFF})$ and $f_0(V_{ON})$ are sufficiently far to fulfill/dismiss the resonant matching between the drive and the slave resonators. In general, there are three possibilities to accomplish this, depending on how the values for V_{OFF} and V_{ON} are selected:

- *sub-resonant* OFF state: $V_{inf,0} < V_{OFF} < V_{ON} \approx V_R$;
- *super-resonant* OFF state: $V_{inf,0} < V_{ON} \approx V_R < V_{OFF}$;
- *static* OFF state: $0 \leq V_{OFF} < V_{inf,0} < V_{ON} \approx V_R$.

The latter choice seems to be the best from the point of view of power consumptions. However, this option leads to severe difficulties in performing continuative transitions between states.

In fact, in this condition, after a switch-OFF commutation is completed, the subsequent switch-ON is not guaranteed (*switch-ON failure*). This issue is completely analogous to the reactivation problem investigated in Section 9.6.1, since it depends on the residual charges on the drive at the end of the latter switch-OFF commutation. This suggests the better option is that of a sub-resonant OFF condition: in this case, in fact, the drive pillar remains in shuttle regime even when the current on the slave is inhibited, so that the repeatability, from the point of view of switch-ON transients, is guaranteed (condition (IV)).

Finally, condition (V) is required in order to guarantee the feasibility of switch-OFF commutations. This problem has no analogies with the analysis of a single QSM. The point is that, in a multiple-QSM device, it is required the slave(s) self-excitation regime does not rely on electrostatic forces (as it is for the drive), but rather on the resonant response elastically excited by the drive. Otherwise, a *switch-OFF failure* condition occurs, where the slave(s) remains in the shuttle regime also when the drive voltage is lowered to $V_0 = V_{OFF}$. In the following parts, we concisely refer to this inopportune condition as *locking*. In order to avoid locking, an upper limit has to be considered for the slave voltage, $V_1 < V_{lock}$ which identifies condition (V).
The value V_{lock} is indeed defined as the minimum voltage V_1 for which locking occurs, i.e. the electrostatic forces on the slave are just sufficient to sustain its shuttle regime, independently from the drive motion. Notice that, except for severe locking conditions ($V_1 \gg V_{lock}$), the switch-OFF is often possible by using "emergency" maneuvers, for example, by imposing voltages $V_0 < V_{OFF}$, or even $V_0 = 0$.

In conclusion, an overview of the possible working regimes a single-slave NMT can establish is qualitatively sketched in Fig.2.21. In particular, the chance of correctly perform ON and OFF states or undergo to switch-ON or switch-OFF failures exclusively depends on accomplishing or dismissing conditions (I)-(V), respectively.

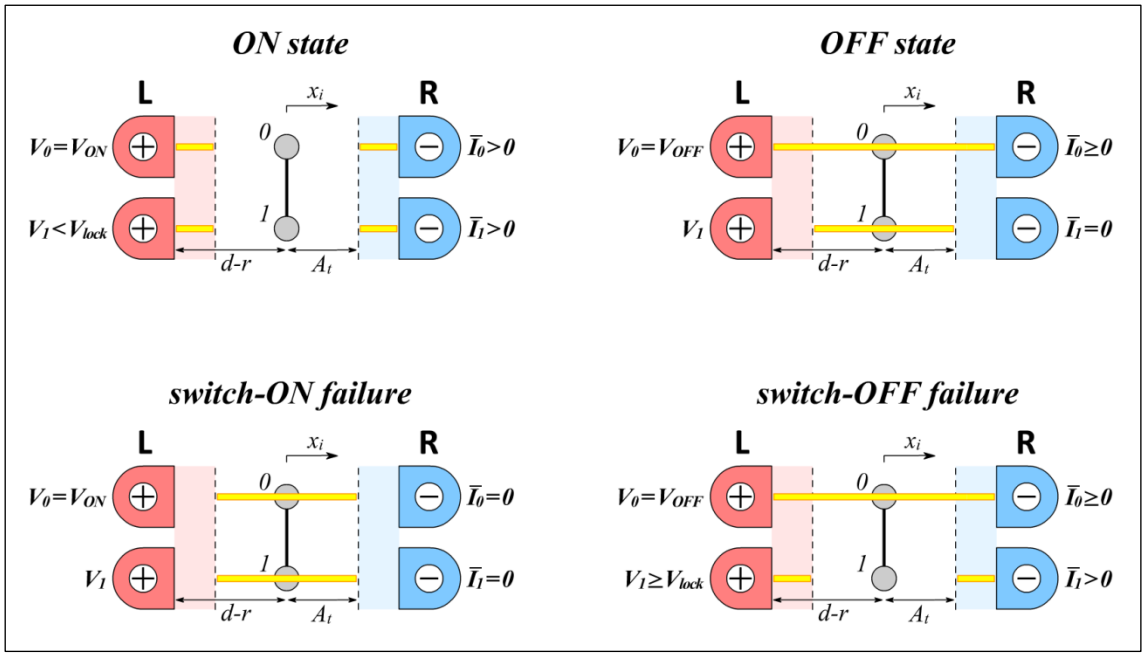

Figure 2.21 – *Schematic representation of possible working conditions for a single-slave NMT. The yellow line describes the locus of admitted turning points in the oscillation of each pillar.*

10.1.3 Role of damping in collisions: durability

A further question is related to the possible occurrence of inopportune collisions, both on the drive and/or the slave resonators, when correctly performing ON or OFF states. For the drive, this possibility is related to the surpass of a voltage $V_{sup,0}$. For the slave it is instead related to a more complex dynamics occurring when V_1 is close to V_{lock} . Since collisions may reduce the *durability* of the device, they would be preferably avoided at the design stage. This introduces a somehow optional condition, in addition to the (I)-(V) previously discussed:

VI) *Prevent pillars collisions (improve durability):* $\begin{cases} \text{(a) for the drive} & V_0 < V_{sup,0} \\ \text{(b) for the slave} & V_1 \ll V_{lock} \end{cases}$

Limit our analysis to the drive (condition (VIa)), and to the case of a sub-resonant OFF state ($V_{inf,0} < V_{OFF} < V_{ON} \approx V_R$) . Since $V_{OFF} < V_{ON}$, it is always possible to select $V_{OFF} < V_{sup,0}$, so that collisions are limited to the only ON state, and (VIa) specifies into $V_{ON} < V_{sup,0}$. The feasibility of the latter inequality is related to the choice of the damping ratio ζ_0. In fact, consequently to the analysis performed in Section 9.6.2, a QSM characterized by $\zeta_0 \approx 1$ generally manifests a better modulability in frequency, since it is characterized by a larger interval $V_{sup,0} - V_{inf,0}$. Conversely, in the case $\zeta_0 \ll 1$, then $V_{inf,0} \approx V_{sup,0}$, and, to achieve a sufficient modulability in frequency †, one has to select $V_{ON} > V_{sup,0}$: the latter inequality dismissing condition (VIa). Reassuming, in general, the achievement of condition (VIa) is possible only for relatively large values of the damping ratio for the drive.

On the other hand, a low damping ratio ζ_0 is preferred for the slave. In fact, conditions (II) and (III) imply a sufficiently sharp resonant response, naturally associated to low dissipations.
The previous considerations lead to consider two different design options:

- *Different-damping system*: $\zeta_1 \ll \zeta_0 \approx 1$ (condition (VIa) is satisfied) ;
- *Equal-damping system*: $\zeta_0 = \zeta_1 \ll 1$ (condition (VIa) is not satisfied) .

Notice how the first option improves the durability of the whole NMT, but it is technologically complex to achieve. The converse considerations hold for the second option.

10.1.4 Numerical experiments

In order to verify the switch functionality for a NMT with a single ($N = 1$) slave module, in the next pages we show the results of a series of numerical experiments carried out by fulfilling conditions (I)-(V). In every simulation, a succession of switch-ON and switch-OFF commutations is attempted by switching the drive voltage V_0 between two design values V_{ON} and V_{OFF} : the desired functionality is achieved if a series of consecutive ON and OFF states, respectively consenting and inhibiting the current passage on the slave I_1, are alternatively performed.

In Fig.2.22a and Fig.2.23a the whole succession of switch-ON and switch-OFF transients is successfully achieved, correctly establishing ON and OFF states. In Fig.2.22b and Fig.2.23b switch-ON failure occurs. Last, Fig.2.22c and Fig.2.23c show a switch-OFF failure (locking).
Plots in Fig.2.22a,b,c refer to a *different-damping* system, whereas those in Fig.2.23a,b,c are in the case of an *equal-damping*. Remarkably, in Fig.2.22a,b,c, differently from Fig.2.23a,b,c, the ON state is characterized by continuative collisions of the drive pillar with the fixed electrodes, because the different-damping condition is not compatible with condition (VIa).

† Since, from conditions (II) and (III), the ON state forced frequency has to be sufficiently far from that in the OFF state.

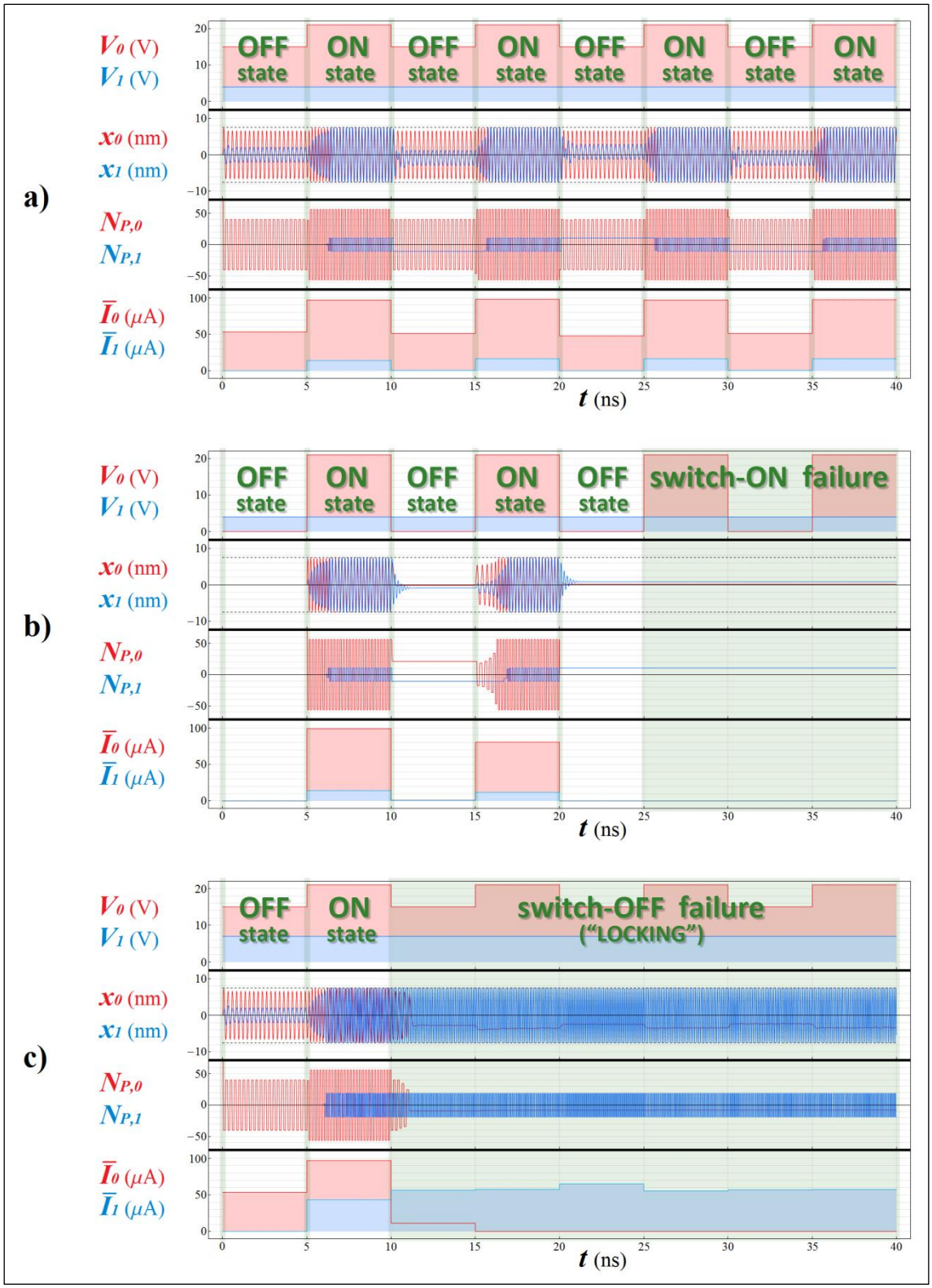

Figure 2.22 – *a single-slave ($N = 1$), different-damping ($\zeta_0 = 0.8$, $\zeta_1 = 0.1$) NMT, undergoes 4 switch-ON attempts. Time histories of three different simulations (a,b,c) based on equations (2.14) are reported: bias voltages (V_0, V_1), pillar positions (x_0, x_1), pillar electrons ($N_{P,0}$, $N_{P,1}$), macroscopic currents ($\bar{I}_0$, $\bar{I}_1$). Simulations only differ for voltage applications: (a) $V_{OFF} = 15\ V$, $V_{ON} = 21\ V$, $V_1 = 4\ V$; (b) $V_{OFF} = 0\ V$, $V_{ON} = 21\ V$, $V_1 = 4\ V$; (c) $V_{OFF} = 15\ V$, $V_{ON} = 21\ V$, $V_1 = 7\ V$, with $V_{lock} \approx 5\ V$. For both the drive and slave modules the reference values of internal parameters (Tab.2.3), except for $m_0 = 2 \times 10^{-21}\ kg$ (gold cap), $m_1 = m_0/4$ (silver cap), $k_0 = k_1 = 0.5\ N/m$, $k_{0,1} = k_0/5$.*

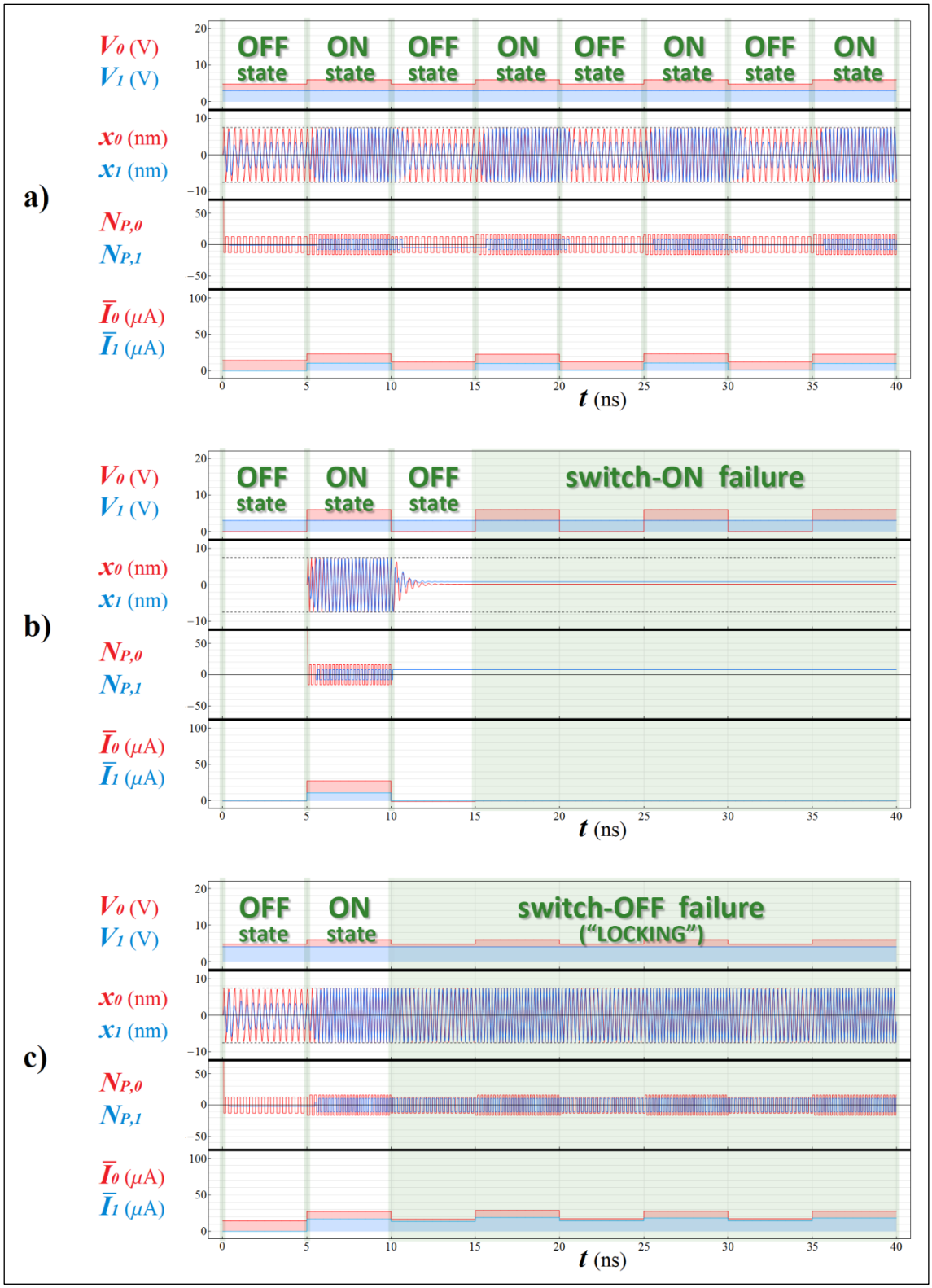

Figure 2.23 – *a single-slave ($N = 1$), equal-damping ($\zeta_0 \equiv \zeta_1 = 0.1$) NMT, undergoes 4 switch-ON attempts. Time histories of three different simulations (a,b,c) based on equations (2.14) are reported for the same quantities as in Fig.2.22. Simulations only differ for voltage applications: (a) $V_{OFF} = 5\,V$, $V_{ON} = 6\,V$, $V_1 = 3\,V$; (b) $V_{OFF} = 0\,V$, $V_{ON} = 6\,V$, $V_1 = 3\,V$; (c) $V_{OFF} = 5\,V$, $V_{ON} = 6\,V$, $V_1 = 4\,V$, with $V_{lock} \approx 3.25\,V$. Simulations share the same internal parameters of Fig.2.22 except $k_1 = 0.25\,N/m$.*

10.2 Amplifier operation

10.2.1 Single slave module ($N = 1$)

Consider the same NMT investigated for the switching operation, in which a single slave module is present ($N = 1$). Since we are interested in the current amplification, consider $\overline{I_0}$ and $\overline{I_1}$ as the input and output signals, respectively. From (2.1c), the current gain can be introduced as:

$$\alpha \triangleq \frac{\overline{I_1}}{\overline{I_0}} \tag{2.34}$$

However, $\overline{I_1}/\overline{I_0} \approx V_1/V_0$ (see Section 11.1.1 for details). Therefore, the gain can be estimated as $\alpha \approx V_1/V_0$. Since, from (V), $V_1 < V_{lock}$, the incipient locking condition maximizes the gain:

$$\alpha_{max} \triangleq \max\left(\frac{\overline{I_1}}{\overline{I_0}}\right) \approx \frac{V_{lock}}{V_{inf,0}} \tag{2.35a}$$

In conclusion, for $N = 1$, the chance of an effective current amplification relies on condition:

$$\alpha_{max} > 1 \quad \Leftrightarrow \quad V_{lock} > V_{inf,0} \tag{2.35b}$$

Notice that devices characterized a large electromechanical coupling for the drive K_0 manifest a relatively smaller $V_{inf,0}$, whereas those with smaller K_1 a relatively larger V_{lock}. Follows that, in general, condition (2.35b) appears to be more easily satisfied for larger $\mathrm{K}_0/\mathrm{K}_1$ ratios.
However, a large number of numerical experiments never exhibited a larger-than-unity gain, even exploring several configurations where drive and slave were characterized by far-different internal parameters. For example, in the simulations in Fig.2.22 (different-damping system) we obtained $\alpha = \overline{I_1}/\overline{I_0} \approx 1/6$, whereas in Fig.2.23 (equal-damping) $\alpha = \overline{I_1}/\overline{I_0} \approx 1/2$.
In order to improve the current amplification performances of a NMT, the natural strategy seems to be, as suggested in Blick's patent [77], adding more slave QSMs; thus, increase N .

10.2.2 Set of slave modules ($N > 1$)

Consider a NMT consisting of a single drive and $N > 1$ identical slave modules. From (2.1a,b):

$$V_{dr} \triangleq V_0 \ , \quad I_{dr} \triangleq \overline{I_0} \ , \quad V_{sl} \triangleq V_1 \equiv V_2 \equiv \cdots \equiv V_N \ , \quad I_{sl} \triangleq \overline{I_1} + \overline{I_2} + \cdots + \overline{I_N} \tag{2.36}$$

Analogous symbols are used for all the parameters, thus replacing subscripts 0 and 1 (from the case $N = 1$), with DR and SL, respectively. All considerations made for $N = 1$ can be generalized to the case $N > 1$: in particular, control strategies (I)-(V) and the optional requirement (VI) still apply, and a direct generalization of the correctly performed and failure working conditions portrayed in Fig.2.21 is possible. Nonetheless, two additionally possibilities exist when $N > 1$:

- consequently to a switch-ON commutation, only *some* of the slave pillars establish the shuttle regime, whereas the others remain in static regime (*partial switch-ON*);
- after to a switch-OFF, only some slave pillars reach the static regime, the others continuing to perform the shuttle regime (*partial switch-OFF failure*, that is a "partial locking").

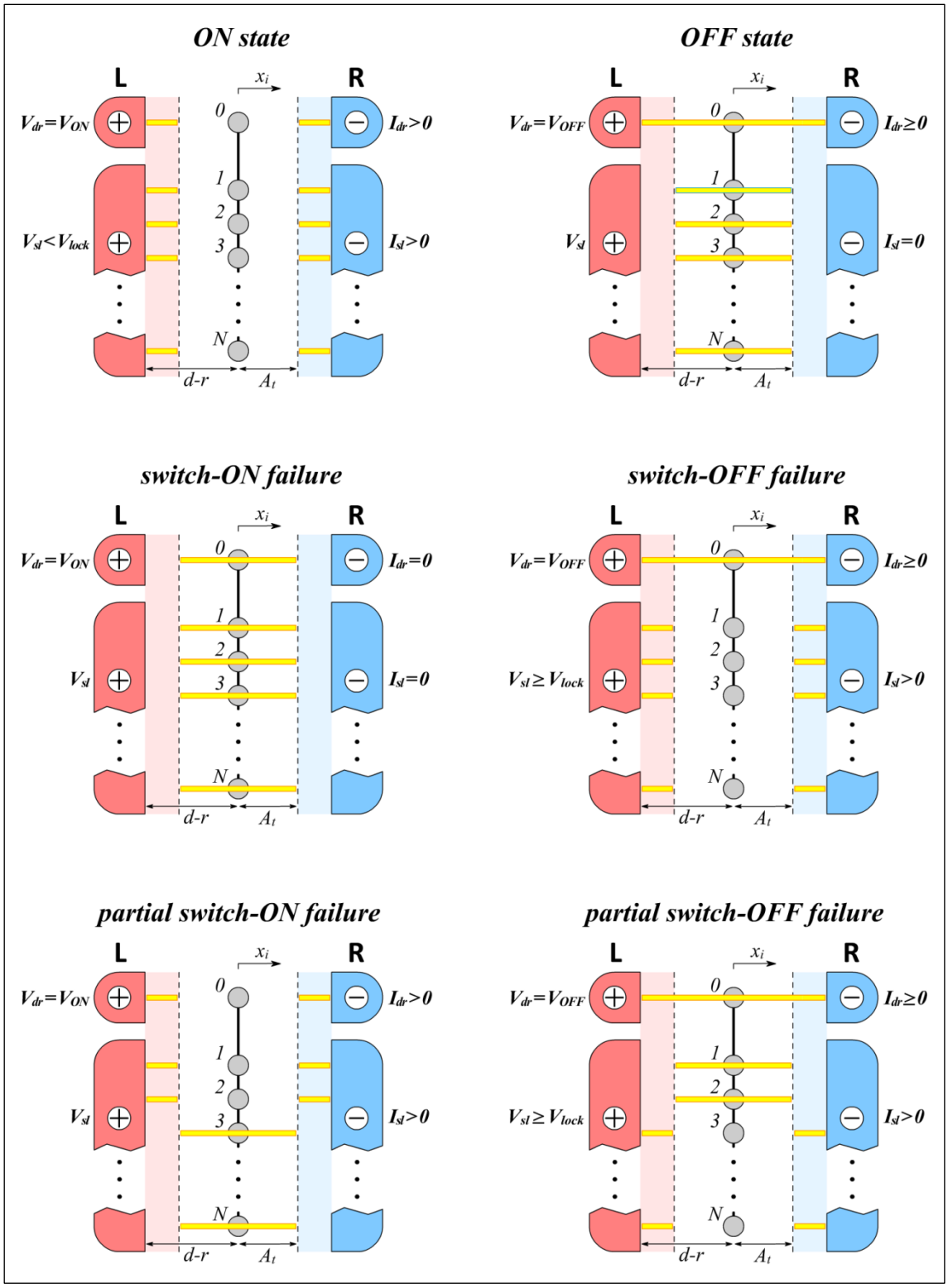

Figure 2.24 – *Schematic representation of the possible working conditions for a multiple-slave NMT ($N > 1$) as a direct generalization single-slave case ($N = 1$, Fig.2.21). The yellow line describes the locus of admitted turning points in the oscillation of each pillar.*

Notice that (differently from the partial switch-OFF) the partial switch-ON is not a failure condition, since it could be used to modulate the current amplification (the gain). In fact, depending on the effective number of slave pillars which reach the tunneling region and achieve the shuttle mechanism, the overall current flowing through the slave set I_{sl} can be regulated.

10.2.3 Design requirements to produce actual amplification

The presence of a large number of slave QSMs does not automatically benefit the current amplification performances. In order to make presence of a multitude of slave pillars effective to produce a larger-than-unity current gain, a few additional conditions, not related with the device control, but with its preliminary design, has to be introduced.

First, the strategy of controlling the slaves vibration through resonant excitation tuned by the drive is still the key control strategy. Consequently, the first additional requirement is:

VII) *Similar slave pillars geometry:* $f_0(V_R) \approx f_{R,1} = f_{R,2} = \cdots = f_{R,N} \triangleq f_{R,sl}$

Notice as this condition is consistent with the assumption of using identical slave pillars. If condition (VII) holds, one can assume $\overline{I_1} \approx \overline{I_2} \approx \cdots \approx \overline{I_N}$ and relations (2.35a,b) generalize into:

$$\alpha_{max} \triangleq \max\left(\frac{I_{sl}}{I_{dr}}\right) \approx N\frac{V_{lock}}{V_{inf,dr}} \tag{2.37a}$$

$$\alpha_{max} > 1 \quad \Leftrightarrow \quad NV_{lock} > V_{inf,dr} \tag{2.37b}$$

Accomplish inequality (2.37b) is less trivial than it appears. In fact, while $V_{inf,dr}$ is constant by definition, several numerical simulations show V_{lock} varies with N, so that adding more slave modules *does not produce* a better amplification effect. Since the dependence $V_{lock} = V_{lock}(N)$ is an intrinsic characteristic of a system, (2.37b) can be satisfied only by systems for which:

VIII) *Current amplification increases with N*: $V_{lock}(N) > V_{lock}(1)/N$

The upper bound for the current amplification is obtained in the hypothesis $V_{lock}(N) \approx const$: in this case directly follows, from (2.37a), $\alpha_{max} \propto N$ (since $V_{inf,dr}$ is constant by definition).
To conclude, notice that, generalizing again from the case $N = 1$ to $N > 1$, the ratio $\mathrm{K}_{dr}/\mathrm{K}_{sl}$ possibly plays a role in controlling the ratio $V_{lock}/V_{inf,dr}$ and, therefore, the value of α_{max} .

10.2.4 Numerical experiments

Simulations in Fig.2.25 and Fig.2.26 exemplify the dynamic response in the case of $N > 1$ slave modules, in the different and equal-damping case, respectively †.
In both cases, the system undergoes some switch-ON and switch-ON transients: the ON state is performed by using a slave voltage $V_1 \lesssim V_{lock}$, in order to maximize the gain and compatibly guarantee repeatability (in particular, avoid the switch-OFF failure). These simulations show a phenomenology analogous to those already discussed in Paragraph 1 about the switch operation.
During the ON states, the advantage of having $N > 1$ in the current gain is neatly visible by comparing such results with those in Fig.2.22a and Fig.2.23a. In the different-damping case, the gain increases of about 50% by passing from 1 (Fig.2.22a) to 4 slaves (Fig.2.25). In the equal-damping case, the gain doubles by adding only one slave module (Fig.2.23a, Fig.2.26). Several numerical simulations show the effect of increasing N on the current gain is usually relevant in the equal-damping case. In such systems, a larger-than-unity gain can be reached, as in Fig.2.21.

† Generalizing definitions given in Section 10.1.3 to the case $N > 1$ and fulfilling requirement (VII), we consider all the slave set characterized by the same damping ratio: this value is the same (equal-damping) or different (different-damping) of the drive.

‡ Although minimal parameters adjustments are required to keep conditions (I)-(VIII) when the number of slaves N is increased.

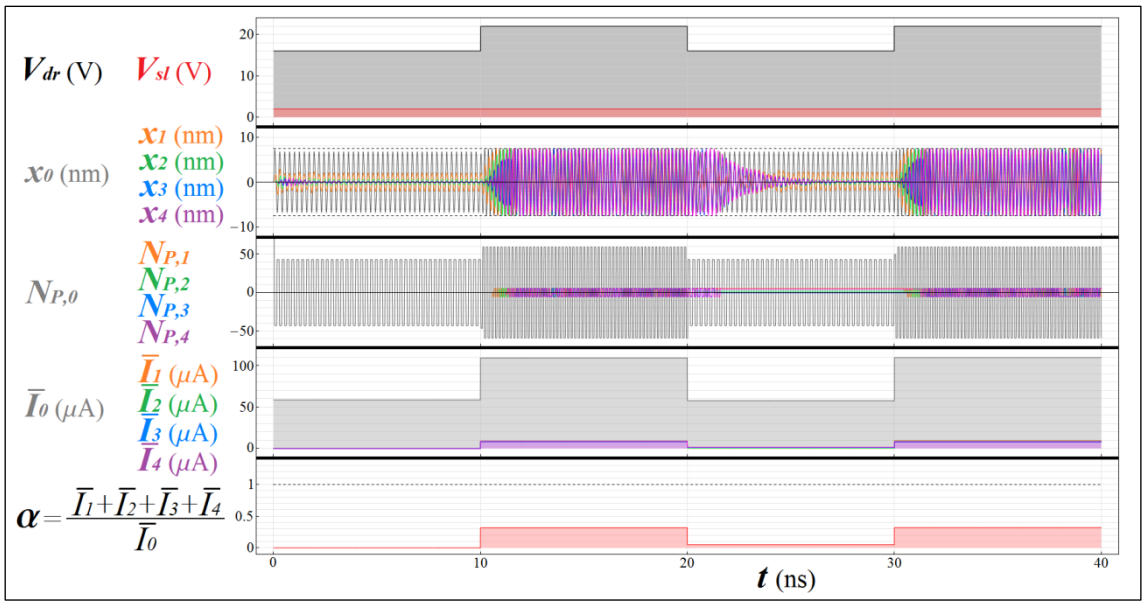

Figure 2.25 – *a multiple-slave ($N = 4$), different-damping ($\zeta_{dr} = 0.8$, $\zeta_{sl} = 0.02$) NMT correctly performs OFF and ON states. Time histories for: bias voltages (V_{dr}, V_{sl}), pillar positions (x_0, x_1, x_2, x_3, x_4), pillar electrons ($N_{P,0}$, $N_{P,1}$, $N_{P,2}$, $N_{P,3}$, $N_{P,4}$), macroscopic currents ($\bar{I}_0$, $\bar{I}_1$, $\bar{I}_2$, $\bar{I}_3$, $\bar{I}_4$), and current gain $\alpha = (\bar{I}_1 + \bar{I}_2 + \bar{I}_3 + \bar{I}_4)/\bar{I}_0$ are shown. Internal parameters as in Fig.2.22. By selecting a value for V_{sl} near to V_{lock}, current amplification is maximized, but the gain still doesn't reach the unity ($\alpha \approx 0.3$).*

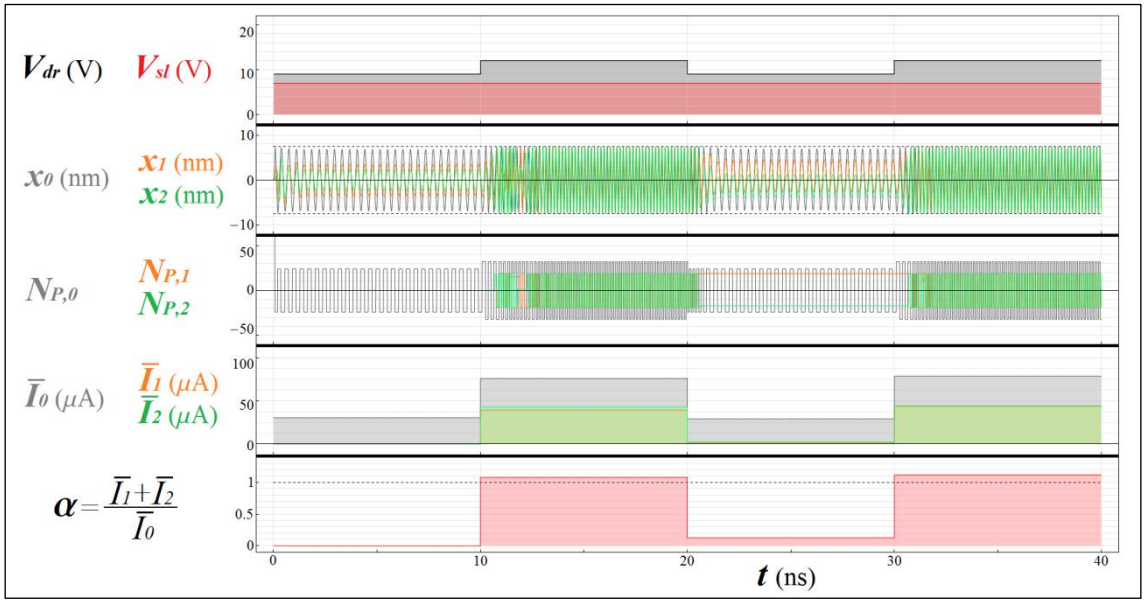

Figure 2.26 – *a multiple-slaves ($N = 2$), equal damping ($\zeta_{dr} \equiv \zeta_{sl} = 0.1$) NMT correctly performs OFF and ON states. Time histories for: bias voltages (V_{dr}, V_{sl}), pillar positions (x_0, x_1, x_2), pillar charges ($N_{P,0}$, $N_{P,1}$, $N_{P,2}$), average currents ($\bar{I}_0$, $\bar{I}_1$, $\bar{I}_2$), and current gain $\alpha = (\bar{I}_1 + \bar{I}_2)/\bar{I}_0$ are shown. Internal parameters as in Fig.2.25, except for $m_1 = m_0/8$ and $k_1 = k_0/4$. By selecting a value for V_{sl} very near to V_{lock} , current amplification is maximized, and a slightly larger-than-unity gain is achieved ($\alpha \approx 1.1$).*

Although having a large N can play a crucial role in enhancing the amplifier functionality, large gain values $\alpha \gg 1$ appear to be unfeasible. A first reason for this is that the selection of the internal parameters to accomplish conditions (I)-(VIII) is far less trivial than in the case $N = 1$. Actually, the more subtle reason is that it is never possible to perfectly fulfill the requirement (VIII). This will be investigated in the following Chapter by using simple energetic arguments.

Chapter 11

Electric performance of a NanoMechanical Transistor

11.1 Switch functionality with respect to conventional devices

This Paragraph is devoted to investigate the electric characteristics of a NMT, focusing on its voltage-driven switching performances, thus, we consider a single-slave device ($N = 1$).
In order to obtain a first-order evaluation, we compare its black-box properties with those of an *ideal switch*. In electronics, an ideal switch is characterized by: i) no current limit during the ON state, ii) no voltage limit during the OFF state, iii) zero rise and fall time between commutation transients, iv) absence of "bouncing" during commutations. In the following sub-Paragraphs we analyze these points one by one. At the end of the Paragraph, the external characterization of the NMT is completed by drawing some characteristic I-V curves.

11.1.1 ON state current limit

In hard shuttle, the tunnel current is negligible. Conversely, in the soft case both the shuttle and tunnel contribution to current can be considerable; in particular, a not null current passes independently from the vibrational state of the pillar. Consequently to this, in Chapter 7, the hard nature of shuttle was set as one of the design requirements for each QSM composing a NMT.
This choice enables for a simple estimation of the the maximum current achievable during the ON state. From formula (1.29), the shuttle current is proportional to the mechanical vibration frequency: $\bar{I} \approx \bar{I}_s = 2\eta e N^* f$. From (1.27b), $N^* \propto V$, then, assuming efficient shuttle ($\eta = 1$), follows $\bar{I} \propto Vf$. During the ON state, both the drive and the slave pillars undergo the shuttle regime, therefore $\bar{I}_0 \propto V_0 f_0$ and $\bar{I}_1 \propto V_1 f_1$. From condition (I), constraint $f_0 \approx f_{1,R}$ leads to $\bar{I}_1/\bar{I}_0 \approx V_1/V_0$ †; during the ON state, in turn, one has $V_1/V_0 = V_1/V_{ON}$. Last, again from (I) $V_{ON} \geq V_{inf,0}$; while, from condition (V) about the locking failure, $V_1 < V_{lock}$.
Combining the estimations above, the ON state output (slave) current limit is obtained:

$$I_{1,max}{}^{(ON)} \triangleq \frac{\bar{I}_0}{V_{inf,0}} V_{lock} \tag{2.38}$$

In conclusion, during the ON state, one expects an output current $I_1 \leq I_{1,max}{}^{(ON)}$ (notice how this inequality is consistent with relations (2.35a) ‡, and, by extension, with (2.37a)).
Remarkably, since from relation (2.15) $G_{QSM,0} = \bar{I}_0/V_{inf,0}$, once the internal parameters for the drive QSM are set, the limit $I_{1,max}{}^{(ON)}$ only depends on V_{lock} .

† This is the proportionality used in Section 10.2.1 to produce formula (2.35a). Here, it has been demonstrated.

11.1.2 OFF state voltage limit

We already investigated the occurrence of the locking failure, which introduces a practical limit to the output (slave) voltage V_{lock} during the ON-state. The existence of such a constraint during the OFF-state is strictly related on the soft or hard nature of self-excitation.
However, from Chapter 9, we showed how a system exhibiting hard shuttle for low voltages can *transit* towards the soft behavior over a certain value of the bias voltage V_T . Consequently, for the slave module, one has to observe the constraint:

$$V_{1,max}{}^{(OFF)} \triangleq V_T \tag{2.39}$$

As hinted in Section 9.6, the quantity V_T can be considered the *breakdown voltage* for a switch, since, when $V_1 \geq V_T$, the interrupting state cannot be correctly performed anymore.
Further notice that, for a proper set of internal parameters (use to the reference settings for internal parameters in Tab.2.3), the hard→soft transition occurs at relatively large voltages, so that $V_{lock} \ll V_T$; from this, in turn, $V_1 \ll V_T$. This means that the locking condition usually occurs *before* the ON-state voltage limit V_{lock} is reached (condition (V)): follows that the NMT remains in the hard regime in any practical condition, and the locking (and not the breakdown) voltage remains the "bottleneck" to perform the interrupting state of a switch.

11.1.3 Commutation speed

A conventional voltage-driven switch is a *static* device, therefore its commutation speed depends on electrical rise and fall times, their order of magnitude being that of the time constant of a capacitor with the characteristic size of the switch electrodes. On the other hand, a NMT operating as a switch is not a static device, and its commutations speed in inversely proportional to the duration of its mechanical transients.
At resonance, the slave pillar amplitude of oscillation A_1 increases linearly with time:

$$A_1(t) = \frac{F_{0,1}t}{2m_1\sqrt{1-\zeta_1{}^2}\,\omega_{1,R}} \approx \frac{k_{0,1}(d_1-r_1)t}{2\sqrt{1-\zeta_1{}^2}\sqrt{m_1k_1}} \tag{2.40a}$$

Then, the duration of any switch-ON commutation can be estimated as the period of time required for A_1 to go from 0 (the worst case) to $d_1 - r_1$ (the shuttle amplitude for excess).
Substituting $A_1(t^*) = d_1 - r_1$ into (2.37a), the rise time t^* is:

$$t^* = \frac{2}{k_{0,1}}\sqrt{1-\zeta_1{}^2}\sqrt{m_1k_1} \tag{2.40b}$$

With the choices of internal and external parameters used in numerical simulations in Fig.2.22 and Fig.2.23, one obtains rise times t^* of the order of some ns , corresponding to a commutation speed not faster than 1 GHz .

11.1.4 Bouncing

In an electrical switch, the phenomenon of bouncing can occur during both switch-ON or switch-OFF commutations, and consists in an intermittency between the two states before the final state is stabilized. Bouncing can dramatically decrease the commutation speed of a switch.
In a NMT bouncing occurs also, but only during switch-ON commutations. It consists in a period of time during which the slave pillar alternatively entering/exiting the tunneling region.
However, this phenomenon is rather rare and generally promoted by a severe collision episode during the rise time of the slave. For this reason, bouncing only appears for relatively large slave voltages, usually in near-locking conditions: $V_1 \lesssim V_{lock}$.
In the first part of the simulation in Fig.2.27 a switch-ON transient which bouncing is achieved. It appears the slave pillar undergoes a sort of beat and intermittently enters/exits the tunneling region, until the ON state is definitely stabilized. During this transient, charge transport is intermittent also. Then, a second switch-ON commutation realized with a slightly smaller V_1, is correctly performed without any bouncing phenomenon. Transient durations are highlighted in yellow: one can notice the difference between the two switch-ON transients durations.

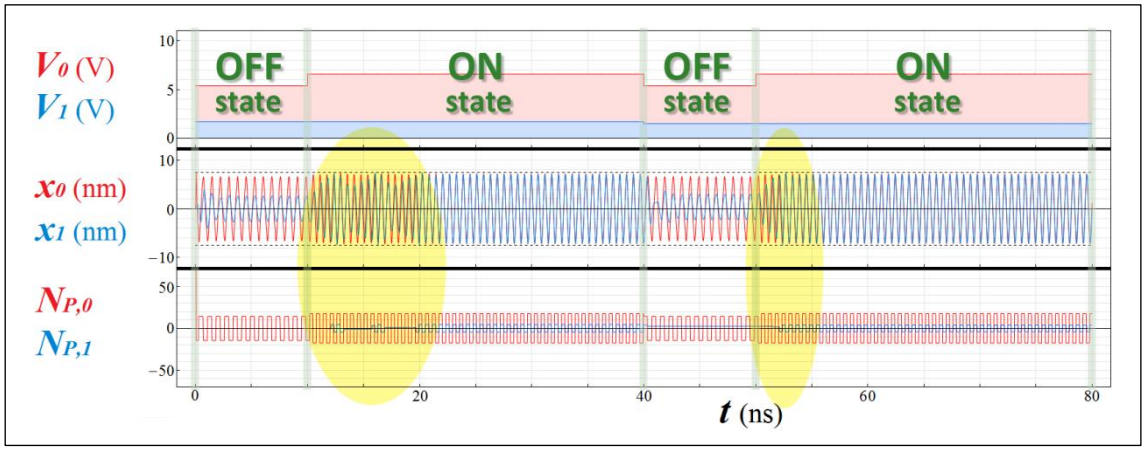

Figure 2.27 – *a single-slave ($N = 1$), different-damping ($\zeta_0 = 0.8$,$\zeta_1 = \zeta_0/10$) NMT undergoes 2 switch-ON commutations, ($V_{OFF} = 5.4\ V$, $V_{ON} = 6.6\ V$) . In the first one, $V_1 = 1.7\ V$ and bouncing occurs; in the second one, $V_1 = 1.5\ V$ and switch-ON is correctly performed. Internal parameters as in the reference system, except for $m_0 = 2 \times 10^{-21}\ kg$, $m_1 = m_0/4$, $k_0 = k_1 = 0.1\ N/m$, $k_{0,1} = k_0/4$.*

11.1.5 External characteristic: I-V curves

Referring to Section 6.1, a NMT, due to its working principle, is a voltage-controlled transistor. Consequently, in its external characterization, an input voltage produces a current as the output. In particular, a set of I-V curves can be plotted, each one corresponding to a certain input (drive) voltage V_{dr}, with the output (slave) current I_{sl} as a function of the output voltage V_{sl} . Different choices of the internal and the external parameters individuates a specific set of I-V curves.
Consider the equal-damping and single-slave NMT to which results in Fig.2.23 were referred †. The plot in Fig.2.28 portrays a set of I-V curves for the considered system, by using the data collected in Tab.2.6, coming from a series of numerical simulations, in which the NMT was tested under different bias voltages V_0 and V_1, and the consequent currents $\bar{I}_0$ and $\bar{I}_1$ measured.

† Both the drive and slave modules have reference values for the internal parameters (Tab.2.3), except for $m_0 = 2 \times 10^{-21}\ kg$, $m_1 = m_0/4$, $k_0 = k_1 = 0.5\ N/m$, $k_{0,1} = k_0/5$. Also, $\zeta_0 = \zeta_1 = 0.1$.

Table 2.6 – *electrical characterization of a single-slave ($N = 1$), equal-damping ($\zeta_0 \equiv \zeta_1 = 0.1$) NMT. Data obtained from a set of numerical simulations based on equations (2.14) with different voltage applications. Simulations share the same internal and external parameters as in Fig.2.23. Cells highlighted in yellow refer to simulations in which "intermittent shuttle" (continuative beats) is performed. Cells highlighted in grey, refer instead to locking failure conditions.*

$V_1(V)$	$\bar{I}_1\ (\mu A)\ [\bar{I}_0\ (\mu A)]$				
	$V_0 = 5.5\ V$	$V_0 = 6\ V$	$V_0 = 6.5\ V$	$V_0 = 7\ V$	$V_0 = 7.5\ V$
0.25	0.77 [16.99]	0.32 [22.66]	1.10 [28.46]	1.26 [35.26]	1.45 [43.47]
0.5	1.55 [17.00]	0.75 [22.67]	2.19 [28.46]	2.52 [35.26]	2.90 [43.47]
0.75	2.32 [17.00]	1.07 [22.67]	3.38 [28.66]	3.87 [36.06]	4.36 [43.47]
1	3.22 [17.70]	2.48 [22.67]	4.51 [29.30]	5.16 [36.06]	5.93 [43.46]
1.25	4.02 [17.70]	4.86 [23.35]	5.65 [29.30]	6.59 [36.86]	7.40 [44.42]
1.5	3.28 [17.71]	5.84 [23.35]	6.96 [30.12]	8.08 [36.87]	8.90 [44.44]
1.75	3.15 [18.42]	7.01 [24.04]	8.12 [30.13]	9.42 [37.65]	10.82 [46.36]
2	3.86 [18.70]	8.25 [24.73]	9.54 [30.97]	10.99 [38.47]	12.37 [46.34]
2.25	4.35 [19.13]	9.79 [26.10]	11.32 [32.65]	12.62 [39.27]	14.19 [47.32]
2.5	5.82 [19.83]	11.17 [26.79]	12.56 [32.65]	14.33 [40.06]	16.10 [48.29]
2.75	10.98 [21.96]	12.60 [27.47]	14.17 [33.50]	16.38 [41.66]	18.07 [49.27]
3	12.36 [22.67]	14.43 [28.85]	15.85 [34.33]	18.21 [42.47]	20.08 [50.21]
3.25	14.24 [24.09]	16.01 [29.54]	18.00 [36.00]	20.09 [43.23]	22.20 [51.49]
3.5	15.78 [24.79]	18.04 [30.91]	20.24 [37.65]	22.44 [44.87]	24.36 [52.80]
3.75	17.87 [26.21]	19.76 [31.60]	22.22 [38.53]	24.46 [45.69]	26.59 [54.11]
4	19.58 [26.92]	21.98 [32.98]	24.73 [40.12]	26.57 [46.46]	28.85 [55.41]

One can compare the NMT characteristic *I-V* curves in Fig.2.28 to those of a conventional (electronic) voltage-driven transistor, like the FET in Fig.2.3b. In the case of a NMT the *ohmic region* is wide and presents a rather good linearity. Also, reaching of the locking region does not produce any visible effect on the conductive properties of the system. Last, the *pinch-off region* is obtained by applying drive voltages smaller than $V_0 = 5.5\ V$. Notice that the saturation region is not reached, since, in the simulations performed, from (2.39), we used $V_1 \ll V_T \sim V_\eta$.

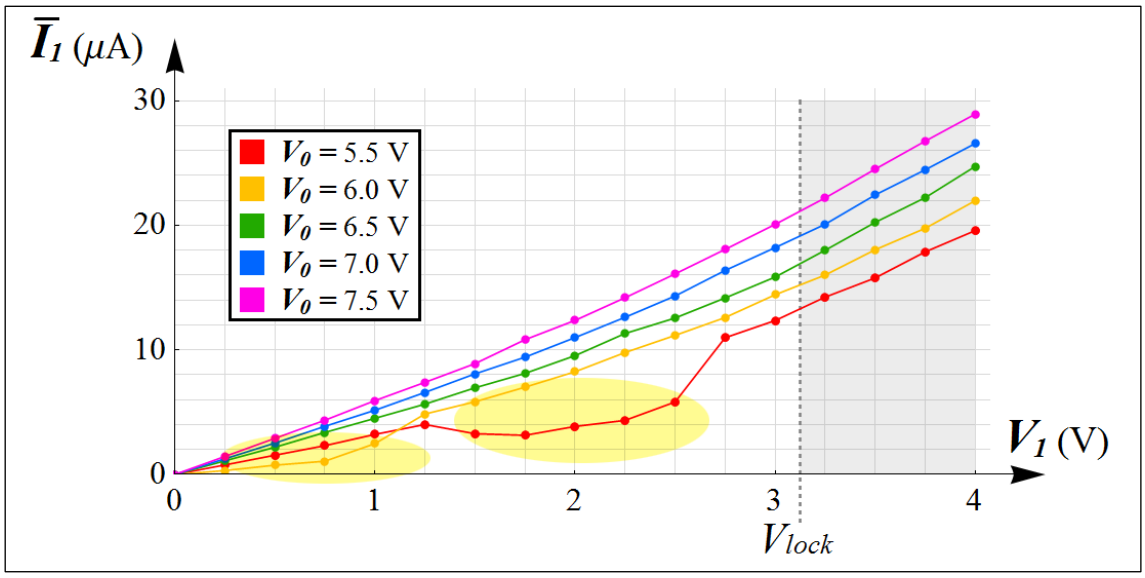

Figure 2.28 – *Characteristic I-V curves for the NMT whose data in Tab.2.6 are referred. Data highlighted in yellow refer to intermittent shuttle, while those in grey, refer to the surpass of V_{lock} .*

11.2 Energetic considerations on the amplifier functionality

In Section 10.2, the chance for a NMT to mimic the functionality of a conventional amplifier, with the gain α defined as the ratio between the slave and drive current, has been discussed. In particular, the feasibility to achieve an actual amplification $\alpha > 1$ in a single-slave ($N = 1$) and a multiple-slave ($N > 1$) depends on satisfying inequalities (2.35b) and (2.37b), respectively.
However, simulations shown in Fig.2.25 and Fig.2.26 highlight a certain difficulty for a NMT to obtain a large current amplification ($\alpha \gg 1$). This is because the effect of adding more slave pillars, explicitly suggested in the patent [77], has the drawback the to lower the threshold V_{lock}, so that (2.37b) cannot be trivially accomplished by "wildly" increase the number of slaves N .
This means the design condition (VIII) cannot be accomplished neither.
Since reaching the locking failure plays the role of bottleneck in achieving a large gain, some energetic considerations to estimate the value of V_{lock} can be useful achieve a more deep understanding of the limitations in direct current amplification of a NMT.

Consider a single-DOF damped oscillator. Respectively let $\Delta\mathcal{E}_{in}$ and $\Delta\mathcal{E}_{out}$ the amounts of pumped and (considered positive) dissipated energy per cycle. In general, a stable orbit is established only when an energy balance $\Delta\mathcal{E}_{in} = \Delta\mathcal{E}_{out}$ is reached. In a QSM, the oscillator is the shuttling element (the pillar). The energy is injected via electrostatic self-excitation, thus $\Delta\mathcal{E}_{in} = \Delta\mathcal{E}_{es}(V)$, being V the bias voltage (see Section 9.2.2). On the other hand, in the limit of weak electromechanical coupling, the mechanically dissipated energy per cycle is, by definition:

$$\Delta\mathcal{E}_d = 2\pi\frac{\mathcal{E}_{mech}(A)}{Q} = 2\pi k A^2 \zeta \tag{2.41}$$

Where $Q = 1/2\zeta$ is the *quality factor*, and $\mathcal{E}_{mech}(A) = kA^2/2$ the total energy stored in oscillations of amplitude A . In general electromechanical coupling conditions, $\Delta\mathcal{E}_d$ remains an increasing function of both A and ζ . Reassuming, a QSM triggers a limit-cycle which establishes a stable orbit with amplitude A^* when the following balance is reached:

$$\Delta\mathcal{E}_{es}(V) \equiv \Delta\mathcal{E}_d(A^*) \tag{2.42}$$

In the hard-limit approximation, constraint $A_{inf} \leq A^* \leq A_{sup}$ holds, being $A_{inf} = A_t$ the minimal amplitude compatible with QT (where the tunneling region begins), and $A_{sup} = d - r$.
Following the nomenclature proposed in Chapter 9, $A^* = A_{inf}$ when $V = V_{inf}$ and $A^* = A_{sup}$ when $V = V_{sup}$. However, as shown in Fig.2.19, the amplitude modulability of a QSM is usually more weak with respect to the frequency modulability. This means in (very) hard systems, $A_{inf} \approx A_{sup}$; and, consequently, the amplitude can be assumed constant and in proximity of to the leads. In conclusion, in these systems, the mechanically dissipated energy per cycle $\Delta\mathcal{E}_d$ can be considered constant with respect to the more relevant variations in the term $\Delta\mathcal{E}_{es}$.
The arguments and demonstrations presented in this Paragraph are thus valid under the approximation the term $\Delta\mathcal{E}_d$ is constant. In particular, in the following sub-Paragraphs, we distinctly analyze the cases $N = 1$ and $N > 1$.

11.2.1 Estimation of the locking voltage with $N = 1$

Consider one drive and $N = 1$ slave modules. If the mechanical coupling is not present, a shuttle regime is achieved in both the drive and slaves when two distinct energy balances hold:

$$\begin{cases} \Delta\mathcal{E}_{es,0}(V_0) = \Delta\mathcal{E}_{d,0} \\ \Delta\mathcal{E}_{es,1}(V_1) = \Delta\mathcal{E}_{d,1} \end{cases} \tag{2.43}$$

Now, add the mechanical interaction. Once every beat-like phenomenon is concluded, a net stationary energy exchange between the two systems is established. Indicate this amount of energy with the term $\Delta\mathcal{E}_{0\to1}$. If one assumes the pillars share the same internal parameters, in particular the same geometry, then $\Delta\mathcal{E}_{es} \triangleq \Delta\mathcal{E}_{es,0} \equiv \Delta\mathcal{E}_{es,1}$, and one obtains:

$$\begin{cases} \Delta\mathcal{E}_{es}(V_0) - \Delta\mathcal{E}_{0\to1}(V_0, V_1) = \Delta\mathcal{E}_{d,0} \\ \Delta\mathcal{E}_{es}(V_1) + \Delta\mathcal{E}_{0\to1}(V_0, V_1) = \Delta\mathcal{E}_{d,1} \end{cases} \tag{2.44}$$

First consider the case in which the ON state is performed. Then:

$$\forall\, V_1 \geq 0 \quad , \quad \begin{cases} \Delta\mathcal{E}_{es}(V_{ON}) - \Delta\mathcal{E}_{0\to1}(V_{ON}, V_1) \geq \Delta\mathcal{E}_{d,0} \\ \Delta\mathcal{E}_{es}(V_1) + \Delta\mathcal{E}_{0\to1}(V_{ON}, V_1) \geq \Delta\mathcal{E}_{d,1} \end{cases} \tag{2.45a}$$

Notice that, since $A \approx const \approx d - r$, the sign " $>$ " refers to an ON state achieved with continuative collisions, whereas " $=$ " establishes shuttle regimes with $A < A_{sup}$. The case of minimal energetic injection is the most interesting (and it surely accomplishes condition (VI), also). By posing $V_1 \approx 0$, from equations (2.45a) useful relations are obtained:

$$V_1 = 0 \quad , \quad \begin{cases} \Delta\mathcal{E}_{es}(V_{ON}) - \Delta\mathcal{E}_{0\to1}(V_{ON}, 0) = \Delta\mathcal{E}_{d,0} \\ \Delta\mathcal{E}_{0\to1}(V_{ON}, 0) = \Delta\mathcal{E}_{d,1} \end{cases} \tag{2.45b}$$

During the OFF state, equations (2.44) specify into either of the following:

$$\forall\, V_1 < V_{lock} \quad , \quad \begin{cases} \Delta\mathcal{E}_{es}(V_{OFF}) - \Delta\mathcal{E}_{0\to1}(V_{OFF}, V_1) = \Delta\mathcal{E}_{d,0} \\ \Delta\mathcal{E}_{es}(V_1) + \Delta\mathcal{E}_{0\to1}(V_{OFF}, V_1) < \Delta\mathcal{E}_{d,1} \end{cases} \tag{2.46a}$$

$$\forall\, V_1 < V_{lock} \quad , \quad \begin{cases} -\Delta\mathcal{E}_{0\to1}(0, V_1) < \Delta\mathcal{E}_{d,0} \\ \Delta\mathcal{E}_{es}(V_1) + \Delta\mathcal{E}_{0\to1}(0, V_1) < \Delta\mathcal{E}_{d,1} \end{cases} \tag{2.46b}$$

Equations (2.46a) refer to a sub-resonant OFF state, whereas (2.46b) to a static OFF state.
Last, the locking failure is characterized by the balances:

$$\forall\, V_1 \geq V_{lock} \quad , \quad \begin{cases} \Delta\mathcal{E}_{es}(V_{OFF}) - \Delta\mathcal{E}_{0\to1}(V_{OFF}, V_1) = \Delta\mathcal{E}_{d,0} \\ \Delta\mathcal{E}_{es}(V_1) + \Delta\mathcal{E}_{0\to1}(V_{OFF}, V_1) \geq \Delta\mathcal{E}_{d,1} \end{cases} \tag{2.47a}$$

$$\forall\, V_1 \geq V_{lock} \quad , \quad \begin{cases} -\Delta\mathcal{E}_{0\to1}(0, V_1) < \Delta\mathcal{E}_{d,0} \\ \Delta\mathcal{E}_{es}(V_1) + \Delta\mathcal{E}_{0\to1}(0, V_1) \geq \Delta\mathcal{E}_{d,1} \end{cases} \tag{2.47b}$$

Similarly, (2.47a) refer to locking failure consequent to attempting a sub-resonant OFF state, while (2.47b) is for a static OFF state.

Again, useful relations are obtained in the less energetic condition (incipient locking):

$$V_1 = V_{lock} \quad , \quad \begin{cases} \Delta\mathcal{E}_{es}(V_{OFF}) - \Delta\mathcal{E}_{0\to1}(V_{OFF}, V_{lock}) = \Delta\mathcal{E}_{d,0} \\ \Delta\mathcal{E}_{es}(V_{lock}) + \Delta\mathcal{E}_{0\to1}(V_{OFF}, V_{lock}) = \Delta\mathcal{E}_{d,1} \end{cases} \tag{2.47c}$$

$$V_1 = V_{lock} \quad , \quad \begin{cases} -\Delta\mathcal{E}_{0\to1}(0, V_{lock}) < \Delta\mathcal{E}_{d,0} \\ \Delta\mathcal{E}_{es}(V_{lock}) + \Delta\mathcal{E}_{0\to1}(0, V_{lock}) = \Delta\mathcal{E}_{d,1} \end{cases} \tag{2.47d}$$

Focus on relations (2.46a,b) and (2.47c,d). Since locking is a failure condition, assume we are interested to find the maximizing condition for V_{lock} . From (2.47c), one would prefer the limit $\Delta\mathcal{E}_{0\to1}(V_{OFF}, V_{lock}) \to 0$, however, from (2.46a), one understands this occurs correspondingly to the condition of minimal electrostatic energy injection, which is when $\Delta\mathcal{E}_{es,0}(V_{OFF})$ is minimal, compatibly with the shuttle regime of both pillars. Similar considerations are valid by comparing (2.47d) with (2.46b).
Consider the situation in which $V_{OFF} = V_{inf,0} + dV$, with $dV \to 0$. Then, introduce:

$$\text{maximizing condition for } V_{lock} \quad \Leftrightarrow \quad \begin{cases} V_{OFF} = V_{inf,0} & \text{subresonant OFF state} \\ V_{OFF} = 0 & \text{static OFF state} \end{cases} \tag{2.48}$$

Now, $V_{lock,max}$ can be estimated by applying (2.48) to the energy balances (2.46b) and (2.47c).

First treat the sub-resonant case. From (2.48), $V_{OFF} = V_{inf,0}$, and let $V_{ON} = V_{inf,0} + \Delta V$. Summing up the two equations in (2.46b) and in (2.47c), one respectively obtains:

$$\Delta\mathcal{E}_{es}(V_{inf,0} + \Delta V) = \Delta\mathcal{E}_{d,0} + \Delta\mathcal{E}_{d,1} \tag{2.49a}$$

$$\Delta\mathcal{E}_{es}(V_{inf,0}) + \Delta\mathcal{E}_{es}(V_{lock,max}) = \Delta\mathcal{E}_{d,0} + \Delta\mathcal{E}_{d,1} \tag{2.49b}$$

Combining (2.49a) and (2.49b), the following estimation is attained:

$$\Delta\mathcal{E}_{es}(V_{lock,max}) = \Delta\mathcal{E}_{es}(V_{inf,0} + \Delta V) - \Delta\mathcal{E}_{es,0}(V_{inf,0}) \tag{2.50}$$

Now consider the static OFF state. From (2.48), $V_{OFF} = 0$, then, let $V_{ON} = V_{inf,0}$. Sum up equations in (2.46b), and impose, in (2.47c), $\Delta\mathcal{E}_{0\to1}(V_{OFF}, V_{lock}) = 0$. Follows that:

$$\Delta\mathcal{E}_{es}(V_{inf,0}) = \Delta\mathcal{E}_{d,0} + \Delta\mathcal{E}_{d,1} \tag{2.51a}$$

$$\Delta\mathcal{E}_{es}(V_{lock,max}) = \Delta\mathcal{E}_{d,1} \tag{2.51b}$$

From (2.51a) and (2.51b), one obtains:

$$\Delta\mathcal{E}_{es}(V_{lock,max}) = \Delta\mathcal{E}_{d,1} \equiv \Delta\mathcal{E}_{es}(V_{inf,0}) - \Delta\mathcal{E}_{d,0} \tag{2.52}$$

In conclusion, relations (2.50) and (2.52) allow for an estimation of the maximum value of voltage which leads to a locking failure, $V_{lock,max}$.

11.2.2 Feasibility of current amplification with $N = 1$

The maximum gain in a single-slave NMT is, from (2.35a), $\alpha_{max} \approx V_{lock}/V_{inf,0}$. However, one can demonstrate α_{max} is strictly related with the different- and same-damping design options. In fact, neglecting the mechanical coupling and using (2.41), stable oscillations are achieved for:

$$\Delta\mathcal{E}_{es}(V) \approx \Delta\mathcal{E}_d = 2\pi k A^2 \zeta \tag{2.53}$$

If $\Delta\mathcal{E}_{es}(V)$ increases with V (see Section 9.5), then $V_0 \propto \zeta_0$, and, analogously, $V_1 \propto \zeta_1$. Thus:

$$\alpha_{max} \propto \frac{\zeta_1}{\zeta_0} \tag{2.54}$$

and in a different-damping NMT amplification is discouraged, since $\zeta_1/\zeta_0 > 1$ (Section 10.1.3).

From the increasing monotonicity of $\Delta\mathcal{E}_{es}(V)$ another relevant consideration follows. In fact, one can assume $V_{lock}/V_{inf,0} \propto \Delta\mathcal{E}_{es}(V_{lock})/\,\Delta\mathcal{E}_{es}\big(V_{inf,0}\big)$, thus concluding:

$$\alpha_{max} > 1 \quad \Leftrightarrow \quad \Delta\mathcal{E}_{es}\big(V_{lock,max}\big) > \Delta\mathcal{E}_{es}\big(V_{inf,0}\big) \tag{2.55}$$

First consider the case of sub-resonant switch-OFF. Applying (2.49b) to (2.55), one obtains:

$$\alpha_{max} > 1 \quad \Leftrightarrow \quad \Delta\mathcal{E}_{es}\big(V_{inf,0} + \Delta V\big) > \Delta 2\mathcal{E}_{es}\big(V_{inf,0}\big) \tag{2.56a}$$

Now consider the case of static switch-OFF. By using (2.52), relation (2.53) specifies into:

$$\alpha_{max} > 1 \quad \Leftrightarrow \quad \Delta\mathcal{E}_{es}\big(V_{inf,0}\big) > \Delta\mathcal{E}_{es}\big(V_{inf,0}\big) + \Delta\mathcal{E}_{d,0} \tag{2.56b}$$

Let us discuss the estimations achieved above. The first inequality, (2.56a), is hardly verified, especially if ζ_0 is low. Unfortunately, $\zeta_0 \ll 1$ is a preferred condition, since from (2.54), amplification is promoted by using $\zeta_1/\zeta_0 \sim 1$, and, simultaneously, condition $\zeta_1 \ll 1$ is required to provide a sufficient (mechanical) amplification of the slave oscillations. This holds for a sub-resonant switch-OFF. The second inequality (2.56b), instead, is neatly impossible, since both $\Delta\mathcal{E}_{es}$ and $\Delta\mathcal{E}_{d,0}$ are positive quantities. In conclusion, we stated the difficulty, and, in some situations, the impossibility, to obtain amplification in a NMT with a single slave ($N = 1$).

11.2.3 Estimation of the locking voltage with $N > 1$

Naturally extend our discussion to a case in which $N > 1$ slave QSMs are present in the NMT. It is possible to directly generalize many results from Section 11.2.1 by assuming the amount of energy coming from the oscillation of the drive is equally distributed into each of the slave resonators †. Thus, each of the N slave pillars receives a stationary amount of energy per cycle:

$$\forall\, i > 0 \;\; , \quad \Delta\mathcal{E}_{0\to i} = \frac{\Delta\mathcal{E}_{dr\to sl}(V_{dr}, V_{sl})}{N} \tag{2.57}$$

† Actually, this condition is strictly verified only in a parallel configuration among the drive and slaves, while the case of study is that of a series coupling between pillars. However, this is a simple approximation which produces neat and useful results.

In a manner completely similar to Section 11.2.1, energy balances (2.43)-(2.47) can be generalized to the case $N > 1$. Also, under the hypothesis (from condition (VII)) that each slave pillar is geometrically similar to the others, it is possible to estimate the value of $V_{lock,max}$ by using a demonstration which leads to final results analogous to relations (2.50) and (2.52). Thus, omitting analytical details, for a sub-resonant OFF and a static OFF state, one respectively obtains:

$$\Delta\mathcal{E}_{es}\left(V_{lock,max}\right) = \frac{\Delta\mathcal{E}_{es}\left(V_{inf,dr} + \Delta V\right) - \Delta\mathcal{E}_{es}\left(V_{inf,dr}\right)}{N} \tag{2.58}$$

$$\Delta\mathcal{E}_{es}\left(V_{lock,max}\right) = \Delta\mathcal{E}_{d,sl} = \frac{\Delta\mathcal{E}_{es}\left(V_{inf,dr}\right) - \Delta\mathcal{E}_{d,dr}}{N} \tag{2.59}$$

11.2.4 Feasibility of current amplification with $N > 1$

From relation (2.37a), the maximum obtainable gain in the case $N > 1$ is:

$$\alpha_{max} \approx N\frac{V_{lock,max}}{V_{inf,dr}} \tag{2.60}$$

Also, if $\Delta\mathcal{E}_{es}(V)$ is an increasing function, $V_{lock}/V_{inf,dr} \propto \Delta\mathcal{E}_{es}(V_{lock})/\Delta\mathcal{E}_{es}\left(V_{inf,dr}\right)$, and:

$$\alpha_{max} > 1 \quad \Leftrightarrow \quad N\Delta\mathcal{E}_{es}\left(V_{lock,max}\right) > \mathcal{E}_{es}\left(V_{inf,dr}\right) \tag{2.61}$$

Consider both of sub-resonant and static switch-OFF cases. Respectively plugging (2.58) and (2.59) into (2.61), one obtains a couple of relations completely analogous to (2.56a,b):

$$\alpha_{max} > 1 \quad \Leftrightarrow \quad \Delta\mathcal{E}_{es}\left(V_{inf,dr} + \Delta V\right) > 2\Delta\mathcal{E}_{es}\left(V_{inf,dr}\right) \tag{2.62a}$$

$$\alpha_{max} > 1 \quad \Leftrightarrow \quad \Delta\mathcal{E}_{es}\left(V_{inf,dr}\right) > \Delta\mathcal{E}_{es}\left(V_{inf,dr}\right) + \Delta\mathcal{E}_{d,dr} \tag{2.62b}$$

It has be remarked the term N has disappeared in both (2.62a,b). This fact states the fundamental point that, in a first approximation and, limited to the case of same geometry between drive and slave pillars, increasing the number of slaves N does not trivially produce a positive effect on the amplification performances. One can say that, due to energetic arguments, the locking voltage V_{lock} has a decreasing dependence from the number of slaves N. Additionally, in this Chapter we demonstrated that, at least in some situations, V_{lock} is inversely proportional to N:

$$\frac{V_{lock}(N)}{V_{lock}(1)} = \frac{1}{N} \quad \Leftrightarrow \quad V_{lock}(N) \propto \frac{1}{N} \tag{2.63}$$

Statements (2.63) are visibly in disagreement with the amplification requirement (VIII).

For completeness sake, one can consider a more general context in which more drive modules are consented. For a NMT with $N_{dr} \geq 1$ drives and $N_{sl} \geq 1$ slaves, holds the relation:

$$\left.\frac{\Delta V_{lock}(N_{sl})}{\Delta N_{sl}}\right|_{N_{sl}=N_{sl}^{*}} < 0 \tag{2.64}$$

Conclusions & Perspectives

In this thesis, the main subjects behind a compelling technological challenge – achieving the transistor functionalities from a mechanical working principle – have been explored and investigated. The properties of two nanomechanical devices, respectively pioneered by the fundamental works of Gorelik and Blick, have been analyzed: a single QSM and a composite NMT.
Specifically, the latter, in the Author's knowledge, is not investigated in NEMS literature, yet.
Consequently, the main original contribution of this research work is the theoretical study of the NMT, synthetized by the suggestions of a set of design requirements and control strategies.
Both the voltage-driven switch and the current amplification functionalities have been analyzed.

Numerical simulations carried out in Chapter 10 demonstrate how the switching operation can be definitely mimicked, at least from a functional point of view. However, as indicated by Blick in [60] and confirmed here in Chapter 11, the characteristic working frequencies of a NMT could not compete with top-category conventional microchips, but are surely compatible with some mundane applications. Thus, multiple NMTs arranged in specifically designed circuital topologies could represent a step innovation in the computing industry, assembling shuttle-based logic gates, characterized by some peculiar advantages highlighted already in the Preface.

On the other hand, consequently to some numerical results shown in Chapter 10 and the more rigorous motivations explained in Chapter 11, the functionality of a conventional amplifier seems to be much more difficult to be reproduced. First of all, it has been showed a larger-than-unity current gain can be obtained only by using more than one slave resonator ($N > 1$). At the moment, by increasing the number of slave pillars in numerical simulations, only a slight amplification effect has been experienced (however sufficient to provide the minimal fan-out effect, as highlighted in [77]). To the aim of enhancing the amplification performances, further investigations continuing the work of the present thesis are definitely required.
In particular, since, by increasing N, the success in obtaining an actual amplification effect is related to a precise selection of the NMT internal parameters, a rigorous study of energy exchanges among the drive and the slave set has to be approached through a general methodology.
As a second question, different – and potentially more effective – mechanical couplings between resonators can be considered. For example (see Fig.2.29), a *parallel configuration* among the slave pillars and the drive can possibly enhance the stability and repeatability of operation, with respect to a *series* one (which is the one proposed in [60,77] and investigated in this thesis).

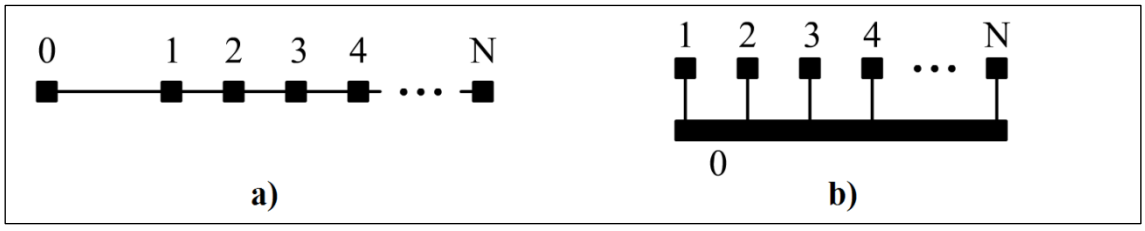

Figure 2.29 – *Sketch of a: (a) series, (b) parallel configuration between the slaves and drive pillar.*

Advantages of a parallel configurations would be: i) better control of the slave pillars vibrations, leading to a reduction of unpredicted collisions with leads, thus enhancing the device durability; ii) better energetic equipartition among the slave pillars with respect to a series coupling, which lowers the risk of a resonance condition not contemporarily reached by all the slaves.
This second point, in particular, highlights that, if N is increased in a series configuration, the energetic considerations presented in Sections 11.2.3 and 11.2.4, and in particular inequalities (2.62a,b) actually represent a "best case", whereas they are accurate if they refer to a parallel configuration, for which hypothesis (2.57) is much larger reliable. On the contrary, if (2.57) does not correctly hold, at least 2 failure conditions, peculiar of the case $N > 1$, should be considered: i) *partial switch-ON failure*, ii) *partial switch-OFF failure* ("partial locking"); respectively associated to any switch-ON or switch-OFF attempt. All these considerations, lead to prefer a parallel coupling. As a last consideration, a drawback of increasing N (shared by both the series and parallel configurations), is that the switch-ON or switch-OFF commutation durations results roughly proportional to N . This means the effort in increasing the amplification performances in a NMT is antagonist to its switching speed: another challenging question which surely requires additional studies. For all these reasons, the convenience in using of $N > 1$ slave pillars can be considered a debated point, since it introduces much more design issues with respect to the case of a single slave pillar, sufficient for the switching operation.

Actually, it can be remarked that it is always possible to obtain a considerable current amplification $\alpha = I_{sl}/I_{dr} \gg 1$ by simply skipping condition (V) about switch-OFF failure. For example, by using $V_{dr} = V_{dr} > V_{lock}$, one obtains $\alpha \approx N$, but the drawback is that a severe locking regime is established, compromising the switching-OFF functionality of the whole NMT and, thus, the repeatability of operation, which clearly represents a design requirement.

In conclusion, this work remains exquisitely theoretical. To the Author's conviction, attempting an experimental activity prior of having an intimate comprehension of the basic behaviors of such complex systems would have been premature. In fact, due to the absence of pre-existing benchmark, any experimental setup would have demanded for wise design choices, in turn requiring a tout-court theoretical analyses: this is the strategy I attempted to follow in the thesis.

In the wait of the first experimental validations, natural perspectives of the research presented in this thesis include: i) theoretical investigation on the hybrid shuttle phenomenology (which, in Chapter 5, has been only outlined); ii) the develop of more accurate analytical models to describe both the mechanical and electrical parts of the system (additional modes of vibration, pillars coupling, electrostatics); iii) both QSM and NMT testing and optimization using COMSOL® (or similar multiphysics software); iv) definitive design of the NMT (with emphasis to the manufacturing process and technological limits).

APPENDICES

Appendix A

Quantum tunneling equivalent conductances

The QT effect can be profitably included in a semi-classical circuital model by using a non-linear equivalent conductance G_t . Many closed-form relations have been proposed in literature. In this thesis, we use one of the most most-cited approaches: the *Simmons formulae* [86,136]. They return an accurate estimation of $G_t = G_t(d,V)$, depending on the insulator thickness d and the applied voltage V (specifying the tunneling length dependence $\lambda = \lambda(V)$ hinted in (1.1b)). In particular, we use the formula referred to a "rectangular barrier with image force included":

$$G_t(d,V) \triangleq \frac{J_0 S}{V}\left[\phi_I \, \mathrm{e}^{-B\sqrt{\phi_I}} - (\phi_I + eV)\mathrm{e}^{-B\sqrt{\phi_I+eV}}\right] \qquad \text{(A. 1)}$$

$$J_0 = \frac{e}{2\pi h(d_2-d_1)^2} \quad , \qquad \phi_I = \phi_L - \frac{eV}{2d}(d_1+d_2)$$

$$B = \frac{4\pi(d_2-d_1)}{h}\sqrt{2m_{el}} \quad , \qquad \psi = \frac{e^2 \ln 2}{8\pi\epsilon d}$$

$$d_1 = \frac{1.2\,\psi d}{\phi} \quad , \qquad d_2 = \begin{cases} \left(1 - \dfrac{9.2\,\psi}{3\phi + 4\psi - 2eV}\right)d + d_1 & \text{if } V < \phi/e \\ \dfrac{(\phi - 5.6\,\psi)d}{eV} & \text{if } V \geq \phi/e \end{cases}$$

and h is the Planck constant, m_{el} the electron mass, ϕ the electrodes working function, S their average area, and ε the insulator permittivity. Though Simmons analytically derived this formulae decades ago, they are in good agreement with experimental data. In Fig.A.1, the conductance G_t is plotted as a function of d and for stepped values of V by using formula (A.1). Notice that, although the dependence of G_t from the voltage V is important †, but the most relevant one is that from the distance d, exponential indeed. The latter represents a peculiarity of QT already highlighted in the first works of Fowler-Nordheim, which explains why its effect produces sensible consequences only within distances of a few nanometers.

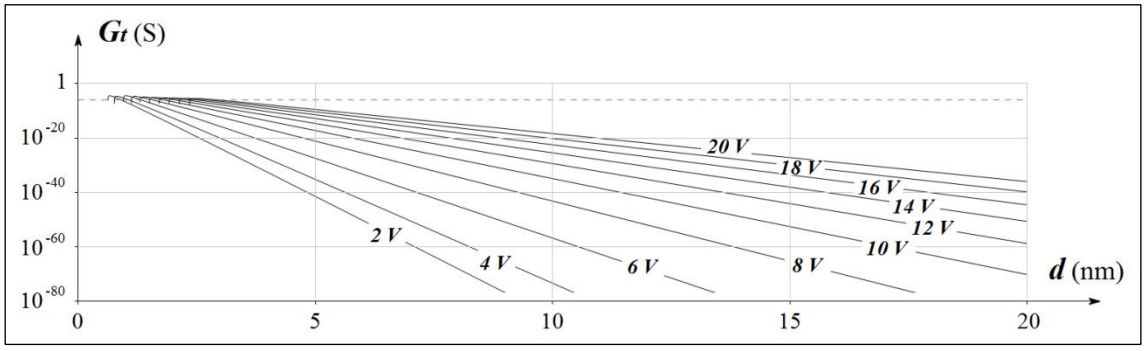

Figure A.1 – *curves $G_t(d,V)$ in logarithmic scale, obtained from formula (A.1).*

Last, the dependence of $G_t = G_t(V)$ is particularly interesting to perform numerical simulations in which the bias voltage is not constant.
Relation (A.1) can be further specified to calculate QT conductances G_{LP}, G_{PR} and G_{LR} , in turn representing the coefficients of the conductance matrices **G** and $\mathbf{G_0}$ to be used in (2.5):

$$G_{LP} \triangleq G_t(d - r + x, V_L - V_P) \tag{A. 2a}$$

$$G_{PR} \triangleq G_t(d - r - x, V_P - V_R) \tag{A. 2b}$$

$$G_{LR} \triangleq G_t(2d, V_L - V_R) \tag{A. 2c}$$

Appendix B

Capacitance matrix

In the most general case, the electrostatics of an N-conductors system is completely described by a $N \times N$ symmetrical capacitance matrix $\mathbf{C}$. Its coefficients depend only on the conductors geometry and their reciprocal positions. Two standard – and equivalent – definitions are used in literature to introduce such capacitance matrix:

$$\mathbf{C} \triangleq \begin{bmatrix} c_{1,1} & c_{1,2} & \cdots & c_{1,N} \\ c_{1,2} & c_{2,2} & \cdots & c_{2,N} \\ \vdots & \vdots & \ddots & \vdots \\ c_{1,N} & c_{2,N} & \cdots & c_{N,N} \end{bmatrix} \tag{B.1a}$$

$$\mathbf{C} \triangleq \begin{bmatrix} (C_1 + C_{12} + \cdots + C_{1N}) & -C_{12} & \cdots & -C_{1N} \\ -C_{12} & (C_{21} + C_2 + \cdots + C_{2N}) & \cdots & -C_{2N} \\ \vdots & \vdots & \ddots & \vdots \\ -C_{1N} & -C_{2N} & \cdots & (C_{1N} + C_{2N} + \cdots + C_N) \end{bmatrix} \tag{B.1b}$$

The first definition, (B.1a), refers to the *ground capacitance matrix*, its terms $c_{i,j}$ are usually called *electrostatic induction coefficients* and do not have any immediate physical interpretation. On the other hand, (B.1b) is the *lumped capacitance matrix*, its coefficients C_i representing the *self-capacitances* (capacitance of a spherical conductor with respect to the surroundings), whereas coefficients C_{ij} correspond to the *floating capacitances* (capacitance of the capacitor formed by the conductors i and j). The latter definition is used in the followings.

In absence of sharp edges or vertexes, it is feasible to approximate the capacitance matrix of an N-conductors system by using N equivalent spheres with same surfaces and relative position. Under this assumption, the investigated three-conductors QSM can be profitably described by the means of a 3×3 (lumped) capacitance matrix:

$$\mathbf{C} = \begin{bmatrix} C_L + C_{LP}(x) + C_{LR} & -C_{LP}(x) & -C_{LR} \\ -C_{LP}(x) & C_P + C_{LP}(x) + C_{PR}(x) & C_{PR}(x) \\ -C_{LR} & -C_{PR}(x) & C_R + C_{PR}(x) + C_{LR} \end{bmatrix} \tag{B.2}$$

Therefore, in (B.2), self- and floating capacitance terms are associated to a system composed by three conductive spheres: the left electrode, the pillar's cap and the right electrode. This approach allows to use simple closed-form expressions to complete the whole capacitance matrix. In fact, all the coefficients in (B.2) can be determined on the basis of the Maxwell-Kirchhoff formulation for spherical conductors †, exposed ahead.

† The original formulation by Russell [137] has been recently revised by many authors. Here, we report, among the others, second the approach used in [138].

Consider two conductive spheres of radii A and B, with $A \geq B$ and a center-to-center distance $D > A + B$. The 2×2 capacitance matrix referred to such two-spheres system is:

$$(\mathbf{C})_{\boldsymbol{AB}} = \begin{bmatrix} (c_{1,1})_{AB} & (c_{1,2})_{AB} \\ (c_{1,2})_{AB} & (c_{2,2})_{AB} \end{bmatrix} \triangleq 4\pi\varepsilon\lambda \begin{bmatrix} +\sum_{n=0}^{\infty} \frac{1}{\sinh(\alpha + n\sigma)} & -\sum_{n=0}^{\infty} \frac{1}{\sinh[(1+n)\sigma]} \\ -\sum_{n=0}^{\infty} \frac{1}{\sinh[(1+n)\sigma]} & +\sum_{n=0}^{\infty} \frac{1}{\sinh(\beta + n\sigma)} \end{bmatrix} \quad \text{(B. 3)}$$

$$\sigma = \text{ArcSinh}\left(\frac{\Lambda D}{AB}\right) \quad , \quad \alpha = \text{ArcSinh}\left(\frac{\Lambda}{A}\right) \quad , \quad \beta = \text{ArcSinh}\left(\frac{\Lambda}{B}\right)$$

$$\Lambda = \frac{\sqrt{(D + A + B)(D - A - B)(D + A - B)(D - A + B)}}{2D}$$

Then, it is possible to calculate the floating capacitance of the capacitor associated to the pair of spherical conductors A and B with:

$$C_{AB}^{float}(D) \triangleq \frac{(c_{1,1})_{AB}(c_{2,2})_{AB} - (c_{1,2})_{AB}^{\ 2}}{(c_{1,1})_{AB} + (c_{2,2})_{AB} + 2(c_{1,2})_{AB}} \quad \text{(B. 4)}$$

whereas the self-capacitance of a sphere of radius A is simply:

$$C_A^{self} \triangleq 4\pi\epsilon A \quad \text{(B. 5)}$$

By using relations (B.4) and (B.5) it is possible to compute the self- and floating capacitance terms which appear in matrix (B.2) for any position x of the pillar:

$$C_{LP} = C_{Rr}^{float}(d + x + R) \quad (B.\,6\text{a})$$

$$C_{PR} = C_{Rr}^{float}(d - x + R) \quad (B.\,6\text{b})$$

$$C_{LR} = C_{RR}^{float}(2d) \quad \text{(B. 6c)}$$

$$C_L \equiv C_R = C_R^{self} \quad (B.\,6\text{d, e})$$

$$C_P = C_r^{self} \quad \text{(B. 6f)}$$

where r is the radius of the pillar's cap, and $R > r$ that of the left and right electrodes.

Appendix C

Electrostatic force

Different approaches can be considered to model the electrostatic acting on the pillar, some take into account the effect of electrostatic induction, some others not. Depending on the ratios R/d , r/d and $Q_P/Q_{L,R}$ a model can result more feasible than others or vice versa.

The simplest case arises by assuming the voltage applied through the fixed electrodes generates an electric field which is *uniform* in the whole oscillating region $\mathcal{O} = [-d + r, d - r]$:

$$F_P \triangleq \frac{V_L - V_R}{2d} Q_P \tag{C.1}$$

A first model introducing the dependence from position $x(t)$ comes by using the classical Coulomb law and considering the total charges $Q_L(t)$, $Q_R(t)$ and $Q_P(t)$ as concentrated *in the center* of the three spherical conductors L , R and P , respectively (time dependences omitted):

$$F_P \triangleq \frac{1}{4\pi\varepsilon}\left[\frac{Q_L}{(d + x + R)^2} - \frac{Q_R}{(d - x + R)^2}\right] Q_P \tag{C.2}$$

Formulae (C.1) and (C.2) represent, in some cases, rather poor approximations. In particular, the uniform field assumption is not accurate when the pillar is close to the leads. Remarkably, these regions are crucially important since the most relevant QT currents occur just when the pillar-electrode distance is minimal. On the other hand, the proposed Coulomb force approach provides for a good approximation in the limit the center-to-center distance between the spheres is much larger than their radii, namely in the validity of limit $R/d \to 0$. In particular, in the case $R \sim d$, the charge distribution on the left and right spheres is not homogeneous at all and the effect of the Coulomb law is that to underestimate the force on the pillar.

Consequently, it is possible to introduce a first-order correction which assumes the total charge in the left and right spheres is concentrated in a point *deviated from their centers*, so that formula (C.2) transforms in:

$$F_P \triangleq \frac{1}{4\pi\varepsilon}\left\{\frac{Q_L}{[d + x + R(1 - \chi)]^2} - \frac{Q_R}{[d - x + R(1 - \chi)]^2}\right\} Q_P \tag{C.3}$$

The symbol χ represents an appropriate *correction factor*, introduced in order to take into account the charge displacements due to electrostatic induction effects. Since left and right electrodes polarity are opposed, χ assumes a positive value, specifically $0 \leq \chi < 1$.
A suitable expression for χ can be determined by using the procedure † described above.

† The method presented here is partly inspired to [139].

Consider the two-conductors system comprising only the left and right electrodes and construct the capacitance matrix $(\mathbf{C})_{\boldsymbol{LR}}$ associated to them, then, calculate the inverse matrix. The electrostatic force between them comes by applying the definition of electrostatic force:

$$F_{LR} = -\frac{\partial \mathcal{U}_{LR}}{\partial \ell}\bigg|_{\ell=2d} = -\left[\frac{1}{2}\frac{\partial (p_{1,1})_{LR}}{\partial \ell} {Q_L}^2 + \frac{\partial (p_{1,2})_{LR}}{\partial \ell} Q_L Q_R + \frac{1}{2}\frac{\partial (p_{2,2})_{LR}}{\partial \ell} {Q_R}^2\right]_{\ell=2d}$$

$$(\mathbf{C})_{\boldsymbol{LR}}{}^{-\mathbf{1}} = \begin{bmatrix} (p_{1,1})_{LR} & (p_{1,2})_{LR} \\ (p_{1,2})_{LR} & (p_{2,2})_{LR} \end{bmatrix}$$

Then, the correction factor is calculated by comparing F_{LR} with the Coulomb law:

$$\chi = \begin{cases} 0 & if\ F_{LR} = 0 \\ 1 + \dfrac{d}{R} - \dfrac{1}{2R}\sqrt{\dfrac{1}{4\pi\varepsilon}\dfrac{Q_L Q_R}{F_{LR}}} & if\ F_{LR} \neq 0 \end{cases}$$

The (attractive) force F_{LR} between left and right electrodes has been calculated in the hypothesis the presence of the pillar is negligible. This is reasonable, since usually $R \gg r$ and $Q_{L,R} \gg Q_P$.

Formula (C.3) provides an accurate estimation of F_P for every R/d ratio. However, it doesn't include electrostatic induction effects on the pillar, which are considerable if condition $r/d \to 0$ does not hold †. Since, in general, $R > r$ and $Q_{L,R} \gg Q_P$, the electrostatic induction *on the pillar* can be relevant, whereas that produced *by the pillar* is negligible. Therefore, it is still possible to consider the total charges Q_L and Q_R as concentrated in little spheres of radii $\rho \ll r < R$, with centers in $-d - R(1-\chi)$ and $d + R(1-\chi)$, respectively. The electrostatic force on the pillar is consequently split into two parts, the left-pillar force F_{LP} and the pillar-right F_{PR} :

$$F_P \triangleq F_{LP} - F_{PR} \tag{C.4}$$

In turn, these terms can be calculated by using an approach analogous to (C.3) and alternatively neglecting the presence of the remaining sphere ‡ :

$$F_{LP} = -\left[\frac{1}{2}\frac{\partial (p_{1,1})_{LP}}{\partial \ell} {Q_L}^2 + \frac{\partial (p_{1,2})_{LP}}{\partial \ell} Q_L Q_P + \frac{1}{2}\frac{\partial (p_{2,2})_{LP}}{\partial \ell} {Q_P}^2\right]_{\ell=(d+x)+R(1-\chi)-(r+\rho)}$$

$$F_{PR} = -\left[\frac{1}{2}\frac{\partial (p_{1,1})_{PR}}{\partial \ell} {Q_P}^2 + \frac{\partial (p_{1,2})_{PR}}{\partial \ell} Q_P Q_R + \frac{1}{2}\frac{\partial (p_{2,2})_{PR}}{\partial \ell} {Q_R}^2\right]_{\ell=(d-x)+R(1-\chi)-(r+\rho)}$$

Procedure (C.4) may seem laborious but, as it is highlighted ahead, it returns results consistent with the more orthodox one (C.3).

In Fig.C.1, a comparison among the electrostatic force calculated by using formulations (C.1), (C.2), (C.3) and (C.4) is portrayed. Curves refer to different: QSM geometries R/r and d/r (with $r = r_{ref}$), voltages $V = V_L - V_R = \{5,10,15\}\,V$, electrons $N_P = \{1,5,25\}$ are shown.

† Notice that characteristic times for electron redistribution in the pillar's metallic cap are considerably smaller with respect to the mechanical period of oscillation of the pillar itself.

‡ This procedure is justified since the electrostatic induction among the large spheres is already included in the corrective term χ .

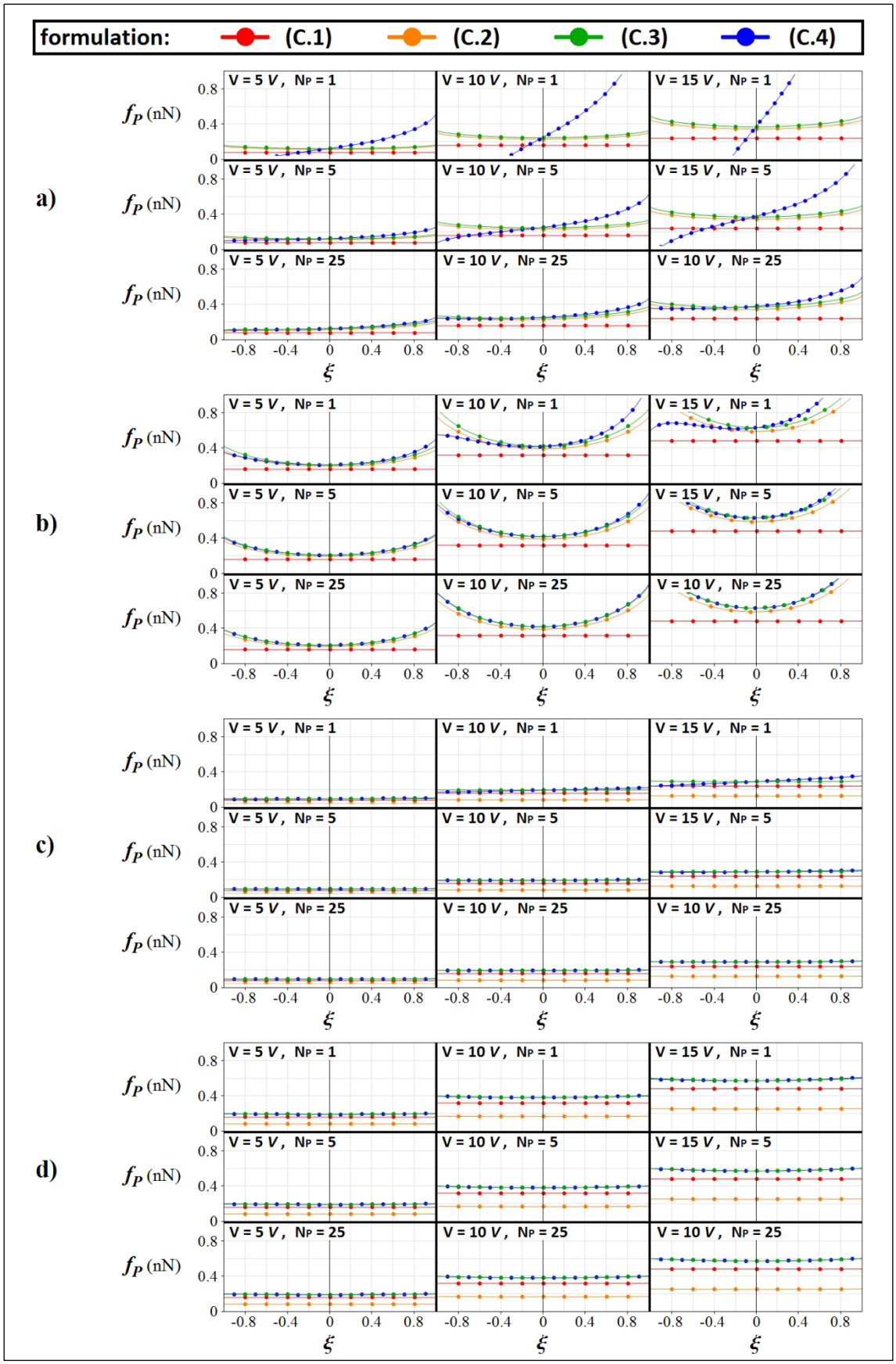

Figure C.1 – *electrostatic force* $f_P \triangleq F_P/N_P$ *as a function of the pillar position* $\xi \triangleq x/(d-r)$ *. Various combinations of applied voltages* V*, electrons* N_P*, and QSM geometries (a)* $d/r = 2$ *,* $R/r = 2$ *; (b)* $d/r = 10$ *,* $R/r = 10$ *; (c)* $d/r = 2$ *,* $R/r = 20$ *; (d)* $d/r = 10$ *,* $R/r = 100$ *, are shown, with* $r = r_{ref}$*.*

A brief analysis of plots in Fig.C.1 demonstrates the consistence of all the approaches (C.1), (C.2), (C.3) and (C.4). In particular, formulation (C.4) coincides to (C.3) in the limit $r/d \to 0$; in turn (C.3) matches with (C.2) in the case $R/d \to 0$. Last, notice how formula (C.2) does not trivially collapse in (C.1), which represents a rather raw approximation.

Electrostatic induction effects are more relevant if $r \sim R$ and/or $r \sim d$, and produce not-symmetric forces. Equations (C.4) constitute the most general and accurate model, in which electrostatic induction on the pillar produces a non-zero force on the pillar also in absence of a net charge on its cap ($N_P = 0$). The validity of the latter statement is highlighted in Fig.C.2.

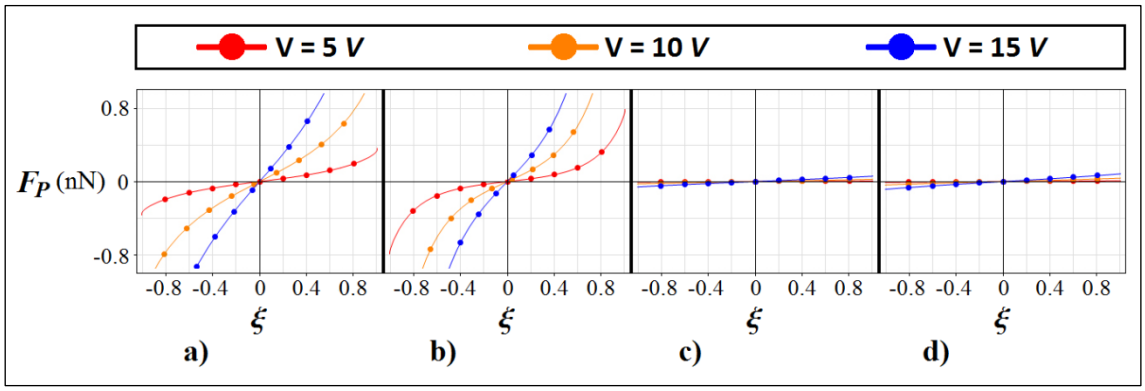

Figure C.2 – *electrostatic force F_P as a function of the pillar position $\xi \triangleq x/(d-r)$, in the case $N_P = 0$. Formulation (C.4) is used for QSM geometries: (a) $g/r = 2$, $R/r = 2$; (b) $g/r = 10$, $R/r = 10$; (c) $g/r = 2$, $R/r = 20$; (d) $g/r = 10$, $R/r = 100$; with $r = r_{ref}$.*

Arguments above suggest to use the latter approach to calculate the electrostatic force term F_P. Therefore, the whole numerics presented in Part Two of this thesis makes use of formula (C.4).

References

[1] E. Eriksen, K. Vøyenli (1976). The classical and relativistic concepts of mass. *Foundations of Physics*, 6(1):115-124.

[2] The equivalence of mass and energy (2001, updated 2012). *Encyclopedia of Philosophy*. http://plato.stanford.edu/entries/equivME/#2.1.

[3] L. Angelani, R. Di Leonardo, G. Ruocco (2009). Self-starting micromotors in a bacterial bath. *Physical Review Letters*, 102:048104.

[4] R. W. Gurney, E. U. Condon (1928). Quantum mechanics and radioactive disintegration. *Nature*, 122:439.

[5] General Electric Research Laboratory (1959). Tunnel diodes.

[6] Woo F. Chow (1964). Principles of tunnel diode circuits.

[7] B. D. Josephson (1973). The discovery of tunneling supercurrents. *Nobel Lecture*.

[8] G. Binnig, H. Rohrer (1986). Scanning tunneling microscopy. *IBM Journal of Research and Development*, 30:4.

[9] R. A. Millikan (1911). The isolation of an ion, a precision measurement of its charge, and the correction of Stokes's law. *Physical Review*, 32:349-397.

[10] H. R. Zeller, I. Giaver (1969). Tunneling, zero-bias anomalies, and small superconductors. *Physical Review*, 181(2):789-799.

[11] C. J. Gorter (1951). A possible explanation of the increase of the electrical resistance of thin metal films at low temperatures and small field strengths. *Physica*, 17:777.

[12] C. Feldman (1963). Temperature dependency of resistance of thin metal films. *Journal of Applied Physics*, 34:1710.

[13] R. I. Shekhter (1973). Zero anomalies of the resistance of tunnel junctions containing metallic inclusions in the oxide layer. *Soviet Physics JETP*, 36:747.

[14] I. O. Kulik, R. I. Shekhter (1975). Kinetic phenomena and charge discreteness effects in granulated media. *Soviet Physics JETP*, 41:308.

[15] D. V. Averin, K. K. Likhare (1986). Superconducting quantum interference devices and their applications. *In* SQUID'85: ed. by H-D Hahlbohm, H. Libbig, *de Gruyter, Berlin*.

[16] L. S. Kuzmin, K. K. Likharev (1987). Direct experimental observation of discrete correlated single-electron tunneling. *JETP Letters*, 45(8):495-497.

[17] T. A. Fulton, G. J. Dolan (1987). Observation of single-electron charging effects in small tunnel junctions. *Physical Review Letters*, 59(1):109-112.

[18] R. P. Andres, T. Bein, et al. (1996). "Coulomb staircase" at room temperature in a self-assembled molecular nanostructure. *Science*, 272(5266):1323-5.

[19] E. S. Soldatov, V. V. Khanin, et al. (1996). Single-electron transistor based on a single cluster molecule at room temperature. *JETP Letters*, 64:556.

[20] D. L. Klein, P. L. McEuen, J. E. B. Katari, R. Roth, A. P. Alivisatos (1996). An approach to electrical studies of single nanocrystals. *Applied Physics Letters*, 68:2574.

[21] D. V. Averin, K. K. Likharev (1991). Single-electronics. *In*: B. Altshuler et al., *Mesoscopic phenomena in solids*. Elsevier, pp. 173-271.

[22] R. I. Shekhter, J. Wan, K. McGreer, L. I. Glazman, A. Goldman (1991). Two-state approximation in the Coulomb-blockade theory: simple analytical results for a double-tunnel junction. *Physical Review B*, 43:938.

[23] E. Ollier, P. Labeye, F. Revol (1995). Micro-opto mechanical switch integrated on silicon. *Electronics Letters*, 31(23):2003-2005.

[24] H. Toshiyoshi, H. Fujita (1996). Electrostatic micro torsion mirrors for an optical switch matrix. *Journal of Microelectromechanical Systems*, 5(4):231-237.

[25] L. Y. Gorelik, A. Isacsson, et al. (1998). Mechanism for charge transfer in Coulomb blockade nanostructures. *Physical Review Letters*, 80(20):4526.

[26] A. Erbe, R. H. Blick, A. Tilke, A. Kriele, J. P. Kotthaus (1998). A mechanically flexible tunneling contact operating at radio frequencies. *Applied Physics Letters*, 73:3751.

[27] A. Isacsson, L. Y. Gorelik, et al. (1998). Shuttle instability in self-assembled Coulomb blockade nanostructures. *Physica B*, 255:150.

[28] L. Y. Gorelik, A. Isacsson, et al. (1998). Micro-mechanical charge transfer mechanism in soft Coulomb Blockade nanostructures. *Physica B*, 249:197.

[29] A. Isacsson (2001). Dynamics of a three-terminal mechanically flexible tunneling contact. *Physical Review B*, 64:2001.

[30] Blick Group, Nanotechnology. http://www.nanomachines.com/nanomachines/Home.html.

[31] R. H. Blick, A. Erbe, et al. (1999). Nanomechanical resonators operating in the radio frequency regime as single charge detectors. *Advances in Solid State Physics*, 39:121.

[32] H. Krömmer, A. Erbe, et al. (2000). Nanomechanical resonators operating as charge detectors in the nonlinear regime. Europhysics Letters, 50(1):101.

[33] P. Lafarge et al. (1991). Direct observation of macroscopic charge quantization: a Millikan experiment in a submicron solid state device. *Comptes Rendus de l'Academie des Sciences, Serie II (Mecanique,-Physique,-Chimie-Sciences-de-la-Terre-et-de-l'Univers)*, 314:883-8.

[34] M. W. Kellera, J. M. Martinis, N. M. Zimmerman, A. H. Steinbachb (1996). Accuracy of electron counting using a 7-junction electron pump. *Applied Physics Letters*, 69:1804.

[35] A. Erbe, G. Corso, et al. (2000). Mechanical mixing in nonlinear nanomechanical resonators. *Applied Physics Letters*, 77:3102.

[36] A. Erbe, C. Weiss, W. Zwerger, R. H. Blick (2001). Nanomechanical resonator shuttling single electrons at radio frequencies. *Physical Review Letters*, 87:096106.

[37] D. V. Scheible, A. Erbe, R. H. Blick (2002). Tunable coupled nanomechanical resonators for single-electron transport. New Journal of Physics, 4:86.

[38] L. Pescini, H. Lorenz, R. H. Blick (2003). Mechanical gating of coupled nanoelectromechanical resonators operating at radio frequency. *Applied Physics Letters*, 82:352.

[39] D. V. Scheible, A. Erbe, R. H. Blick (2003). Dynamic control and modal analysis of coupled nanomechanical resonators. *Applied Physics Letters*, 82:3333.

[40] D. V. Scheible, C. Weiss, R. H. Blick (2004). Effects of low attenuation in a nanomechanical electron shuttle. *Journal of Applied Physics*, 96:1757.

[41] D.V. Scheible, R. H. Blick (2004). Silicon nano-pillars for mechanical single electron transport. *Applied Physics Letters*, 84:4632.

[42] R. H. Blick, D. V. Scheible (2004). A quantum electro mechanical device: the electro-mechanical single electron pillar. *Superlattices and Microstructures*, 33:397.

[43] R. H. Blick, M. Grifoni (2005). Focus on nano-electromechanical system (Editorial). *New Journal of Physics*, 7.

[44] Single-electron transistor goes mechanical (2004). *PhysicsWorld.com*. http://physicsworld.com/cws/article/news/2004/may/26/single-electron-transistor-goes-mechanical.

[45] Single electron transistor created with tiny mechanical arm (2004). *University of Wisconsin-Madison*. https://www.engr.wisc.edu/news/archive/2004/Sep27.html.

[46] T. Novotný, A. Donarini, A-P Jauho (2003). Quantum shuttle in phase space. *Physical Review Letters*, 90:256801.

[47] M. P. Blencowe, J. Imbers, A. Armour (2005). Dynamics of a nanomechanical resonator coupled to a superconducting single-electron transistor. *New Journal of Physics*, 7:236.

[48] T. Novotný, A. Donarini, C. Flindt, A-P Jauho (2004). Shot noise of a quantum shuttle. *Physical Review Letters*, 92:248302.

[49] A. Donarini, T. Novotný, A-P Jauho (2005). Simple models suffice for the single dot quantum shuttle. *New Journal of Physics*, 7:237.

[50] D. Rodrigues, A. D. Armour (2005). Quantum master equation descriptions of a nanomechanical resonator coupled to a single-electron transistor. *New Journal of Physics*, 7:251.

[51] A. A. Clerk, S. Bennett (2005). Quantum nano-electromechanics with electrons, quasiparticles and Cooper pairs, effective bath descriptions and strong feedback effects. *New Journal of Physics*, 7:238.

[52] F. Rüting, A. Erbe, C. Weiss (2005). Self-excitation in nanoelectromechanical charge shuttles below the field emission regime. *New Journal of Physics*, 7:240.

[53] F. Pistolesi, R. Fazio (2006). Dynamics and current fluctuations in an ac-driven charge shuttle. *New Journal of Physics*, 8:113.

[54] A. D. Armour, A. MacKinnon (2002). Transport via a quantum shuttle. *Physical Review B*, 66:035333.

[55] T. Nord and L. Y. Gorelik (2005). Energy pumping in a quantum nanoelectromechanical system. *Low Temperature Physics*, 31:534.

[56] D. Fedorets, L. Y. Gorelik, R. I. Shekhter, M. Jonson (2004). Quantum shuttle phenomena in a nanoelectromechanical single-electron transistor. *Physical Review Letters*, 92:166801.

[57] D. Fedorets, L. Y. Gorelik, R. I. Shekhter, M. Jonson (2004). Quantum precursor of shuttle instability. *Fundamental Problems of Mesoscopic Physics, NATO Science Series II*, 154: 65-73.

[58] H-S Kim, H. Qin, L. M. Smith, M. Westphall, R. H. Blick (2007). Field emission from a single nanomechanical pillar. *Nanotechnology*, 18:065201.

[59] D. V. Scheible, C. Weiss, J. P. Kotthaus, R. H. Blick (2004). Periodic field emission from an isolated nanoscale electron island. Physical Review Letters, 93:186801.

[60] R. H. Blick, H. Qin, H-S Kim, R. Marsland (2007). A nano-mechanical computer: exploring new avenues of computing. *New Journal of Physics*, 9:241.

[61] Proposed 'nanomechanical' computer is both old-school and cutting-edge (2007). *Phys.org*. http://phys.org/news105356632.html.

[62] The mechanical computer that is smaller than a grain of sand (2007). *Daily Mail*. http://www.dailymail.co.uk/sciencetech/article-474540/The-mechanical-smaller-grain-sand.html.

[63] H. Qin, H-S Kim, R. H. Blick (2008). Nanopillar arrays on semiconductor membranes as electron amplifiers. *Nanotechnology*, 19:095504.

[64] D. V. Scheible, R. H. Blick (2010). A mode locked nanomechanical electron shuttle. *New Journal of Physics*, 12:023019.

[65] C. Kim, H-S Kim, H. Qin, R. H. Blick (2010). Coulomb-controlled single electron field emission from a freely suspended metallic island. *Nano Letters*, 10:615.

[66] C. Kim, J. Park, R. H. Blick (2010). Spontaneous symmetry breaking in two coupled nanomechanical electron shuttles. *Physical Review Letters*, 105:067204.

[67] H-S Kim, H. Qin, R. H. Blick (2010). Self-excitation of nanomechanical pillars. *New Journal of Physics*, 12:033008 *(selected as one of the 'Best of 2010' papers by the New Journal of Physics)*.

[68] M. T. Tuominen, R. V. Krotkov, M. L. Breuer (1999). Stepwise and hysteretic transport behavior of an electromechanical charge shuttle. *Physical Review Letters*, 83:3025-3028.

[69] H. Park, J. Park, A. K. L. Lim, E. H. Anderson, A. P. Alivisatos, P. L. McEuen (2000). Nanomechanical oscillations in a single-C60 transistor. *Nature*, 407:57.

[70] F. Pistolesi, R. Fazio (2005). Charge shuttle as a nanomechanical rectifier. *Physical Review Letters*, 94:036806.

[71] N. Pauget, F. Pistolesi (2008). Coulomb blockade for an oscillating tunnel junction. *Physical Review B*, 77:235318.

[72] L. Wang, H-H Chen; X-D He (2011). Active H∞ control of the vibration of an axially moving cantilever beam by magnetic force. *Mechanical Systems and Signal Processing*, 25(8):2863-2878.
[73] R. M. Lin, W. J. Wang (2006). Structural dynamics of microsystems – Current state of research and future directions. *Mechanical Systems and Signal Processing*, 20(5):1015-1043.
[74] D. R. Koenig, E. M. Weig, J. P. Kotthau (2008). Ultrasonically driven nanomechanical single-electron shuttle. *Nature Nanotechnology*, 3:482-485.
[75] D. R. Koenig, E. M. Weig (2012). Voltage-sustained self-oscillation of a nano-mechanical electron shuttle. Applied Physics Letters, 101:213111.
[76] A. I. Ekimov, A. A. Onushchenko (1981). Quantum size effect in three-dimensional microscopic semiconductor crystals. *JETP Letters*, 34:345-349.
[77] R. H. Blick, R. A. Marsland (2008). Nanomechanical computer. *United States Patent 7414437B1*.
[78] P. C. W. Davies (2005). Quantum tunneling time. American Journal of Physics, 73:23-27.
[79] F. E. Low (1998). Comments on apparent superluminal propagation. *Annalen der Physik (Leipzig)*, 7:660-661.
[80] M. Razavy (2003). Quantum theory of tunneling. *World Scientific Publishing Co*.
[81] R. H. Fowler, L. Nordheim (1928). Electron Emission in Intense Electric Fields. *Proceedings of the Royal Society of London*, 119(781):173-181.
[82] W. W. Lui, M. Fukuma (1986). Exact solution of the Schrodinger equation across an arbitrary one-dimensional piecewise-linear potential barrier. *Journal of Applied Physics*, 60:1555.
[83] R. P. Bell (1959). The tunnel effect correction for parabolic potential barriers. *Transaction of the Faraday Society*, 55:1-4.
[84] Y. Ando, T. Itoh (1987). Calculation of transmission tunneling current across arbitrary potential barriers. *Journal of Applied Physics*, 61:1497.
[85] A. Garg (2000). Tunnel splittings for one-dimensional potential wells revisited. *American Journal of Physics*, 68:430.
[86] J. G. Simmons (1963). Generalized formula for the electric tunnel effect between similar electrodes separated by a thin insulating film. *Journal of Applied Physics*, 34:1793.
[87] H. Grabert, H. L. Ingold (1991). Single electron tunneling rates in multijunction circuits. *Zeitschrift für Physik B*, 84(1):143-155.
[88] R. H. Chen, K. K. Likharev (1998). Multiple-junction single-electron transistors for digital applications. *Applied Physics Letters*, 72(1):61.
[89] K. Nakazato, H. Ahmed (1993). The multiple tunnel junction and its application to single electron memory. *Advanced Materials*, 5(9):668-671.
[90] A. N. Korotkov, R. H. Chen, K. K. Likharev (1995). Possible performance of capacitively coupled single-electron transistors in digital circuits. *Journal of Applied Physics*, 78(4):2520.
[91] R. H. Chen, A. N. Korotkov, K. K. Likharev (1996). Single-electron transistor logic. *Applied Physics Letters*, 68:1954.
[92] K. K. Likharev (1987). Possibility of creating analog and digital integrated circuits using the discrete, one-electron tunneling effect. *Mikroelectronikz*, 16:195-209.
[93] C. Schönenberger, H. van Houten, H. C. Donkersloot (1992). Single-electron tunnelling observed at room temperature by scanning-tunnelling microscopy. *EuroPhysics Letters*, 20:249.
[94] E. S. Soldatov et al. (1998). Room temperature molecular single-electron transistor. *Physics Uspekhi*, 41:202-204.
[95] E. S. Soldatov et al. (2003). Molecular cluster based nanoelectronics. *Microelectronic Engineering*, 69:536-548.
[96] C. Joachim, J. K. Gimzewski, A. Aviram (2000). Electronics using hybrid-molecular and mono-molecular devices. *Nature*, 408:541-548.
[97] D. Porath, O. Millo (1997). Single electron tunneling and level spectroscopy of isolated C60 molecules. *Journal of Applied Physics*, 81:2241.
[98] C. Joachim, J. K. Gimzewski, H. Tang (1998). Physical principles of the single-C60 transistor effect. *Physical Review B*, 58(24):16407:16417.

[99] H. W. Ch. Postma, T. Teepen, Z. Yao, M. Grifoni, C. Dekker (2001). Carbon nanotube single-electron transistors at room temperature. *Nature*, 293:76-79.
[100] Y. Q. Feng, R. Q. Zhang, S. T. Lee (2004). Simulation of gate-controlled Coulomb blockades in carbon nanotubes. *Journal of Applied Physics*, 95:5729.
[101] J. Kong, C. Zhou, E. Yenilmez, H. Dai (2000). Alkaline metal-doped n-type semiconducting nanotubes as quantum dots. *Applied Physics Letters*, 77:3977.
[102] M. A. Reed, J. N. Randall et al. (1988). Observation of discrete electronic states in a zero-dimensional semiconductor nanostructure. *Physical Review Letters*, 60:535–537.
[103] U. Meirav, E. B. Foxman (1996). Single-electron phenomena in semiconductors. *Semiconductor Science and Technology*, 11:255-284.
[104] Y. Takahashi, Y. Ono, A. Fujiwara, H. Inokawa (2002). Silicon single-electron devices. *Journal of Physics: Condensed Matter*, 14, R995-R1033.
[105] L. Zhuang, L. Guo, Y. Stephen (1998). Silicon single-electron quantum-dot transistor switch operating at room temperature. *Applied Physics Letters*, 72(10):1205-1207.
[106] L. P. Kouwenhoven et al. (1997). Electron transport in quantum dots. *Conference Proceedings of Advanced Study Institute on Mesoscopic Electron Transport*, edited by L. P. Kouwenhoven, L. L. Sohn, G. Schön (Kluwer 1997).
[107] S. J. Tans et al. (1997). Individual single-wall carbon nanotubes as quantum wires. *Nature*, 386:474-477.
[108] K. W. Chan et al. (2011). Single-electron shuttle based on a silicon quantum dot. *Applied Physics Letters*, 98:212103.
[109] A. V. Moskalenko et al. (2009). Fabrication of shuttle-junctions for nanomechanical transfer of electrons. *Nanotechnology*, 20:485202.
[110] A. A. Andronov, A. A. Vitt, S. E. Khaikin (1966). Theory of oscillators. *Pergamon, Oxford*, Ch. IX, §9.
[111] M. B. Haider et al. (2009). Controlled coupling and occupation of silicon atomic quantum dots at room temperature**.** *Physical Review Letters*, 102:046805.
[112] A. N. Cleland (2002). Foundation of Nanomechanics. *Springer*.
[113] L. D. Landau (1976). Mechanics. *Course of Theoretical Physics, Vol.1, Third Edition*, p. 80.
[114] G. E. Moore (1965). Cramming more components onto integrated circuits. *Electronics Magazine*, p. 4.
[115] S. J. Tans, A. R. M. Verschueren, C. Dekker (1998). Room-temperature transistor based on a single carbon nanotube, *Nature*, 393:49-52.
[116] R. M. Westervelt (2008). Graphene nanoelectronics. *Science*, 320(5874):324-325.
[117] A. Bachtold, P. Hadley, T. Nakanishi, C. Dekker (2001). Logic circuits with carbon nanotube transistors. *Science*, 294(5545):1317-1320.
[118] T-H Lee, S. Bhunia, M. Mehregany (2010). Electromechanical computing at 500°C with silicon carbide. *Science*, 329(5997):1316-1318.
[119] T. Hasegawa et al. (2011). Volatile/Nonvolatile Dual-Functional Atom Transistor. *Applied Physics Express*, 4:015204.
[120] H. Iwamura, M. Akazawa, Y. Amemiya (1998). Single-electron majority logic circuits. *IEICE Transactions on Electronics*, E81-C:42-48.
[121] N. Yoshikawa, C. Fukuzato, M. Sugahara (1999). Single electron transfer logic gate family. *Japanese Journal of Applied Physics*, 38:433-438.
[122] K. Uchida, J. Koga, R. Ohba, A. Toriumi (2000). Room-temperature operation of multifunctional single-electron transistor logic. *Electron Devices Meeting, IEDM 2000*, 863-865.
[123] S. J. Kim et al. (2006). Single-electron logic cells and SET/FET hybrid integrated circuits. *JSTS*.
[124] K. S. Park, S. J. Kim, et al. (2005). SOI single-electron transistor with low RC delay for logic cells and SET/FET ICs. *IEEE Transactions on Nanotechnology*, 4(2):242-248.
[125] K. S. Park, S. J. Kim, et al. (2004). THz ultra-fast single-electron transistors fabricated on SOI structures by PADOX. *Semiconductor Science and Technology*, 19:L39-41.
[126] K. Jain, G. W. Pratt Jr. (1976). Optical transistor. *Applied Physics Letters*, 28:719.

[127] K. Jain, G. W. Pratt Jr. (1983). Optical transistors and logic circuits embodying the same. *United States Patent 4382660.*

[128] E. H. Witlicki, C. Johnsen, et al. (2011). Molecular logic gates using surface-enhanced raman-scattered light. *Journal of the American Chemical Society*, 133:7288-7291.

[129] Simulating physics with computers. http://www.cs.berkeley.edu/~demmer/papers/feynman.pdf.

[130] T. Kubota et al. (2004). A 7-nm nanocolumn structure fabricated by using a ferritin iron-core mask and low-energy Cl neutral beams. *Applied Physics Letters*, 84:1555.

[131] C-W Kuo et al. (2003). Fabrication of size-tunable large-area periodic silicon nanopillar arrays with sub-10-nm resolution. *The Journal of Physical Chemistry B*, 107(37):9950-9953.

[132] C. Li, T-W Chou (2003). Single-walled carbon nanotubes as ultrahigh frequency nanomechanical resonators. *Physical Review B*, 68:073405.

[133] C. Li (2004). Vibrational behaviors of multiwalled-carbon-nanotube-based nanomechanical resonators. *Applied Physics Letters*, 84(1):121-123.

[134] S. Bauerdick, A. Linden, C. Stampfer, T. Helbling, C. Hierold (2006). Direct wiring of carbon nanotubes for integration in nanoelectromechanical systems. *Journal of Vacuum Science & Technology B*, 24:3144.

[135] J. E. Hopcroft, J. D. Ullman (1979). Introduction to automata theory, languages, and computation. Reading, Massachusetts. *Addison-Wesley, 1st Ed*.

[136] J. G. Simmons (1963). Electric tunnel effect between dissimilar electrodes separated by a thin insulating film. *Journal of Applied Physics*, 34:2581.

[137] A. Russell (1921). The capacity coefficients of spherical electrodes. *Proceedings of the Physical Society of London*, 23:352.

[138] A. C. M. de Queiroz (2003, updated 2012). Capacitance calculations.

[139] Y. Nakajima, T. Sato (1999). Calculation of electrostatic force between two charged dielectric spheres by the re-expansion method. *Journal of Electrostatics*, 45:213-226.

Publications

On the thesis topic:

1. A. Scorrano, A. Carcaterra (2011). Modelling and simulations of a nanomechanical transistor. *ENOC 2011, Rome, Italy; AIMETA 2011, Bologna, Italy*.
2. A. Scorrano, A. Carcaterra (2012). Vibration-based nano-mechanical transistor: theoretical modelling and numerical simulations. *NOVEM 2012, Sorrento, Italy*.
3. A. Scorrano, A. Carcaterra (2012). Self-excitation of electro-mechanical resonators: nano-mechanical transistor. *ISMA 2012, Leuven, Belgium*.
4. A. Scorrano, A. Carcaterra (2013). Semi-classical modelling of nano-mechanical transistors. *Mechanical Systems and Signal Processing (Elsevier).*
5. A. Scorrano, A. Carcaterra (2013). Investigation on nanomechanical transistor. *Meccanica (Springer).*
6. M. E. Peña-Aza, A. Scorrano, L. Y. Gorelik (2013). Parametric excitation of dc current in a single-dot shuttle system via spontaneous symmetry breaking. *Physical Review B (APS Physics).*

On the project "SEALAB: JointLab Marine Vehicle Technology" (http://w3.uniroma1.it/sealab):

7. A. Carcaterra, A. Scorrano, G. Pepe. SEALAB: aero-hydromechanics of a 3-wings jumping vehicle. *HSMV 2011, Naples, Italy*.
8. G. Pepe, A. Carcaterra, A. Scorrano. Stability analysis of a three-wings high-speed craft. *AIMETA 2011, Bologna, Italy*.
9. A. Carcaterra, A. Scorrano, G.Pepe. Aero-hydro mechanics of an extreme-speed marine vehicle. *AIMETA 2011, Bologna, Italy*.

Conferences Participations

CISM 2010 (Variational Models and Methods in Solid and Fluid Mechanics)
International Centre for Mechanical Sciences, Udine, Italy, 12-16 July, 2010

9° Symposium HSMV 2011 (High Speed Marine Vehicle)
Università degli Studi di Napoli "Federico II", Naples, Italy, 26-27 May 2011

7th Conference ENOC 2011 (European Nonlinear Dynamics Conference)
Università degli Studi di Roma "La Sapienza", Rome, Italy, 24-29 July 2011

XX Congresso AIMETA 2011 (Associazione Italiana Meccanica Teorica e Applicata)
Complesso Monumentale " Santa Cristina", Bologna, Italy, 12-15 September 2011

GA7 Meeting, MID-FREQUENCY (Seventh Framework Programme)
Università degli Studi di Roma "La Sapienza", Rome, Italy, 15-16 March 2012

NOVEM 2012 (Noise and Vibration: Emerging Methods)
Hotel Royal, Sorrento, Italy, 1-4 April, 2012

25th Conference ISMA 2012 (International Conference on Noise and Vibration)
Katholieke Universiteit, Leuven, Belgium, 17-19 September 2012

Abstract (extract from the Preface)

The most basic example of charge transport is represented by the collective motion of free charge carriers in a conductive medium. In the context of electromechanical devices, more complex forms of charge transport, labeled with the umbrella term *electron shuttle*, exist.
The simplest system exhibiting a shuttle mechanism comprises a set of three conductors: two fixed electrodes and a vibrating element between them. Under certain boundary conditions a limit-cycle is established, and the oscillator alternatively takes and releases a finite amount of electrons while approaching the electrodes. Since this form of charge transport relies on the presence of mechanical vibrations, the described phenomenon constitutes the archetype of a "mechanical charge carrier".

Although the first concept of electron shuttle is over two centuries old, only in recent times [Gorelik and Isacsson, 1998] it found reinvigorated interest in the field of nanotechnology, producing a novel branch of both theoretical and experimental research. In fact, the introduction of quantum effects in shuttle devices produces interesting motion regimes peculiar of nanoscale. Refer to such systems as *Quantum Shuttle Modules* (QSMs).

Many original architectures have been conceptualized and realized in the last decade. A promising application is contained in a patent [Blick and Marsland, 2008] which proposes a switching element based on electron shuttle and capable of reproducing the main functionalities of a conventional transistor, depicted as composed by an array of mechanically coupled QSM subsystems, whose vibrating elements are nanocantilevers. Refer to this invention as the *Nano-Mechanical Transistor* (NMT). At the present day, the NMT is an unexplored concept: no experimental setup has been realized nor theoretical model has been proposed yet.

The research work contained in this thesis is intended to provide a first theoretical description and an early design stage for such NMT device. Notice that, since the NMT is composed by a set of QSMs, a preliminary study of these systems is needed. This work is consequently divided in two Parts: the first one focuses on the QSMs with an exquisitely theoretical approach, while the second one is intended to assess the feasibility of a real application, the NMT.
A brief description of the thesis contents is presented ahead.

Part One begins by introducing the fundamental concepts of quantum tunneling and Coulomb blockade. Then, the general scheme of a QSM is presented. As usual in literature, a concentrated parameters model is used, and the state of the system is reduced to a couple of lagrangian descriptors: the oscillator position and charge. Conductive and dynamical properties are investigated with both analytical and numerical approaches. Then, a systematic study of QSMs is attempted by considering two basic shuttle mechanisms: in the first case, the oscillator is self-excited by a shuttle current between electrodes at different voltages; in the second case, the oscillator vibrates under parametric resonance and a shuttle current is established between two electrodes at the same voltage. The portrayed phenomenologies are complementary, meaning each QSM presents a combination of these two fundamental forms of electron shuttle.

Part Two opens with an overview of the conventional transistors and an analysis of the NMT patent. Follows the choice of the characteristic scales of the device and the typology of QSM to be the best candidate as NMT subsystem. Under suitable approximations, closed-form formulae for capacitances, quantum tunneling and electrostatic force are produced. A flexible set of equations is obtained, allowing to perform a large number of numerical experiments. First, a single QSM subsystem is considered: a predictive model is proposed in which a QSM is related to a Turing machine whose admitted states are represented by the feasible motion regimes. Then, more QSM subsystems are arranged to realize the NMT: each module is electrostatically independent but mechanically coupled with its nearest neighbors. A functional analysis of the whole system is presented, in which peculiar motion regimes are investigated, and a set of design and control strategies aimed to correctly reproduce switching and amplification functionalities is proposed. Last, the black-box electrical characterization of the device is outlined.

In conclusion, the main original contributions of this research work are: i) the theoretical study of a novel device – the NMT – which has led to synthetize a series of design requirements and control strategies; II) the conceptualization of a parametric resonant QSM, which – differently from the self-excited one – constitutes a new archetype of electron shuttle.

"An expert is a person who has made all the mistakes
that can be made in a very narrow field."
Niels Bohr

"Science is the belief in the ignorance of experts."
Richard Feynman

"If we knew what it was we were doing,
it would not be called research, would it?"
Albert Einstein

"If you thought that science was certain,
well, that is just an error on your part."
Feynman

"As I have said so many times,
God doesn't play dice with the world."
Einstein

"God was invented to explain mystery.
God is always invented to explain those things
that you do not understand."
Feynman

"The most incomprehensible thing about the world
is that it is at all comprehensible."
Einstein

"I think I can safely say that nobody
understands quantum mechanics."
Feynman

"A witty saying doesn't prove anything."
Voltaire

Printed in Rome, March 2013